KTB REPORT 90-8

KTB Pilot Hole

Results of Geoscientific Investigation
in the KTB Field Laboratory

0–4000,1 m

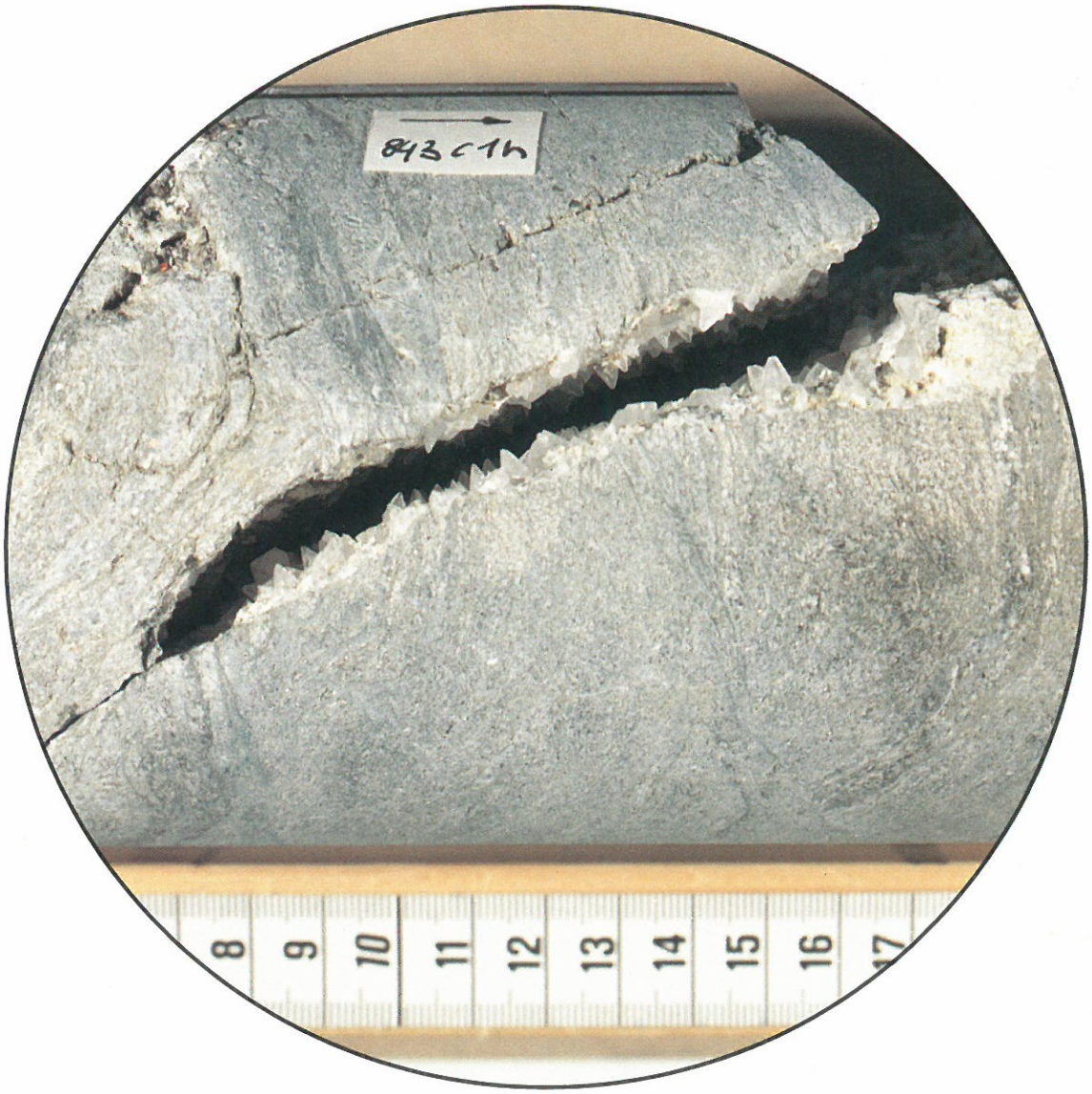

Edited by
the Project Management of the Continental
Deep Drilling Programme of the Federal Republic of Germany
in the Geological Survey of Lower Saxony

R. Emmermann, H.-G. Dietrich, J. Lauterjung, Th. Wöhrl

Redaktion: R. Emmermann, H.-G. Dietrich,
J. Lauterjung, Th. Wöhrl

Druck: Wittmann & Wäsch, 3007 Gehrden

Titelbild: Open fissure as migration path of gaseous and highly saline brines within sillimanite-biotite gneiss, displaying calcite scalenohedrons on the joint planes.

(Core piece 843C1h, 3446.95 m, scale in cm)

Die diesem Bericht zugrundeliegenden Vorhaben wurden mit Mitteln des Bundesministeriums für Forschung und Technologie (Forschungskennzeichen: RG 8604-0) gefördert. Die Verantwortung für den Inhalt dieser Veröffentlichung liegt bei den Autoren.

Anschrift des Herausgebers: Projektleitung KTB im Niedersächsischen Landesamt für Bodenforschung, Postfach 51 01 53, D-3000 Hannover 51. Telefon: (05 11) 643-2675.

KTB drilling rig and field laboratory (0.4/88),
Photo Hoffmannsbeck, No. 992508 / 2170 Luftamt
Nordbayern

KTB Report 90-8
KTB Pilot Hole
Results of Geoscientific Investigation in the KTB Field Laboratory

(0 - 4000.1 m)

CONTENTS

KTB-Report	90-8	A1 - A23	14 Fig.	Hannover 1990

A. INTRODUCTION

[1] Emmermann, R., [3] Dietrich, H.-G., [2] Lauterjung, J. & [3] Wöhrl, Th.

Contents:

Authors addresses:

1) Institut für Geowissenschaften und Lithosphärenforschung der Justus-Liebig-Universität, D-6300 Giessen;

   Director of "Geosciences" in the KTB Project Management and Chief Coordinator of the DFG Priority Program "KTB";

2) Institut für Geowissenschaften und Lithosphärenforschung der Justus-Liebig-Universität, D-6300 Giessen;

3) KTB-Feldlabor, P.O.-Box 67, D-8486 Windischeschenbach.

A.1 INTRODUCTION

R. Emmermann

Establishment of a field laboratory at the drill site had a top priority since the very first discussions about a continental deep drilling program in Germany. Therefore, already in 1983 a working group headed by R. Emmermann was set up in order to define the tasks to be accomplished in the lab and to determine the equipment and personnel necessary. It was agreed that the main purpose of the field laboratory is to collect extensive geoscientific data on cores, cuttings, rock flour, drilling fluids and gases recovered from both the pilot hole and the main borehole.

In particular properties should be measured which :

- are necessary for quick operational decisions concerning drilling, sampling and testing
- have to be determined on a quasi-continuous scale as a function of depth
- are time-dependent and have to be recorded as soon as possible
- are necessary for correlation with data obtained by borehole measurements
- are needed for proper sample selection and serve as basic information for all individual research projects carried out at universities and other research institutions.

In order to meet these requirements a comprehensive scientific program is carried out on-site which includes :

- structural, petrographical and mineralogical investigations on cores and cuttings
- establishment of a "lithologic log" and a first interpretation of geological structures
- determination of major and trace elements on core material, cuttings, rock flour and drilling fluid
- on-line analysis of gases dissolved in the drilling fluid
- measurements of physical properties of cores, cuttings and rock flour.

Figure A.1.1 summarizes the organizational structure and working scheme of the field laboratory. In addition to the specified investigations the field laboratory is responsible for distribution, management and archiving of samples, and for regular publication of all scientific results. Progress reports are published regularly and cover borehole sections of 500 m length (Emmermann et al. 1988, 1989). Thus far, eight KTB-reports containing all data

corroborated in the field laboratory have been published and eight so-called "Sampling Parties" have been held where all scientists who are interested in obtaining material for their investigations are gathered during two days. In the meantime, over 20000 samples have been prepared and distributed by the field laboratory.

The staff currently includes 2 permanently employed assistants of the Project Management, 16 scientists from nine universities and 15 technicians who are mainly from the area around Windischeschenbach. These personnel are assigned to four working groups: Geology-Petrology, Geochemistry, Geophysics and Data Processing.

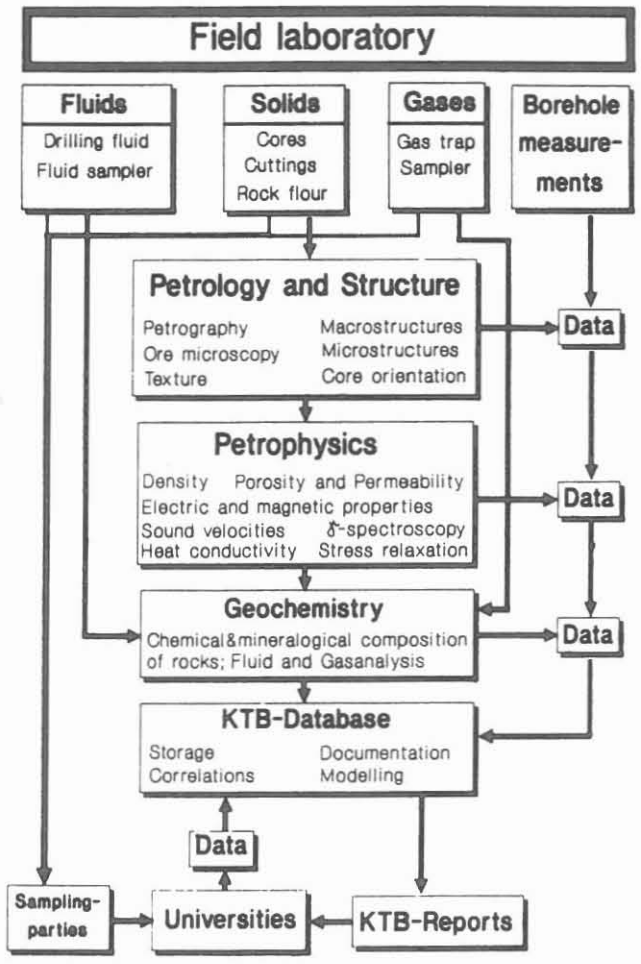

Fig. A.1.1: Sampling and working scheme of the KTB field laboratory

The KTB project management is responsible for the operation of the field laboratory which belongs to the directorate for "Geosciences". The director on site is Dr. H. G. Dietrich and his deputy is T. Wöhrl. Scientific and non-scientific

personnel are financed by the DFG-project, "Staffing of the KTB Field Laboratory" and are employed through private contracts with R. Emmermann at the University of Giessen. Principle investigators of the DFG-project include Prof. Dr. R. Emmermann, Giessen, Prof. Dr. H. Berckhemer, Frankfurt, Prof. Dr. G. Friedrich, Aachen, Prof. Dr. K. von Gehlen, Frankfurt, Prof. Dr. O. Natau, Karlsruhe, Prof. Dr. H. Soffel, München, Prof. Dr.B. Stöckhert, Bochum, Prof. Dr. K. Weber and Prof. Dr. K. H. Wedepohl, Göttingen. These investigators are responsible for the scientific program carried out in the field laboratory and their institutes serve as so-called "parent institutes" for providing qualified personnel and maintaining the equipment.

These "Parent Institutes" are:
Institut für Geowissenschaften und Lithosphärenforschung der Universität Giessen
Institut für Meteorologie und Geophysik der Universität Frankfurt
Institut für Mineralogie und Lagerstättenlehre der RWTH Aachen
Institut für Geochemie, Petrologie und Lagerstättenkunde der Universität Frankfurt
Institut für Boden- und Felsmechanik der Universität Karlsruhe
Institut für Allgemeine und Angewandte Geophysik der Universität München
Institut für Geologie der Ruhr-Universität Bochum
Institut für Geologie und Dynamik der Lithosphäre der Universität Göttingen
Geochemisches Institut der Universität Göttingen

The petrophysical investigations performed at the drilling site include determination of density, seismic velocities, natural remanent magnetization, susceptibitity, electrical resistivity, thermal conductivity, porosity and permeability. An important experiment carried out immediately after core retrieval is the measurement of anelastic strain recovery using a specially designed strain measurement apparatus.

A new X-ray diffraction technique is used to qualitatively and quantitatively determine the mineral composition of cores, cuttings and rock flour separated from the drilling fluid by means of a centrifuge. X-ray fluorescence analysis using a fully automated and computerized XRF spectrometer (Siemens SRS 303) is used for determination of major oxides and selected trace elements on core samples, cuttings and rock flour

A new type of drilling fluid was successfully used for the first time in the KTB pilot hole. This drilling fluid consists of water with about 2 wt. % Dehydril HT, a lithium-

containing sodium, magnesium silicate with a clay mineral like structure, which yields a solid-free thixotropic fluid with a high carrying capacity. An extensive analytical program for a quasi-continuous fluid investigation has been developed and up to 12 cations are analyzed at intervals from 1 - 3 m using an ICP atomic emission spectrometer (ARL 3580). Additionally, Cl- and SO42+ are determined with a chromatography system. The results obtained show that continuous fluid analysis allows immediate and reliable detection of inflow horizons and even provides qualitative information as to the composition of the water

A specially designed gas mass-spectrometer (Vacuum Generators) is used for the qualitative and quantitative determination of gases released from the drilling fluid. Using an on-line technique, 10 gas components (N2, 02, Ar, CO2, H2, CH4, C2H6, C3H8, He and H2S) are determined routinely by this fully automatic system which operates round the clock. Despite a relatively complex interpretation of the gas data, the "gas logs" have been very sensitive indicators of problem horizons and permeable zones. The on-line gas data, therefore, proved to be very useful for quick operational decisions concerning positioning of drill-stem tests and fluid sampling.

A.2 Drilling Technique

The pilot hole KTB OBERPFALZ VB was spudded on September 22, 1987. The first section of the hole down to 27.5 m, was drilled with a 17 1/2" roller cone bit. A 13 3/8" conductor pipe was set and cemented to surface (Fig. A.2.1).

The next borehole section was cored down to 478.5 m was cored using rotary technique with 10 5/8" roller cone core bits (Fig. A.2.2) and a standard 8 1/4" core barrel which yielded 4" (100.6 mm) cores. 451 m were cored and core recovery was 193.05 m (42.8%) with practically no appreciable recovery over the first 80 m.

After an extensive geophysical logging and testing program an 8 5/8" anchor casing was run above 478.0 m and cemented to surface. After drilling the casing shoe the hole was deepened down to 480 m with a 7 7/8" roller bit. Later, a 7" casing was run to a depth of 479.5 m and left uncemented so it could be recovered after completion of the pilot hole. This casing served as a wear protection for the anchor casing and offered the same hydraulic cross section as the following wireline coring phase (Chur, et al., 1989).

From 480.0 m to the final depth of 4000.1 m wireline coring technique with a specially manufactured 5 1/2" drill string and 6" diamond core bits (Fig. A.2.3) was applied. Continuous coring was interrupted by three phases of directional drilling which were necessary to reduce the angle of deviation. These sections were drilled with 6" roller cone bits and 6" diamond bits (Fig. A.2.4).

During all phases of wireline coring which yielded cores with a diameter of 94 mm the total core intervall was 3142.6 m. The total core recovery was excellent and exceeded 3074.7 m (97.8 %). A total of 9 surface set and 62 impregnated diamond core bits were used (Tab. A.2.1 and Tab. A.2.2).

Due to lost bottem hole assemblies after fishing activities two sidetracks were nessecary, the first at 1998 m and the second at 3767 m. At 1998.3 m during a directional drilling phase the drillstring got stuck. All attempts failed to free the string completely. The hole was plugged back and a sidetrack was run above the top of the fish at a depth of 1787.4 m. The kick-off point was located at 1709.0 m. The sidetracking was completed at a depth of 1802.0 m (see Fig. A.2.5).

The first part of the hole above 1998.3 m has been named KTB OBERPFAZ VB1; the denotation below the kick-off point was KTB OBERPFALZ VB 1a.

The drillstring got stuck again at a depth of 3893.0 m.
For the sidetrack an open hole packer was placed above the fish and then connected with an orientated wedging device. After sidetracking with a kick-off point at 3766.9 m the hole with the new name KTB OBERPFALZ VB 1b was deepened with a 3 1/2" rotary string and roller cone bits to the final depth

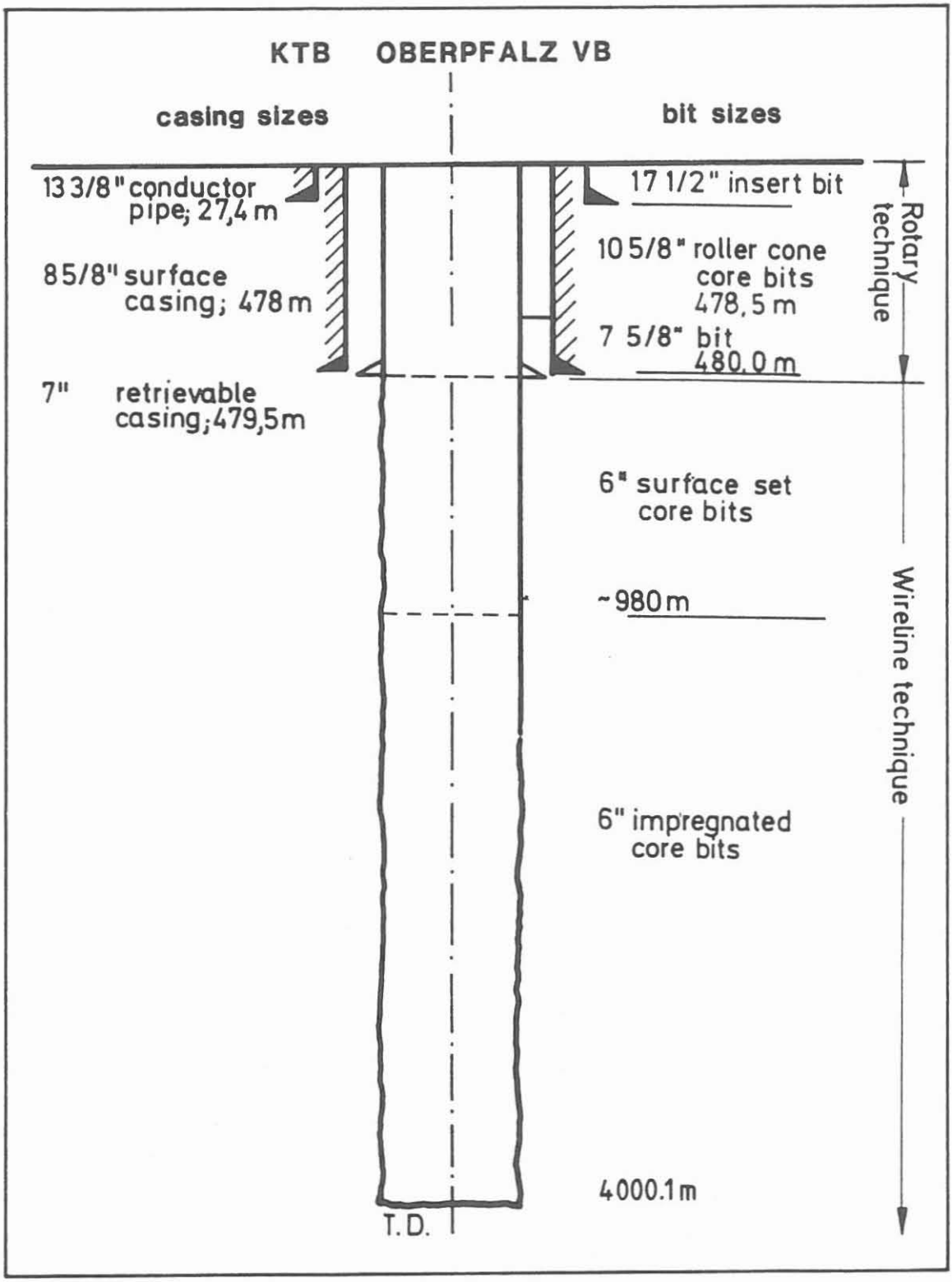

Fig. A.2.1: Casing scheme of the KTB pilot hole

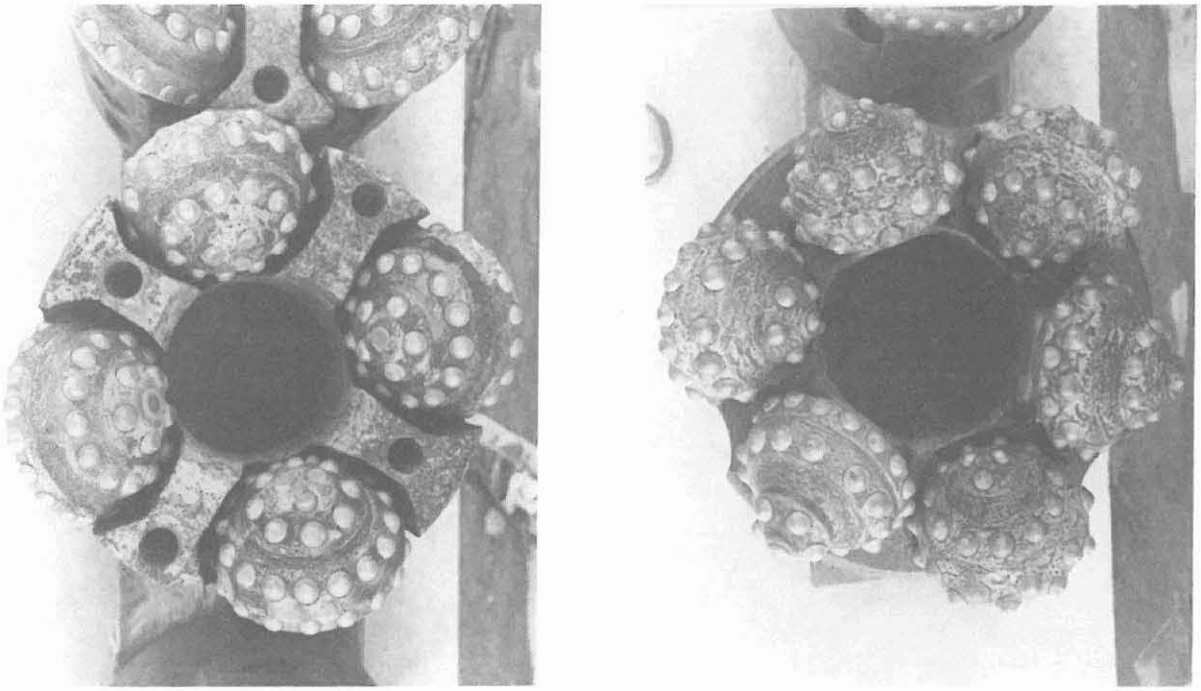

Fig. A.2.2: Two different types of 10 5/8" roller cone bits used during the rotary drilling phase

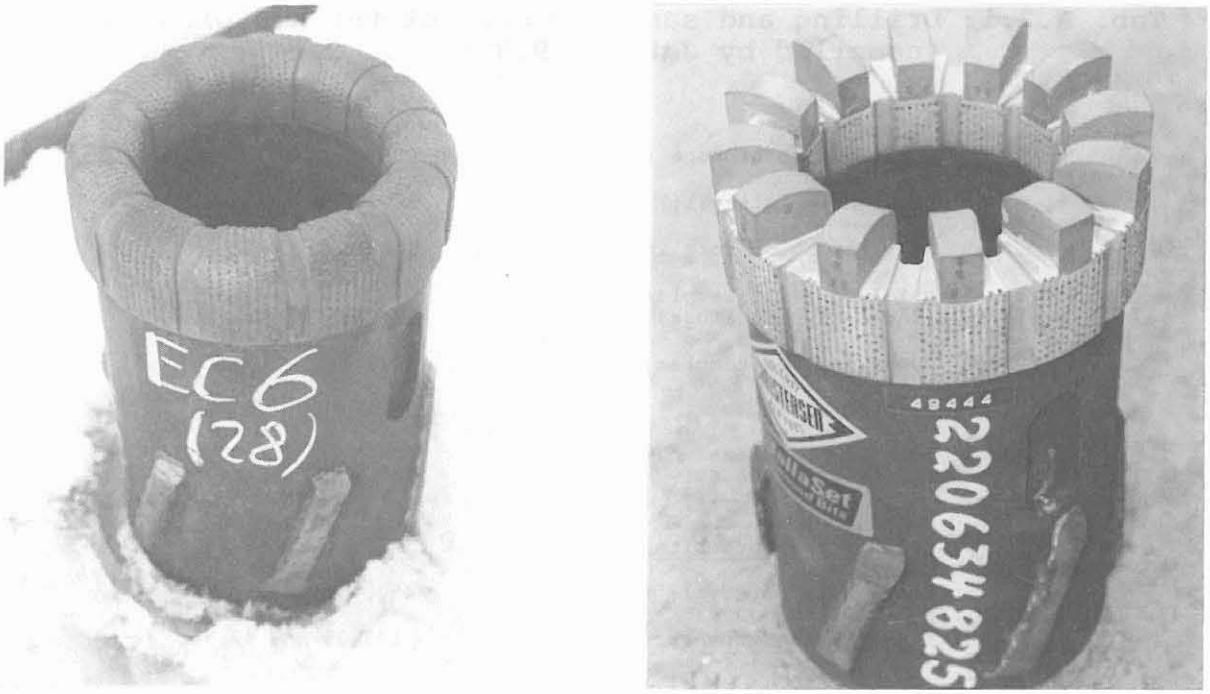

Fig. A.2.3: Two different types of 6" diamond core bits used during wireline coring, surface set (left picture) and impregnated core bit (right picture)

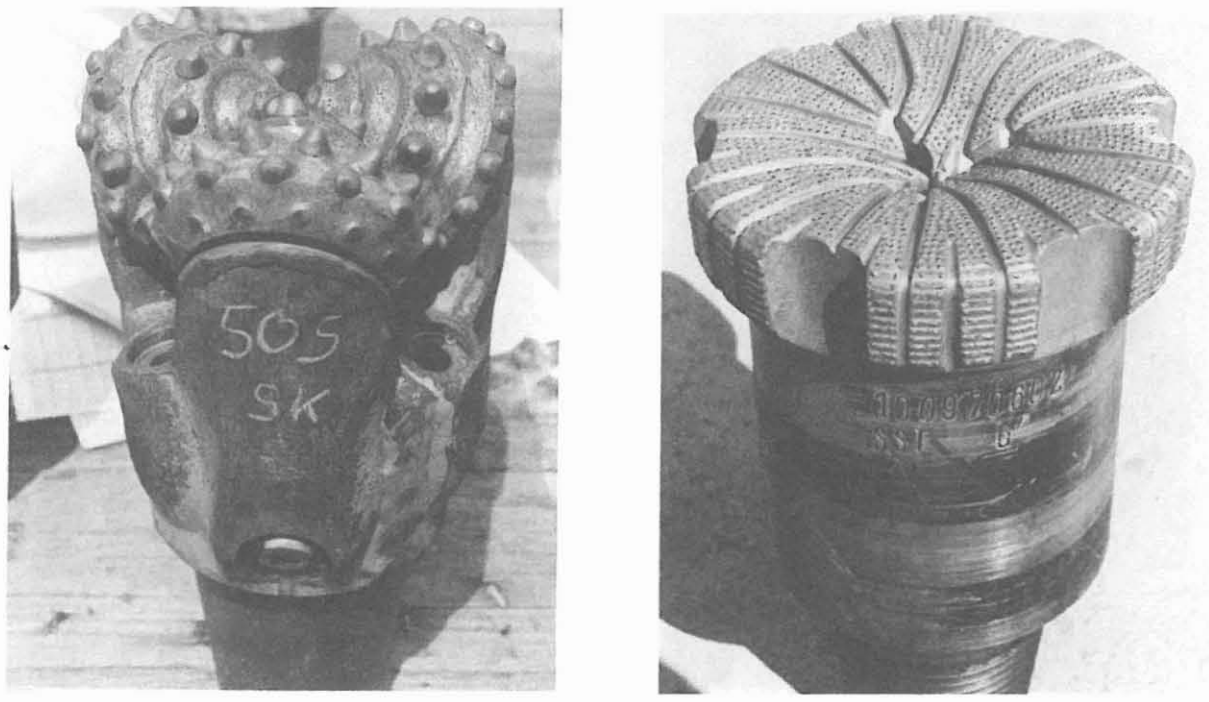

Fig. A.2.4: Two types of 6" bits used during directional drilling, roller cone bit (left picture) and surface set diamond bit (right picture)

Tab. A.2.1: Drilling and sampling data of the KTB pilot hole (compiled by Jatho, 09.89)

total number of core runs:	956
total core interval:	3593.0 m
avg. length of core interval:	3.42 m
numer of solid samples (shaker / centrifuge):	13 069
number of mud samples:	4342
open hole tests:	3
logging programme (22.09.87-04.04.89):	282 runs
<u>roller cone core bits</u>	
total core interval:	450.4 m
total core recovery: %	193.05 m = 42.86
avg. length of core interval:	2.6 m
<u>wireline coring</u>	
total core interval:	3142.6 m
total core recovery: %	3074.74 m = 97.83
avg. length of core interval:	3.56 m

depth range	Operation	bit		avg.bit life	max. bit life	avg. rate of penetration
		No	type			
28,1 m - 478,5 m	conventional coring	9	10 5/8" x 4" roller cone core bits	50,00 m	112,5 m	1,17 m/h
		1	10 5/8" x 4" diamant core bit		0,5 m	1,00 m/h
480 m - 3893 m	wireline coring	9	6" x 94 mm diamant core bits surface set	35,81 m	89,5 m	1,84 m/h
		62	6" x 94 mm diamant core bits impregnated	47,92 m	135,5 m	1,66 m/h
3771,9 m - 4000,1	full hole drilling	18	6" insert bits	12,31 m	26,2 m	0,84 m/h
		1	6" diamant bit		6,4 m	0,75 m/h

Tab. A.2.2: Drilling data of the KTB pilot hole (compiled by JATHO, 09.89)

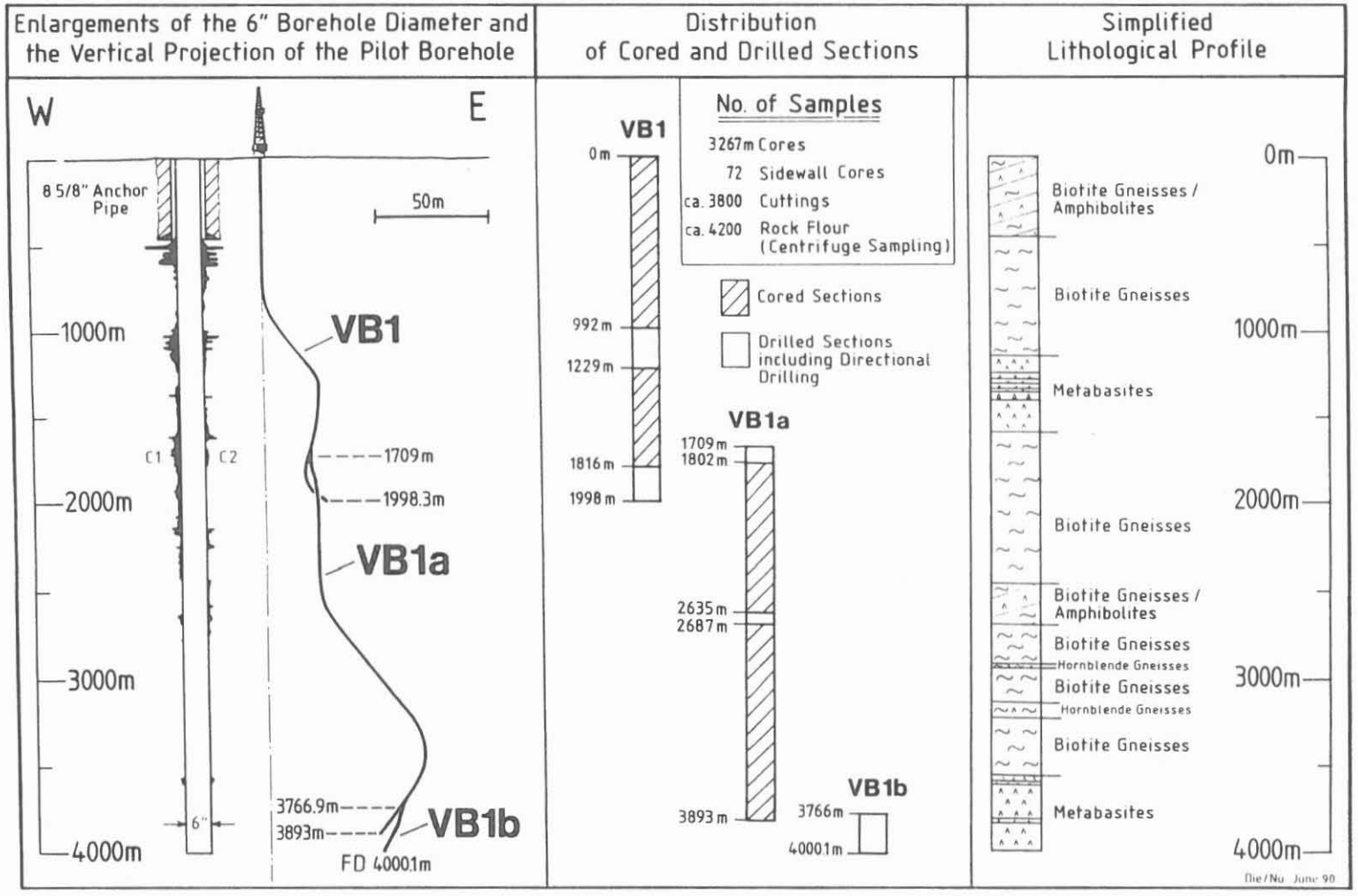

Fig. A.2.5: Borehole trajectory, sample distribution and lithological profile of the KTB pilot hole

of 4000.1 m. This depth was reached on April 4, 1989.

An extensive logging and testing program has been carried out in order to complete the data. In the wireline coring section 4 intermediate logging series and a final borehole measuring program were run (e.g. DRAXLER, 1990; DRAXLER & HÄNEL, 1988; HÄNEL, 1989). During the drilling activities and the following geophysical logging and testing program the hole was left uncased from 480.0 m to the actual depth respectively to the final depth of 4000,1 m (Fig. A.2.1). All activities in the hole are given on the drilling progress curve (Fig. A.2.6).

Before the final hydraulic test of the lowest 150 m a 5 1/2"/5" casing was run to a depth of 3850 m and cemented up to about 3650 m.

Figure A.2.7 presents an overview of the actual situation of the pilot hole KTB OBERPFALZ VB 1b with the mounted wellhead which was installed on April, 13 1990.

A.3 Samples

For scientific investigations there are different types of samples available:

- solids (cores, side wall cores,cuttings, rock flour)
- drilling mud, fluid from fluid samplers
- gases dissolved in the drilling mud

Cuttings from the shakers, rock flour from the centrifuge as well as drilling mud samples from the flowline were generally taken at 1.0 m intervals. During directional drilling phases cuttings were taken every 0.5 m. The quantity of all samples are listed in Table A.3.1 and Tab. A.3.2. Furthermore, a bit basket was used during the drilling of the borehole section VB 1b in order to sample lost bit material an coarser grained cuttings. A summary of that bit basket sampling is given by SIGMUND & DIETRICH (1990) and is shown in Figs. A.3.1 - A.3.4.

For gas analyses a gas trap, installed in the possum belly of the drilling rig, was directly connected with the gas mass spectrometer in the field laboratory (Fig. A.3.5). This way the dissolved gases in the drilling mud were analysed on line over the complete depth of the well.

The depth correlation of cuttings, rock flour, mud and gas samples was made by calculation of the lag time. This is the time samples take to be transported from the bottom to the surface by the drilling fluid.

The depths given on the cores always refer to the driller's depth. This causes a difference between the core depth and the logger's depth.

To get the orientation of cores of the metamorphic rocks in the KTB pilot well two different methods have been applied

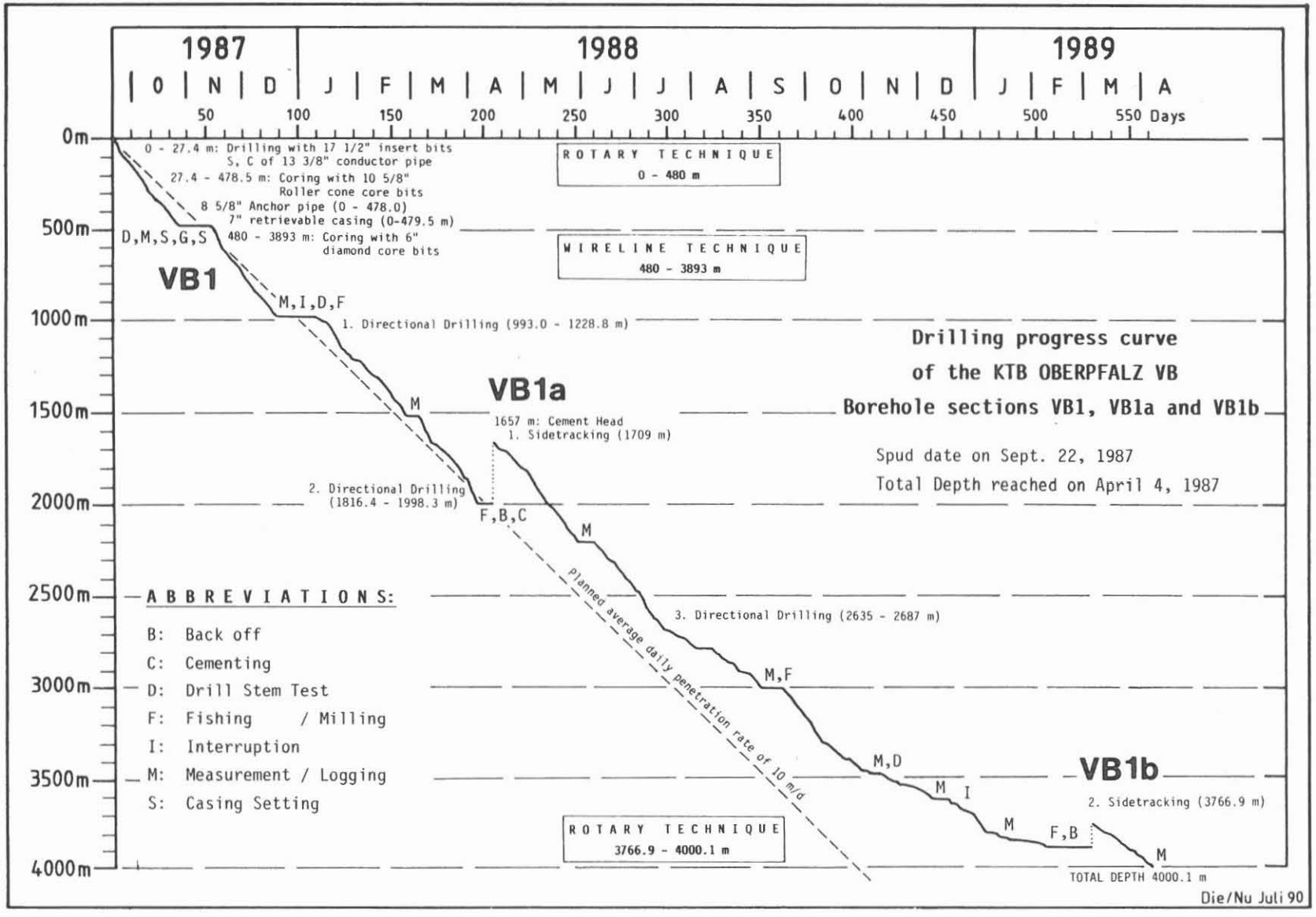

Fig. A.2.6: Drilling progress curve of the KTB pilot hole

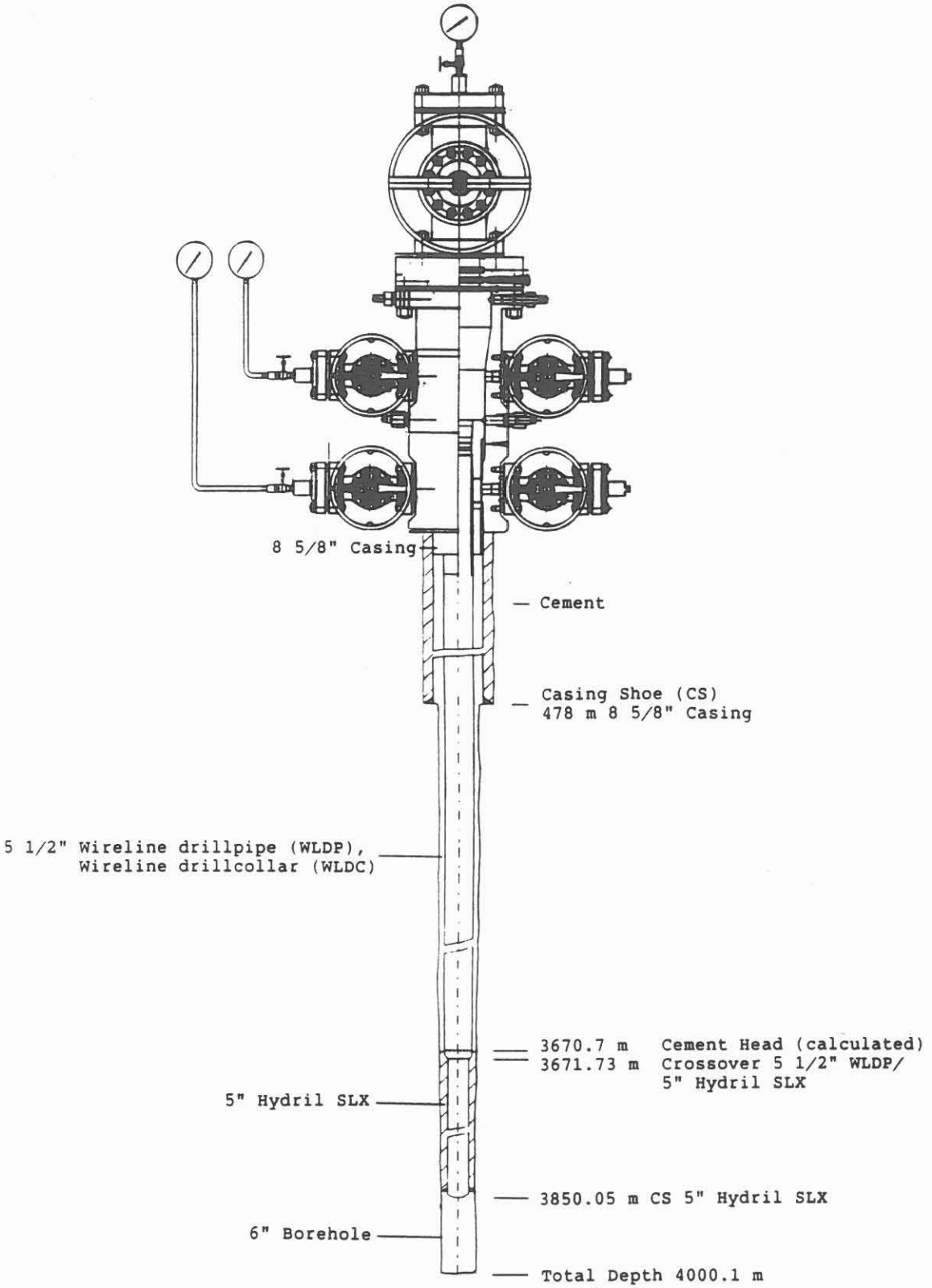

Fig. A.2.7: Well head end-flange of the KTB pilot hole (compiled by Jatho, 05.90)

Year Month	No. of core runs	Corelength (m)	Core Recovery m	%	Core Loss m	%	Type of Core bit
VB 1							
09.87	16	113.2	13.65	12.0	99.55	88.0	10 5/8" RCCB and
10.87	57	337.2	179.28	53.2	157.92	46.8	10 5/8" DCB
11.87	78	275.8	273.79	99.3	2.01	0.7	
12.87	101	236.2	234.77	99.4	1.43	0.6	"
01.88	2	6.5	6.40	98.5	0.10	1.5	"
02.88	65	300.1	295.67	98.5	4.43	1.5	"
03.88	89	287.0	281.46	98.1	5.54	1.9	"
Total	408	1556.0	1285.02	82.6	270.98	17.4	9 RCCB 30 DCB
VB 1a							
04.88	1	4.8	4.5	93.8	0.3	6.2	6" DCB
05.88	102	393.8	376.27	95.6	17.53	4.4	"
06.88	95	284.8	278.41	97.8	6.39	2.2	"
07.88	67	246.7	241.25	97.8	5.45	2.2	"
08.88	52	174.5	170.40	97.7	4.10	2.3	"
09.88	56	238.8	233.40	97.7	5.40	2.3	"
10.88	69	278.9	277.85	99.6	1.05	0.4	"
11.88	25	102.4	96.60	94.3	5.80	5.7	"
12.88	45	189.8	188.70	99.4	1.10	0.6	"
01.89	31	101.8	97.89	96.2	3.91	3.8	"
02.89	5	20.7	17.30	83.6	3.40	16.4	"
Total	548	2037.0	1982.57	97.3	54.43	2.7	42 DCB
VB 1b 03.-04.89	no coring activities		----	----	----	----	----
Grand Total	**956**	**3593.0**	**3267.59**	**90.9**	**325.41**	**9.1**	9 RCCB 72 DCB

RCCB: Roller Cone Core Bit, DCB: Diamond Core Bit

Tab. A.3.1: Monthly core balance of the KTB pilot hole

Month/ Year	Interval (m)	Number of Samples: Wet Samples Shakers	Wet Samples Centrifuge	Dry Samples Shakers	Dry Samples Fine	Dry Samples Coarse	Mud Samples	Special Samples	Remarks
09.87	VB 1 4- 114.5	141	-	121	121	141	95	-	86.5 - 1231.5 m: cuttings every 0.5 m (samples from shaker)
10.87	115- 478.5	727	284	308	355	355	318	-	
11.87	481- 758.0	Interval 72	271 Interv. 19	-	-	-	272	-	
12.87	759- 992	Interval 44	235	-	-	-	233	51	
01.88	944-1229	462	228	243	231	231	230	-	
02.88	1230-1529	344	292	268	293	292	306	62	1287.5 - 1343 m,
03.88	1529-1927	504	402	380	377	377	396	68	1355.5 - 1393.5 m and 1816.5 - 1998.5 m: cuttings every 0.5 m
04.88	1927-1998	85	71	71	71	71	72		
	VB 1a								
04.88	1677.5-1806	244	128	117	135	136	125	13	1677.5 - 1805.0 m: cuttings every 0.5 m
05.88	1807-2200	348	387	391	416	391	392	51	
06.88	2201-2485	273	274	275	276	275	282	74	
07.88	2468-2784	332	287	278	299	282	289	54	2635.0 - 2684.0 m: cuttings every 0.5 m
08.88	2785 - 2959	168	173	175	174	175	174	45	
09.88	2960 - 3198	238	238	233	236	237	238	42	
10.88	3199 - 3478	272	279	257	274	267	278	2	
11.88	3479 - 3580	99	99	96	96	99	99	-	
12.88	3580 - 3772	187	186	185	187	187	192	1	
01.89	3773 - 3872	96	95	92	95	96	96		
02.89	3873 - 3893	21	21	21	21	21	21		
	VB 1b								
03.89	3767 - 3976	407	220	210	209	209	210	2	3767.0 - 4000.0 m: cuttings every 0.5 m
04.89	3976 - 4000	47	24	24	24	24	24		
Total	0 - 4000	5111	4213	3745	3893	3866	4342	465	Grand Total: 25.635 Samples

Tab. A.3.2: List of samples from the KTB pilot hole

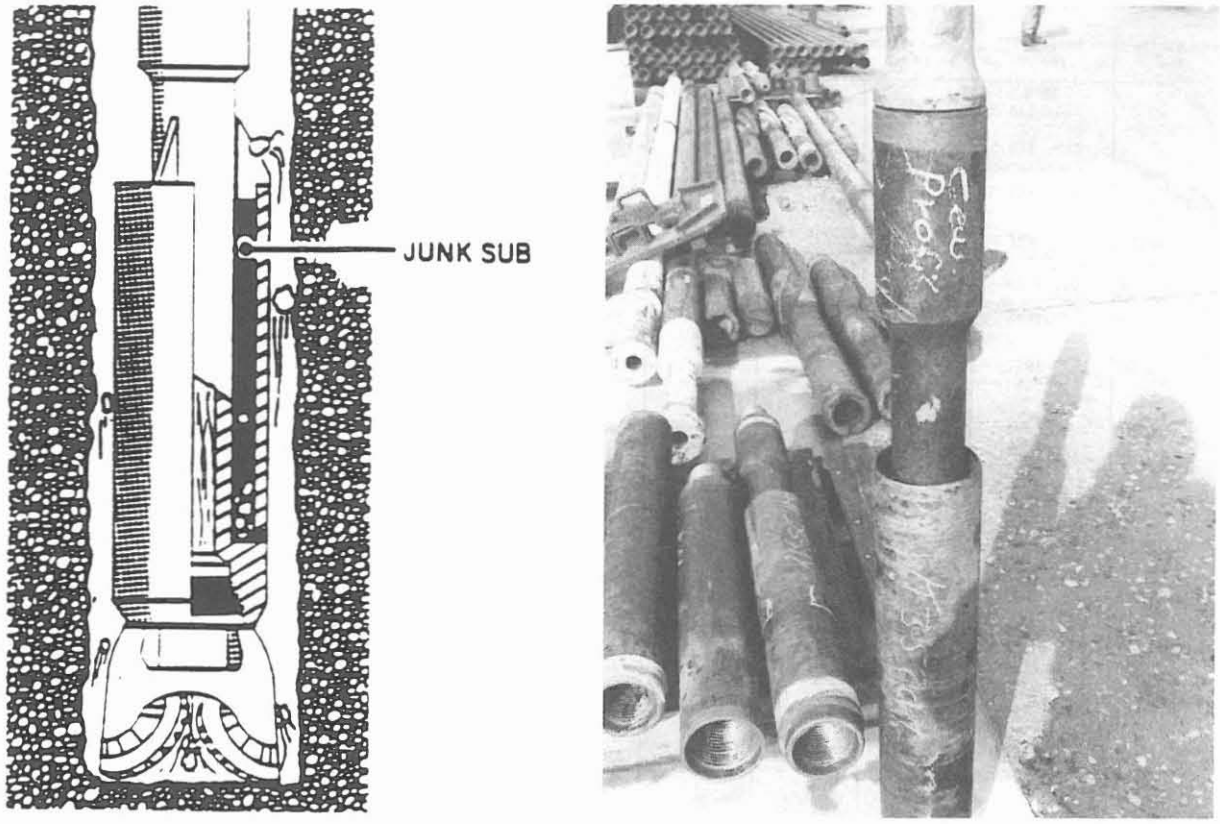

Fig. A.3.1: Sketch (left after Whittaker, 1985) and photograph (right) of used bit basket

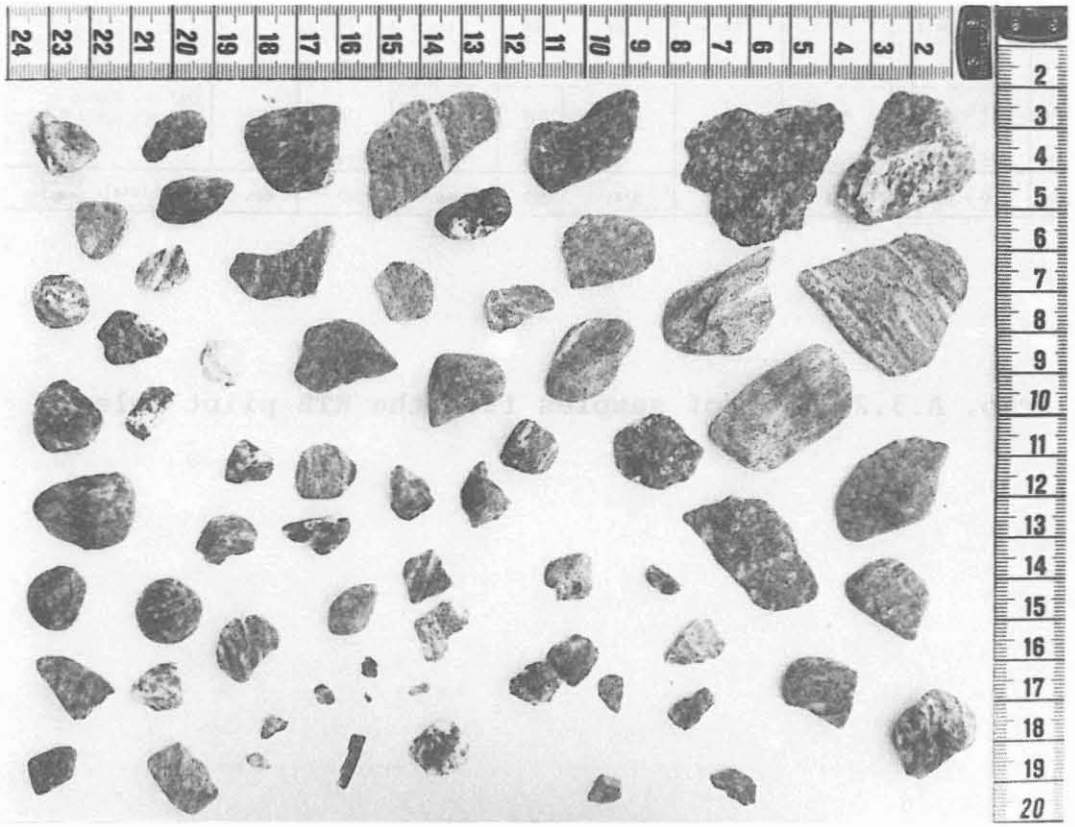

Fig. A.3.2: Sample from bit basket KTB VB 1b 3832.1 - 3843.6m

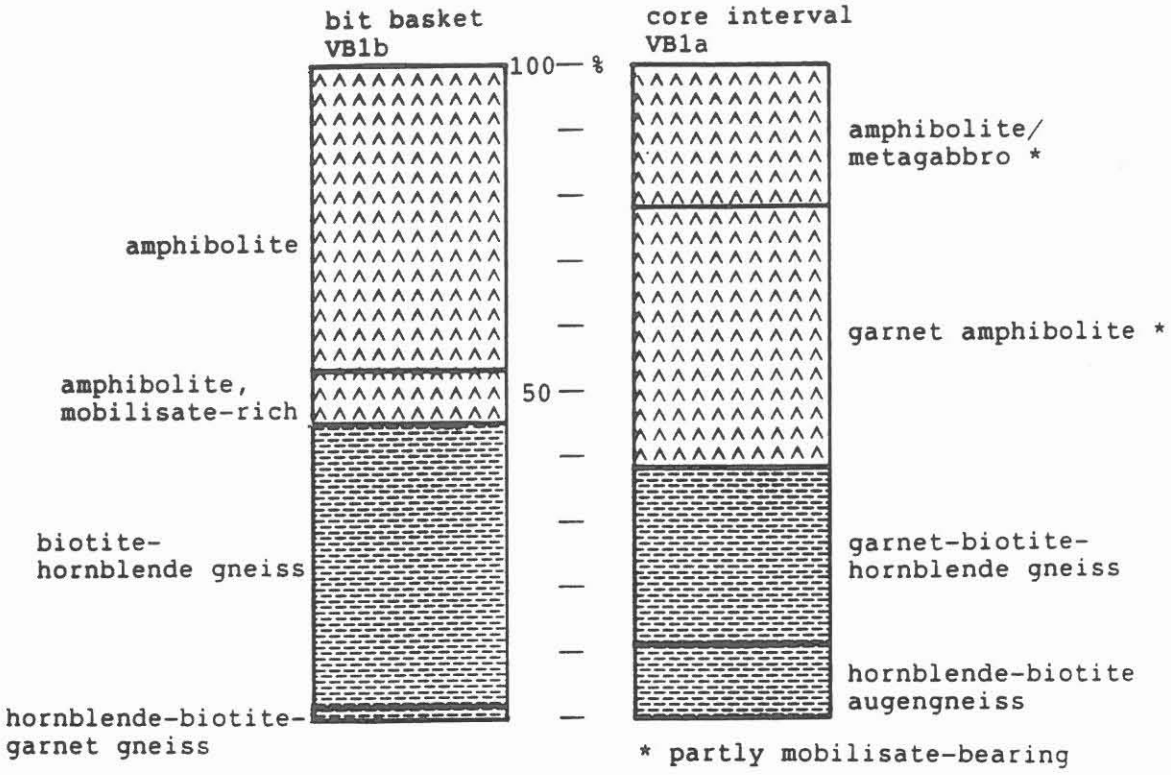

Fig. A.3.3: Lithological comparison of core interval between 3832.1 - 3843.6 m in VB 1a and sample from bit basket collected during drilling the same depth interval in VB 1b in per cent.

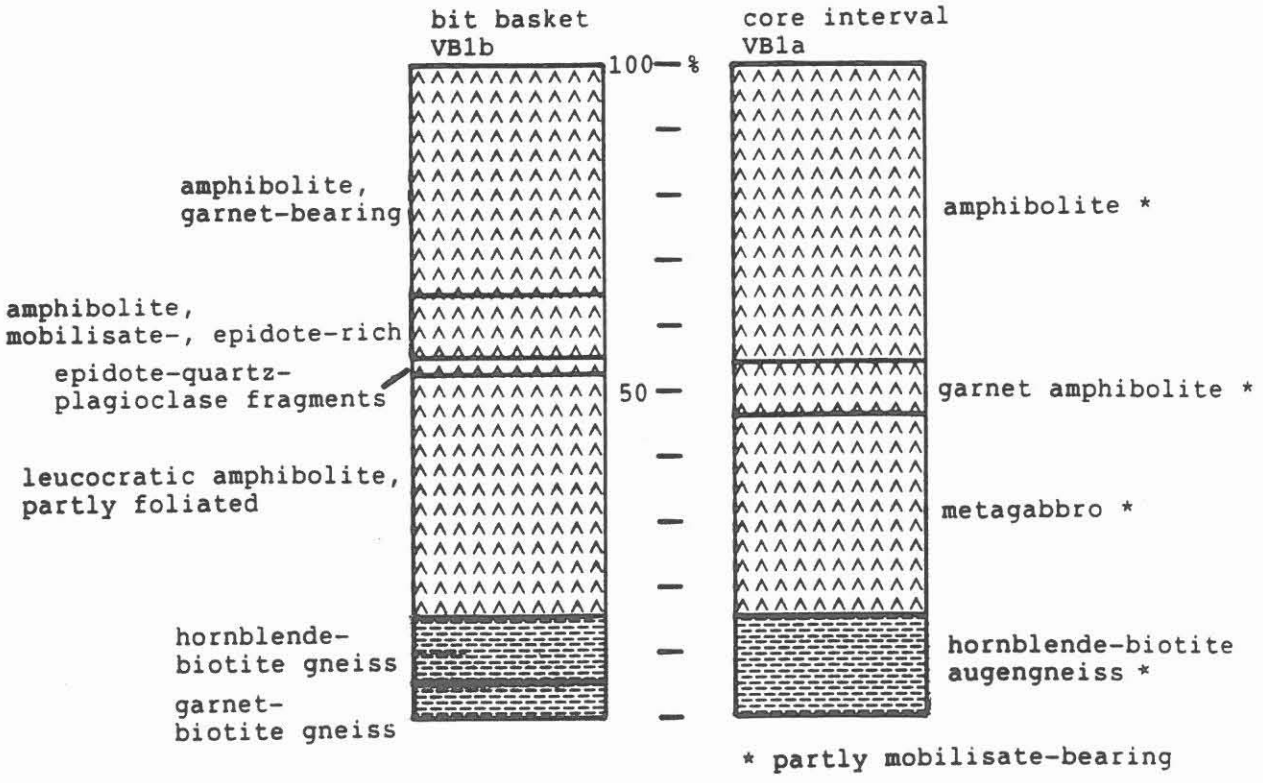

Fig. A.3.4: Lithological comparison of core interval between 3843.6 - 3855.8 m VB 1a and sample from bit basket collected during drilling the same depth interval in VB 1b in per cent.

successfully (SCHMITZ et al., 1989). The direct method gives fast information for only single depth ranges whereas continuous orientation data of nearly the whole core material becomes available by the indirect method.

A.4 Mud Logging

In addition to the parameters measured in the field laboratory an important source of information for the interpretation of the measured data is the mud logging, which continuously measures drilling fluid parameters (see Fig. A.3.5) and technical parameters. The most important parameters listed in Tab. A.4.1.

Tab. A.4.1: Mud Logging Parameters

Drilling Parameters	Mud Parameters
rate of penetration	mud flow
depth	density
weight on bit	pH
rotary speed of drill string	redox
torque	conductivity
pump strokes	temperatur
standpipe pressure	pit levels
block velocity	total hydrocarbons
cable wear	$C_1 - C_5$
torque	H_2S
overshot depth	
cable velocity	
cable tension	
annules pressure	
choke manifold pressure	

All data are depth corrected. The recording interval is 20 cm.

The total rig time of 560 days with an average daily penetration of 7.14 m includes all coring, drilling, measuring and cementation as well as tests and fishing activities. A share of 13.4 % of the total time was spent for measurements and tests. 33.5 % of the time were needed for coring and drilling operations including directional drilling and sidetracking. 36.1 % were needed for pulling and running the drillpipes including tripping core barrel and changing bits (Tab. A.4.2 and Fig. A.4.1).

This evaluation of the rig time shows (RISCHMÜLLER, 1989) that, despite the good results of bit life, ROP, and the excellent core recovery of 98%, there is potential and need for furher improvement of drilling technology (1) directional drilling and fishing can be avoided by using a straight hole drilling technology and (2) the time for tripping the drill string and the core barrel can be reduced.

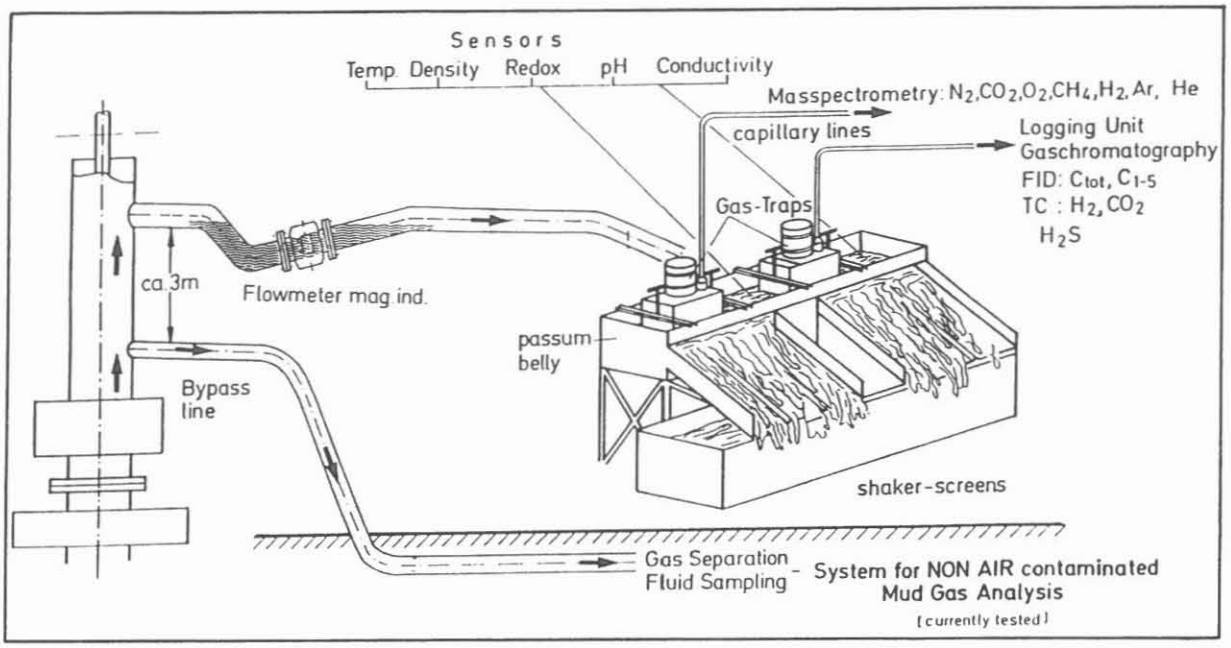

Fig. A.3.5: Mud flowout measuring technology for KTB pilot hole (after Chur et al., 1989)

Tab. A.4.2: Well databank of KTB pilot hole (total depth (TD) = 4000.1 m)

Well name: KTB Oberpfalz VB

Spud date: 22.09.87
TD reached: 04.04.89
Total days: 560

Kind of work	h	%
Coring / Drilling	2633	19.6
Directional Drilling / Sidetracking	1406	10.5
Circulating / Reaming	460	3.4
Measuring + Testing	1800	13.4
Tripping Core Barrel	2116	15.7
Roundtripping	2735	20.4
Reparing	607	4.5
Fishing	893	6.6
Miscellaneous	790	5.9
Grand Total	**13440**	**100**

	PLANNED	REACHED
BIT LIFE (DCS) (m)	20	48
AVERAGE CORE LENGTH (m)	4	3.5
AVERAGE ROP (m/h)	1.5	1,68
TRIPPING DRILLSTRING (h/1000 m)	3	4.5
TRIPPING WL-CORE-BARREL (h/1000 m)	1.15	0.95
CORE RECOVERY (%)	85	98

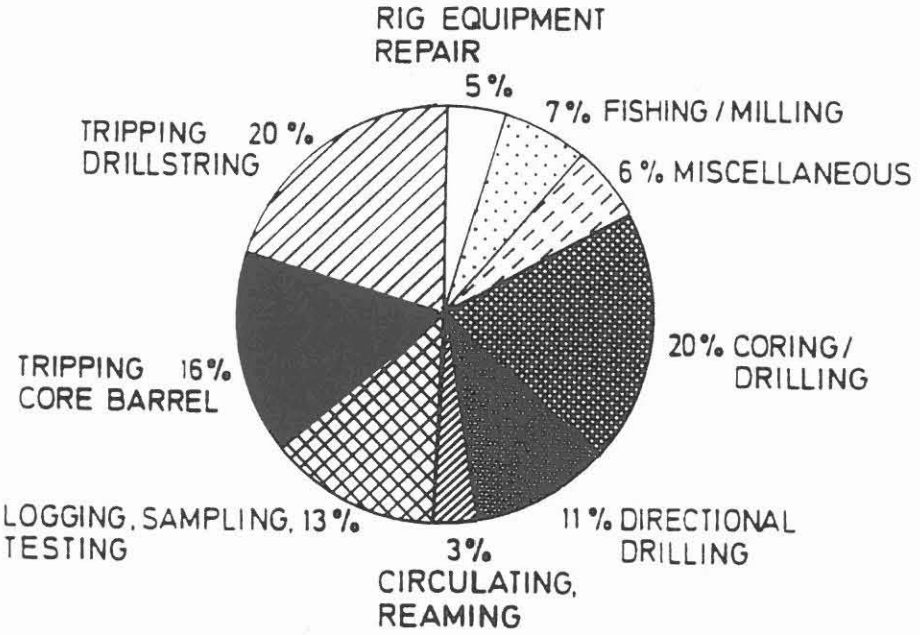

Fig. A.4.1: Rig time break down and performance data of the KTB pilot hole (after Rischmüller, 1989).

A.5 References

CHUR, C., ENGESER, B. & WOHLGEMUTH, L. (1989): KTB Pilot Hole - Results and Experiences of One Year Operation - OIL GAS - European Magazine, 1,89, pp 14 - 19.

DRAXLER, J.K. (1990): Grundlagenforschung und Bohrlochgeophysik (Bericht 8). Bohrlochmessungen in der KTB Oberpfalz VB (Intervall 3009.7 - 4000.1 m), KTB-Report 90-1, Projektleitung KTB im NLfB, Hannover.

DRAXLER, J.K. & HÄNEL, R. (1988): Grundlagenforschung und Bohrlochgeophysik (Bericht 5). Bohrlochmessungen in der KTB Oberpfalz VB (Intervall 1529.4 - 3009.7 m), KTB-Report 88-7, Projektleitung im NLfB, Hannover.

EMMERMANN, R. (1989): The KTB Pilot Hole: Tectonic Setting, Technical Data and First Results. - In: EMMERMANN, R. and J. WOHLENBERG (eds.) The German Continental Deep Drilling Program - (Exploration of the Deep Continental Crust) - Site-selection Studies in the Oberpfalz and Schwarzwald. Springer, Berlin Heidelberg New York London Paris Tokyo Hong Kong, pp 527 - 553

HÄNEL, R. (1989): Grundlagenforschung und Bohrlochgeophysik (Bericht 7). Auswertung von Bohrlochmessungen der KTB Oberpfalz VB, KTB-Report 89-1, Projektleitung im NLfB, Hannover.

RISCHMÜLLER, H. (1989): The German Continental Deep Drilling Project - An Overview -. Paper presented at the 28th International Geological Congress, Washington, D.C., USA.

SCHMITZ, D., HIRSCHMANN, G., KESSELS, W., KOHL, J., RÖHR, C. & DIETRICH, H.-G. (1989): Core Orientation in the KTB Pilot Well. Scientific Drilling, 1, pp 150 - 155.

KTB-Report	90-8	B1 - B55	65 Fig.	Hannover 1990

GERMAN CONTINENTAL DEEP DRILLING PROGRAM (KTB) - GEOLOGICAL SURVEY OF THE PILOT HOLE "KTB OBERPFALZ VB"

by

C. Röhr, J. Kohl, W. Hacker, S. Keyssner, H. Müller*, J. Sigmund, A. Stroh, G. Zulauf**

KTB Feldlabor
D-8486 Windischeschenbach
Federal Republic of Germany

---

* present address:
Mineralogisch-petrographisches Institut
Albert-Ludwigs-Universität
Albertstraße 23b
D-7800 Freiburg i. Br.
Federal Republic of Germany

** Geologisch-Paläontologisches Institut
Johann Wolfgang Goethe-Universität
Senckenberg-Anlage 30
D-6000 Frankfurt/Main
Federal Republic of Germany

CONTENTS

ABSTRACT

The KTB pilot hole was drilled through the tectono-metamorphic unit of the Zone of Erbendorf-Vohenstrauss (ZEV) at the western margin of the Bohemian Massif (Central Europe) to a depth of 4000 m.

The drilled crust is built up by the following rock sequences:
- monotonous garnet-Al_2SiO_5-biotite gneisses
- metabasic sequences of amphibolites and meta-gabbros
- interlayering of amphibolites, muscovite - biotite gneisses, biotite-hornblende gneisses and calcsilicate rocks

Gneisses comprise about 70%, metabasites about 30% of the volume. The rocks underwent polyphase metamorphism. An early stage of high-pressure metamorphism ($p > 10$ kbar, T around 700 °C) is documented by parageneses and mineral compositions locally preserved in metabasites. Pervasive re-equalibration has taken place under amphibolite facies conditions ($p = 7\pm1$ kbar, $T = 675\pm50$ °C), which are reflected by the bulk of the metabasites and paragneisses. Later partial retrogression under greenschist facies and lower T conditions is pervasive. It has gone to completion in places. Mineralized fissures and cataclasites indicate significant activity of fluids during the late stage evolution.

The foliation of the gneisses dips steeply to SSW down to 3000 m turning towards the E in the deeper part of the section. This structure is interpreted as a large scale open fold with subhorizontal axial plane. The axis plunges gently towards SSE. It formed late, at temperatures below about 500 °C.

A NE-SW trending fault system has caused several stages of cataclasis with conspicuous graphite mineralization. The maximum principle stress direction has rotated from NE to N during compression in the brittle field. During the subsequent late stage of crustal extension the minimum principle stress direction is about E.

Ore mineralizations are generally sparse and of secondary origin, local enrichments correlate with zones of pronounced alteration. The predominant ore minerals pyrite and pyrrhotite and to a lesser extend base metal sulphides are present throughout the section. Pyrrhotite causes most of the magnetic anomalies. Oxides (ilmenite, rutile, and minor magnetite) dominate in the metabasic and meta-ultramafic rocks.

Open fissures containing brines and mineralized with quartz and calcite have been drilled at depths below 3447 m. Near epidote-rich fissures below 3800 m pyrite is replaced by oxidic ore minerals (magnetite, hematite, goethite, and ilvaite).

B.1 INTRODUCTION

The Continental Deep Drilling Program of the Federal Republic of Germany (KTB) started the pilot hole in September 1987. It reached a final depth of 4000.1 m in April 1989. Core recovery is a total of 3268 m. The main hole will be started in September 1990. It is planned to reach a depth of 10,000 m by the end of 1994.

The drilling site is situated in Eastern Bavaria (Oberpfalz), about 200 km NNE of Munich (Figs. B.1.1, B.1.2), in the exposed basement rocks of the Bohemian Massif, close to its western margin.

B.1.1 Geological Setting

The western part of the Bohemian massif in NE-Bavaria can be subdivided into three Variscan tectono-metamorphic units (Fig. B.1.1): Saxothuringian, Moldanubian and the Zone of Erbendorf-Vohenstrauss. To the west of the NW-SE trending Franconian Line fault system, these crystalline basement rocks are overlain by permo-mesozoic sediments. (Weber and Vollbrecht 1989, Franke 1989):

The Saxothuringian of the Fichtelgebirge consists of Palaeozoic metasediments and mafic and felsic metavolcanic rocks that have suffered a low to medium grade metamorphism at shallow crustal depth. The peak temperatures increase from below 350 °C in the north to more than 600 °C in the south, at the adjacent Moldanubian. The "Zone of Tirschenreuth-Mähring" (ZTM, Schreyer 1966, Stettner 1979, Weber and Vollbrecht 1989) is interpreted as a high temperature shear belt. The age of the low pressure metamorphism was determined to be 320 Ma (Teufel 1988, Kreuzer et al. 1989).

The Moldanubian consists of a presumably Late Proterozoic to Paleozoic, monotonous, metasedimentary sequence with some intercalated variegated units. It has a polymetamorphic history. Eclogites and associated gneisses reflect an evolution from high to low pressures (Blümel 1983, O'Brien 1989). Small kyanite and garnet inclusions in plagioclases of paragneisses document a former equilibration at intermediate pressures (Blümel 1983). The dominating parageneses with cordierite, K-feldspar and sillimanite reflect a late stage of high temperatures at shallow depth dated as about 320 Ma (Teufel 1988, Kreuzer et al. 1989).

The Zone of Erbendorf-Vohenstrauss (ZEV) has formed from a probably Late Proterozoic to Palaeozoic sequence, transformed to paragneisses, amphibolites, calcsilicate rocks, orthogneisses and metagabbros. The dominating intermediate pressure amphibolite facies overprint has taken place about 380 Ma ago. (Teufel 1988, Kreuzer et al. 1989). An earlier metamorphism at higher pressures is locally well documented

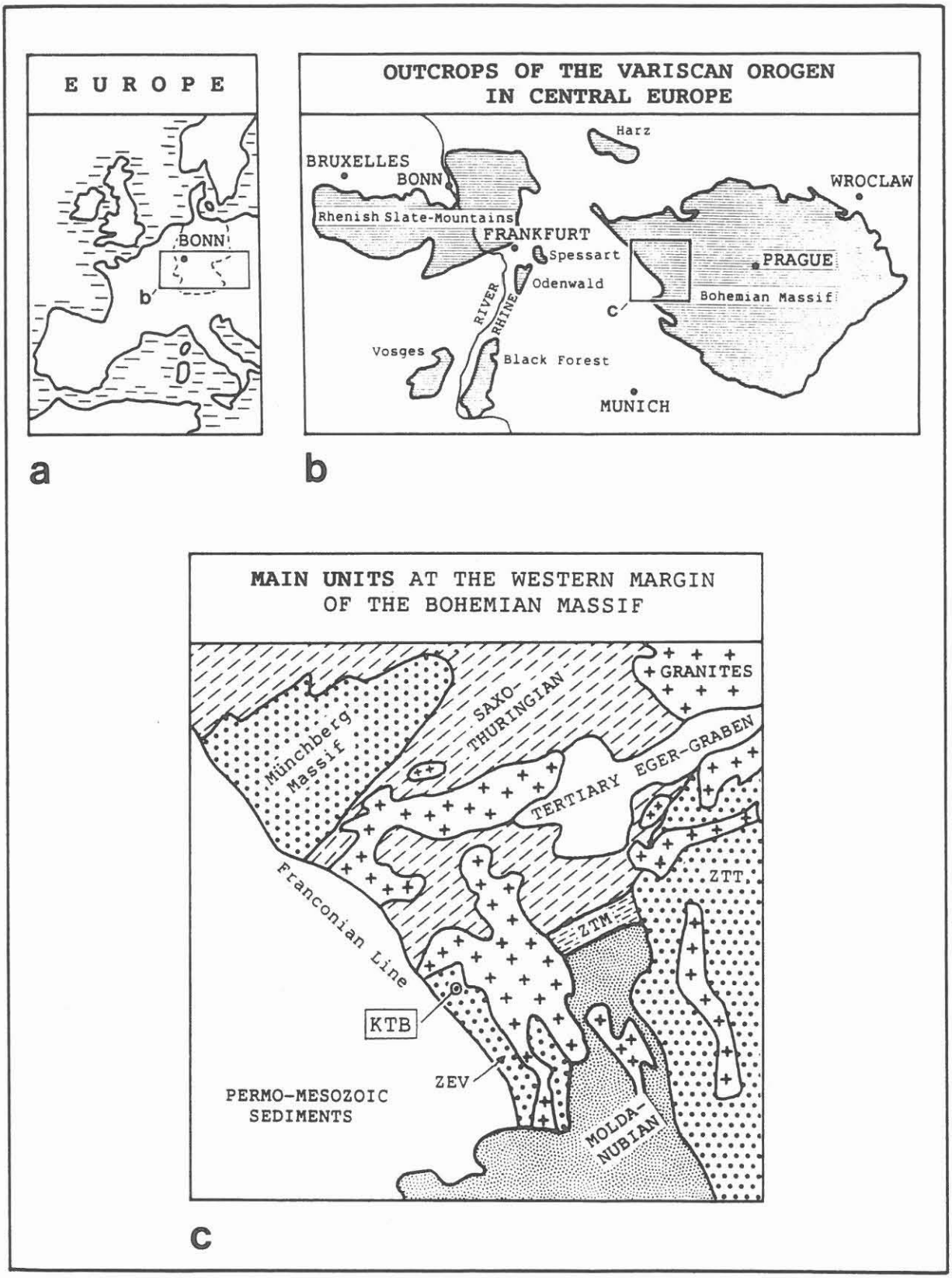

Fig. B.1.1: Geographical and geological sitiuation: a) Europe, b) outcrops of the Variscan orogen in Central Europe and c) the Western Margin of the Bohemian Massif. KTB = drill site, ZEV = Zone of Erbendorf - Vohenstrauss, ZTM = Zone of Tirschenreuth - Mähring, ZTT = Zone of Tepl - Taus.

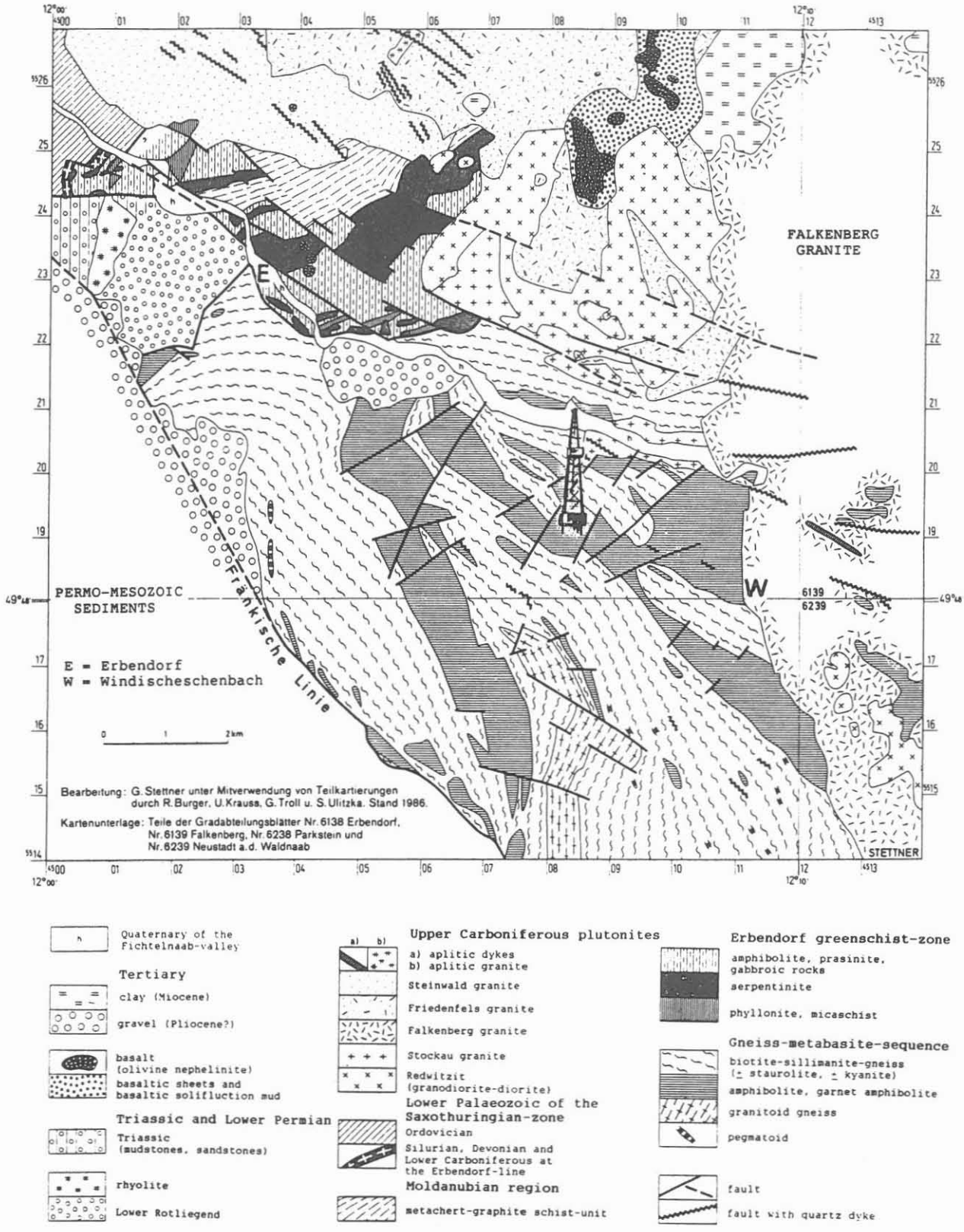

Fig. B.1.2: Geological map of the KTB drilling location, after Stettner in Weber and Vollbrecht (1986).

in metabasites. The ZEV has been interpreted to be part of a large nappe complex covering the Moldanubian and Saxothuringian boundary (Weber and Vollbrecht 1986, 1989). This complex is characterized by the high amount of metabasites and the 380 Ma old intermediate pressure type metamorphism. Other units attributed to this nappe complex are the Münchberg Massif and the Zone of Tepla-Domazlice (= Zone of Tepl-Taus, ZTT). The metabasites of the different units show significant differences in their geochemical character (Okrusch et al. 1989).

The drilling site is situated in the northwestern part of the ZEV, about 3 km NW of the small town of Windischeschenbach. The detailed geological map by Stettner (Fig. B.1.2) shows apophyses of the Falkenberg granite, which covers a greater area to the east, in close vicinity to the drill site. To the north, the ZEV is bordered and underlain by the south-dipping "Erbendorf Greenschist Zone", which consists of amphibolites, metagabbros, greenschists, serpentinites and minor metasediments and the "Wetzldorf Unit", which consists of metalydites, quartzites and phyllitic schists. These rocks are considered to be the lower part of the ZEV nappe complex. One major aspect of the project is to drill through the nappe complex to reach the inferred Saxothuringian/Moldanubian collision zone underneath.

B.1.2 Technical data, sampling

Corresponding to the applied drilling techniques the samples available for geological and geochemical investigations are drill cores (diameter: 94 mm), cuttings (grain size 0.1 - 10 mm) and drill flour ("centrifuge samples", 20 µm - 0.1 mm). Down to 1998 m the well is designated as VB1. Due to technical problems at 1998 m depth the lowermost part of the hole had to be abandoned. After back cementation and directional drilling a new hole (VB1a) was started from 1709 m downwards (cf. chapter A for more detailed information concerning drilling techniques and core recovery). A second kick off point is at 3766 m. From there down to 4000 m the hole is designated as VB1b. Cores from VB1a are available down to 3898 m.

For intervals represented only by cuttings and centrifuge samples, the geological profile had to be constructed from macroscopical and microscopical examination and analyses (chemical, X-ray diffraction) of this material combined with the geophysical borehole logging data. All recovered core material has been reconstructed to its original shape and length followed by itemization and labelling of every piece. Core sections that match together are marked by a straight line. This serves as a reference line for all orientation measurements at the core before the true geographic orientation of the core is reconstructed. Reorientation requires

either the evaluation of Formation Micro Scanner and Borehole Televiewer logs or, in the case of drilling with orientation marks, determination of the actual dip and orientation of the borehole. Mesoscopic structural analysis was done by measurement of cores or copied wrappings (Fig. B.1.3a). Petrographical and microstructural analysis of the samples is based on about 2500 thin sections and 500 polished sections. Furthermore, chemical and modal analyses were performed on these samples by X-Ray Fluorescense Spectrometry and quantitative X-Ray-Diffractometry. More details about these methods can be found in Schmitz et al. (1989) and in chapter A and C of this volume.

B.2 GEOLOGICAL SECTION OF THE PILOT HOLE

Four characteristic rock series are alternating (Fig. B.2.1):

(1) 0 to 460 m: variegated sequence of garnet amphibolites with calcsilicate layers, muscovite-biotite gneisses, biotite-hornblende gneisses and minor marble.

(2) 460 to 1160 m, 1610 to 2470 m and 2690 to 3575 m: monotonous garnet-bearing biotite gneisses with kyanite and/or sillimanite. These gneisses, mainly with compositions corresponding to greywacke, were intruded by some lamprophyric dykes.

(3) 1160 to 1610 m and 3575 to 4000 m: amphibolites, metagabbros and minor ultramafic rocks. The metabasites of basaltic composition show evidence of an early high-pressure metamorphism followed by the dominating amphibolite facies stage.

(4) 2470 to 2690 m: variegated sequence of biotite-hornblende gneisses with frequent interlayering of amphibolites, calcsilicate rocks and sillimanite-biotite gneisses. This sequence resembles (1).

Down to a depth of 1200 m the foliation of the gneisses dips steeply towards SSW. From 1800 - 2500 m it is nearly vertical, switching between SSW and NNE dip direction. Between 2500 and 3150 m the foliation changes gradually into a shallower dipping or subhorizontal position. The dip direction varies between SW and E at 3050 - 3300 m (Fig. B.2.2). This variation of dip is bound to mesoscopic folds as well as to graphite-bearing fault zones. At the depth of 3050 to 3300 m folding and thrusting as well as normal faulting cause a complex structural pattern (Fig. B.2.3b). The structure at the depth of 3000 to 3500 m is considered as the hinge of a large open fold with subhorizontal axial plane. The axis plunges gently to SSE (Fig. B.2.3a).

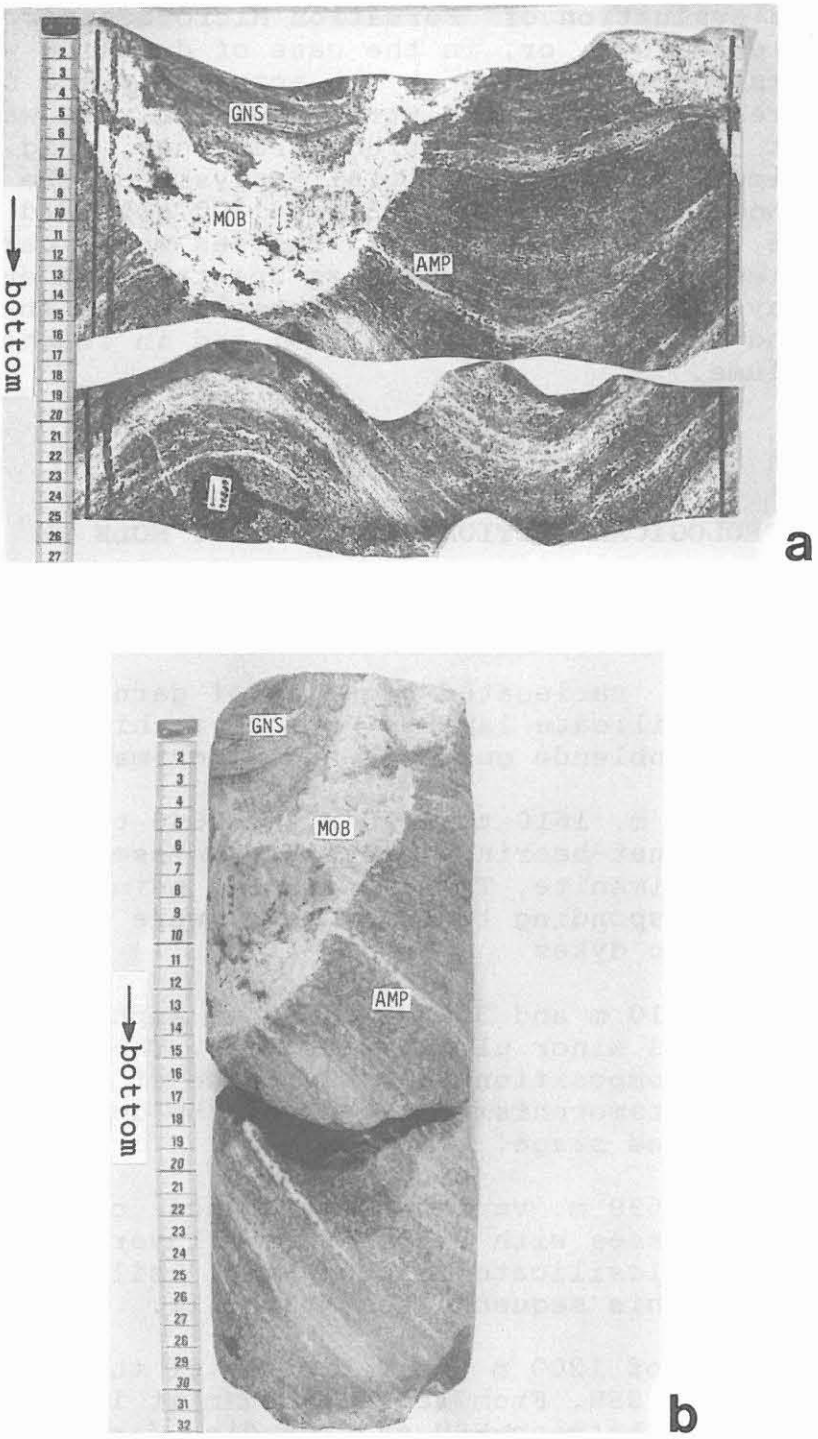

Fig. B.1.3: Unrolled cylinder mantle (a) and normal photograph (b) of two core pieces from 455 m. Discordant contact between garnet-biotite-gneiss (GNS) and amphibolite with calcsilicate layers (AMP), at the contact leucocratic mobilisate (MOB).

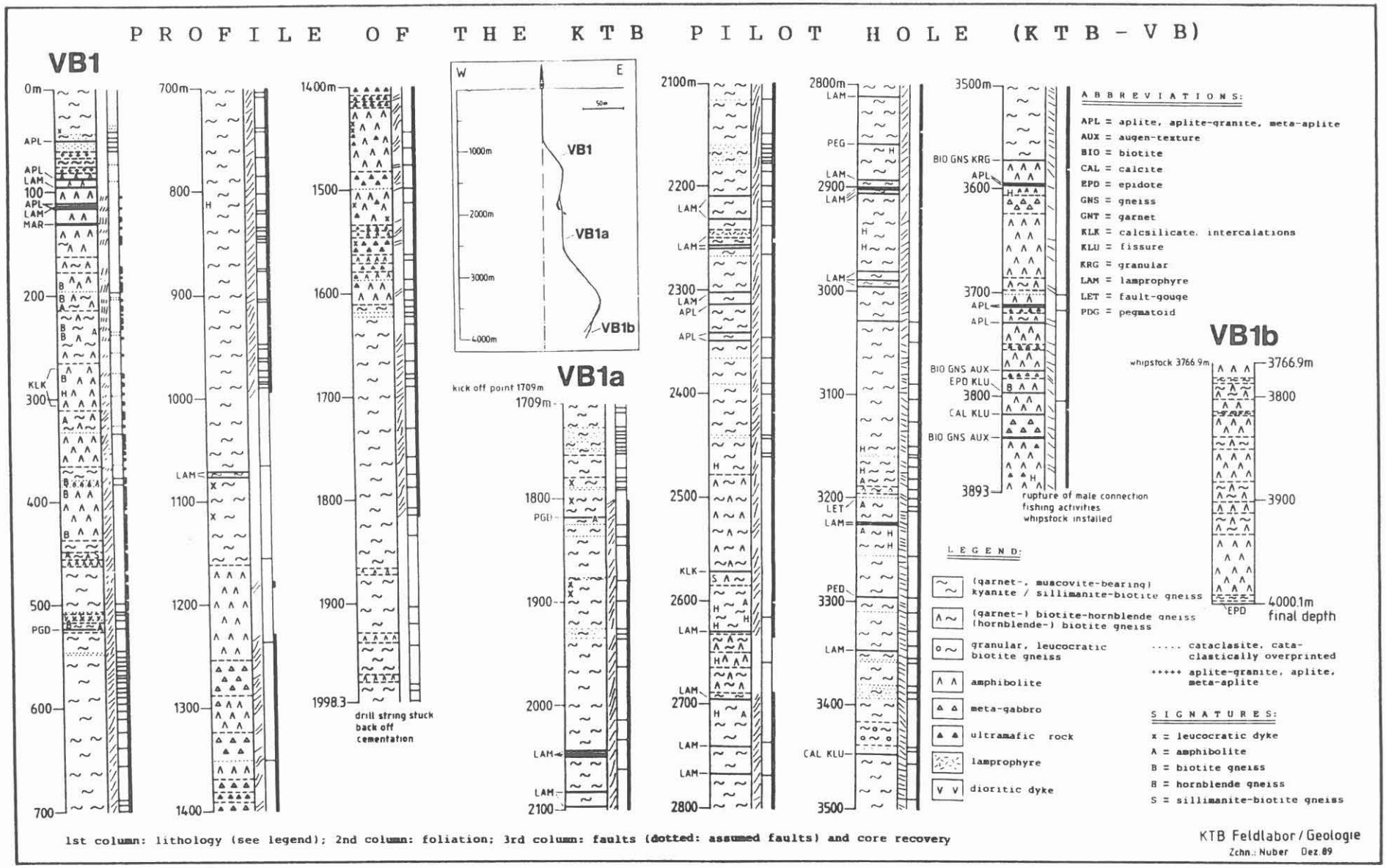

Fig. B.2.1: Geological section of the KTB pilot hole.

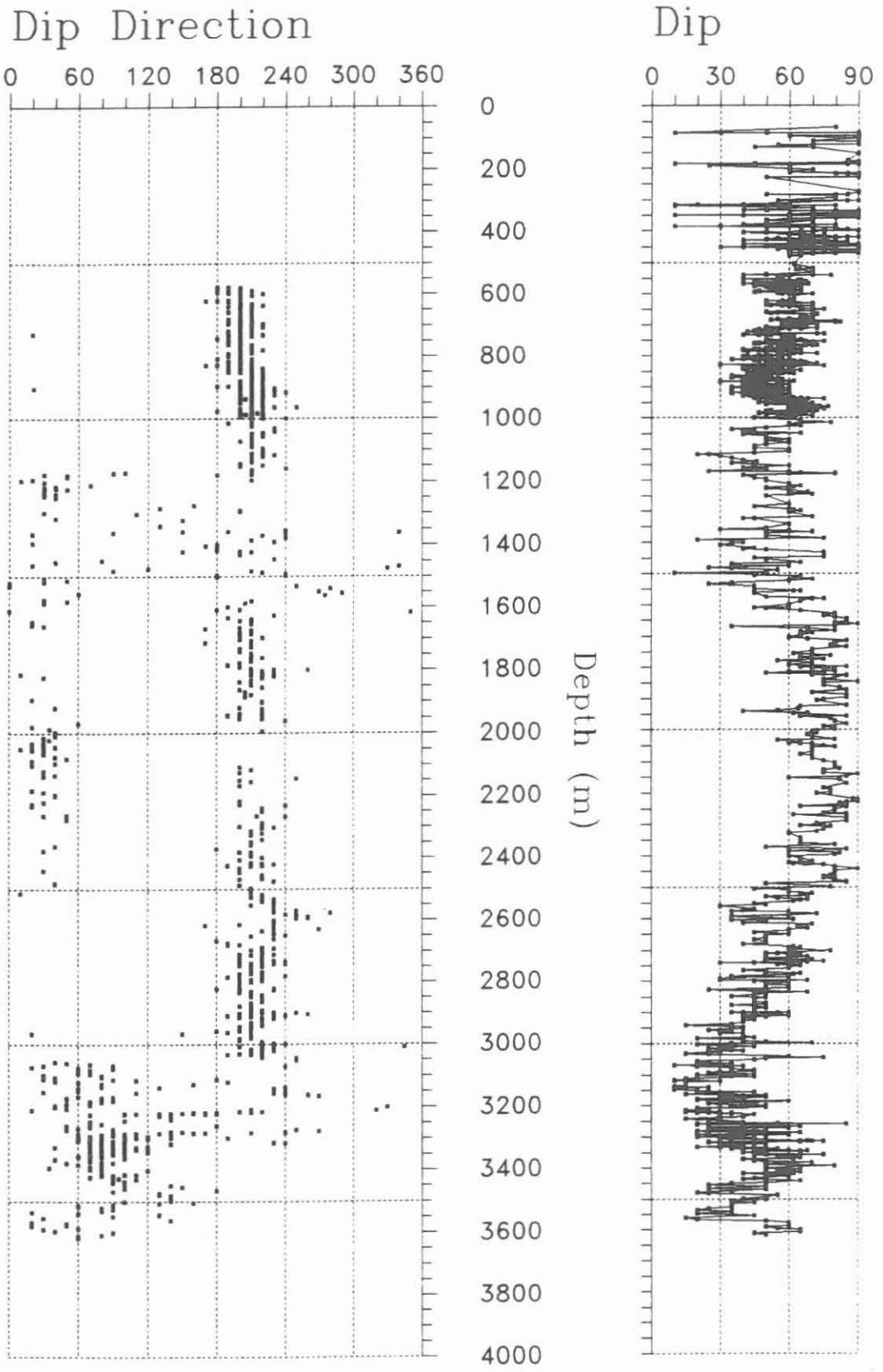

Fig. B.2.2: Dip and dip direction of the foliation.

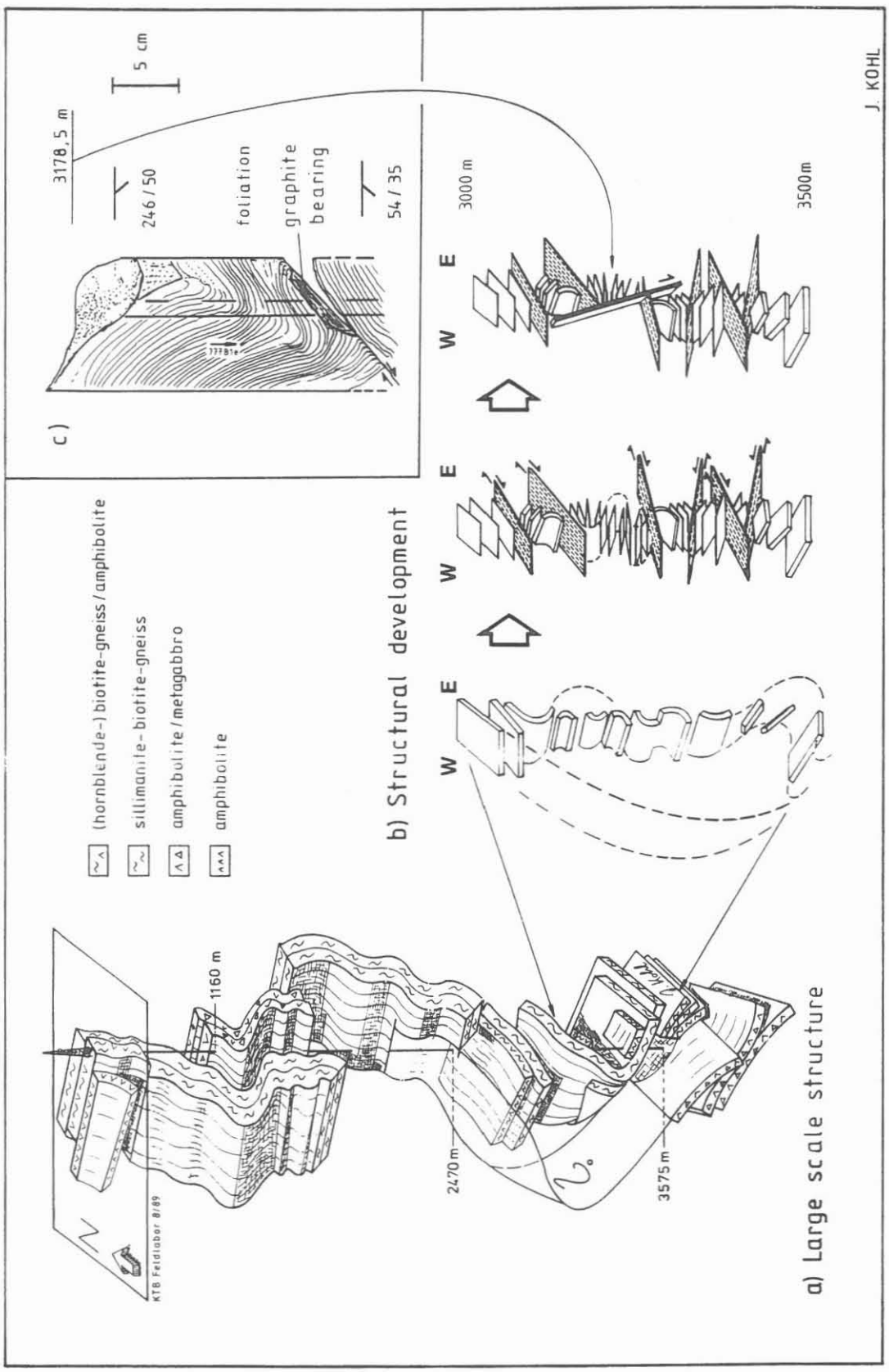

Fig. B.2.3: Schematic sketches of a) large scale structure, b) development of the interval 3000 - 3500 m during different stages of deformation and c) typical mesoscopic fold with reverse graphite-bearing fault.

The chlorite/(chlorite+biotite) ratio, applied as an alteration index, demonstrates the pervasive low-temperature alteration especially in the cataclastic zones 500 - 600 m and 1600 - 1800 m (Fig. B.2.4). The number of fractures per meter is generally decreasing with depth (Fig. B.2.5). The peak at 3580 m results from pronounced core disking at the lithological transition to the metabasites (cf. chapter G).

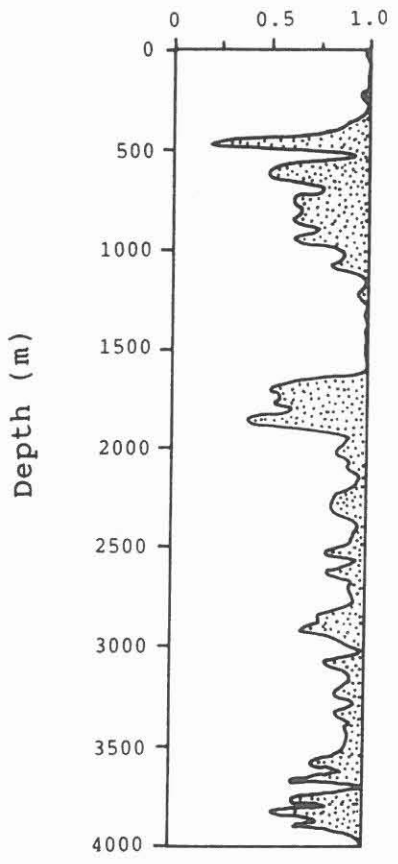

Fig. B.2.4: Plot of chlorite/(chlorite+biotite) versus depth. This parameter is used as an low-temperature alteration-index. Chloritization of hornblende and garnet is subordinate and can be ignored (averaged data from quantitative XRD).

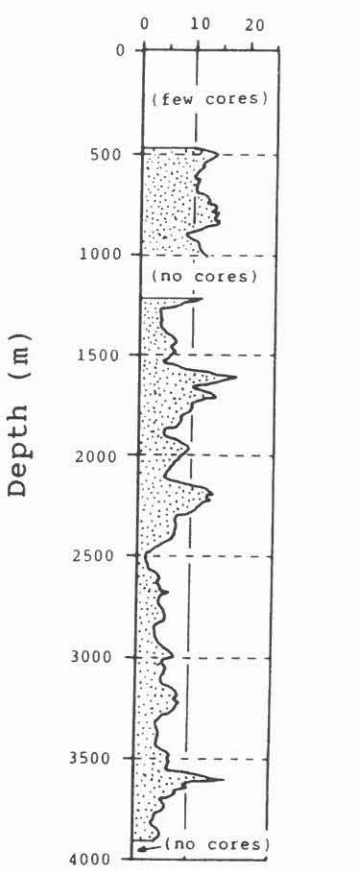

Fig. B.2.5: Averaged number of fractures per meter, measured at cores.

B.3 GNEISSES

B.3.1 Petrography

Garnet-Al_2SiO_5-muscovite-biotite gneisses:

Garnet-Al_2SiO_5-muscovite-biotite gneisses form three monotonous series with minor intercalations of biotite-rich, amphibole-bearing gneisses and calcsilicate rocks. Fabrics vary from fine grained and finely layered to medium grained with flaser texture and layer to lense shaped quartz-feldspar-mobilisates (cf. chapter B.7 for a more detailed discussion of the different structural types). From 500 to 625 m and 950 to 960 m migmatitic phenomena are obvious.

Garnet and muscovite contents are variable. Muscovite has preferably grown in the vicinity of quartz-feldspar-mobilisates, in regions of intense retrogression and often around Al_2SiO_5-minerals (Fig. B.3.1). Garnet cores are often rich in inclusions of quartz, plagioclase or rutile, whereas the rims are free of inclusions. At least two types of garnet occur in the same thin section: large hypidiomorphic grains and smaller embayed ones (Fig. B.3.2).

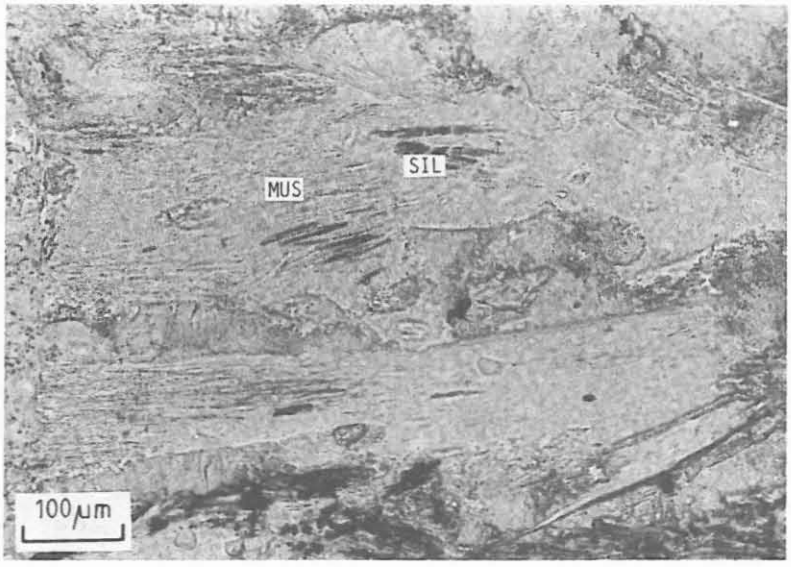

Fig. B. 3.1: Garnet-Al_2SiO_5-biotite gneiss. Relics of sillimanite (SIL) within muscovite (MUS). (Thin section CUT1006, 1006 m, // nicols).

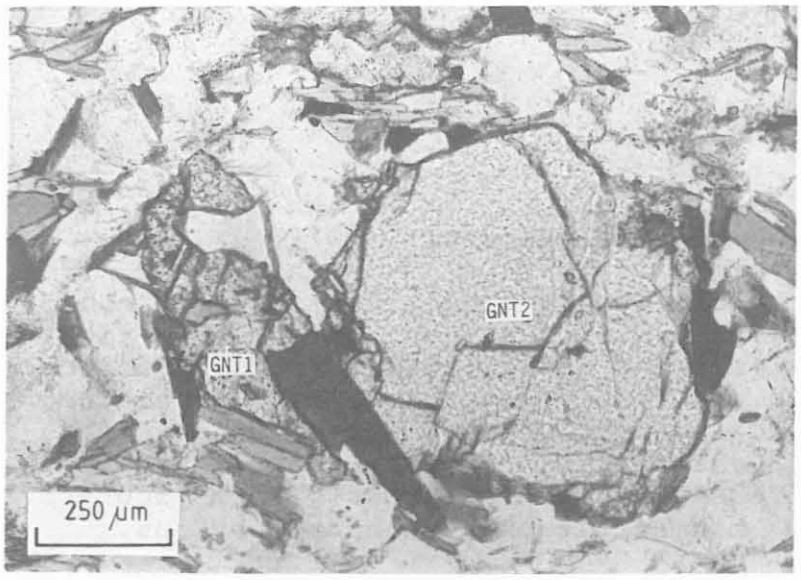

Fig. B.3.2: Garnet-kyanite-biotite gneiss with different garnet types: GNT 1 is small, embayed and rich in inclusions, whereas GNT 2 is roundish-subhedral with inclusions in the core.
(Thin section 71A4T, 420.2 m, // nicols).

Al_2SiO_5-minerals are ubiquitous. Fig. B.3.3 shows the distribution of Al_2SiO_5-minerals with depth. Down to 750 m and in some layers around 2000 m kyanite is present in quite large amounts and is in contact to biotite. Kyanite forms single grains or grain clusters, where the individual grains display different crystallographic orientations (Fig. B.3.4 to B.3.6). In the other gneisses of appropriate compositon kyanite occurs exclusively as minute rounded inclusions in plagioclase (Fig. B.3.7). Sillimanite was first observed in the garnet-muscovite-biotite gneisses at 450 m and becomes more prominent with increasing depth. It forms rare prismatic crystals and - more frequently - fibrolitic aggregates, in most cases intimately intergrown with biotite (Fig. B.3.8). Accessory minerals are zircon, monazite, tourmaline, and graphite. Apatite is occasionally accumulated in some layers.

Biotite-hornblende gneisses:

Biotite-hornblende gneisses occur as small interlayers within the Al_2SiO_5-bearing gneisses but mainly as part of the variegated sequence together with amphibolites and calcsilicate rocks (0 to 460 m and 2470 to 2580 m).

Main constituents of these gneisses are plagioclase, biotite, hornblende, quartz and in places cummingtonite and microcline. The early high-pressure / high-temperature stage is documented by the relictic paragenesis of clinopyroxene+garnet+quartz together with mesoperthites (Fig. B.3.9, B.3.10).

Accessory minerals are zircon, monazite, allanite, titanite, and apatite. Allanite-bearing gneisses are bound to the neighbourhood of amphibolites.

Saussuritization and sericitization of feldspars and chloritization of biotite and hornblende are widespread.

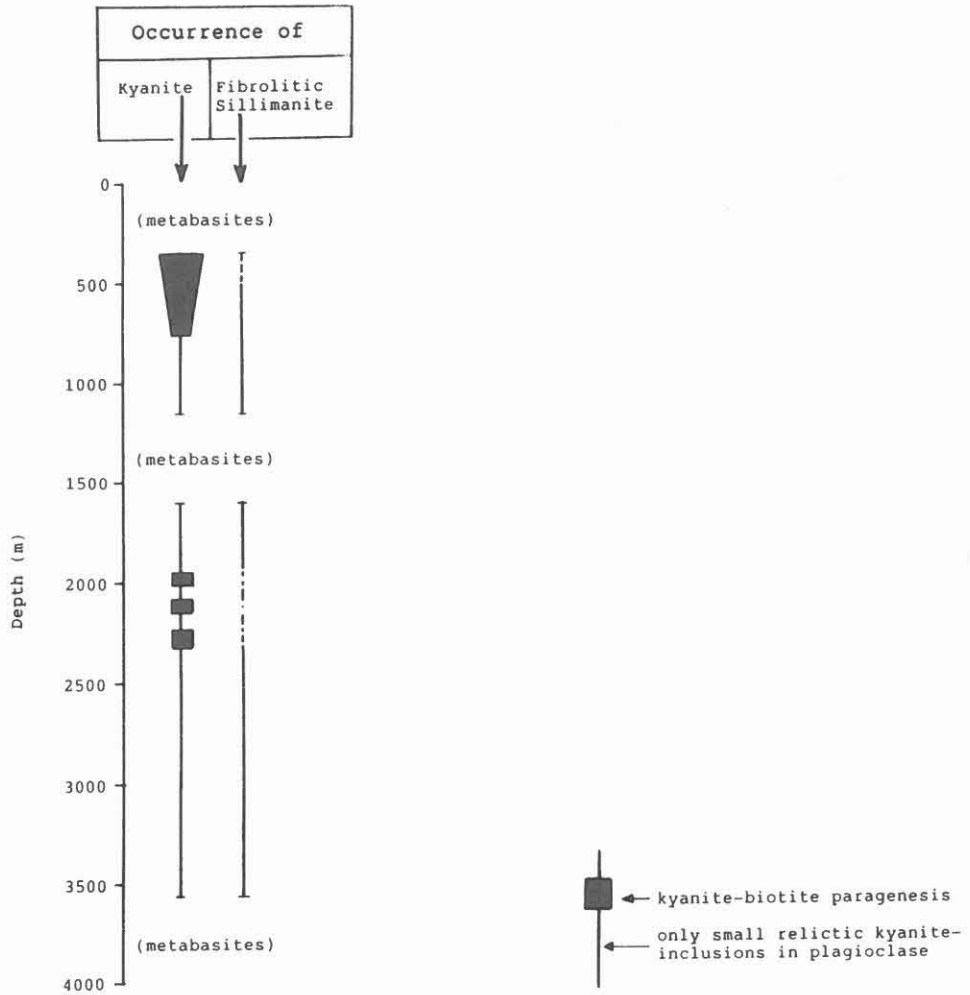

Fig. B.3.3: Distribution of Al_2SiO_5-minerals in meta-greywackeceous and meta-pelitic gneisses.

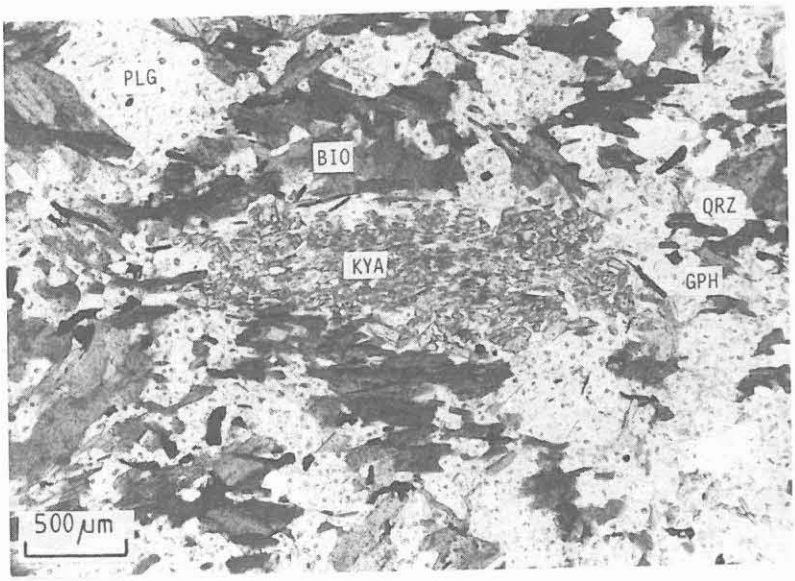

Fig. B.3.4: Graphite-bearing garnet-Al_2SiO_5-biotite gneiss. Aggregate of disintegrated kyanite and small biotite and white mica (KYA). QRZ = quartz, GPH = graphite, BIO = biotite, PLG = plagioclase. (Thin section 53B7tII, 375.9 m, // nicols).

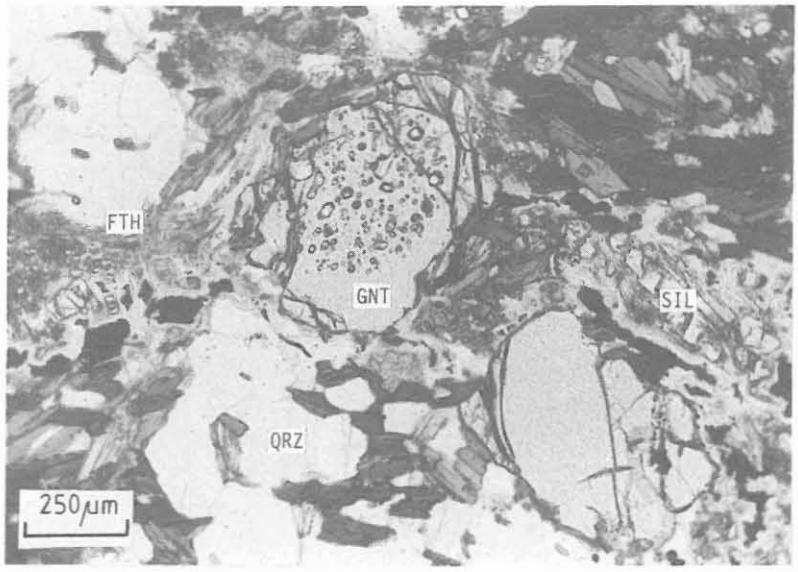

Fig. B.3.5: Garnet-Al_2SiO_5-biotite gneiss. Two types of garnet, one with and the other without inclusions. QRZ = quartz, GNT = garnet, SIL = sillimanite pseudomorphs after kyanite, FTH = fibrolitic sillimanite. (Thin section 97D3h, 546.8 m, // nicols).

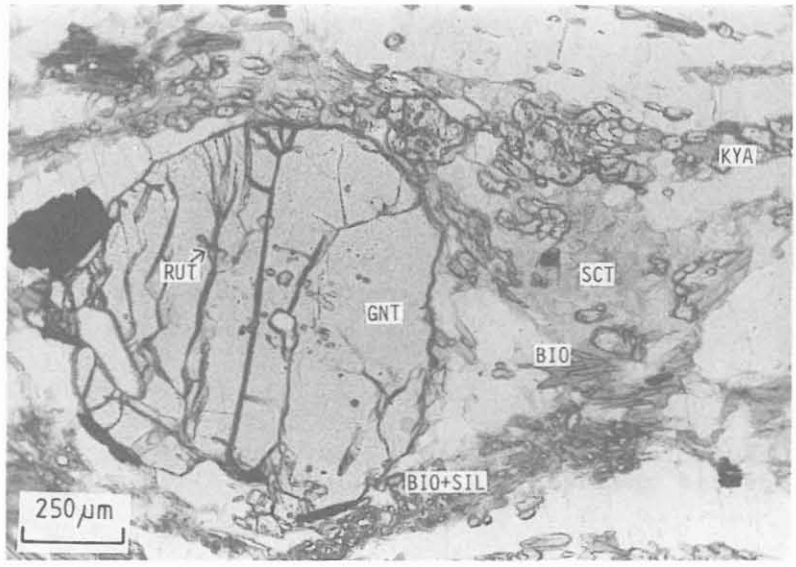

Fig. B.3.6: Garnet-Al_2SiO_5-biotite gneiss. Large garnet with central inclusions, surrounded by a sillimanite - biotite aggregate (BIO+SIL) and small grains of disintegrated kyanite (KYA). GNT = garnet, BIO = biotite, RUT = rutile, SCT = sericitic substance. (Thin section 100B2d, 554.2 m, // nicols).

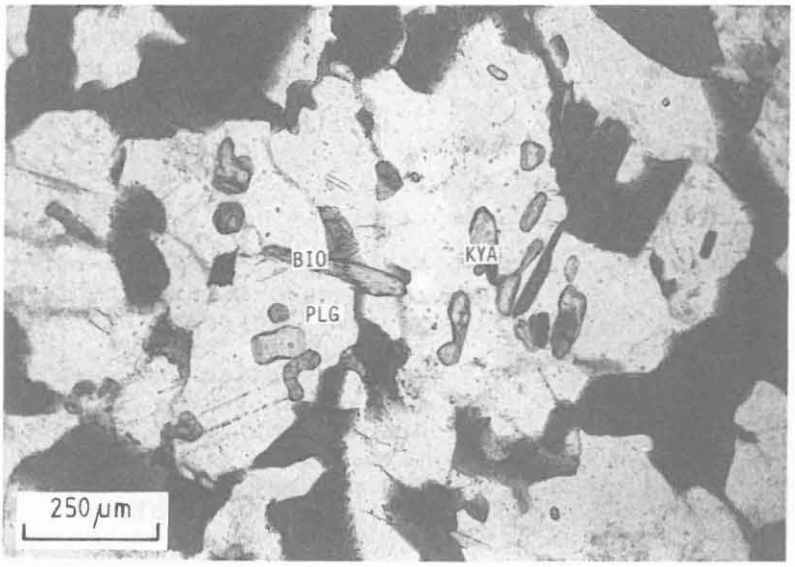

Fig. B.3.7: Garnet-Al_2SiO_5-biotite gneiss. Relictic kyanite grains (KYA) within plagioclase (PLG). BIO = biotite. (Thin section 382B1e, 1730.2 m, // nicols).

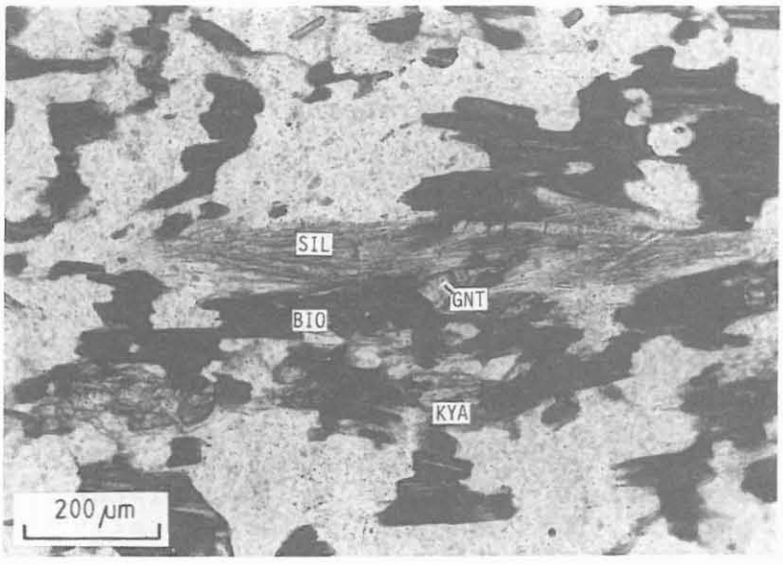

Fig. B.3.8: Garnet-Al_2SiO_5-biotite gneiss. Sillimanite (SIL) and kyanite (KYA) have phase boundaries to biotite (BIO), but not to themselves. GNT = garnet. (Thin section 447E2q, 1979.2 m, // nicols).

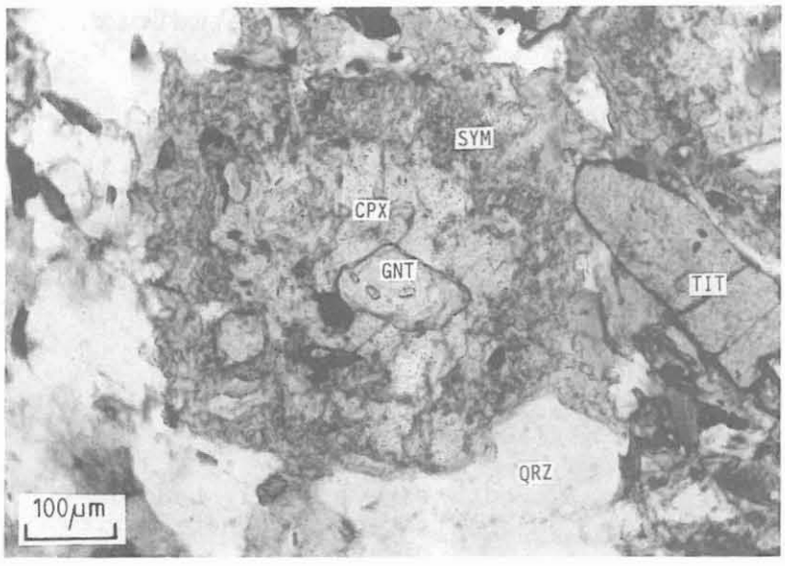

Fig. B.3.9: Clinopyroxene-garnet-hornblende-biotite gneiss. Clinopyroxene (CPX) with inclusion of garnet (GNT) is surrounded by a corona of amphibole-plagioclase symplectite (SYM). QRZ = quartz, TIT = titanite. (Thin section 619E1gk, 2547.10 m, // nicols).

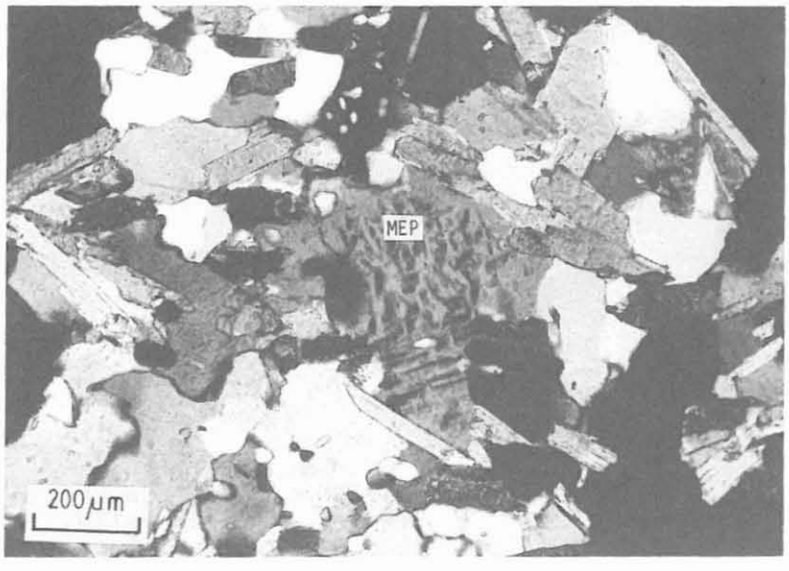

Fig. B.3.10: Hornblende-biotite augengneiss with mesoperthite (MEP). (Thin section CUT3846, 3846 m, + nicols).

Some biotite-hornblende gneisses bear plagioclase porphyroclasts of 1 - 5 mm diameter with small inclusions of drop-like, strain free quartz. At 2480 - 2490 m these porphyroclasts have an isometric shape; in general they are elliptical elongated parallel to the foliation.

Other gneiss-types occuring in subordinate amounts:

From 3420 to 3440 m leucocratic biotite gneisses occur. Granular plagioclase defines a weak foliation (Fig. B.3.11).

Below 3773 m within the metabasites some augengneisses are intercalated. They contain various amounts of hornblende and/or biotite and/or garnet. The marginally or totally recrystallized plagioclase porphyroclasts reach 1 cm diameter normal to foliation and lineation (Fig. B.3.12). Fine grained mesoperthite, microcline and plagioclase occur in the matrix.

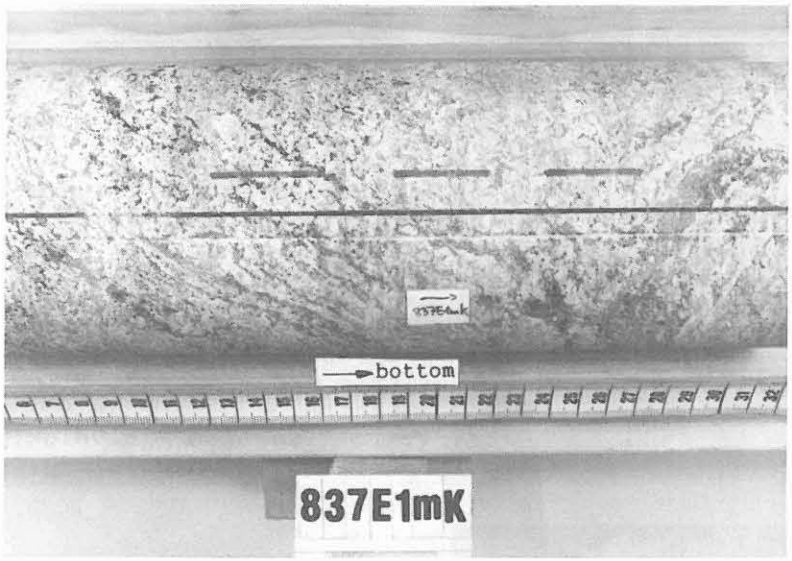

Fig. B.3.11: Leucocratic garnet-biotite gneiss with granular fabric.
(Core piece 837E1mK, 3427.0 m, scale in cm).

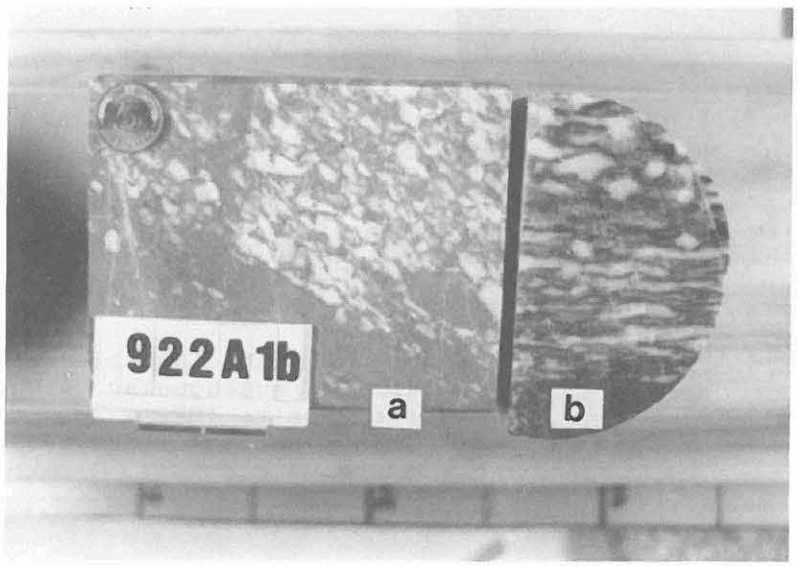

Fig. B.3.12: Augengneis, a) normal to the lineation, b) parallel to the lineation.
(Core piece 922A1b, 3776 m, core diameter 9.4 cm).

B.3.2 Chemical composition

The chemical composition of the garnet-Al_2SiO_5-muscovite-biotite gneisses (Table B.3.1) corresponds to the composition of greywackes, clayey greywackes and claystones, judging from the SiO_2/Al_2O_3 versus K_2O/Na_2O diagram after Wimmenauer (1984; Fig. B.3.13). Greywackeceous compositions predominate, claystone compositions are subordinate. The greywacke/claystone interlayering could be the result of a flysch like sedimentation process. The biotite-hornblende gneisses as well as the leucocratic garnet-biotite gneisses appear interlayered with the meta-greywackes. The composition of those hornblende-bearing gneisses is compatible with that of CaO-rich greywackes.

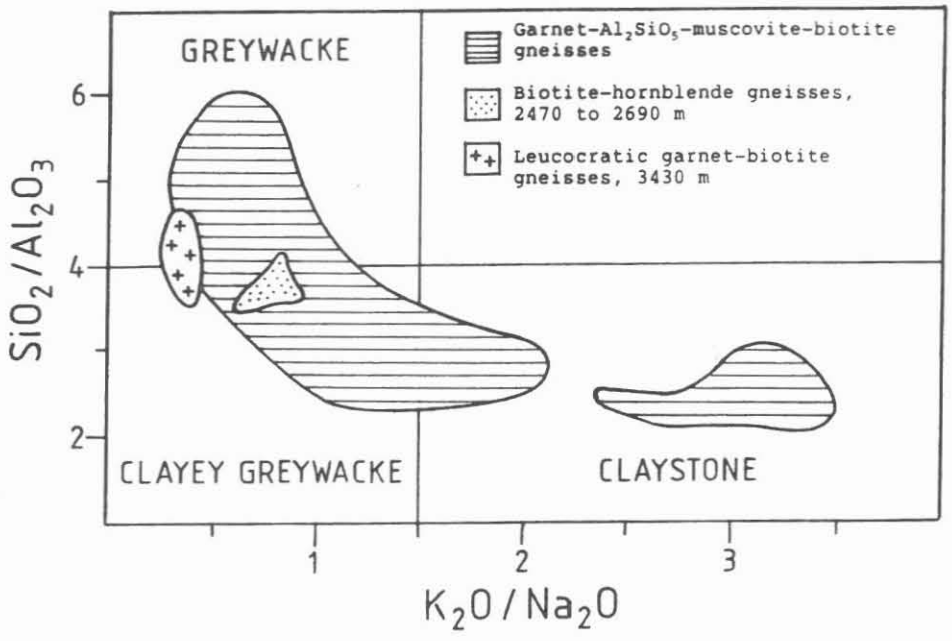

Fig. B.3.13: Plot of chemical analyses of different gneisses into the SiO_2/Al_2O_3 versus K_2O/Na_2O diagram with the field of different clastic sediments after Wimmenauer (1984).

Table B.3.1: Selected chemical (XRF) and modal (XRD) analyses of the main rock types. Main constituents and modal amounts in wt.-%, trace element in ppm. The detection limit of quantitative XRD is 1 to 3 wt.-%.

	Garnet-Al_2SiO_5-biotite gneisses				Biotite-hornblende gneisses			
Core	55A6T	158A1T	419D1ac	790G1w	30B4T	616F1nK	788A1a	946A1a
Depth (m)	384.31	722.20	1855.68	3242.47	217.46	2530.44	3226.70	3858.50
SiO_2	61.5	67.8	57.6	59.6	50.0	54.9	50.9	53.0
TiO_2	0.92	0.81	1.06	1.02	1.27	1.49	1.19	1.48
Al_2O_3	15.6	15.0	20.5	16.8	17.4	15.5	14.5	15.4
Fe_2O_3	7.77	5.22	8.24	7.55	7.13	9.34	8.49	9.12
MnO	0.52	0.07	0.11	0.12	0.13	0.14	0.13	0.13
MgO	2.66	1.83	2.76	2.94	3.31	3.53	9.61	4.23
CaO	2.14	1.26	0.81	1.94	11.41	6.84	5.86	7.44
Na_2O	3.4	2.6	2.1	2.8	3.7	2.9	1.9	3.6
K_2O	1.99	2.56	4.09	2.96	1.38	2.03	2.05	1.24
P_2O_5	0.11	0.07	0.04	0.07	0.55	0.38	0.30	0.29
Zr	201	245	256	232	158	313	218	205
Y	48	32	40	33	26	44	26	44
Sr	348	162	139	247	122	388	444	201
Rb	58	67	109	56	18	52	68	22
Zn	96	85	136	108	178	106	84	84
Cu	25	27	46	36	48	25	31	28
Ni	46	30	45	42	64	49	167	26
Cr	542	67	83	87	328	85	363	109
U	<5	<5	<5	<5	-	<5	<5	<5
Th	10	10	10	7	<5	5	14	<5
Quartz	24	46	27	32	4	25	23	11
Chlorite	13	8	5	12	9	-	15	4
Amphibole	-	-	-	-	8	31	23	31
K-Feldspar	-	-	-	-	7	-	-	-
Biotite	2	9	19	-	-	9	11	2
Garnet	6	-	-	-	-	-	-	5
Plagioclase	54	24	30	33	41	35	28	47
White Mica	-	13	13	22	-	-	-	-
Sillimanite	-	-	5	-	-	-	-	-
Prehnite	-	-	-	-	29	-	-	-
Calcite	-	-	-	-	2	-	-	-

	Amphi-bolite	Meta-ultramaf.	Meta-gabbro	Amphi-bolite	Amphi-bolite	Meta-gabbro	Amphi-bolite	Amphi-bolite
Core	50D14T	300G1j	324E1l	325E2u	613E1hK	883A1bK	889A1b	922C1q
Depth (m)	353.74	1449.29	1549.11	1554.90	2514.10	3607.15	3633.54	3777.63
SiO_2	46.3	42.7	44.6	47.9	51.4	45.9	48.8	46.6
TiO_2	2.53	0.84	1.11	1.07	1.67	1.17	1.44	1.36
Al_2O_3	16.5	6.0	15.3	14.8	15.5	16.2	15.3	15.2
Fe_2O_3	12.56	15.26	9.74	9.20	11.08	10.22	10.46	10.97
MnO	0.17	0.18	0.14	0.13	0.19	0.15	0.16	0.17
MgO	7.48	26.91	9.52	8.32	3.85	8.95	8.47	8.34
CaO	6.03	3.70	10.00	9.01	8.06	9.61	9.32	9.59
Na_2O	3.5	0.4	2.5	3.4	3.5	2.8	3.0	2.6
K_2O	1.34	0.13	0.47	0.75	2.16	0.51	0.78	0.67
P_2O_5	0.39	0.11	0.13	0.11	0.52	0.13	0.16	0.14
Zr	200	90	93	89	341	99	107	119
Y	51	17	20	18	46	21	28	33
Sr	342	44	301	335	269	319	238	192
Rb	42	10	11	15	37	10	18	17
Zn	113	100	66	80	134	74	76	90
Cu	49	215	68	64	33	58	44	39
Ni	109	692	129	55	44	84	81	89
Cr	333	919	261	227	66	103	231	228
U	-	<5	-	-	<5	1	1	2
Th	2	<5	3	3	5	1	3	2
Quartz	-	-	-	-	7	-	4	4
Chlorite	21	17	3	-	3	-	4	-
Amphibole	36	39	70	43	39	56	42	61
K-Feldspar	4	-	-	-	-	-	-	-
Garnet	-	-	4	-	-	-	13	-
Plagioclase	39	-	23	57	44	44	37	35
Titanite	-	-	-	-	7	-	-	-
Serpentine	-	43	-	-	-	-	-	-

B.4 METABASITES

B.4.1 Petrography

Metabasites appear in two main types:

(1) thick amphibolite-metagabbro sequences and
(2) thin amphibolite layers and lenses intercalated within different gneisses.

Amphibolite-Metagabbro Sequence:

From 1160 - 1610 m and from 3575 to 4000 m two sequences composed of dominating garnet amphibolites, subordinate metagabbros and small meta-ultramafic lenses were intersected. Locally, small leucocratic gneisses occur.

The main constituents of the garnet amphibolites are plagioclase, hornblende and garnet; quartz and biotite are subordinate. Their dominating fabric is massive, medium grained, and streaked with quartz-plagioclase schlieren (Fig. B.4.1).

The metagabbros are massive, medium to coarse grained rocks and differ from the amphibolites by their relictic, magmatic, ophitic texture with pseudomorphs after plagioclase laths included in 1 cm large clinopyroxenes (Fig. B.4.2 and B.4.3). Metagabbro with corona fabric occurs subordinately (Fig. B.4.4). Hornblende, plagioclase and garnet are the main constituents. Quartz-plagioclase schlieren are almost missing.

In local shear zones the amphibolites and metagabbros show a pronounced foliation.

Meta-ultramafic rocks (chlorite-amphibole fels to schist) appear as 0.1 to 6 m thick layers and lenses mainly within the metagabbros. The mineralogical composition of these rocks and their fabric is very variable. It is characterized by up to 1 cm large poikilitic porphyroclasts of brown hornblende and clinopyroxene with inclusions of pseudomorphs after olivine, now consisting of different sheet-silicates. These porphyroclasts are surrounded by a fine grained matrix of various amphiboles, chlorite, serpentine, ilmenite, brown spinel, magnetite, and sulphides.

Contacts between meta-ultramafic rocks and metabasites as well as between amphibolites and metagabbros are variable. Some boundaries appear to be intrusive with local formation of mobilisates in the contact zone. Others are cataclastic.

Some metagabbros are syntectonically altered to amphibolites. The meta-ultramafics are interpreted to be cumulates of the gabbros.

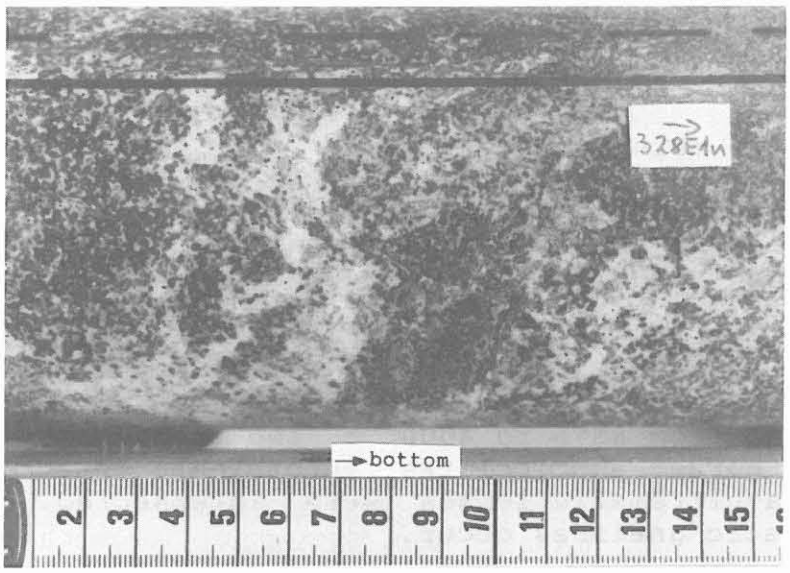

Fig. B.4.1: Garnet-amphibolite with characteristic leucocratic quartz-plagioclase mobilisates. (Core piece 328E1n, 1572.2 m, scale in cm).

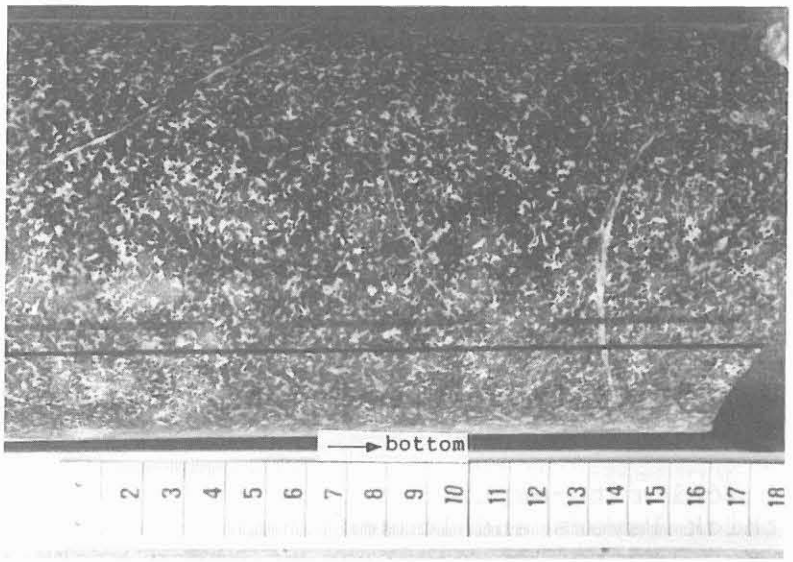

Fig. B.4.2: Typical massive metagabbro with relictic, igneous, ophitic fabric. (Core piece 263C10a, 1259.30 m, scale in cm).

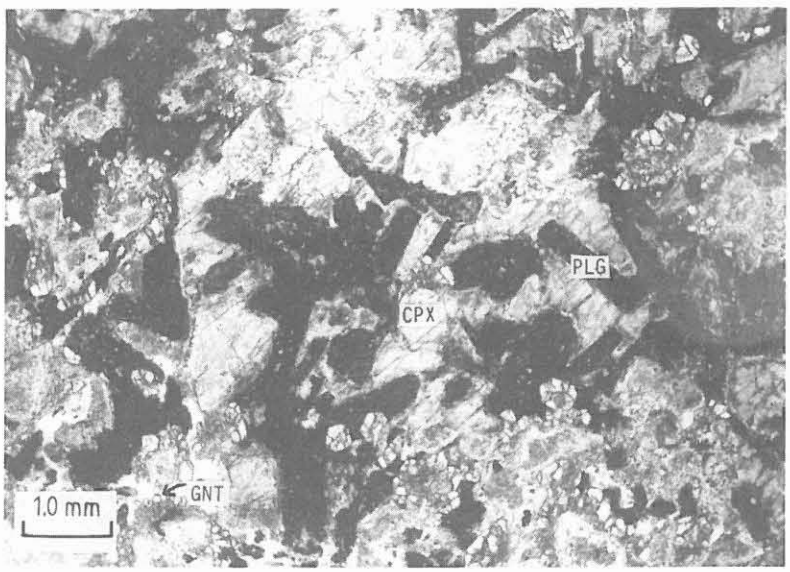

Fig. B.4.3: Ophitic fabric of metagabbro. Large crystal of clinopyroxene (CPX) includes dark, altered laths of plagioclase (PLG). Garnet (GNT) mostly forms coronas around hornblende-plagioclase symplectite. (Thin section 264H4nT, 1269.6 m, // nicols).

Thin amphibolites intercalated with gneisses:

Thin amphibolites with thicknesses in the range of decimeters to meters appear mainly as members of the variegated sequences from 0 to 460 m and 2470 to 2690 m. In the upper variegated sequence they form partly fine grained, banded, epidote-rich layers, partly massive garnet amphibolites and partly amphibolites with centimeter-thick calcsilcate bands of clinopyroxene + plagioclase + titanite. The amphibolites of the lower variegated sequence are similar, but coarse grained garnet amphibolite boudins are especially characteristic. Down to 200 m the amphibolites show an almost complete alteration under greenschist facies conditions.

B.4.2 Metamorphic evolution

The amphibolites and metagabbros show different stages of metamorphism (Röhr et al. 1990):

(a) early high-pressure stages,
(b) a dominating amphibolite facies stage, and
(c) a late low temperature stage.

a) High-pressure stages:

A typical metagabbro with good preservation of the old high-pressure stage contains large clinopyroxenes (Jd10) with lamellar amphibole, rutile, quartz, and plagioclase (An23) inclusions. These clinopyroxenes are surrounded by vermicular clinopyroxene(Jd1-14)-plagioclase(An17-25)-quartz symplectites. Further minerals are coronitic garnet, Ti-rich, brown hornblende, zoned, granoblastic plagioclase (center: An21 -> rim: An84), rutile-ilmenite aggregates, quartz, and biotite (Fig. B.4.5 to B.4.7).

The composition of weakly zoned garnet in this rock is characteristically around Alm45, Pyr30, Gross25. Garnet includes kyanite, zoisite, plagioclase (An33 to An92), clinopyroxene (up to Jd30), rutile and quartz.

The pseudomorphs after magmatic plagioclase laths (Fig. B.4.5) consist of an aggregate of plagioclase (An9-32), (clino)zoisite and subordinate phengitic white mica.

b) Amphibolite facies stage

Subsequently, the high pressure rocks were adapted to amphibolite facies conditions. This happenend in several steps of reaction. Some of the reactions were frozen in and various stages are preserved now side by side.

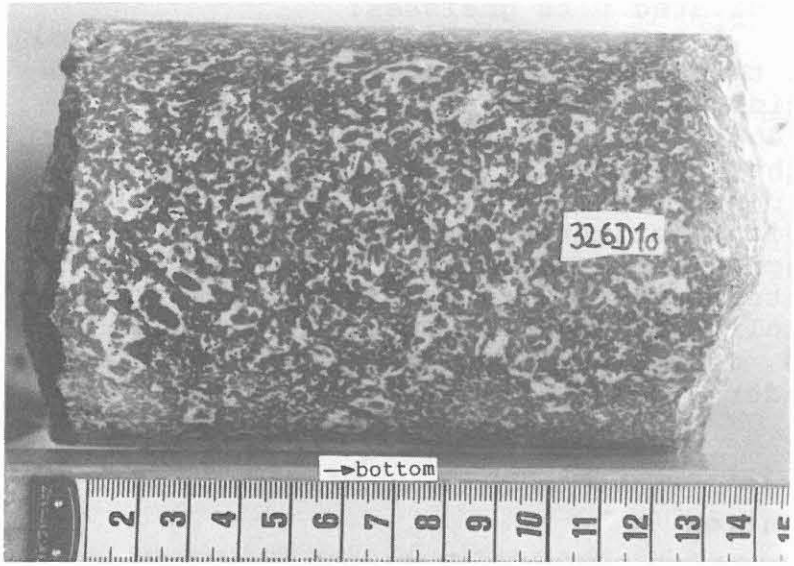

Fig. B.4.4: Massive metagabbro with coronitic fabric. Plagioclase coronas surround roundish hornblende crystals. (Core piece 326D1o, 1559.8 m, scale in cm).

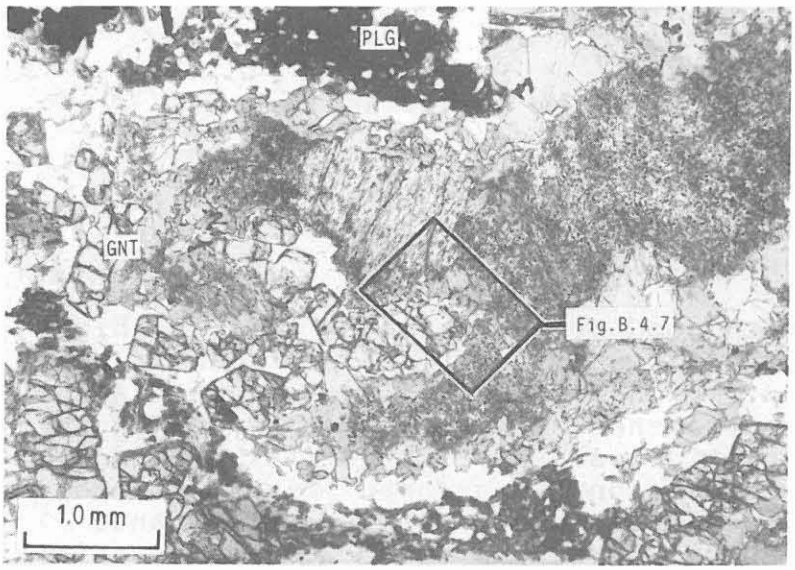

Fig. B.4.5: Overview of the typical fabric of metagabbros from the lower amphibolite - metagabbro sequence. Clinopyroxene with lamellar inclusions is surrounded by clinopyroxene-plagioclase symplectite. GNT = coronitic garnet, PLG = altered plagioclase laths. (Thin section 885C3n, 3620.2 m, // nicols).

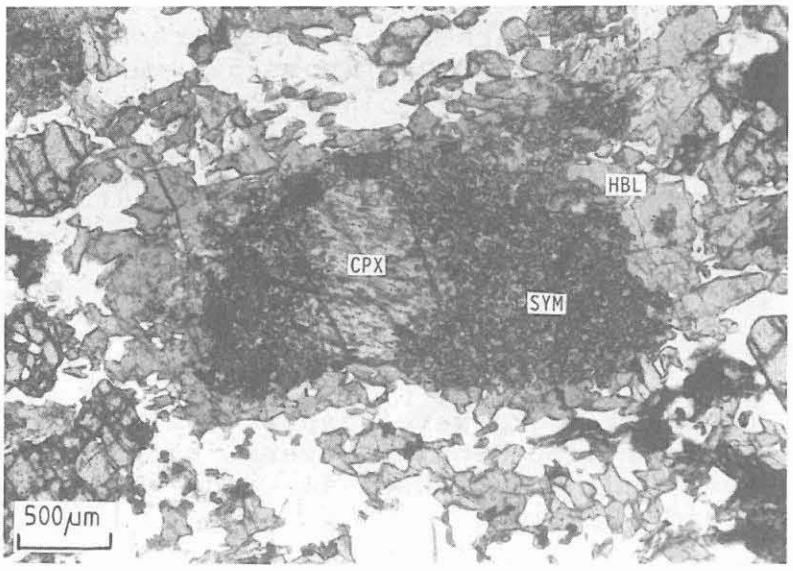

Fig. B.4.6: Metagabbro. Large clinopyroxene (CPX) with inclusions of plagioclase, lamellar quartz, and rutile is surrounded by clinopyroxene - quartz -plagioclase symplectite (SYM). These are surrounded by a corona of brown hornblende (HBL). (Thin section 885C3n, 3620.2 m, // nicols).

The adaption led to:

(1) the formation of hornblende-plagioclase-quartz symplectite after clinopyroxene-plagioclase-quartz symplectite and finally to a granoblastic hornblende and plagioclase matrix;

(2) the development of coronas of plagioclase ± hornblende around garnet leading to the total replacement of garnet by pseudomorphs of plagioclase ± hornblende ± biotite (Fig. B.4.8);

(3) the widespread formation of green, Ti-poor hornblende;

(4) the development of coronas of titanite around ilmenite and rutile leading to the total replacement of rutile.

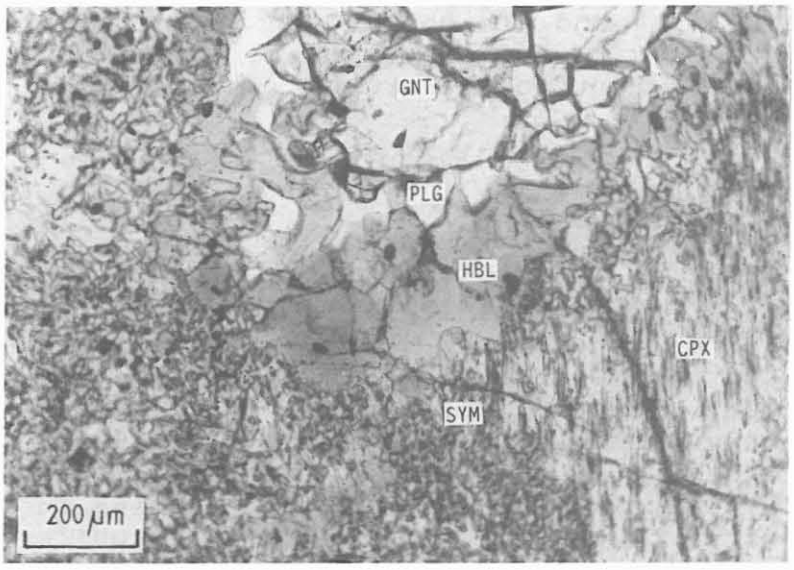

Fig. B.4.7: Metagabbro, detail from Fig. B.4.5. Contact between large clinopyroxene (CPX, including lamellae of quartz and plagioclase) and clinopyroxene - plagioclase - quartz symplectite (SYM). A corona of plagioclase (PLG) and hornblende (HBL) is developed between garnet (GNT) and clinopyroxene, probably due to amphibolite facies overprint.
(Thin section 885C3n, 3620.20 m, // nicols).

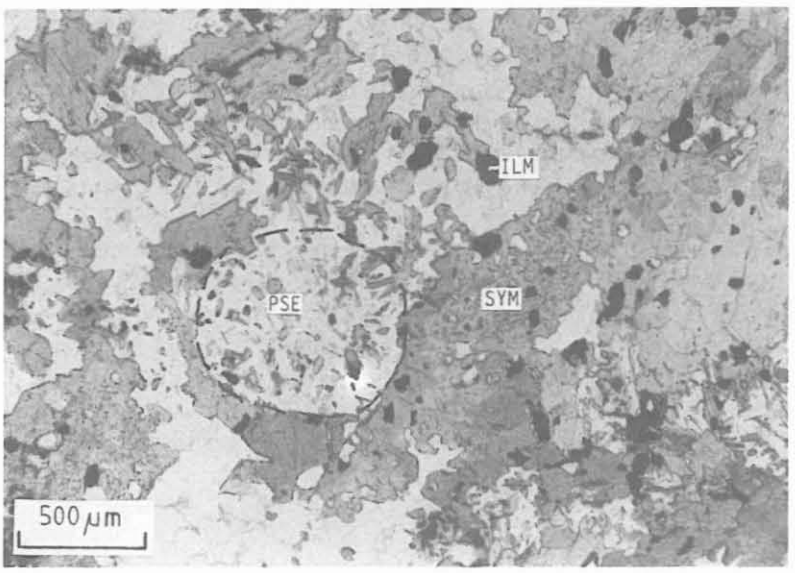

Fig. B.4.8: Amphibolite. Due to the adaption to amphibolite facies the high - pressure garnet reacted to form pseudomorphs (PSE) of plagioclase + hornblende + biotite + ilmenite. The clinopyroxene symplectite is transferred to poikilitic hornblende symplectite (SYM). Ilmenite (ILM) is surrounded by titanite.
(Thin section 919A1aII, 3758.9 m, // nicols).

With depth there is some change in the extent of adaption to amphibolite facies conditions:

(1) At the surface of the ZEV, clinopyroxene and hornblende symplectites and garnet coronas are very rare. Only coronas of plagioclase ± hornblende ± biotite around garnet were observed by Schüssler (1987).

(2) Within the upper amphibolite-metagabbro sequence from 1160 to 1610 m of the pilot hole, high pressure relics (symplectites and garnet coronas) are rare.

(3) Within the lower amphibolite-metagabbro sequence from 3575 to 4000 m high-pressure relics are common.

c) Late low temperature stage:

The last metamorphic event led to local development of greenschist facies and lower-grade minerals, e.g. disintegration of plagioclase to clinozoisite and albite, growth of epidote, chlorite, prehnite, pumpellyite and development of light green rims of hornblende to actinolite around green hornblende.

B.4.3 Chemical composition

The chemical composition of the metabasites (Table B.3.1) is equivalent to subalkaline, tholeiitic basalts. Iron and garnet-rich amphibolites can be interpreted as forming the typical Fe-enriched part of tholeiitic trends. Only a few amphibolites with clinopyroxene-rich layers from 0 to 460 m may be para-amphibolites (Fig. B.4.9) and are excluded from the further discussion. Patzak et al. (1989) discriminated the different metabasites by comparison of their immobile elements with those of modern basalts of different geotectonic settings.

Patzak et al. conclude that the amphibolites of the variegated unit from 0 to 460 m are similar to modern tholeiites of ocean islands (OIT) or anomalous segments of mid ocean ridges (E-MORB) because of their elevated content of TiO_2 and P_2O_5 and their specific rare earth element pattern.

Composition of metabasites of the thick amphibolite-metagabbro sequence is clearly different from the amphibolites above 460 m. The metagabbros from 1160 to 1610 m have compositions equivalent to modern mid ocean ridge basalts of normal segments (N-MORB), the composition of associated garnet amphibolites is similar to E-MORB. All metabasites investigated by Patzak et al. show a distinct enrichment of the mobile elements Sr, K, Rb and especially Ba.

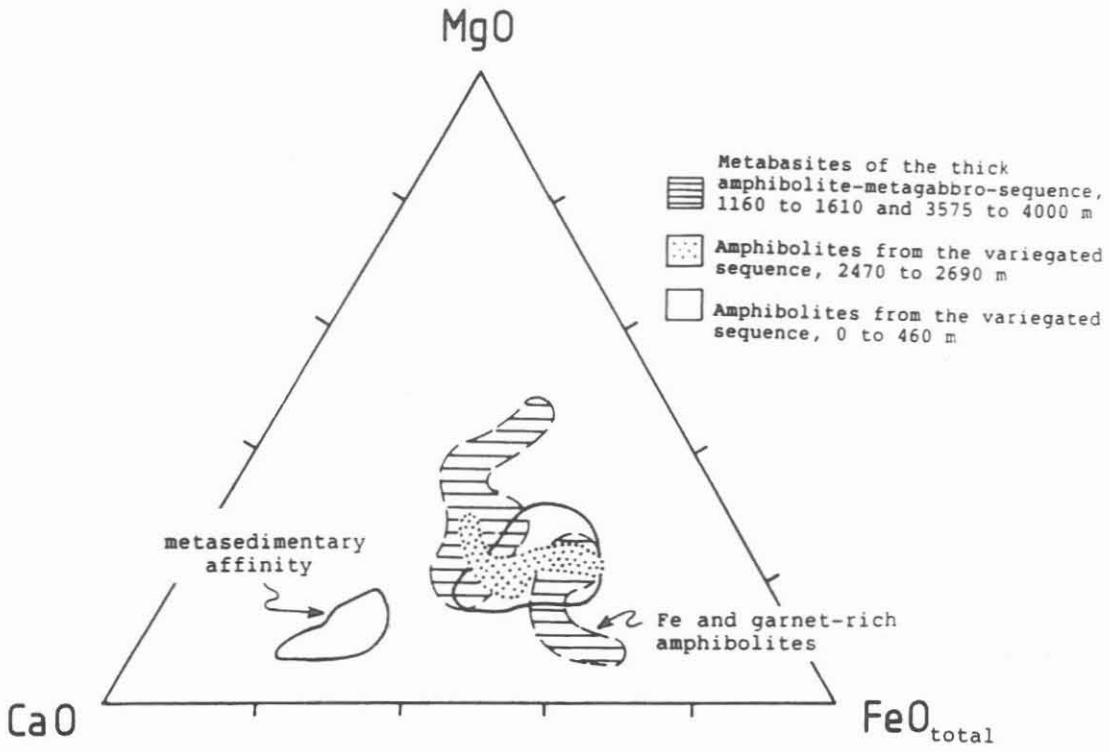

Fig. B.4.9: Compositions of metabasic rocks in the CaO-MgO-FeO_t-diagram.

B.5 LATE DYKES

The metamorphic rocks are crosscut by numerous, partly deformed lamprophyres and a few aplites. These rocks serve as important time-markers but radiometric data for the dykes are not yet available.

B.5.1 Lamprophyres

The lamprophyres are fine-grained, brownish igneous rocks, that penetrated the gneisses mainly discordantly to the foliation. They are missing within the metabasites. Their thickness ranges from centimeters to several meters. Xenoliths of graphite-rich cataclasitic gneiss prove the graphite-cataclastic event to be older than the lamprophyre intrusion.

Plagioclase is the prevailing matrix mineral. Variable amounts of biotite and brown hornblende appear as phenocrysts. Some dykes bear equal amounts of plagioclase and K-feldspar. Pseudomorphs after olivine up to 2 mm in size bear brown spinel inclusions and are totally replaced by calcite, quartz and chlorite. Low-temperature alteration of the lamprophyres is pervasive leading to the formation of chlorite, sericite, pyrite, carbonate and quartz. The dykes themselves are cut by numerous later veins filled with calcite, prehnite, K-feldspar etc.

Ore minerals within these dykes are dispersed. Pyrite, chalcopyrite, pyrrhotite, pentlandite, sphalerite, galena, siegenite, ilmenite, anatase/rutile and spinel were identified. In places, gneissic xenoliths within lamprophyres show a marginal sulphide enrichment.

On the base of modal and chemical composition these dykes are classified as calcalkalic lamprophyres (kersantite, spessartite and vogesite).

B.5.2 Aplites

Aplite granites are limited to the depth interval 50 to 120 m were they form several, up to 6 m thick, cataclastically deformed dykes. Further, decimeter thick rocks of this kind appear around 2330 m and below 3575 m within the metabasites. They consist of quartz, plagioclase (with oscillatory zoning), microcline, perthite, white mica and chloritized biotite. These rocks may be genetically related to the large Falkenberg granite outcropping north and east of the pilot hole. More or less deformed pegmatites with white mica up to cm size (Fig. B.5.1) are subordinately present.

Fig. B.5.1: Quartz-plagioclase pegmatoid with biotite lenses, on the right contact to amphibolite. (Core piece 699A2b, 2858.1m, scale in cm).

B.6 ORE MINERALIZATION

Ore minerals identified within the 4000 m section of the pilot hole are

(1) **sulphides** (in decreasing order of abundance):

pyrite, pyrrhotite, marcasite, chalcopyrite, sphalerite, galena, pentlandite, molybdenite, millerite, arsenopyrite, Ag-pentlandite, siegenite, cobaltite, gersdorffite, polydymite, violarite, loellingite, and

(2) **oxides:**

ilmenite, rutile, anatase, leucoxene, titanite, magnetite, hematite, goethite, Cr-spinel (picotite).

In addition variable amounts of graphite and zircon are present, rare ilvaite and traces of tellurobismutite have been identified.

In a few zones of alteration or cataclasis the amount of disseminated pyrite mineralization exceeds 1 %. The down-hole distribution of major sulphide and oxide phases as well as graphite is shown in Table B.6.1.

B.6.1 Ore mineralisation of gneisses

Pyrite and pyrrhotite are the dominant sulphides of this lithological unit. Within the rock groundmass they occur as disseminated single grains showing a preferred orientation parallel to metamorphic foliation or as small lenses. Both minerals also occur as joint fillings. Along shear zones or in zones of cataclastic deformation, euhedral pyrite is abundant and often associated with graphite. Frequently, pyrrhotite in those zones is replaced by marcasite. Supergene alteration causes limonitization of sulphides down to 33 m.

Pyrrhotite of greater depth shows small flamelike exsolution bodies of pentlandite; it is often intergrown with pyrite and marginally replaced by chalcopyrite, locally together with sphalerite (Fig. B.6.1). Pyrrhotite may also form rims around sphalerite. Deformation twinnings are abundant in pyrrhotite close to shear zones.

Chalcopyrite, sphalerite and rare galena form single grains in the rock groundmass; but, like pyrite and pyrrhotite, they may also occur in individual veins (mm to cm width; Fig. B.6.2). Locally arsenopyrite occurs in form of disseminated grains; in a quartz-feldspar dyke it is replaced partially by galena. Argentian pentlandite is intimately intergrown with chalcopyrite, pyrite and pyrrhotite. Here, pyrrhotite contains flame-like exsolutions of pentlandite (Fig. B.6.3).

Tab. B.6.1: Distribution of main opaque minerals within the KTB pilot hole; most of the minerals are ubiquitous; 1 = variegated sequence, 2 = garnet-Al_2SiO_5-biotite-gneiss, 3 = amphibolite-metagabbro sequence, 4 = variegated sequence (similar to 1).

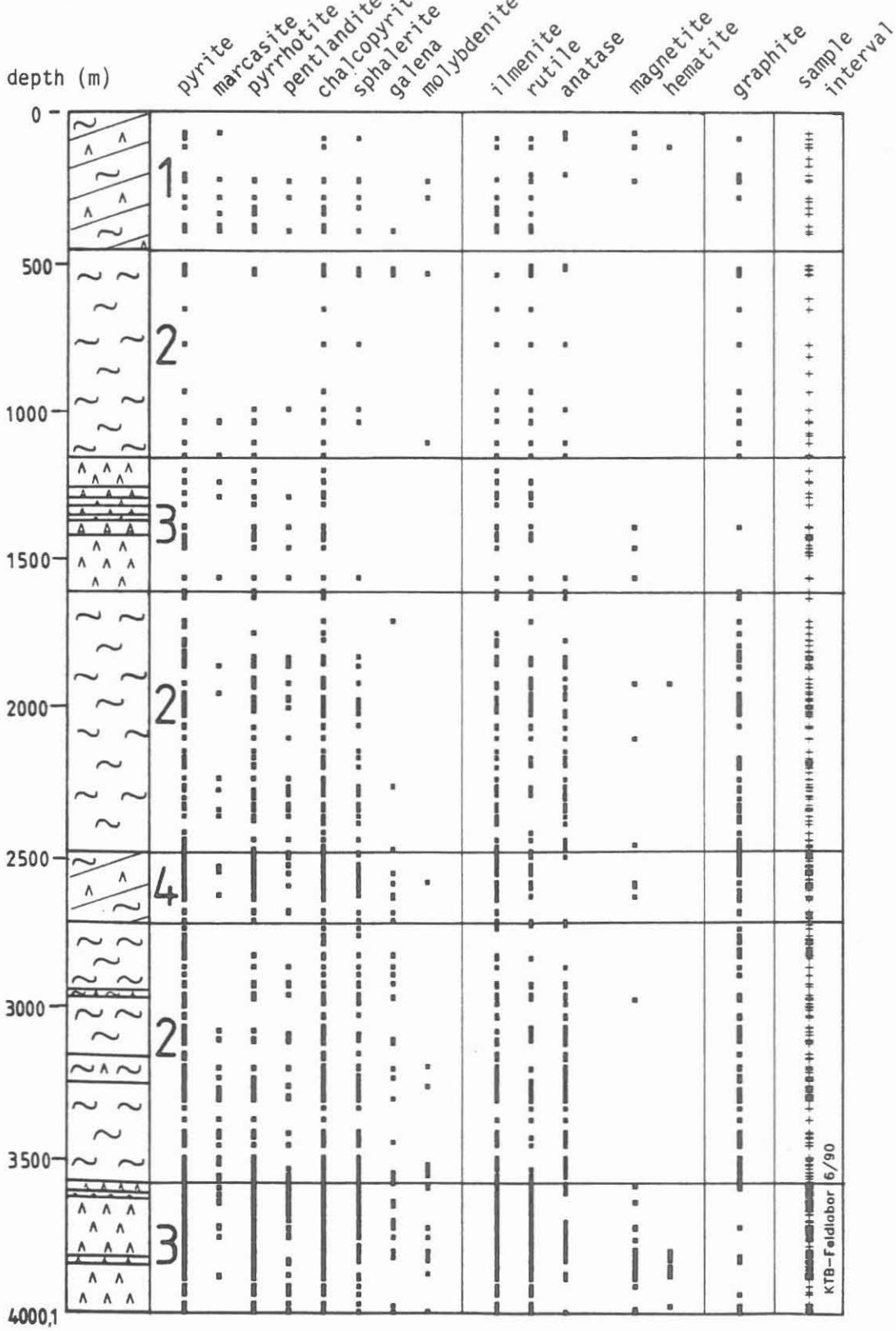

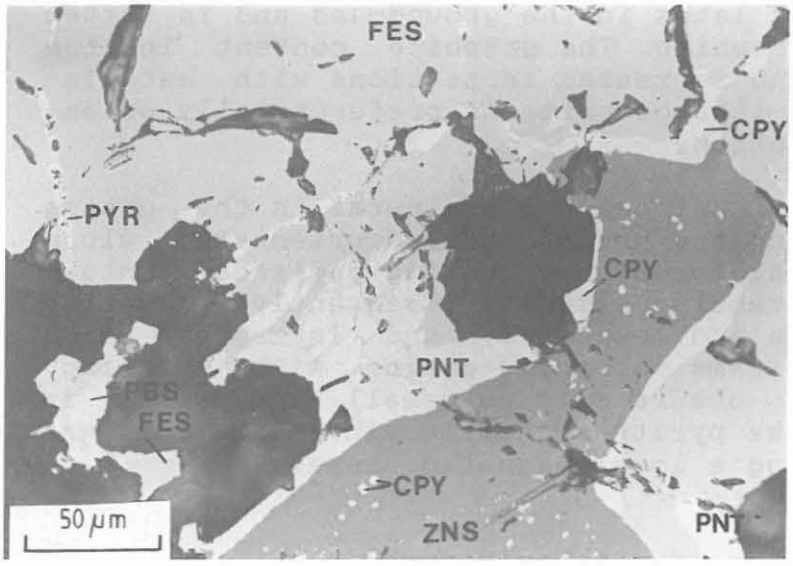

Fig. B.6.1: Complex aggregate of pyrrhotite (FES) with flame-like pentlandite (PNT) exsolutions and inclusions; euhedral pyrite (PYR) grains along cracks; replacement of pyrrhotite by chalcopyrite (CPY) and sphalerite (ZNS) with chalcopyrite ("chalcopyrite disease"?) and by galena (PBS) in garnet-sillimanite-biotite gneiss. (Polished section 695A8R, 2848.49 m, // nicols).

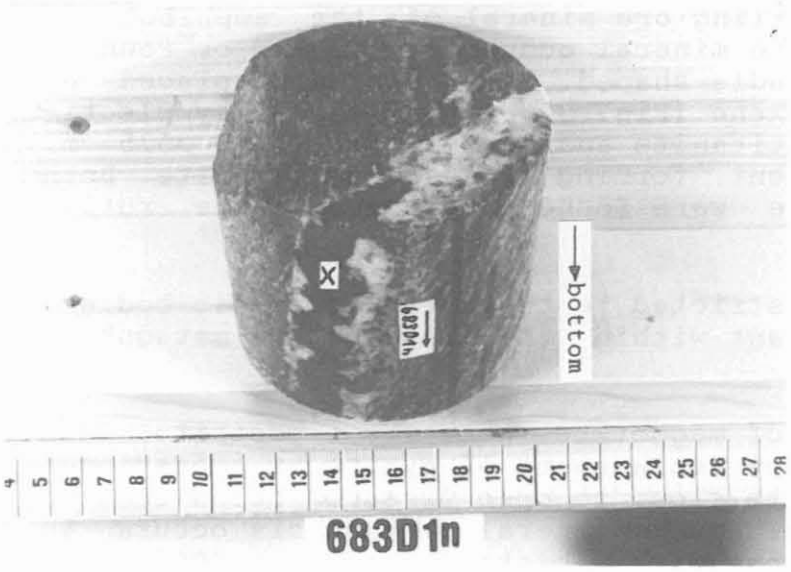

Fig. B.6.2: Vein-like hydrothermal sphalerite mineralization (X) in garnet-bearing sillimanite-biotite gneiss. (Core piece 683D1n, 2808.09 m, scale in cm).

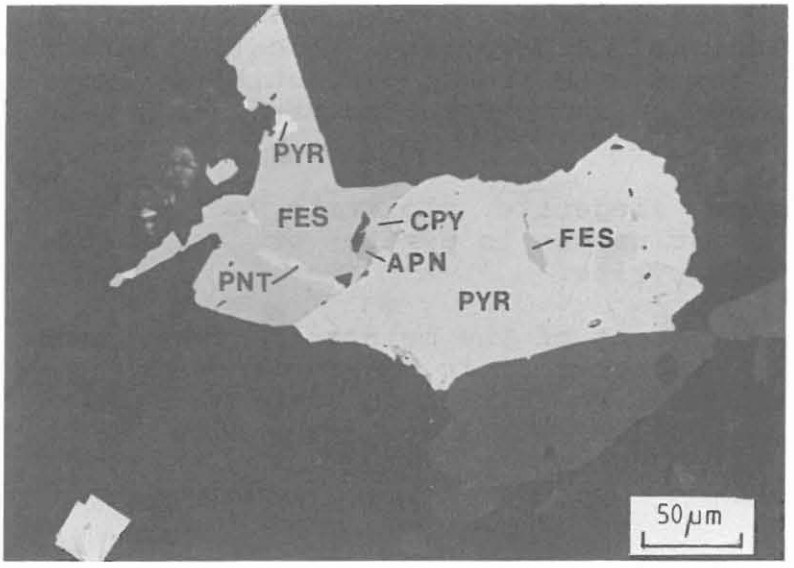

Fig. B.6.3: Pyrite (PYR) and pyrrhotite (FES) with pentlandite (PNT) exsolutions, intergrown with chalcopyrite (CPY) and Ag-pentlandite (APN) in biotite-hornblende gneiss. (Polished section 617B1h, 2533.21 m, // nicols).

Molybdenite forms small laths in the groundmass and is often closely related to graphite. The graphite content in the gneisses is variable and increases in sections with cataclastic deformation; lath-like graphite is preferentially orientated parallel to foliation.

Ilmenite is the predominant oxide ore mineral in the gneiss series. It forms elongated grains often orientated along cleavage planes of mica. Hornblende bearing gneisses contain much larger and more tabular ilmenite. Frequently, ilmenite is altered to anatase and leucoxene, and intergrown with rutile. Rutile also forms isometric grains with twinning. Subordinate magnetite occurs only as small inclusions in pyrite, but a lense-like pyrite-magnetite mineralization was found at 2955 m, causing a local magnetic anomaly.

B.6.2 Ore mineralization of metabasic rocks

Ilmenite is the prevailing ore mineral of the amphibolite-metagabbro sequence. The mineral occurs as tabular or rounded grains, sometimes needle-shaped. It is often replaced by rutile, anatase, leucoxene (Fig. B.6.4) and shows symplectitic intergrowth with titanite and hornblende. Below 3575 m, titanite is more frequent, forming rims around ilmenite. Both ilmenite and titanite were found replacing large rutile grains.

Magnetite is mostly restricted to the meta-ultramafic bodies; it becomes more abundant within the amphibolite-metagabbro sequence below 3575 m.

Late stage formation of magnetite, hematite, goethite, and ilvaite is documented by replacement of pyrite or accretional intergrowth with pyrite close to open fissures below 3800 m (Fig. B.6.5, B.6.6). The same mineral paragenesis occurs in the form of a small lense within biotite gneiss at 2955.2 m.

Major sulphides in metabasic units are pyrite and pyrrhotite with pentlandite exsolutions. Chalcopyrite, locally intergrown with sphalerite, forms rims around pyrrhotite; flame-like marcasite replaces pyrite and pyrrhotite marginally and along subgrain boundaries.

Small amounts of millerite, siegenite, violarite, polydymite, and cobaltite occur as inclusions in pyrite or as minute grains together with chalcopyrite.

Graphite is a minor constituent of the metabasic rocks forming lath-like, curled or spherolitic aggregates in the groundmass. Graphite has been identified in several samples of amphibolite at the gneiss/metabasic transition below 3575 m.

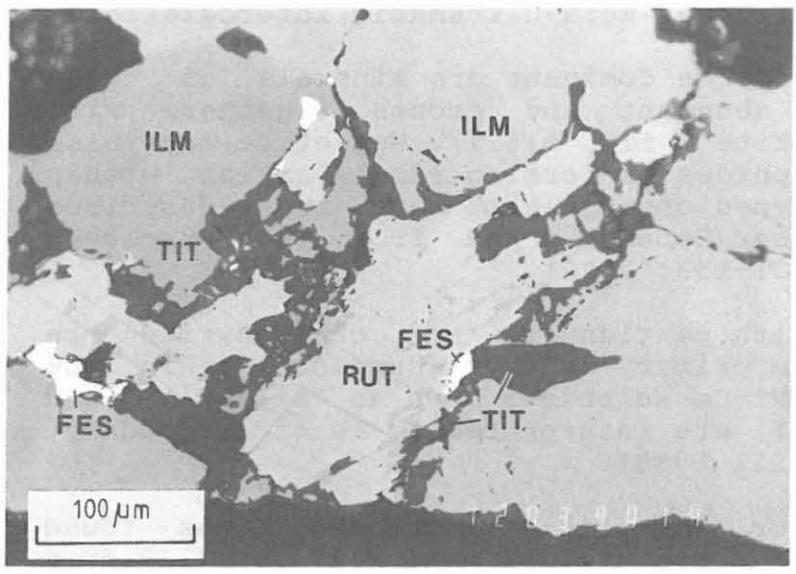

Fig. B.6.4: Relic rutile (RUT) with twin lamellae replaced by medium-grey ilmenite (ILM) and dark-grey titanite (TIT); pyrrhotite (FES) along alteration fronts in garnet-rich amphibolite.
(Polished section 875C21T, 3577.50 m, // nicols, oil).

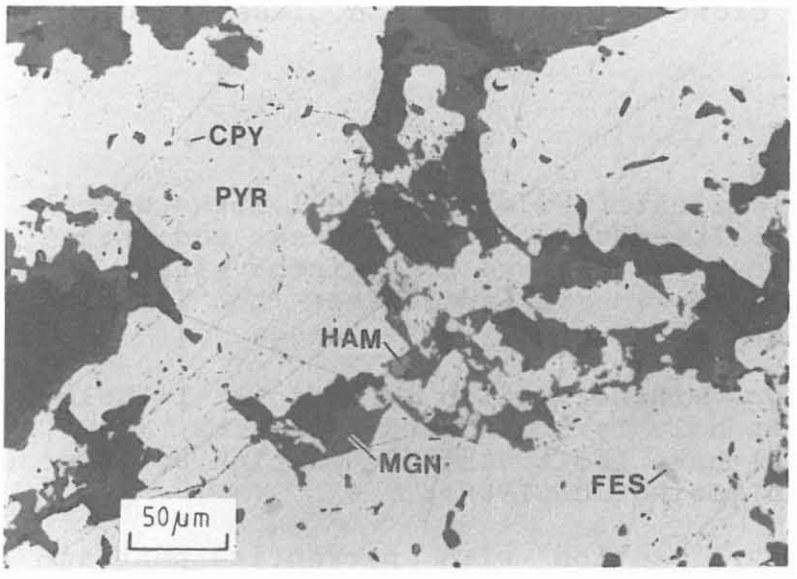

Fig. B.6.5: Pyrite (PYR) with inclusions of chalcopyrite (CPY) and pyrrhotite (FES) replaced by magnetite (MGN), hematite (HAM), goethite (GOE), and ilvaite (ILV) in garnet-amphibolite close to open fissure.
(Polished section 928E1nK, 3808.74 m, // nicols, oil).

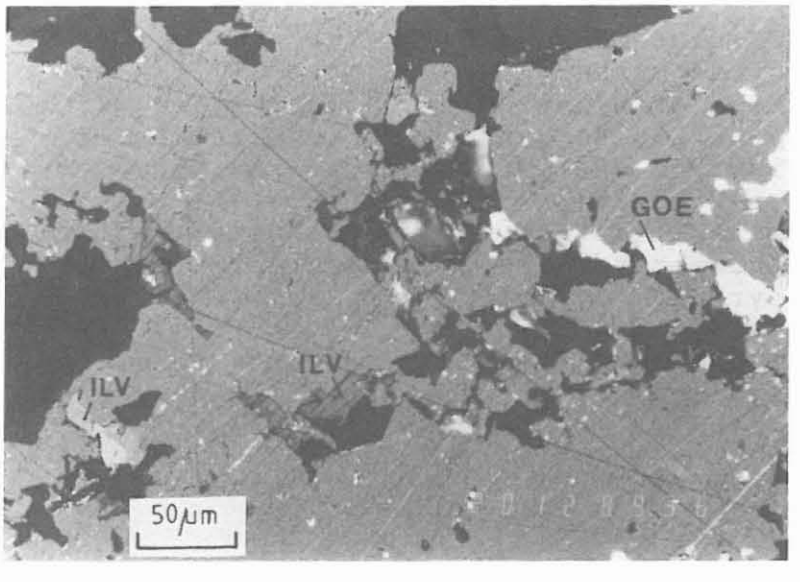

Fig. B.6.6: Distribution of tabular, homogenious, dark-grey ilvaite (ILV) and goethite (GOE) with abundant internal reflections (here white); as Fig. B.6.5 but with + nicols.

B.6.3 Ore mineralization of meta-ultramafic intercalations

Ilmenite and rutile are the dominant ore minerals of these units. Magnetite is abundant and occurs together with chromian spinel (picotite - Fig. B.6.7). Magnetite may also occur surrounding sulphides or forming single grains within silicates. Similar types of magnetite have been described from serpentinites near Erbendorf and from the Münchberg Massif (Dill 1985 p. 131-133; 1988).

Pyrite, pyrrhotite with pentlandite and chalcopyrite are thought to derive from primary sulphur abundance within the ultramafic melt. Fe-Ni-Co sulphides such as millerite and cobaltite (Fig. B.6.8) are interpreted to be of secondary, hydrothermal origin (Dill 1985).

Graphite, as curled or spherolitic aggregates, was found within meta-ultramafic rocks at 1381 m as well as 3719.5 m (Fig. B.6.9). Small single grains or clusters occur within the rock groundmass or close to magnetite and, less frequent, ilmenite.

B.6.4 Conclusions

The bulk of ore minerals identified occur in all lithological units: gneisses, amphibolite-metagabbro sequences, and meta-ultramafic bodies. Although oxides are predominant within the metabasites, a relation of mineral parageneses to lithological units can be established in only a few cases.

Microprobe studies of ore mineralization in various lithological units of the pilot hole by Kontny and Friedrich (1989) and Kontny et al. (1990) have led to the distinction of four types of mineralization (Friedrich 1989):

(1) intra-magmatic mineralization with pyrrhotite-pentlandite-chalcopyrite-magnetite as typical for meta-ultramafic units;
(2) mineralization with metamorphic overprint in gneisses (sphalerite-pyrrhotite-pyrite);
(3) mineralizations mobilized by metamorphic processes with pyrrhotite-pyrite-pentlandite-chalcopyrite-sphalerite-Ag-pentlandite associations and veinlike Te-bismutite, Bi bearing galena and pyrrhotite;
(4) post metamorphic mineralization of hydrothermal origin represented by low temperature Fe poor sphalerite, galena, arsenopyrite, pyrite).

Cogenetic inclusions of chalcopyrite and pyrrhotite in pyrite of gneisses and metabasic rocks yield formation temperatures of 334 +/-17 °C (Yund and Kullerud 1966) and 328 +/-5 °C (Sugaki et al. 1975).

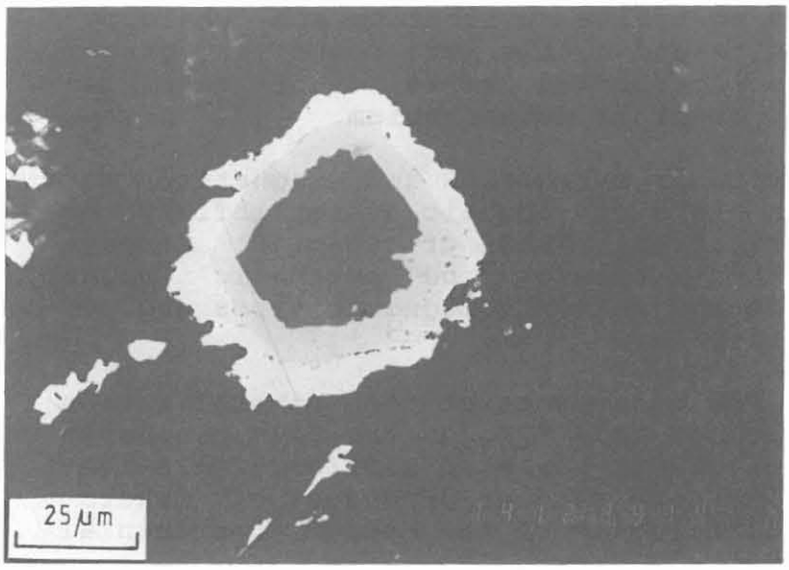

Fig. B.6.7: Very dark-grey spinel (picotite) with zoned rim of magnetite; inner, darker rim consists of chrome-rich magnetite, outer rim is of pure magnetite; in serpentine-chlorite-hornblende fels. (Polished section 911F1ahK, 3719.51 m, // nicols, oil).

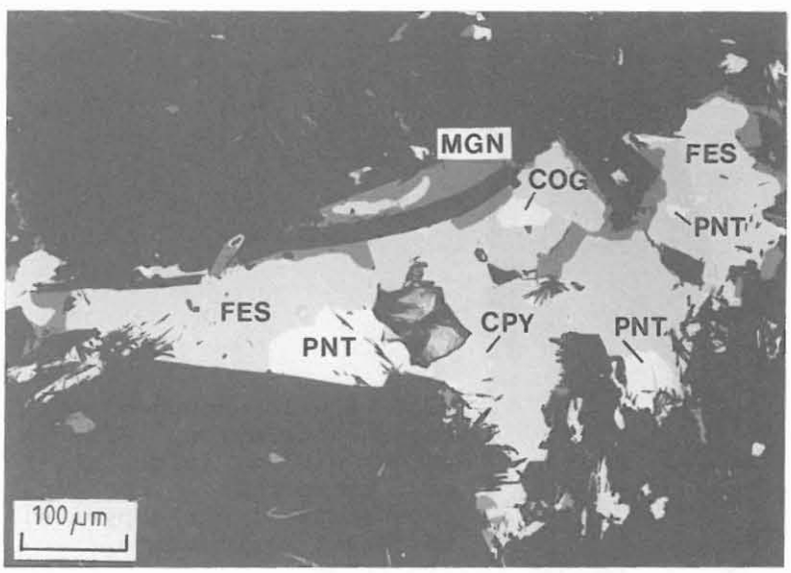

Fig. B.6.8: Complex sulphide-oxide aggregate; pyrrhotite (FES) with flame-like pentlandite (PNT), surrounded by magnetite (MGN), chalcopyrite (CPY) inclusions and cobaltite (COG) accretions; at the far left rim magnetite is bordered by ilmenite; in serpentine-bearing chlorite-hornblende fels. (Polished section 300G1j, 1449.30 m, // nicols).

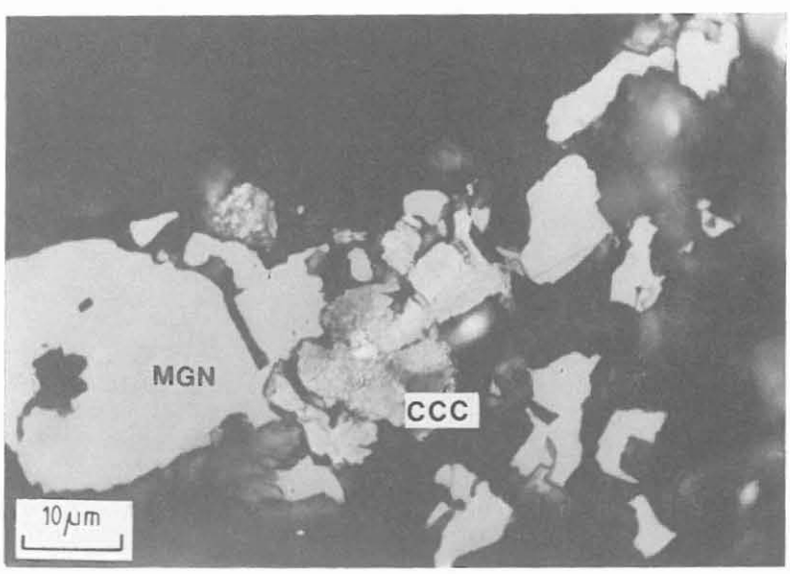

Fig. B.6.9: light-grey, homogeneous magnetite (MGN) intergrown with grey, spherolitic graphite (CCC) in serpentine-chlorite-hornblende fels. (Polished section 911F1ahK, 3719.51 m, // nicols, oil).

Occasionally, inclusions of pyrite, pyrrhotite and chalcopyrite, as well as ilmenite and rutile were found in garnet (Fig. B.6.10) and may be interpreted as relics of mineralization related to early, prograde metamorphism.

The irregular distribution of pyrrhotite and magnetite may easily be recognized in plots of magnetic suszeptibility or natural remanent magnetization (NRM - cf. chap. D: Geophysics). Pyrrhotite within gneisses and metabasic rocks consists of ferrimagnetic and antiferromagnetic types and of combinations of both varieties.

The comparison of type and occurrence of ore mineralization within the KTB pilot hole and hole SG-3 on the Kola peninsula in the USSR (Genkin et al. 1984) revealed similar mineralization and therefore may indicate similar processes of mineralization in equivalent lithologies of the deeper continental crust (Kontny et al. 1990).

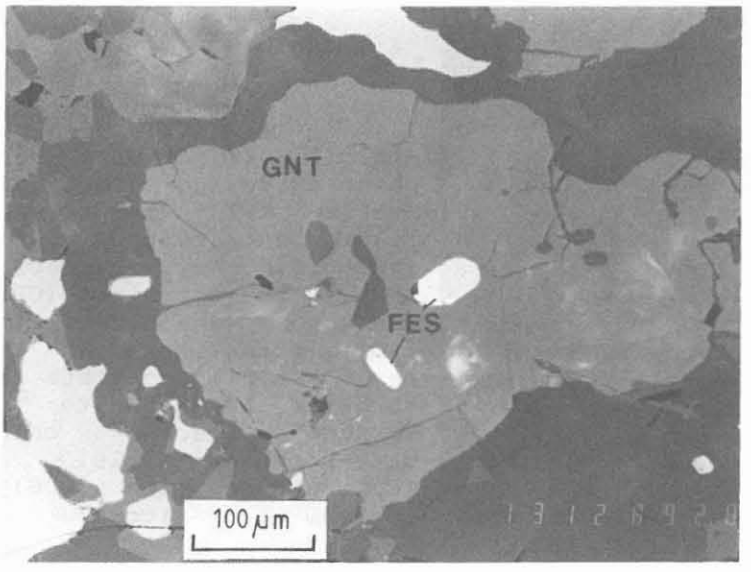

Fig. B.6.10: Rounded pyrrhotite inclusions (FES) in garnet (GNT); large grain of pyrrhotite contains inclusions of chalcopyrite; in garnet amphibolite. (Polished section 916B1f, 3743.14 m, // nicols).

B.7 TECTONIC EVOLUTION

B.7.1 Early ductile deformation

The prominent structural feature documenting intense ductile deformation of the crust at high temperature is the foliation of the gneisses and metabasites. This foliation is partly refolded and a second generation schistosity has developed in the course of progressive deformation (Fig. B.7.1).

In the gneisses three types (end members) of fabrics can be distinguished, each reflecting a certain combination of original fabric, imposed strain and crystallization of the minerals:

(1) medium-grained, flaser structure (Fig. B.7.2)
(2) medium-grained, differentiated layering (Fig. B.7.3)
(3) fine-grained, pronounced compositional banding (Fig. B.7.4)

Fabrics of type (1) are due to growth of plagioclase porphyroblasts after development of a pronounced schistosity (Fig. B.7.5). The same holds true for type (2) fabrics which reflect a stronger compositional differentiation during the earlier stages of progressive deformation and metamorphism (Fig. B.7.6). Fabrics of type (3) are interpreted to have developed in zones of high strain accumulation. The microfabrics are characterized by equigranular fine-grained aggregates of plagioclase obviously formed by dynamic recrystallization of coarse grains. These are locally preserved as porphyroclasts embedded in the fine-grained matrix ("core and rim structure"; Fig B.7.7, B.7.8). Quartz forms coarse-grained ribbons (Fig. B.7.9). Biotite reveals a sharp preferred orientation. The high angle grain boundaries in the feldspar aggregates form "120° triple junctions"; all minerals are optically strain-free, as far as not affected by later deformation (Fig. B.7.10). This points to low stress annealing after high-temperature flow of the rock. Fabrics of type (3) may result from deformation of rocks resembling type (1) and (2) in shear zones developed after the growth of the porphyroblastic plagioclase. The long axes of the aggregates of recrystallized plagioclase and of the quartz ribbons, as well as streaks of fragmented garnet define a stretching lineation. This lineation is paralleled by the axes of small tight to isoclinal folds.

The fabrics of the metabasites reflect a highly inhomogeneous strain-field. In places, the metagabbros have remained essentially unstrained with their magmatic fabrics preserved despite extensive metamorphic reactions. The amphibolites are in part derived from the same protoliths and owe their distinct fabric to a higher strain suffered during high-temperature deformation (Fig. B.7.11). The foliation of these

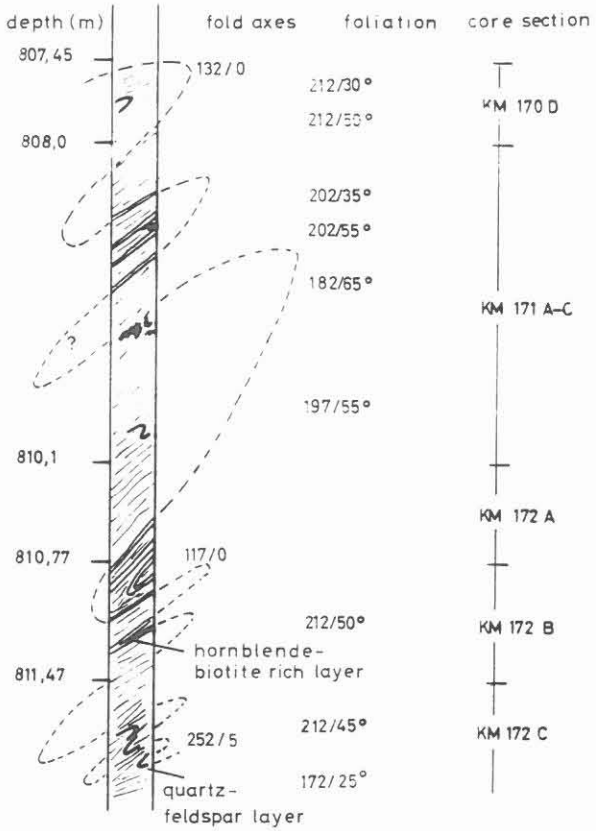

Fig. B.7.1: Folded interlayering of hornblende-biotite gneiss and sillimanite-biotite gneiss between 807.45 and 812.20 m.

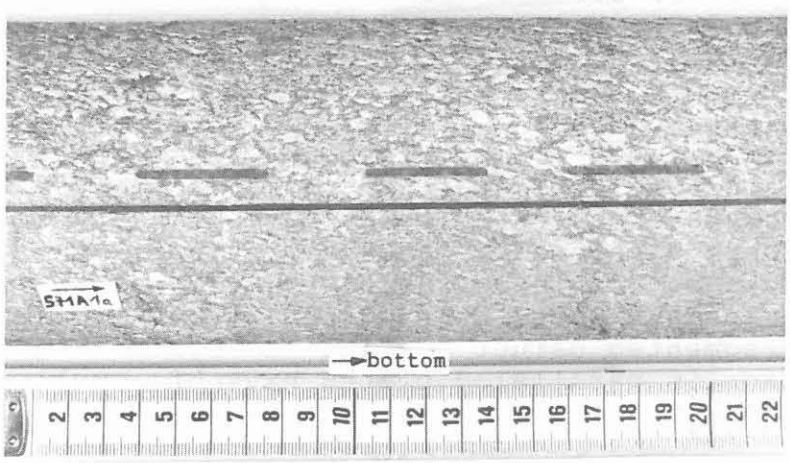

Fig. B.7.2: Sillimanite-biotite gneiss with medium grained flaser fabric of type (1).
(Core piece 571A1a, 2360.4 m, scale in cm).

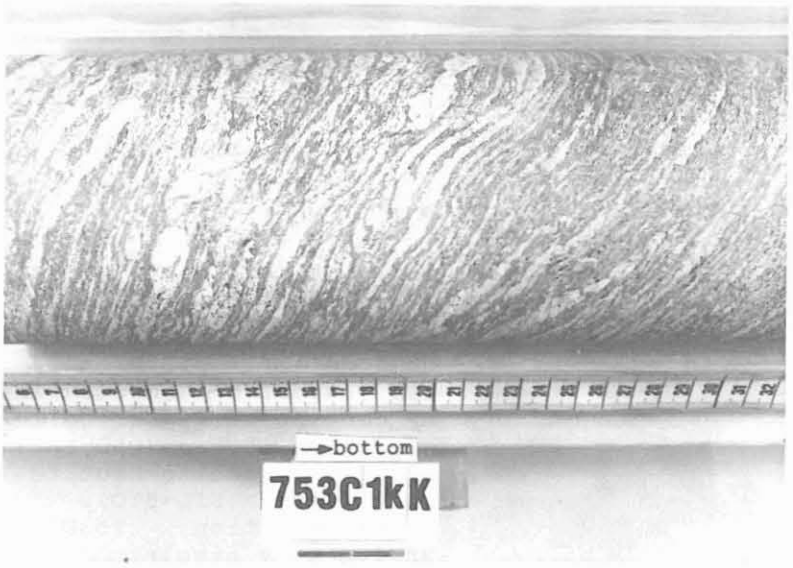

Fig. B.7.3: Sillimanite-biotite gneiss with medium grained, differentiated layered fabric of type (2).
(Core piece 753C1kK, 3075.9 m, scale in cm).

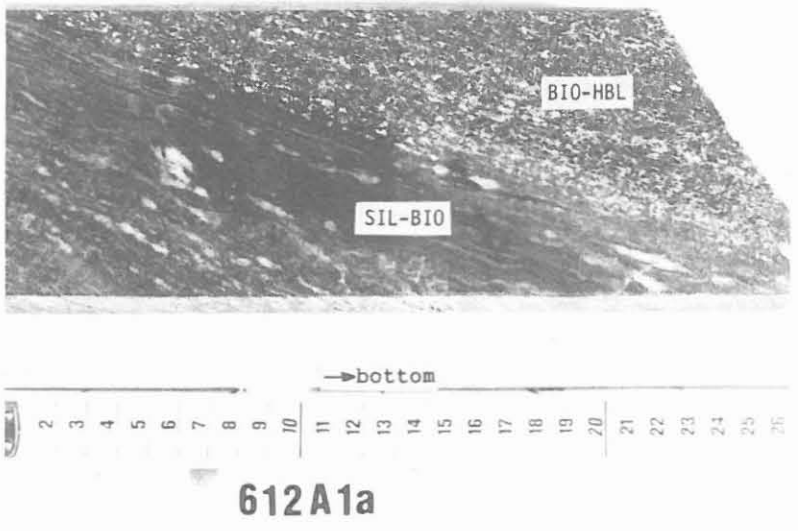

Fig. B.7.4: Fine-grained, mylonitic sillimanite-biotite gneiss of fabric type (3) (SIL-BIO) in contact with biotite-hornblende gneiss (BIO-HBL). The hornblende gneiss shows granular plagioclase and a weak foliation.
(Core piece 612A1a, 1997.7 m, scale in cm).

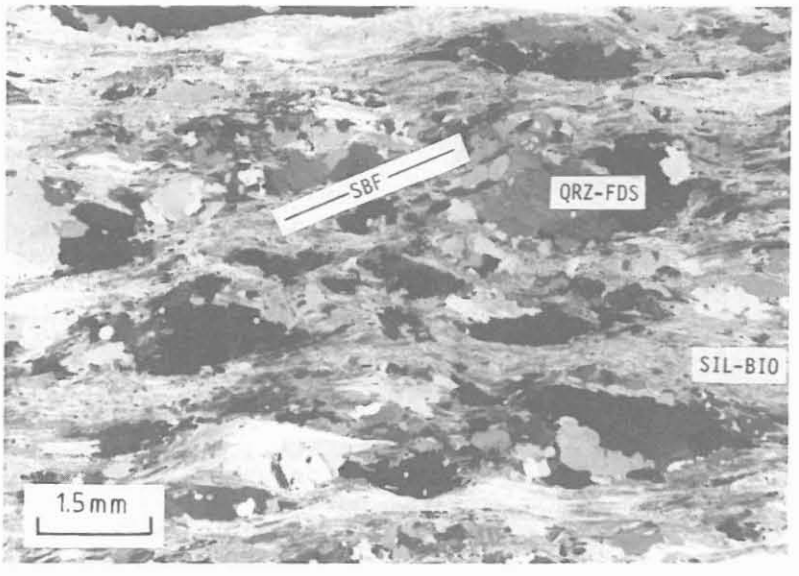

Fig. B.7.5: Flaser structure of gneiss fabric type (1). Sillimanite-biotite layers (SIL-BIO) and elongated quartz-feldspar (QRZ-FDS) augen form an anastomosing foliation. A shear band foliation (SBF) is weakly developed.
(Thin section 571A1a, 2360.4 m, + nicols).

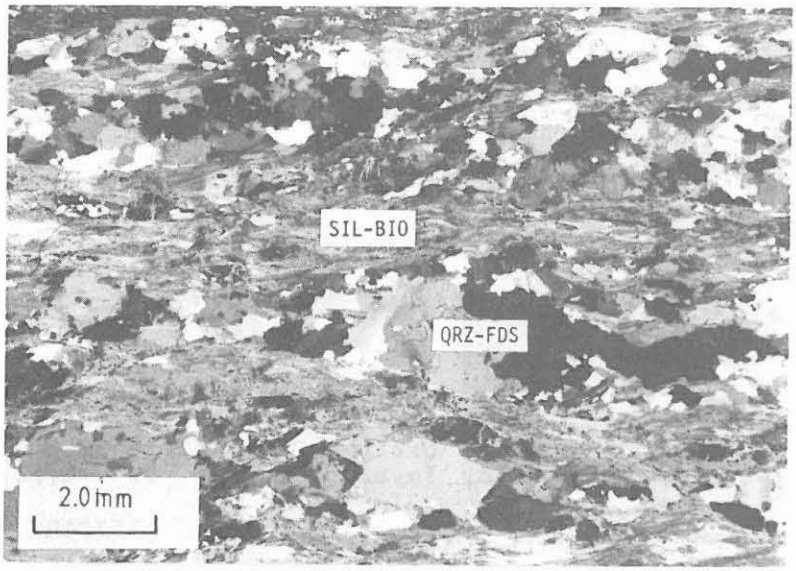

Fig. B.7.6: Gneiss fabric of type (2). Differentiated layering, documented by continuous quartz-feldspar-rich layers (QRZ-FDS) and sillimanite-biotite-rich layers (SIL-BIO). (Thin section 753D1m, 3076.5 m, + nicols).

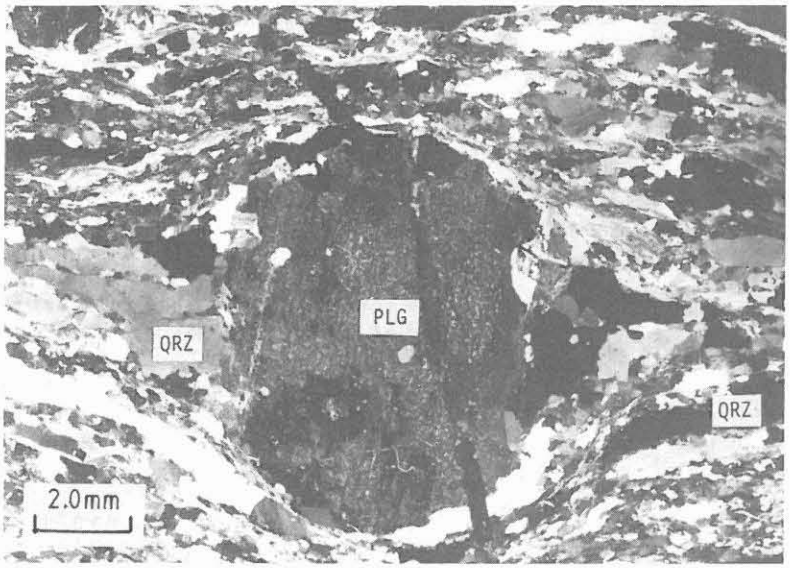

Fig. B.7.7: Plagiclase clast (PLG) without recrystallized seam in gneiss of fabric type (3). An asymmetric shape of sigma-type is generated by ribbon quartz (QRZ). (Thin section 424G113, 1882.5 m, + nicols).

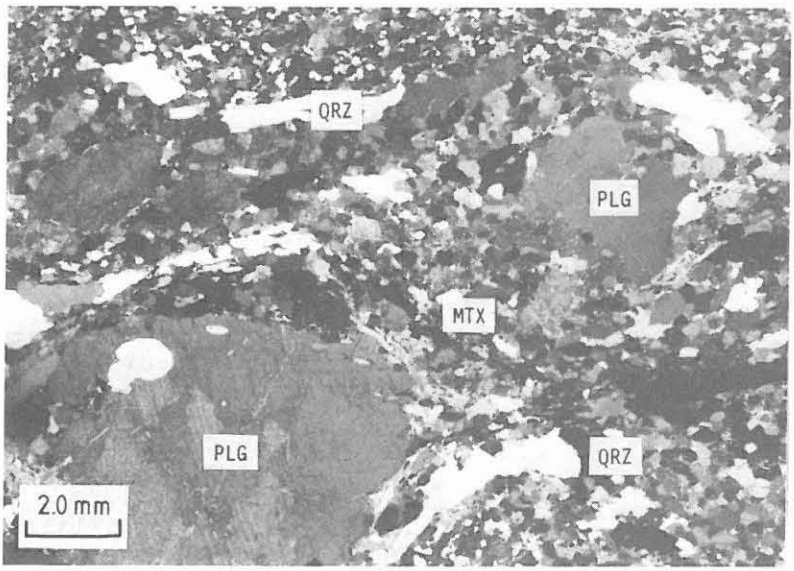

Fig. B.7.8: Plagioclase clasts (PLG) in gneiss of fabric type (3). Coarse host grains are embedded in a fine-grained matrix (MTX) and form "core and rim structures". Elongated, coarse-grained ribbon quartz (QRZ) surrounds the porphyroclasts and defines the foliation. (Thin section 552E1wKII, 2309.6 m, + nicols).

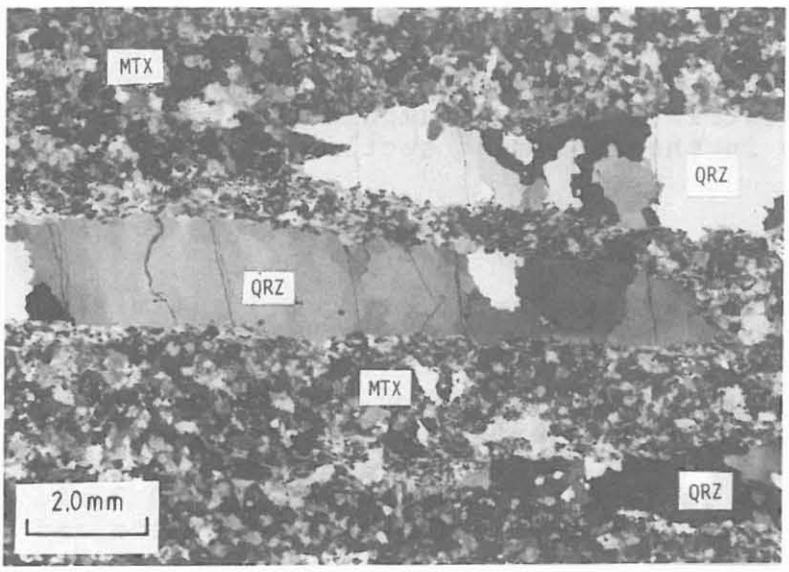

Fig. B.7.9: Gneiss fabric type (3). Coarse-grained ribbon quartz (QRZ) with sutured grain boundaries in a fine-grained quartz-feldspar matrix (MTX). Undulose extinction in quartz results from a late stage of deformation. (Thin section 922A1b, 3775.9 m, + nicols).

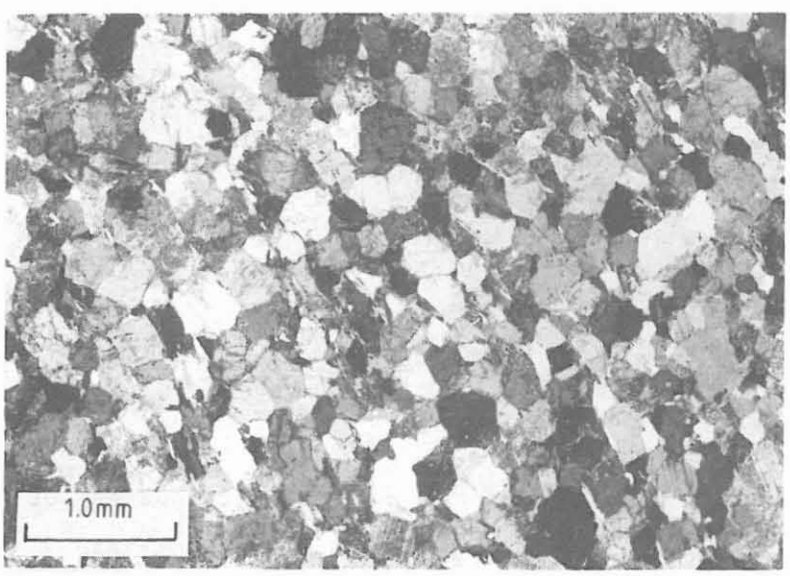

Fig. B.7.10: Plagioclase aggregate in gneiss fabric of type (3). Microfabric is characterized by equigranular grains with straight grain boundaries, forming 120° "triple junctions". (Thin section 139C6T, 705.6 m, + nicols).

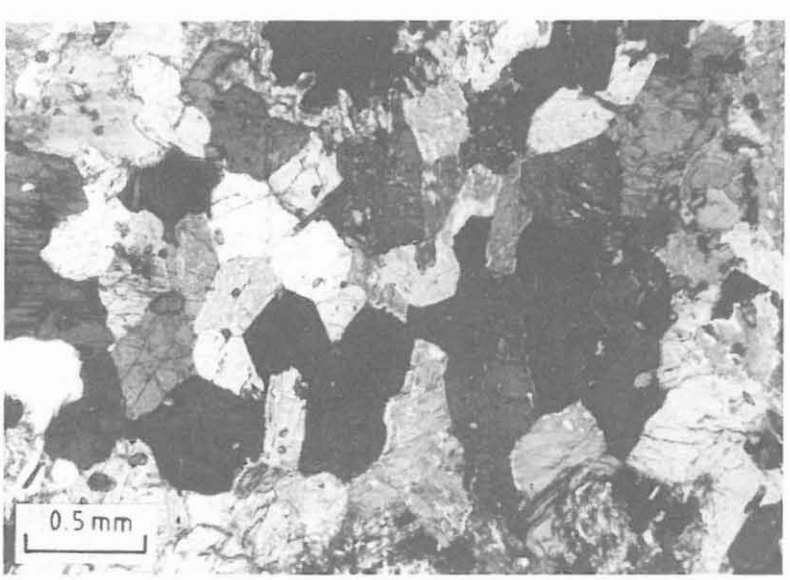

Fig. B.7.11: Microfabric in medium-grained, foliated amphibolite. Grain boundaries in a hornblende aggregate are straight and meet in "triple-junctions". (Thin section 59B6d, 401.2 m, + nicols).

rocks is defined by a weak lattice and shape preferred orientation of the amphiboles. Local shear zones and conspicuous flaser gabbros reflect strain rate gradients. Marked compositional layering is restricted to the amphibolite-calcsilicate series occuring in the uppermost section of the hole down to 460 m.

B.7.2 Late deformation in the semi-brittle and brittle field

The interval 3000 - 3500 m is dominated by mesoscopic folds with 30 to 50° inclined axial planes and compressive kink bands with steep kink band boundaries. Transition into SE-trending reverse faults is frequent (Fig. B.7.12, B.2.3.c). The microfabric of both shows recrystallization of quartz and cataclasis of plagioclase.

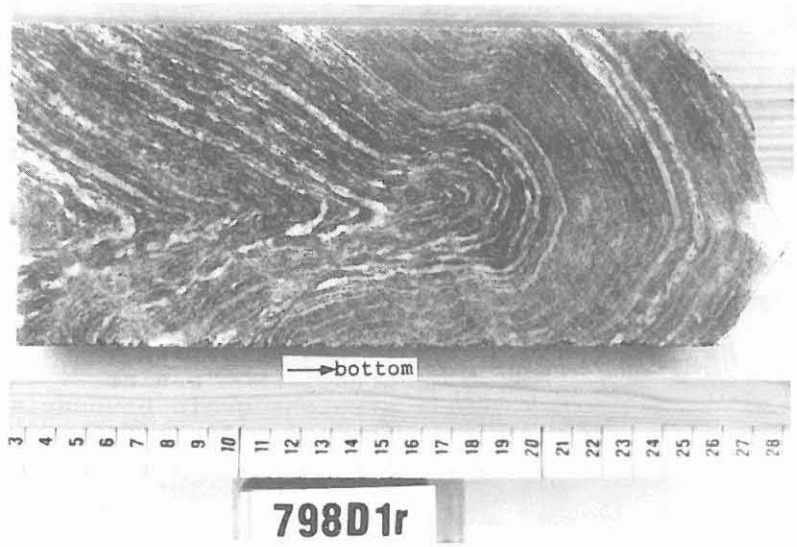

Fig. B.7.12: Tight to open fold in sillimanite-biotite gneiss of type (2).
(Core piece 798D1r, 3272.0 m, scale cm).

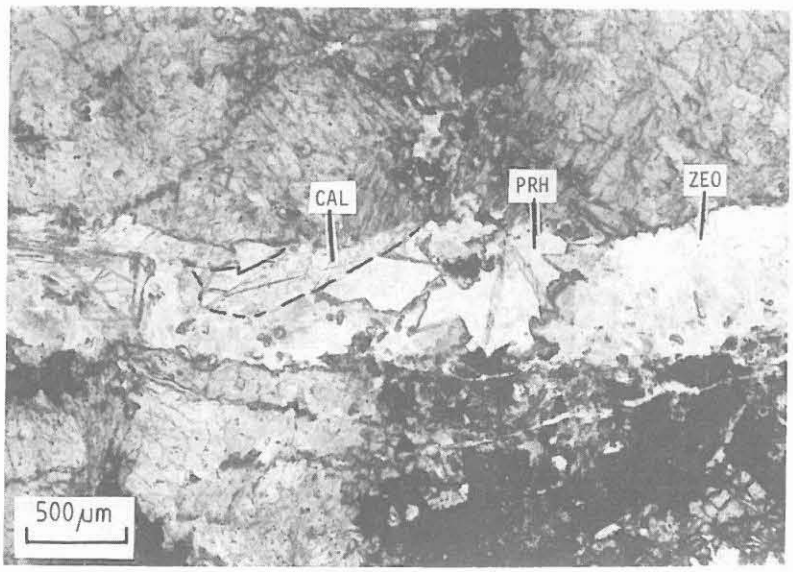

Fig. B.7.13: Low-temperature metamorphic overprint in metagabbro: fissure mineralized with zeolite (ZEO), prehnite (PRH) and calcite (CAL).
(Thin section 326D1p, 1559.9 m, // nicols).

The polyphase deformation in the brittle field has started with the development of subvertical tension gashes primarily within the metabasites (Fig. B.7.13). There they are mineralized with prehnite ± epidote ± actinolite (prehnite-actinolite facies). They never cut other brittle structures. The oldest of three later generations of reverse faults is observed only below 3050 m and is due to an E-W compression (Fig. B.7.14a). The second generation of reverse faults, resulting from NE-SW compression, are observed in the entire hole. They are characterized by graphite enrichment on the fault planes within the corresponding cataclasites of the gneisses (Fig. B.7.14.b and B.7.15). In one case a lamprophyre has intruded a graphite-cataclasite (Fig. B.7.16). As the lamprophyres are probably slightly younger than the granite intrusion age of 311 Ma (Wendt et al. 1986), this might imply a late-Variscan age for this graphite-bearing fault generation. A third generation of (oblique) reverse faults was generated by N-S compression (Fig. B.7.14.c and B.7.17).

Normal faults in metabasites and in gneisses with subhorizontal foliation are the result of an E-W extension. Open folds as well as extensional kinks in sections with nearly vertical foliation (Fig. B.7.18) are other features of this extension direction. Such folds and kink bands are common from 1700 to 2500 m and have near horizontal axial planes and kink band boundaries. The faults are mineralized with laumontite and often follow older structures in their orientation (Fig. B.7.14d).

The volumetric proportion and individual thickness of cataclasites tends to decrease with increasing depth (Fig. B.7.18). Fault breccias of several dm thickness are restricted to the upper part of the hole (Fig. B.7.19). Down to 3575 m, sections with more than 0.5 Vol.-% of cataclastic rock (measured per 50 m) are often bound to large contrasts in competence (Fig. B.7.18). The reduction in thickness of brittle shear zones is probably a consequence of increasing confining pressure due to increasing depth (Sammis et al. 1980, 1986; Anderson et al. 1980, 1983).

Quartz, calcite, chlorite, prehnite, laumontite, feldspars and sulphides represent the fissure minerals (Figs. B.7.13, B.7.20, B.7.21). Calcite is prominent in amphibolites and lamprophyres, whereas it is subordinate in gneisses compared with laumontite. Prehnite (and epidote) mineralization increases with depth, while laumontite decreases (Fig. B.7.18).

From 3447 m to final depth several, maximum 1 cm wide, open fissures filled with methane and helium bearing saline brines were intersected. Dissolved gases without detectable associated formation water were present in some fault zones up to 1100 m (cf. chapter C.2). Fig. B.7.22 shows a normal fault zone consisting of cataclasite and a ultra-cataclasite with fault gouge (3200 m), and Fig. B.7.23 an open fissure with calcite crystals (3447 m): both yielded gas.

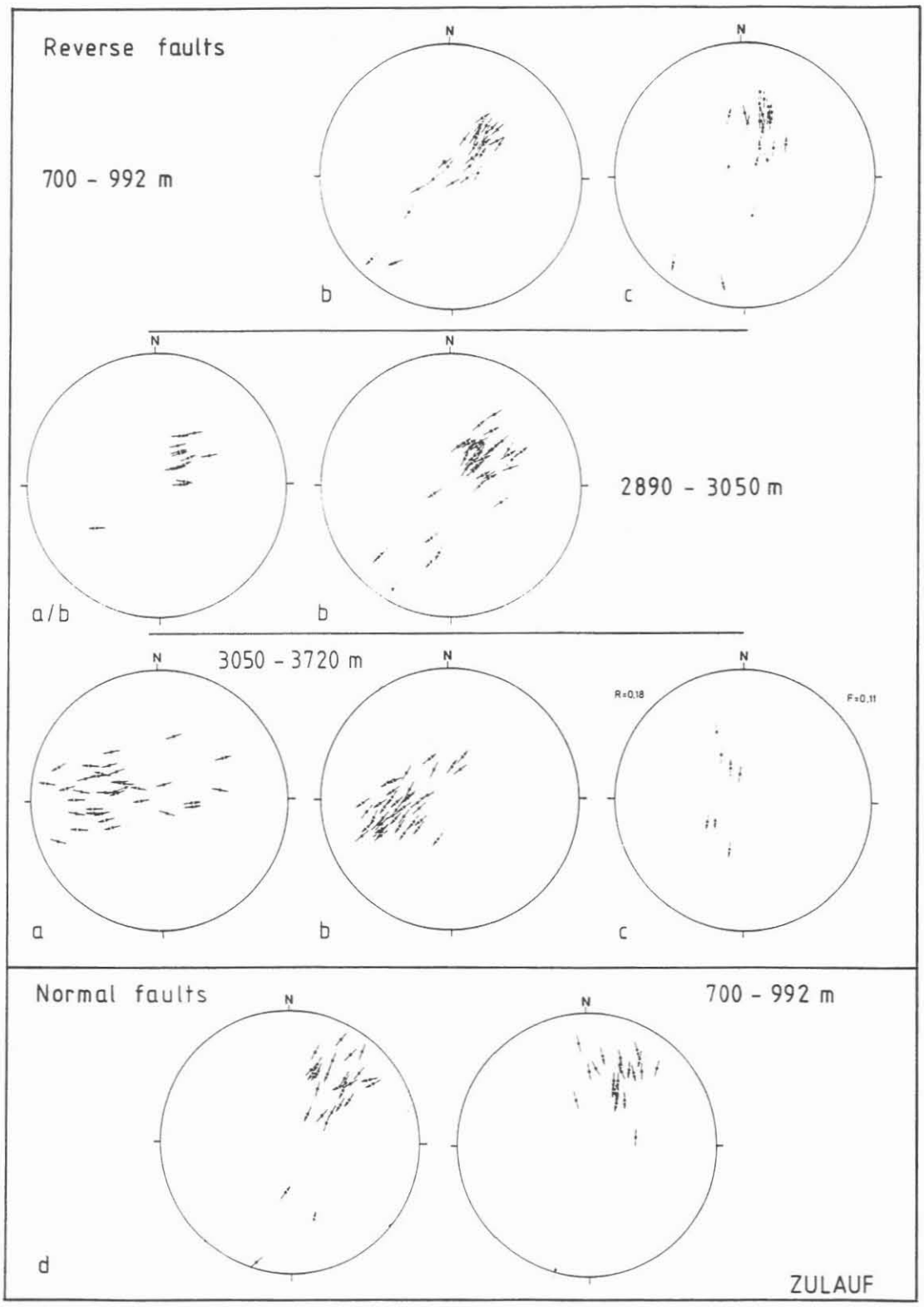

Fig. B.7.14: Fault populations. Poles of slickensides with traces of affiliated striae are shown following Hoeppener (1955). The arrows indicate the shear sense of the hanging-wall. The different generations are indicated by a,b,c,d (early to late).

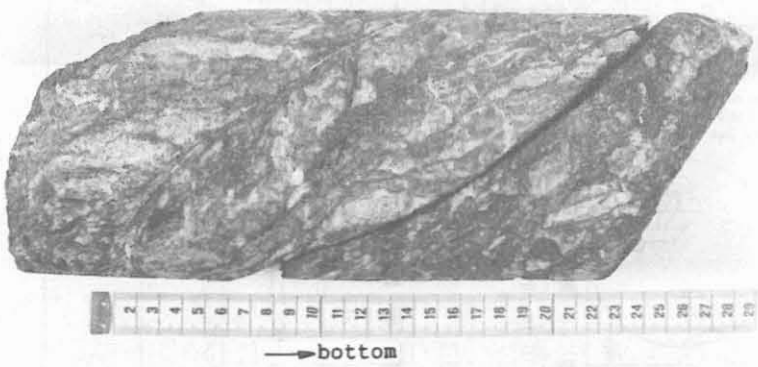

Fig. B.7.15: Cataclasite in the fault zone from 192 - 194 m. Graphite is abundant in the matrix and on slickensides. (Core piece 27A2a, scale in cm).

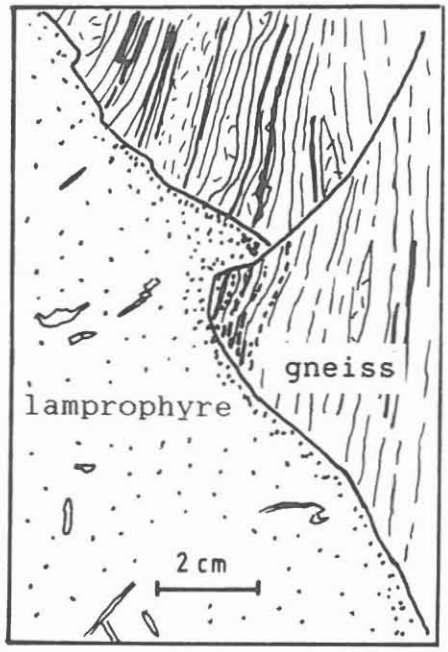

Fig. B.7.16: Small scale reverse fault in paragneiss is cut off by lamprophyre. (Core piece 536A1b, 2257 m).

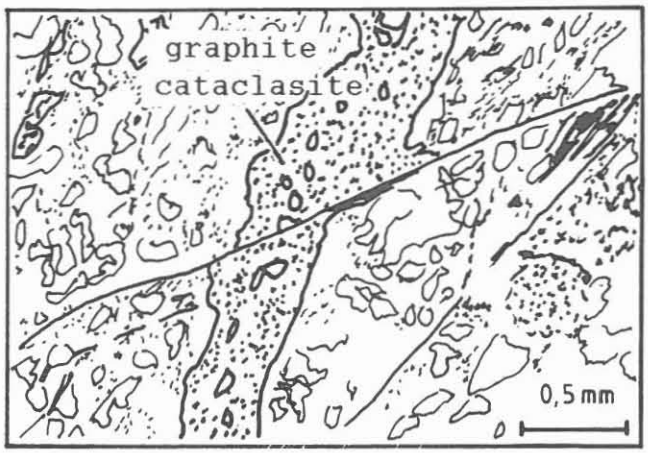

Fig. B.7.17: Graphite-bearing cataclasite is displaced along a reverse fault (drawing from thin section 617H1tK, 2537.8 m).

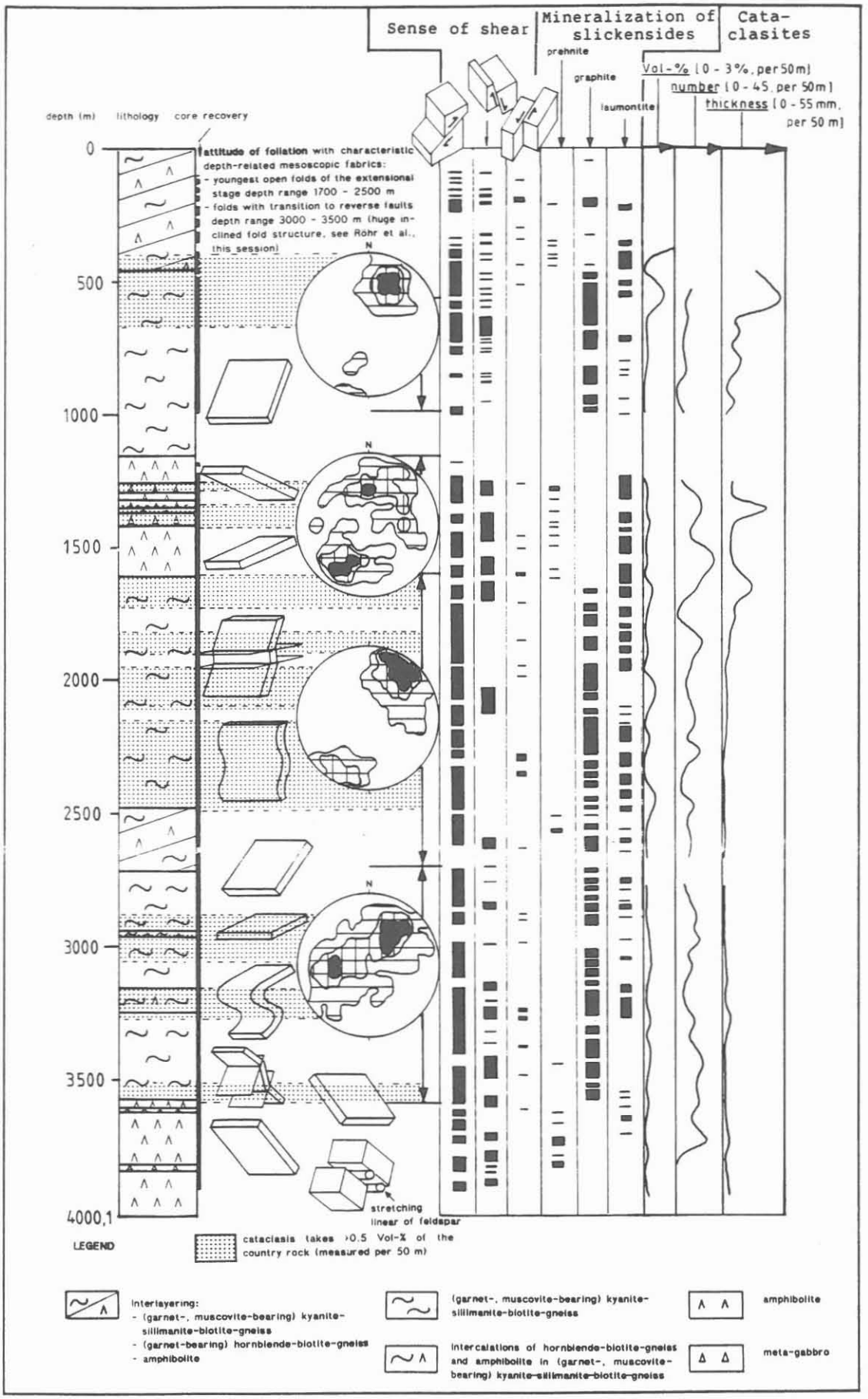

Fig. B.7.18: Synoptic diagram of lithology, attitude of foliation, sense of shear of faults, mineralization of slickensides, Vol.-%, number and thickness of cataclasites versus depth.

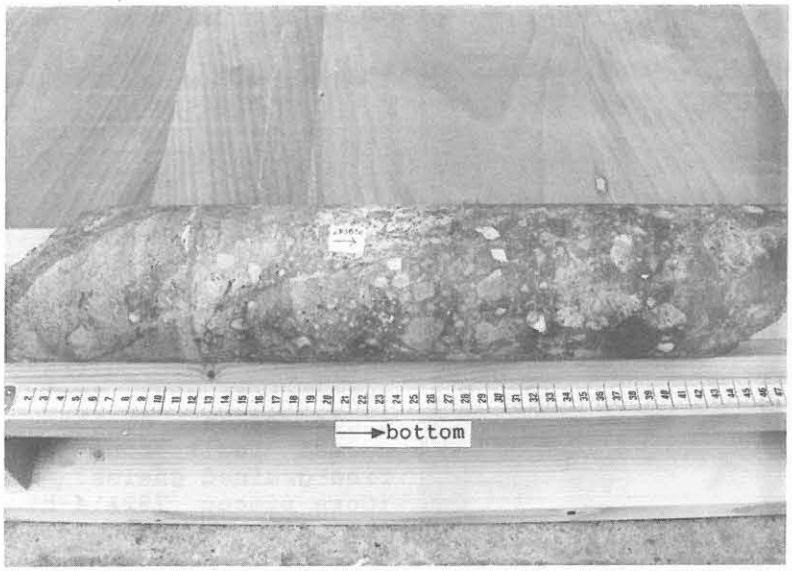

Fig. B.7.19: Fault breccia in amphibolite. Coarse-grained, angular porphyroclasts are embedded in a fine-grained matrix. (Core piece 283B1e, 1351.4 m, scale in cm).

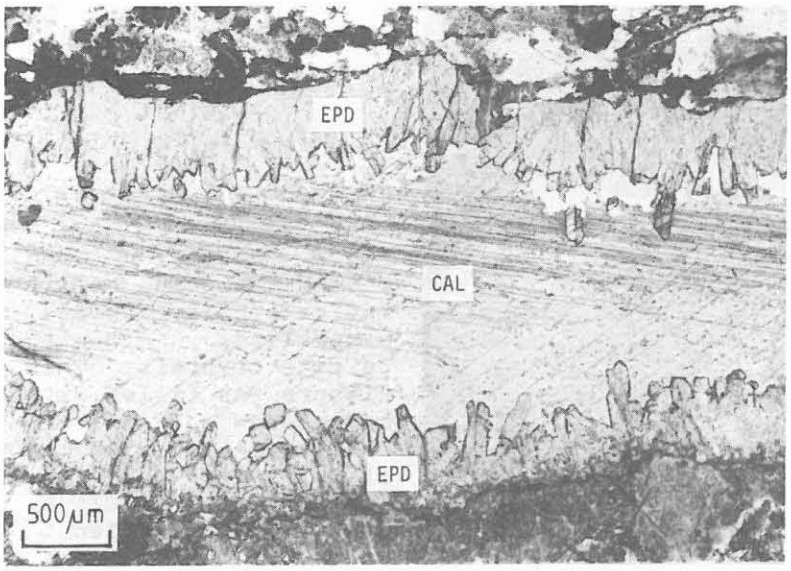

Fig. B.7.20: Fissure within hornblende-biotite gneiss, mineralized with epidote (EPD), grown normal to fissure planes and younger calcite (CAL). (Thin section 633A2aK, 2614.73 m, // nicols).

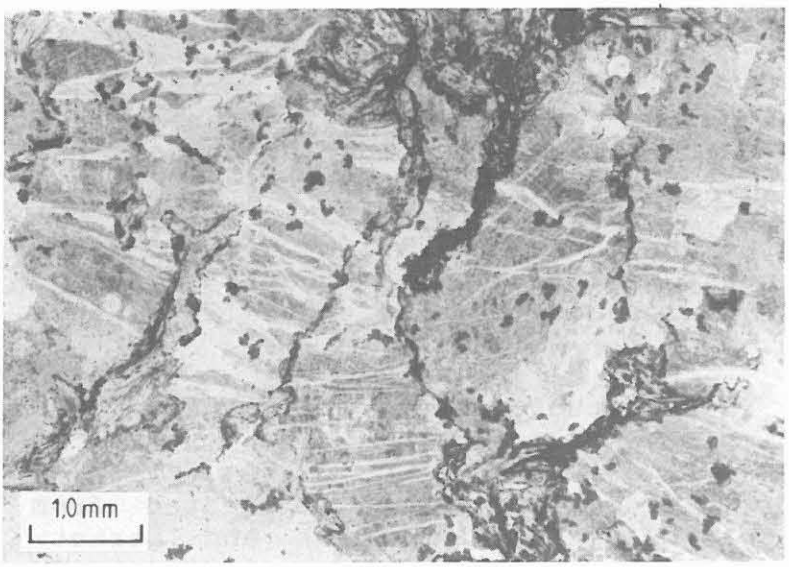

Fig. B.7.21: Fissure within garnet-biotite gneiss, mineralized with albite and/or zeolite. (Thin section 838A1c, 3429.7 m, // nicols).

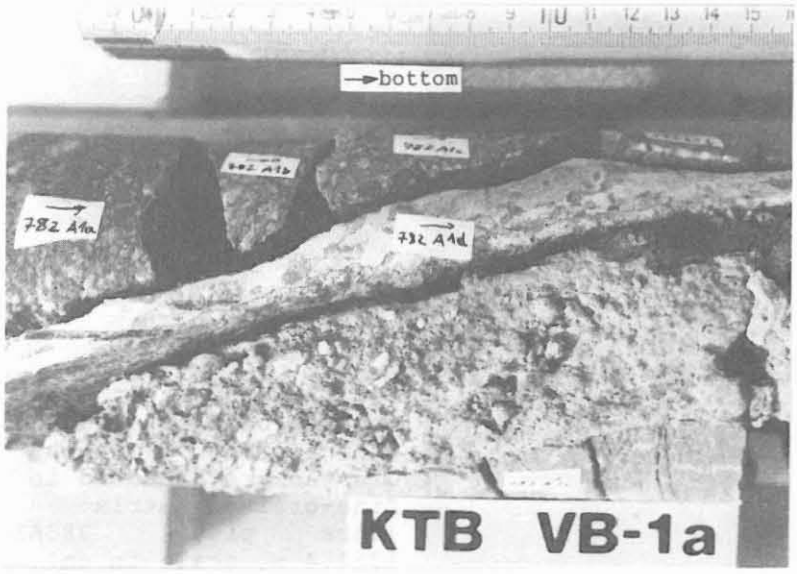

Fig. B.7.22: Cataclasite and thin ultracataclasite with fault gouge of a dm-thick normal fault zone in fine-grained gneiss. (Core pieces 782A1a-h, 3199.4 m, length 15 cm).

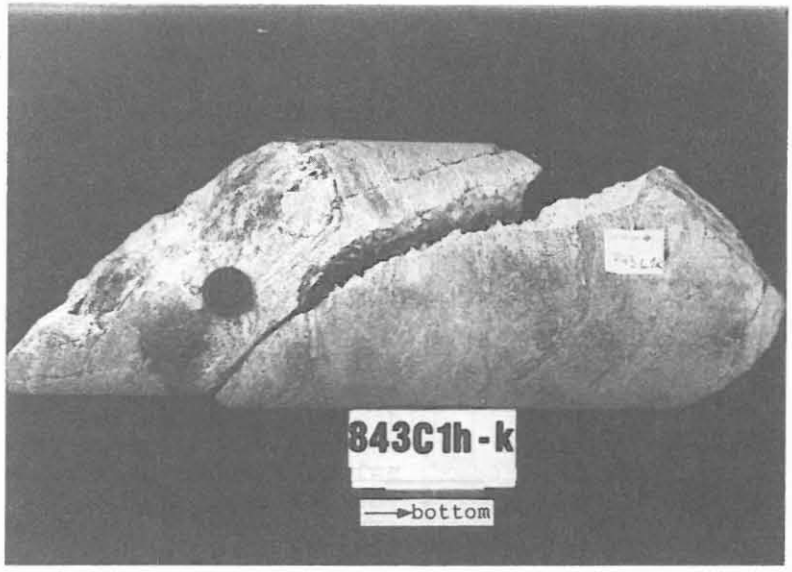

Fig. B.7.23: Open fissure within sillimanite-biotite gneiss, mineralized with calcite crystals. This fissure was filled with a methane- and helium-bearing, high saline brine. (Core pieces 843C1h-k, 3447 m, total length 26 cm).

B.7.3 Synopsis of deformation and metamorphism

The polystage metamorphic development included early high-pressure stages. Judging from recent discovery of an retrogressed eclogitic rock in the immediate neighbourhood of the KTB pilot hole (Röhr et al., in prep.) eclogite facies conditions seem possible for the borehole rocks. This stage was followed by a high-pressure granulite facies stage, documented by various clinopyroxene-plagioclase-quartz symplectites, an amphibolite facies metamorphism and a late low-temperature alteration.

A tentative p-T-path is constructed from preliminary geothermobarometric results:

Minimum conditions of 14 kbar, 730 °C are indicated from albite-jadeite-quartz barometry (Holland 1980) and garnet-clinopyroxene geothermometry (Ellis and Green 1979) using clinopyroxenes included in garnet.

The jadeite-content of the clinopyroxene symplectites around 10 mol-% indicate equilibration around 10 kbar for the inferred temperatures. The same pressure and temperature range is indicated by garnet-kyanite-plagioclase-quartz-geothermobarometry.

Pressure and temperature of the amphibolite facies stage were determined as 675±50°C and 7±1 kbar by Reinhardt and Kleemann (1989) for the garnet-sillimanite-kyanite-biotite paragenesis of the gneisses.

The ductile deformation of the metabasites is characteristic of that formed at high-temperature.

The deformation in the semi-brittle and brittle field took place under greenschist facies conditions. It started with tension gashes and close to open folds. Slickenside and fissure mineralization have developed during stepwise decreasing temperatures and pressures.

B.7.4. Implications for tectonics

The evolution of rocks of the Zone of Erbendorf-Vohenstrauss may be sketched as follows:

(1) Amphibolite-Metagabbro-Sequence => former olivine-tholeiites of mid ocean ridge and ocean island composition => chemical character of oceanic crust,

(2) Garnet-Al_2SiO_5-muscovite-biotite-gneisses => former greywackes and claystones of possible flyschoid character => ? active plate margin sediments,

(3) Eclogite facies metamorphism => deep crustal depth (around 40 km) => ? subduction of melange of oceanic crust and active plate margin sediments,

(4) Uplift, eventually to intermediate crustal depth of around 20 km => from eclogite facies to the high-pressure granulite facies to the dominating amphibolite facies conditions.

(5) Cooling down to about 350 °C and slight uplift

(6) Low temperature deformation in the brittle field.

The continuous boundary between the gneisses of greywacke composition and the amphibolite-metagabbro sequence (Fig. B.7.24) demonstrate that both units had a common history at least since adaption to amphibolite facies conditions.

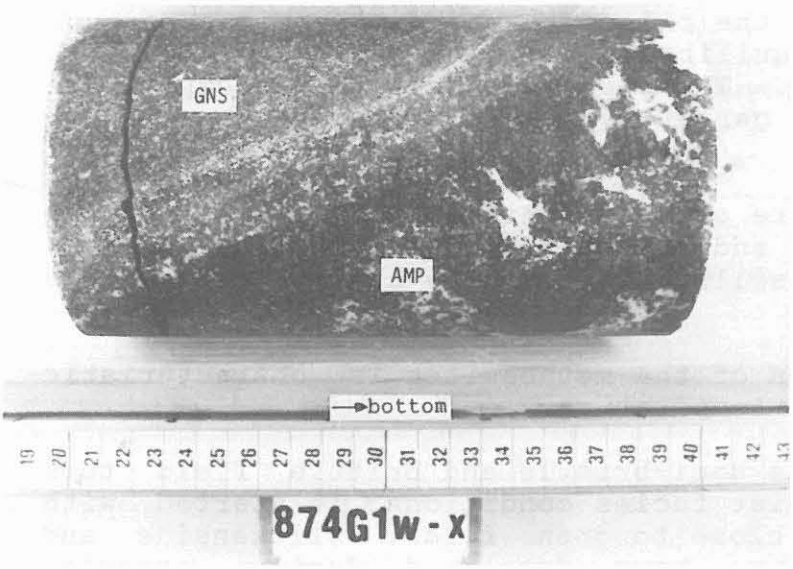

Fig. B.7.24: Concordant boundary between monotonous gneiss (GNS) and the lower amphibolite-metagabbro sequence (AMP) at 3573.5 m. (Core pieces 874G1w-x).

ACKNOWLEDGEMENTS

We thank Prof. Friedrich, Aachen, Prof. von Gehlen, Frankfurt, Dr. Herzig, Aachen, Prof. Stöckhert, Bochum and Prof. Weber, Göttingen for their critical and improving comments. Microprobe measurements were done at Bayerisches Geoinstitut, Bayreuth and at Institut for Mineralogy and Economic Geology, RWTH Aachen. We thank P. O'Brien, Bayreuth, for assistance and helpful discussions about high pressure metamorphism and for improving the English text. G. Hirschmann, Hannover, provided orientation data of the foliation.

REFERENCES

Anderson, J.L., Osborne, R.H., and Palmer, D.F. (1980): Petrogenesis of cataclastic rocks within the San Andreas fault zone, Southern California, U.S.A.- Tectonophysics, 76: 221-249.

Anderson, J.L., Osborne, R.H., and Palmer, D.F. (1983): Cataclastic rocks of the San Gabriel fault: An expression of deformation at deeper levels in the San Andreas fault zone.- Tectonophysics, 98: 209-251.

Blümel, P. (1983): The western margin of the Bohemian Massif in Bavaria.- Fortschr. Mineral., 61, Beiheft 2, 171-195, Stuttgart.

Dill, H. (1985): Die Vererzung am Westrand der Böhmischen Masse - Metallogenese in einer ensialischen Orogenzone.- Geol. Jb., D73, 3-461, Hannover.

Dill, H. (1988): Lagerstätten-Typisierung und metallogenetische Entwicklung im Umfeld der Grenzregion Saxothuringikum-Moldanubikum (Nordbayern) - ein Überblick.- Geol. Bavarica, 92, 133-150, München.

Ellis, D.J. and Green, D.H. (1979): An experimental study of the effect of Ca upon garnet - clinopyroxene Fe-Mg exchange equilibria.- Contrib. Mineral. Petrol., 71: 13-22.

Franke, W. (1989): The geological framework of the KTB drill site, Oberpfalz.- In: Emmermann, R. and Wohlenberg, J. (ed.): The German Continental Deep Drilling Program (KTB): 37-54, Springer-Verlag, Berlin.

Friedrich, G. (1989): Erzpetrologie im Kontinentalen Tiefbohrprogramm: Sulfidmineralisation in Paragneisen und Amphiboliten der KTB-Vorbohrung, Oberpfalz.- Europ. J. Mineralogy, Vol. 1, Beih., 51 (abstract), Stuttgart.

Genkin, A.D., Gorbunov, G.I., Kazansky, V.I., Lanev, V.S., Filimonova, A.A. and Yakovlev, Y.N. (1984): Ore Mineralization.- In: Kozlovsky, Y.A. (ed.): The Superdeep Well of the Kola Peninsula.- S. 199-222, Springer-Verlag, Berlin.

Hansen, B.T., Teufel, S., and Ahrendt, H. (1989): Geochronology of the Moldanubian-Saxothuringian Transition Zone, Northeast Bavaria.- In: Emmermann, R. and Wohlenberg, J. (ed.): The German Continental Deep Drilling Program (KTB): 55-65, Springer-Verlag, Berlin.

Hoeppener, R. (1955): Tektonik im Schiefergebirge.- Geol. Rundsch., **44**: 26 - 58.

Holland, T.J.B. (1980): The reaction albite = jadeite + quartz determined experimentally in the range 600-1200°C.- Amer. Mineral., **65**: 129-134.

Kontny, A. and Friedrich, G. (1989): Bildungstemperaturen im Cu-Fe-Zn-S-System am Beispiel einer metamorphen Sulfidmineralisation in der Zentralzone Erbendorf-Vohenstrauss.- Europ. J. Mineralogy, Vol. 1, Beih., 100 (abstract), Stuttgart.

Kontny, A., Friedrich, G., Herzig, P., Keyssner, S. and Vogtmann-Becker, J. (1990): Erzmineralparagenesen und Mineralisationstypen in der KTB Vorbohrung.-In: Emmermann, R. & Giese, P. (Hrsg.): Beiträge zum 3. KTB-Kolloquium, Gießen, 28.2. bis 2.3.1990. - KTB Report, **90-4** (in press).

Kreuzer, H., Seidel, E., Schüssler, U., Okrusch, M., Lenz, K.-L., and Raschka, H. (1989): K-Ar geochronology of different tectonic units at the northwestern margin of the Bohemian Massif.- Tectonophysics, **157**: 149-178.

O'Brien, P.J. (1989): The petrology of retrograded eclogites of the Oberpfalz Forest, northeast Bavaria, West Germany.- Tectonophysics, **157**: 195-212.

Okrusch, M. Seidel, E. Schüssler, U., and Richter, P. (1989): Geochemical Characteristics of Metabasites in Different Tectonic Units of the Northeast Bavarian Crystalline Basement.- In: Emmermann, R., Wohlenberg, J. (ed.): The German Continental Deep Drilling Program (KTB): 67-79, Springer-Verlag, Berlin.

Patzak, M., Okrusch, M. and Röhr, C. (1989): Metabasite der KTB-Vorbohrung: Vorläufige Ergebnisse bis 1610 m.- In: Emmermann, R. and Giese, P. (ed.): Beiträge zum 2. KTB-Kolloqium, Giessen, 15.-17.3.1989.- KTB Report, **89-3**, 67-80.

Reinhardt, J. and Kleemann, U. (1989): Phasenpetrologische Analyse und Geothermobarometrie der Metapelite in der Zone von Erbendorf-Vohenstrauss (ZEV), Oberpfalz.- Europ. J. Mineralogy, Vol. 1, Beih., 152 (abstract), Stuttgart.

Röhr, C., Patzak, M., and Okrusch, M. (1990): Metamorphose-Entwicklung der Metabasite der KTB Vorbohrung.- In: Emmermann, R. and Giese, P. (ed.): Beiträge zum 3. KTB-Kolloqium, Giessen, 28.2 bis 2.3.1990.- KTB Report, **90-4** (in press).

Sammis, C.G., Osborne, R.H., Anderson, J.L., and Banerdt, M. (1980): Reading stress from cataclastic rocks.- EOS Trans. Amer. Geophys. Union, **61**: 1118.

Sammis, C.G., Osborne, R.H., Anderson, J.L., Mavonwe, B., and White, P. (1986): Self-similar cataclasis in the formation of fault gouge.- Pure appl. Geophys., **124**: 53-78.

Schmitz, D., Hirschmann, G., Kessels, W., Kohl, J., Röhr, C., and Dietrich, H.-G. (1989): Core orientation in the KTB pilot well.- Scientific Drilling, **1**: 150-155.

Schreyer, W. (1966): Metamorpher Übergang Saxothuringikum - Moldanubikum östlich Tirschenreuth/Opf., nachgewiesen durch phasenpetrologische Analyse.- Geol. Rdsch., **55**: 481-509.

Schüssler, U. (1987): Petrographie, Geochemie und Metamorphosealter von Metabasiten im KTB-Zielgebiet Oberpfalz.- Ph.D. thesis, Würzburg.

Stettner, G. (1979): Der Grenzbereich Saxothuringikum - Moldanubische Region im Raum Tirschenreuth - Mähring (Oberpfalz) und die Situation des Uran-führenden Präkambriums.- Z. Dtsch. Geol. Ges., **130**: 561-574.

Sugaki, A., Shima, H., Kitakaze, A. and Harada, H. (1975): Isothermal phase relations in the system Cu-Fe-S under hydrothermal conditions at 350 °C and 300 °C.- Econ. Geol., **70**, 806-823, El Paso.

Teufel, S. (1988): Vergleichende U-Pb- und Rb-Sr-Altersbestimmungen an Gesteinen des Übergangsbereiches Saxothuringikum/Moldanubikum, NE-Bayern.- Göttinger Arb. Geol. Paläont., **35**: 87 p.

Weber, K. and Vollbrecht, A. (ed.) (1986): Ergebnisse der Vorerkundungsarbeiten - Lokation Oberpfalz.- 2. KTB-Kolloquium 19.-21.9.1986, Seeheim/Odenwald, 186 p. (unpublished).

Weber, K. and Vollbrecht, A. (1989): The Crustal Structure at the KTB Drill Site, Oberpfalz.- In: Emmermann, R. and Wohlenberg, J. (ed.): The German Continental Deep Drilling Program (KTB): 5-36, Springer-Verlag, Berlin.

Wendt, I., Kreuzer, H., Müller, P., and Schmid, H. (1986): Gesamtgesteins- und Mineraldatierung des Falkenberger Granits.- Geol. Jahrb. **E34**: 5-66.

Yund, R.A. and Kullerud, G. (1966): Thermal stability of assemblages in the Cu-Fe-S-system.- J. of Petrol., **7**, 454-488.

KTB Report	90-8	C1-C37	14 Fig.	Hannover 1990

Drill Hole KTB Oberpfalz VB, Geoscientific Investigations in the KTB-Field-Laboratory, Depth interval 0 - 4000.1 m

C. Geochemistry / Mineralogy

Stroh, A., Hansmann, J., Heinschild, H.-J., Homann, K.D., Tapfer, M., Wittenbecher, M., Zimmer, M. *)

*) Authors address: KTB Feldlabor
D-8486 Windischeschenbach

Summary

Extensive geochemical investigations of cores, cuttings, rock flour, drilling fluid, formation waters, and dissolved gases formed an essential part of the geoscientific work in the KTB field laboratory.

Investigation of mineralogical and chemical composition of solids proved that identification of drilled rocks is possible using only cuttings or rock flour (centrifuge samples). These data correspond to a high degree to the lithostratigraphic profile obtained from petrological core data and microscopic description.

The profile established on rock flour samples can be described as follows:

In the interval 0-460 m a metabasic-metapelitic sequence was encountered. The metapelites are garnet-biotite-gneisses, kyanite-sillimanite-garnet-biotite-gneisses, and hornblende gneisses. The metabasites comprise mainly amphibolites and consist of amphibole, plagioclase, chlorite, ±garnet, ±alkali feldspar and ±sphene.

From 460 - 1160 m monotone sillimanite-biotite-paragneisses with subordinate quartz-diorite and amphibolite were penetrated.

The depth interval 1160 - 1610 m exhibits a variegated unit of amphibolites, metagabbros, and meta-ultramafic rocks.

The section 1610 - 2470 m is characterized by a sequence of sillimanite-garnet-biotite-gneisses with interlayers of lamprophyres, calcsilicates and amphibolites.

From 2470 down to 2586 m biotite-hornblende-gneisses predominate.

Between 2586m and 2634m and from 2680m down to 3572m sillimanite-biotite-gneisses, partly garnet bearing, with minor intercalations of biotite-hornblende-gneisses and amphibolites, prevail.

In the metabasic rock sequence, encountered from 3570m down to the final depth of 4000.1m, epidotization (3860m) with epidote concentrations of locally > 50 wt.-% and anomalously high Ca, P, Sr, Y and Zr concentrations occurs.

In the KTB pilot hole a new drilling fluid system was applied for the first time using Dehydril-HT as mud additive. Dehydril-HT is an inorganic viscosifier with high temperature stability. It has an excellent carrying capacity for drilled cuttings and rock flour and does not impair the geochemical analysis for solids and dissolved gases. The mud additive has

low and constant initial concentrations of Na, Ca, K, and Cl- and, therefore, allows detection of small amounts of inflowing saline formation water.

A strong inflow of saline formation fluids composed mainly of sodium, calcium and chloride was evident at three depth intervals (3447 m, open joint; 3817 m, open joint and 4000 m, epidotization horizon). The chemical composition differed greatly at 3447m and 4000 m, respectively.

Because the drilling fluid does not contain any organic compounds continuous analysis of hydrocarbons is possible. Methane and helium have been found to be excellent indicators for the detection of fluid containing horizons, because these fluids are strongly enriched in these gases. Different fluid systems can be distinguished by their methane/helium ratio.

Gas data can be used to predict graphite bearing cataclastic shear zones which may provide technical problem zones for drilling.

C.1 Analysis of solids

C.1.1 Introduction

The drilled solids, namely core material, cuttings and rock flour (separated from the drilling fluid by a centrifuge), were continuously investigated. These investigations included:

- continuous sampling of cuttings and rock flour every meter
- close sampling of core material
- measurement of chemical composition (major and trace elements) by X-Ray fluorescence spectrometry (XRF)
- measurement of quantitative mineralogical composition by X-Ray diffraction (XRD)

The pilot hole was almost entirely cored providing the unique possibility of a direct comparison of the results of core material and cuttings. A reconstruction of the lithostratigraphic profile using cutting and rock flour data was established. Altogether, 2500 rock flour samples, 430 cuttings and 950 core samples have been analyzed by XRF and XRD.

C.1.2 Sampling and preparation

The pilot hole was mainly drilled using a wire line coring technique with thin kerfed diamond bits which allowed for excellent core and rock flour recovery. During directional drilling phases, however, only cuttings and rock flour were obtained.

Cuttings and rock flour samples (50 - 100 g) were taken at intervals of 1 m. The samples were dried at 105°C and ground in a tungsten carbide ball mill for 25 minutes. The powder was then pressed into standardized pellets which were used for both XRD and XRF measurements.

For core material investigations core pieces or plugs were available. The core material was crushed in a tungsten carbide jaw breaker and then processed in the same way as the rock chip material.

C.1.3 Methods

C.1.3.1 X-Ray diffractometry (XRD)

The qualitative and quantitative mineralogical phase analysis of crystalline rock material is performed by X-Ray powder diffraction using a SIEMENS D 500 diffractometer. During the preliminary stages of KTB a new method for quantitative phase analysis by X-Ray diffraction was developed (STROH, 1988). This method is based on the comparison of the diffraction spectrum of the unknown sample with those of pure minerals. The powder diffraction data of the minerals are stored in a database built of approx. 220 natural mineral phases separated from various kinds of igneous and metamorphic rock types. The complete analysis is automatically carried out by computer. As a rule the detection limit for this method lies between 1 and 3 wt.%. With the results of the quantitative phase analysis a mineralogical "rock composition log" can be achieved.

C.1.3.2 X-Ray fluorescence spectrometry (XRF)

Analysis of major and trace elements on cores, rock flour and cuttings was performed with a SIEMENS SRS 303 AS X-Ray fluorescence spectrometer. 10 main constituents (SiO_2, TiO_2, Al_2O_3, Fe_2O_3, MnO, MgO, CaO, Na_2O, K_2O, P_2O_5) and 10 trace elements (Cr, Ni, Cu, Zn, Rb, Sr, Y, Zr, Th, U) were determined on a routine basis. With XRF results a "chemical data log" was computed.

C.1.4 Results

For proper interpretation of XRD and XRF results of rock flour it is necessary that the sample material represents the actually drilled rock. Contamination, dispersion, delay and mixing of cuttings and rock flour are the main problems that can occur.
Fig. C.1.4.1 shows the grain size distribution of gneiss and amphibolite rock flour. Besides the homogeneity of rock flour material an important characteristic of this material is the very small grain size range with pronounced maxima between 20 and 40 µm. Material with an average grain size of about 30 µm form a single phase medium together with the drilling fluid and does not seem to be affected by dispersion (WOLFF, 1987).

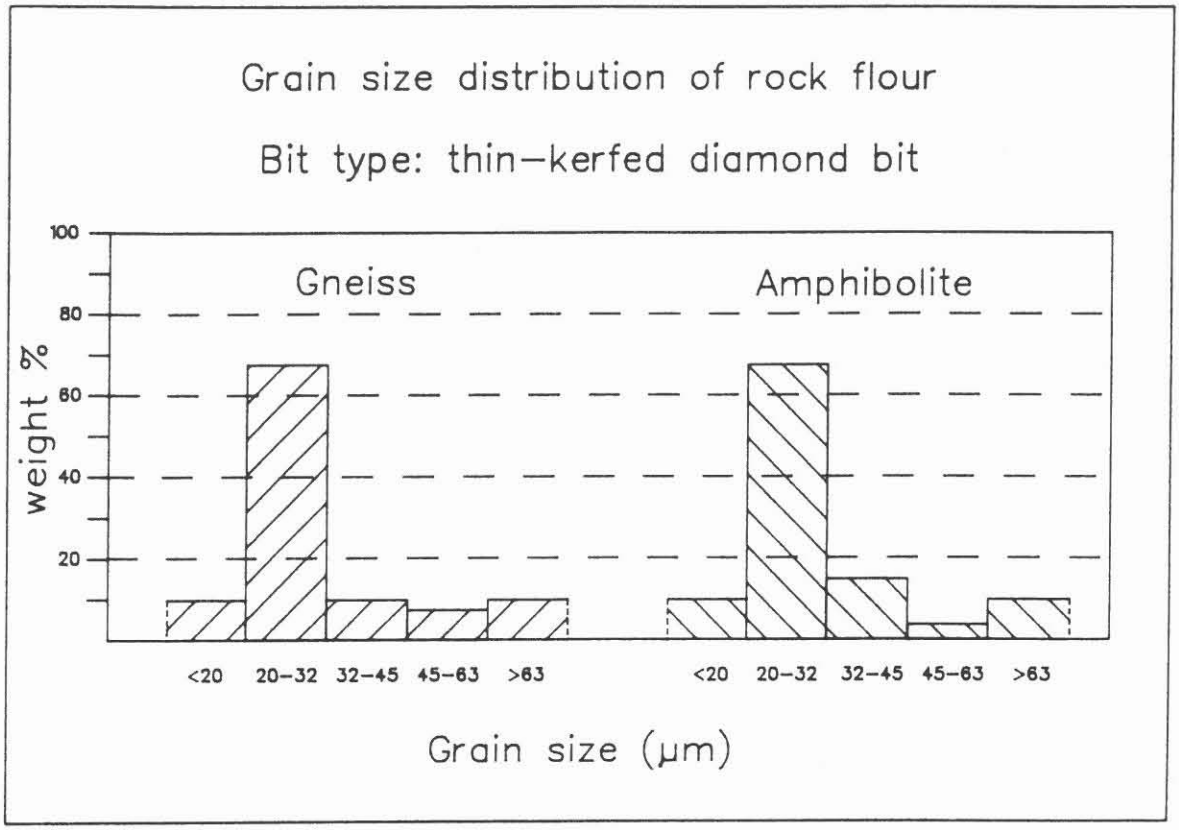

Fig. C.1.4.1: Grain size distribution of rock flour

In order to investigate effects of mixing or "smearing out" during transportation, 2 m^3 of fresh drilling fluid containing 20 kg of cristobalite, a SiO_2 polymorph, as tracer (with grain size distribution comparable to rock flour material) was fed into the drilling fluid system during drilling. This test was carried out at a depth of 3896 m, simulating an artifical cristobalite horizon. Rock flour samples of the centrifuge were taken every minute and analyzed in the field laboraty. Interpretating the onset of a new mineral (cristobalite) as a lithological change a depth resolution of 10 - 20 cm was observed at a drilling rate of 1 - 2m/h (STROH & WÖHRL, 1989). It follows from this test that even small intercalations of different rocks can be resolved by rock flour samples.

Rock flour and especially cuttings can be contaminated by cavings particularly when drill tools are frequently changed. To prevent this the mud volume in the annulus of the borehole must be completely circulated out before each trip.

Small lithological units (< 2 m) e.g. meta-ultramafics often appear thicker in the rock flour profile compared to the core profile. Thicker layers (> 2 m) can be delimited exactly in the rock flour profile with boundaries corresponding closely to depth assignments of the core profile. The resolution depends on the sampling distance which is every 1 - 2 m on average in the pilot hole.

Distinguishing of lithological units by rock flour analysis involves the consideration of the mineral and element concentrations. The major rock types, gneiss or amphibolite, can be easily identified in the mineralogical/chemical data due to the difference in the quartz or amphibole content (see Appendix).

Also the "fine structure" of the lithostratigraphic profile is resolved. Fig C.1.4.2 shows an example of a lithological sequence in the interval 1250 - 1500 m. Here a sequence of amphibolites and metagabbros embedded with meta-ultramafics of different thickness can be identified. Indicative are the increase of the mineral amphibole and the element Ni, and the decrease of plagioclase in the meta-ultramafics compared to amphibolites and metagabbros.

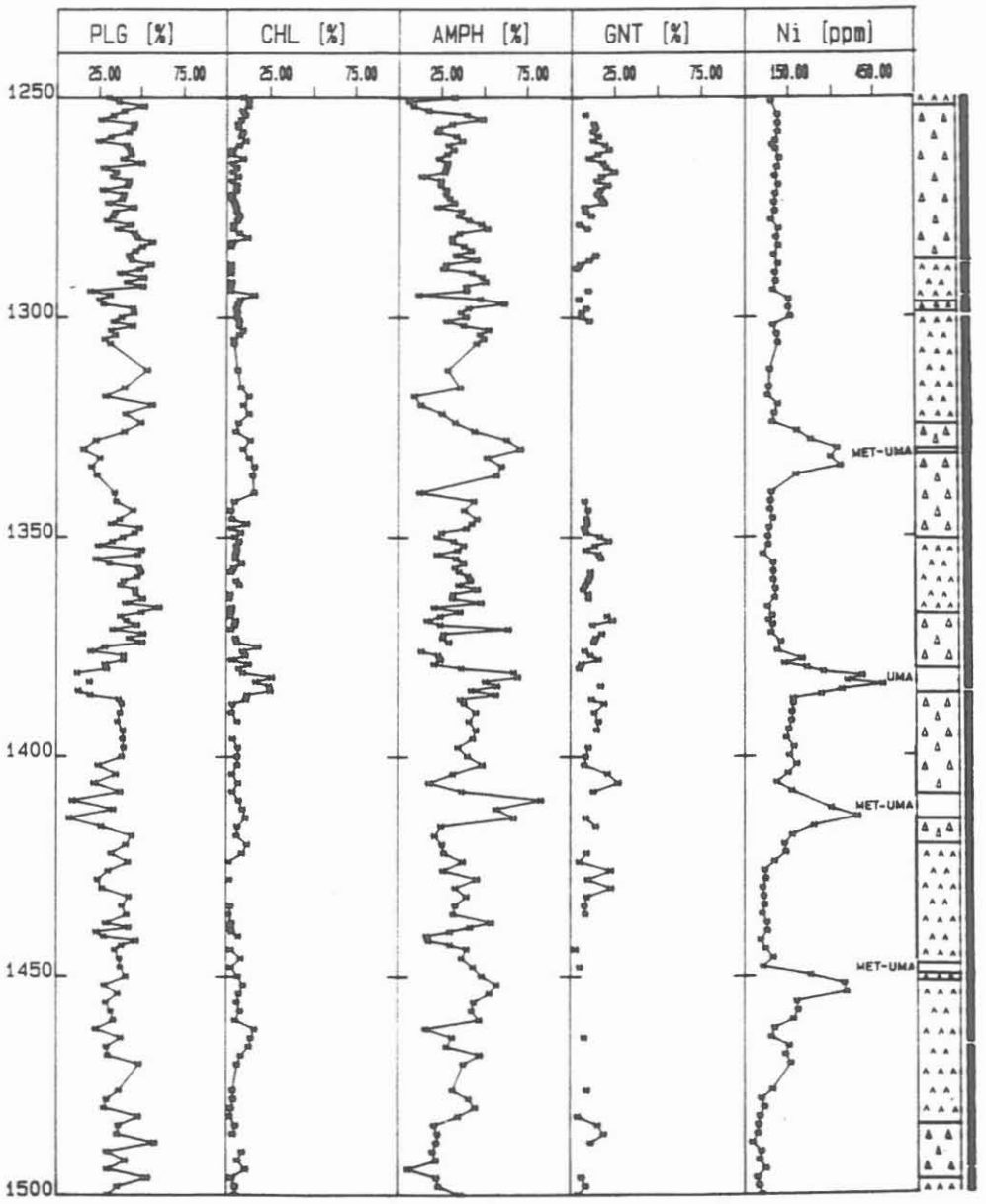

Fig. C.1.4.2: Results of XRF and XRD analyses of rock flour material in the interval 1250 m to 1500 m in comparison to the core profile showing a lithological sequences of amphibolite (Λ) and metagabbro (Δ) embedded with thin layers of meta-ultramafics.

Another benefit of the continuous X-Ray analysis is the mineralogical indication of cataclastic shear zones. In the interval 1900-2000 m drilling problems occurred. This horizon was indicated by changes of the mineralogical composition while entering a cataclastic zone below 1980 m. The rock flour profile identified this graphite impregnated shear zone by increasing concentrations of chlorite, white mica and particularly pyrite and decreasing concentrations of quarz and plagioclase (Fig. C.1.4.3). Together with gas analysis (see Cap. C.2) these observations are ideal indicators of rock alteration.

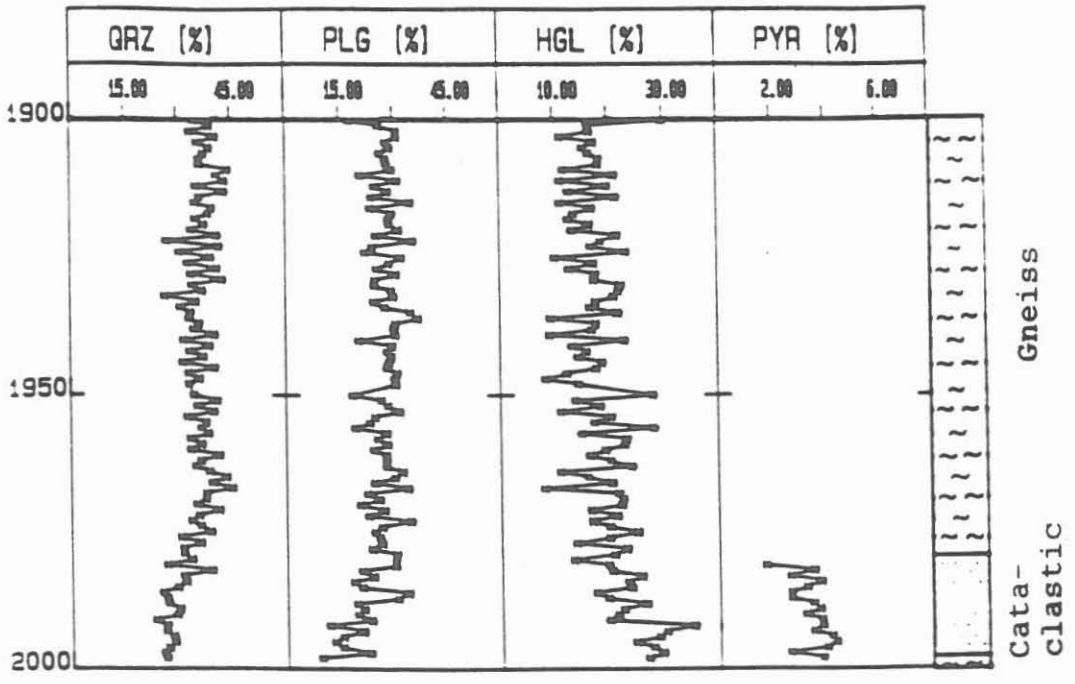

Fig. C.1.4.3: Results of rock flour analysis between 1900 m and 2000 m, corresponding to gneisses and a cataclastic zone in the core profile.

Fig. C.1.4.4 shows the litholostratigraphic profile (0-4000.1m) based on rock flour analysis versus core profile. It is evident that the major lithological units can be delimited in the rock flour profile and correspond to the core profile depth.

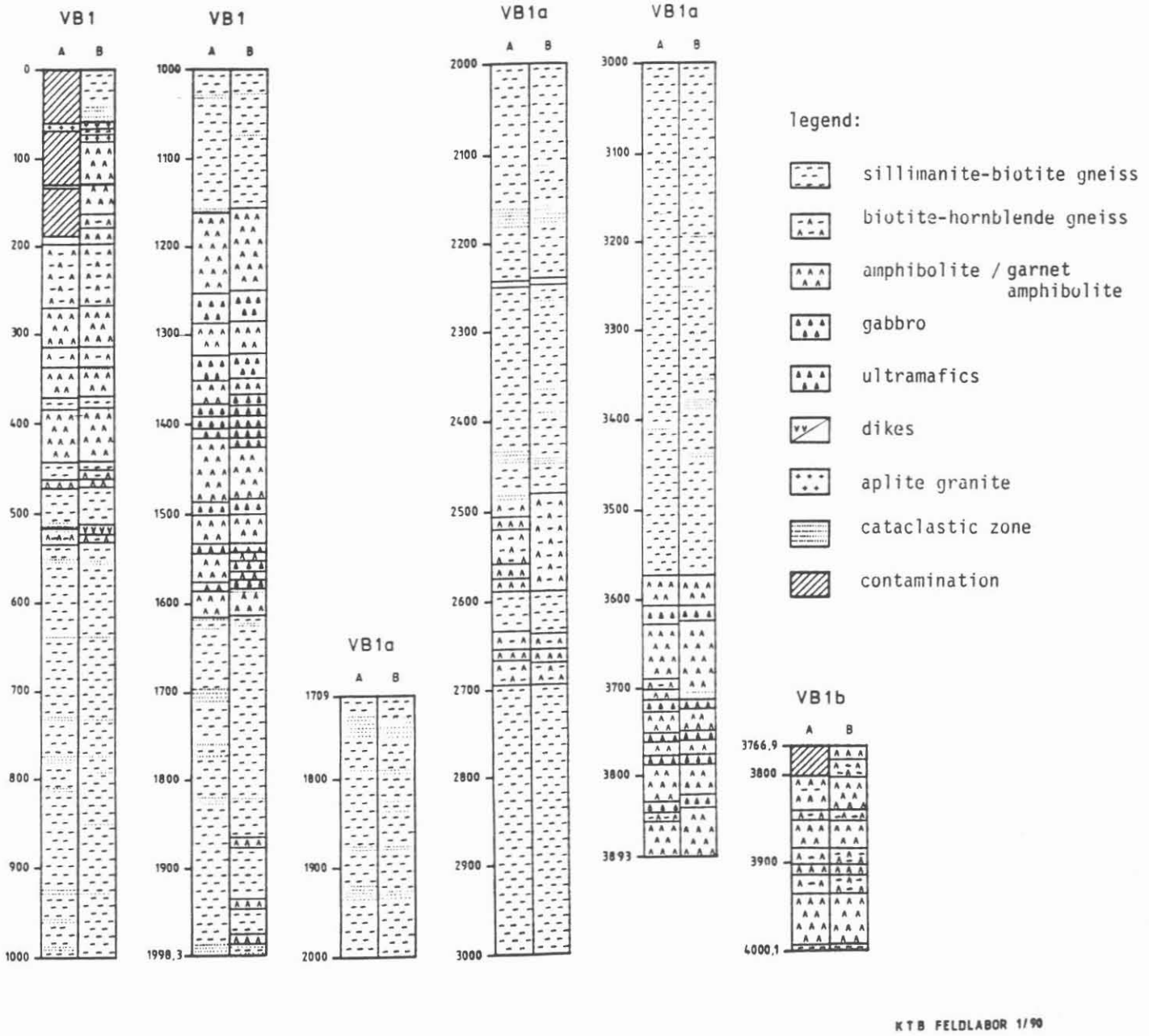

Fig. C.1.4.4: Lithological profile (0 - 4000.1m) based on rock flour analysis (A) and core profile (B).

C.1.4.1 Physical parameters calculated from mineral composition

Starting at a depth of 1500 m rock density was computed from the quantitative mineral composition calculated from XRD-measurements.

XRD densities calculated from centrifuge samples and densities measured on cores using the buoyancy method (see also Part D. Geophysics) correlate well. The calculated densities provide matrix densities, whereas the buoyancy method determines total densities which are generally lower due to porosities.

The densities in paragneisses are on average around 2.7 g/ccm, while densities between 2.9 g/ccm and 3.05 g/ccm predominate in the amphibolites.
In the garnet rich amphibolites below 3570m, density reaches values over 3.25 g/ccm.
A downhole variation plot of the calculated rock densities (XRHO) is shown in Fig. C.1.4.5, clearly indicating the lithological changes.

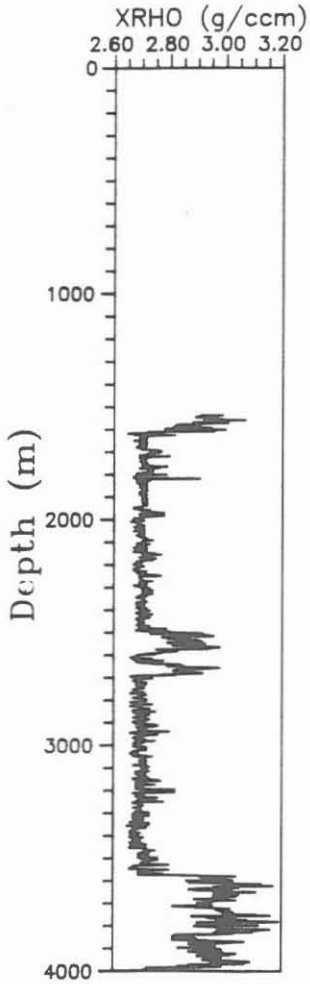

Fig. C.1.4.5: Densities calculated from XRD-measurements.

C.2 Drilling fluid analysis

C.2.1 Introduction

During the drilling phase of the pilot hole the chemical composition of the drilling fluid and the dissolved gases was continuously measured at the drill site.
The main objective of this drilling fluid analysis was the detection of influxes such as connate or formation waters and/or gases, thus allowing a direct sampling of potentially fluid containing horizons. Continuous gas analysis also allowed to measure the variation of gas composition as a function of depth.

Experience has shown that results of the drilling fluid analysis are also necessary for explaining and controlling changes of mud properties such as viscosity or pH.

C.2.2 Dehydril HT - the mud additive

In the KTB pilot hole a completely new mud additive was used for the first time. Low percentages (1 - 2 wt.%) of Dehydril HT powder (Henkel KGaA, Düsseldorf) is added to water, yielding a high temperature resistent colloidal silicate gel. Dehydril HT drilling fluid has thixotropic properties. Both the thixotropy and the viscosity of the drilling fluid depend on the concentration of the drilling additive, the pH value and the electrolyte content of the drilling mud (see HEROLD et al., 1987). The mud additive Dehydril HT consists mainly of Si, Mg, Na, Li and H_2O. The chemical composition of the pure Dehydril HT powder is given in Tab. C.2.1.

Tab. C.2.1: Chemical composition of the mud additive Dehydril HT (Henkel KGaA, Düsseldorf) analysed by the KTB laboratory with ICP-AES and IC. The values refer to air-dry Dehydril HT powder; LOI = loss on ignition

SiO_2	51.3	wt.%	Ca	1300 ppm
MgO	22.9	wt.%	Fe	400 ppm
Na_2O	2.3	wt.%	Al	330 ppm
Li_2O	0.65	wt.%	K	180 ppm
H_2O LOI	22.0	wt.%	Sr	< 10 ppm
			Cl^-	100 ppm
total	99.15	wt.%	SO^4	2300 ppm

Dehydril has low and constant initial concentrations of the elements Na, Ca, K, Sr, Fe, Li, Cl^- and SO_4^{2-}. Therefore, the identification of fluid containing horizons is possible, due to the fact that naturally occurring waters exhibit the elements Na and Ca (in saline waters also Cl^-) as main cations.

At concentrations between 1 to 2 wt.% the synthetic Dehydril HT mud (mixed with bidestilled water) contains 0.24 - 0.48 wt.% Si, 0.14 - 0.28 wt.% Mg, 170 - 340 ppm Na, and 30 - 60 ppm Li. The initial background concentrations of Ca, Sr, Fe and K and the anion concentrations of Cl^- and SO_4^{2-} are less than 40 ppm.

C.2.3 Analytical methods

The concentrations of the following elements in the drilling fluid were continuously measured during the drilling phase:

- Cations (Mg, Li, Ca, Na, K, Sr, and Fe)
- Anions (Cl^-, and SO_4^{2-})
- Gases (N_2, O_2, Ar, CO_2, CH_4, H_2, and He)

An atomic emission spectrometer, an ion chromatographic system, and a mass spectrometer were used for drilling fluid and gas analysis.

C.2.3.1 Atomic emission spectrometry (ICP-AES) and preparation method

Cation concentrations of the drilling fluid are measured with an atomic emission spectrometer (ARL 3580 Vacuum) with inductively coupled plasma. Detailed descriptions of the equipment and measuring programmes are given in STROH et al., (1988).

However, before starting the investigations all fine rock flour particles must be removed in order to avoid contaminations. Due to the cation-absorbing properties of the mud additive a simple preparation method like dilution and filtration of the drilling fluid to is not possible. Therefore, the measured cation concentration of the filtered solution depends on the degree of dilution as well as on the pore size of filter material (see HEINSCHILD et al., 1988).
A new preparation method was devoloped and proved to be effective:

step 1: - dilution
step 2: - ultrasonic treatment in order to destroy large charged D-HT particles
step 3: - centrifuging to remove fine-grained solids

C.2.3.2 Ion chromatography (IC) and preparation methods

For quantitative anion determination in the field laboratory, a chromatography system (Waters) was applied. This equipment and the principles of the method are described in the KTB Report 88-2 (HEINSCHILD et al., 1988).
Because the anions are not absorbed on the charged Dehydril HT particles, dilution followed by filtration (0.45 µm) was applied.

C.2.3.3 Mass spectrometry (MS)

A single focussing magnetic sector mass spectrometer was used for continuous gas analysis (Vacuum Generators LTD, MM8- 80). The operation principle of the mass spectrometer has been explained by STROH et al. (1988).
The dissolved gases are liberated from the drilling fluid using a gas trap (see Figure C.2.1).
The mass spectrometer and the gas trap were installed three months after the pilot hole was spudded. Because of this continuous analysis could not begin before 1200 m.

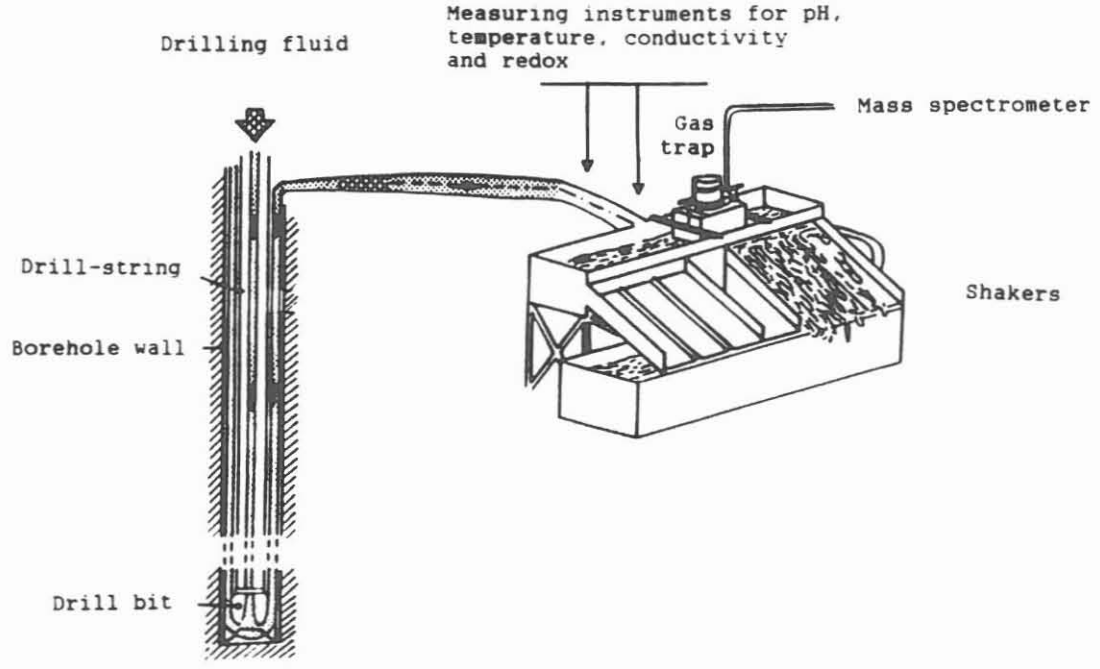

Fig. C.2.1: Drilling fluid circuit including gas trap position

C.2.4 Results

The results of continuous drilling fluid analysis indicated no inflow of formation water in the upper 3000 m (a "dry" hole). Below 3400 m four horizons showing an inflow of saline water and gases were observed (Figure C.2.2 and C.2.3). Methane and helium enrichments became evident in some intervals. A selection of measured parameters is shown as a data log 0 - 4000 m in the Appendix.

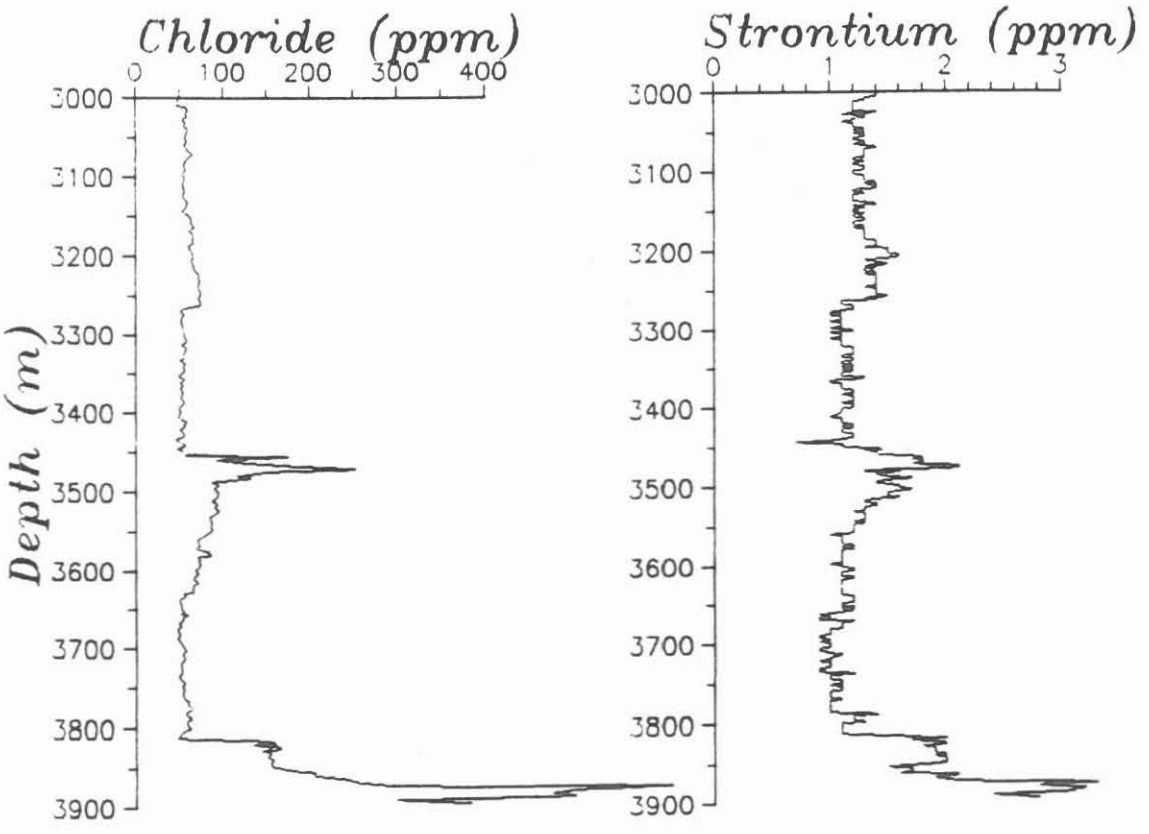

Fig. C.2.2: Strontium and chloride content of the drilling fluid

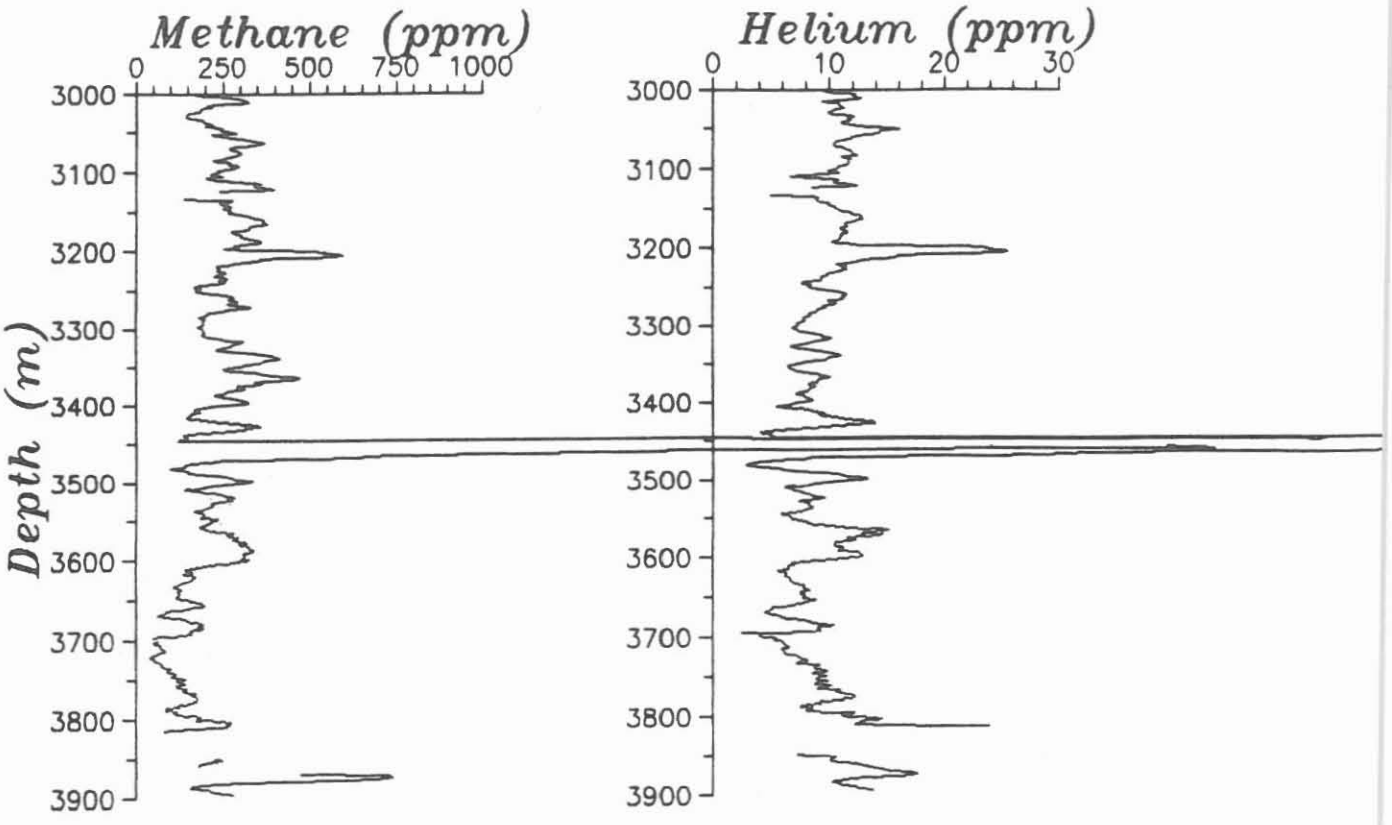

Fig. C.2.3: Variation of methane and helium of the liberated gas phase with depth. The results were averaged every two meters over a 20 meter intervall

In the KTB pilot hole the zones of increased methane and helium concentrations coincided with graphite bearing cataclastic horizons, cataclastic shear zones, faults and open joints.

An increase of Na, Ca, Sr, and Cl^- together with a large enrichment of methane and helium at about 3450 m indicate an influx of gas-bearing saline waters. This fluid horizon correlates with an open joint (calcite crystals) preserved in the core (3447 m, see cover photograph). The fluids from this horizon were collected directly with gastight fluid samplers and a drill-stem test was performed. The fluids collected by the sampler turned out to be a mixture of drilling fluid and formation water. The results of the analysis are shown in Table C.2.2.

Tab. C.2.2: Composition of drilling fluid collected by a fluid sampler at 3447.0 m (28.10.88)

Na	2600 ppm	N_2	71.89 vol.%
Ca	4000 ppm	Ar	-
K	200 ppm	CO_2	1.02 vol.%
Sr	55 ppm	CH_4	24.39 vol.%
Cl^-	8700 ppm	H_2	2.03 vol.%
		He	0.68 vol.%

For a drill collar sample from 3447 m an element balancing was performed, assuming that no reactions between formation water and drilling fluid and/or precipitation of elements occured. The calculated composition of formation water at 3447 m is shown in Table C.2.3.

Tab. C.2.3: Calculated fluid composition at 3447 m

Na	7600 ppm
Ca	16200 ppm
Sr	390 ppm
Cl^-	35600 ppm

At depths of about 3817 m (partly open calcite joint), 3860 - 3880 m (porosity zone) and at 3980 - 4000 m further horizons showed the described characteristics of saline water influx: enrichment of Na, Ca, Sr, Cl^-, helium and methane.

The KTB pilot hole (VB) was completed in April 1989. One year later a flow test at 3850 - 4000 m was executed. From this test more than 35 m^3 of uncontaminated fluid was collected from a total of 71 m^3 entering the borehole. The average values of the fluid analysis are summarized in Table C.2.4.

Tab. C.2.4: Analysis of the saline water collected by the flow test (April 1990)

Na	6300 ppm	N_2	70 vol.%	He	0.55 vol.%
Ca	15400 ppm	O_2	0 vol.%	CO_2	0.04 vol.%
Sr	245 ppm	Ar	0.1 vol.%	^{222}Rn	3000 decreased to 2000 Bq/m^3-gas
Cl^-	37000 ppm	CH_4	28 vol.%		
pH	8.1				
conductivity	62.7 mS/cm				
gas content	800 l gas/m^3 fluid				

Evident influx of gases and/or saline waters are summerized in Table C.2.5.

Tab. C.2.5: Main inflow horizons in the KTB pilot hole including observed gases, cations, anions and mineralization.
bio=biotite, hbl=hornblende, chl=chlorite, pyr=pyrite, ccc=graphite, hgl=white mica, cal=calcite, epi=epidote

Depth (m)	Lithology	Fluid Gas	Ions	Mineral-ization
VB				
505	bio-gneiss	"ground water"		chl
648	bio-gneiss	"ground water"		
1240 - 1250	amphibolite	He, CH_4		chl,pyr
1500 - 1530	amphibolite	He, CH_4		pyr
1690 - 1710	bio-gneiss	He, CH_4		ccc
1980 - 1998	bio-gneiss	He, CH_4		ccc, pyr, hgl, chl
VB1a				
1930 - 1960	bio-gneiss	He, CH_4		ccc
2150 - 2180	bio-gneiss	He, CH_4		ccc,pyr, chl
3202	bio-gneiss	He, CH_4		cataclastic fault gauge
3447	open joint bio-gneiss	He, CH_4 ;	Ca, Na, Sr, Cl^-	cal-joint
3800 - 3820	open joint amphibolite/ metagabbro	He, CH_4 ;	Ca, Na, Sr, Cl^-	cal-joint
3860 - 3880	porosity zone amphibolite	He, CH_4 ;	Ca, Na, Sr, Cl^-	epi
VB1b				
3980 - 4000	hbl-gneiss	He, CH_4 ;	Ca, Na, Sr, Cl^-	epi

Graphite-indicating method

Figure C.2.3 shows the concentrations of methane and helium from 1970 - 2000 m including a graphite-bearing cataclastic horizon (1981 - 1998 m).
Helium increased steadily when entering the graphite-bearing zone. Methane, however increases before encountering this zone, thus methane may serve as a sensitive indicator of graphite-bearing zones before actually drilling them.

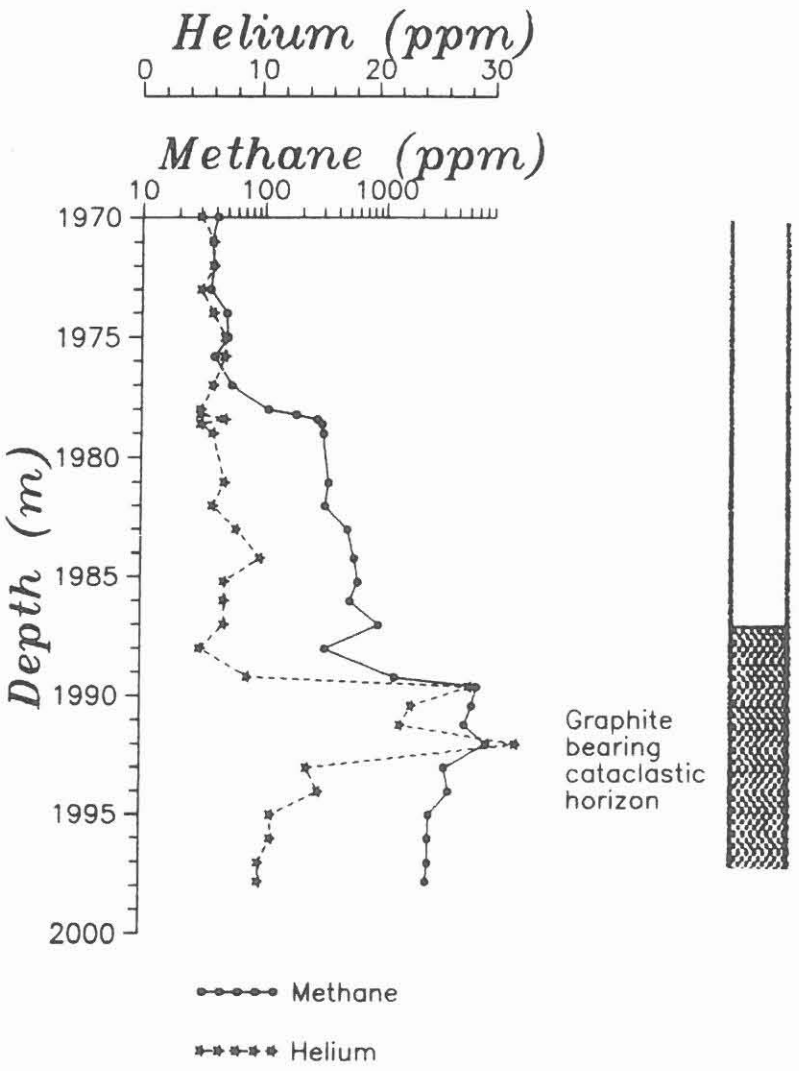

Fig. C.2.4: Concentrations of methane and helium during the interval 1970 - 2000 m including a graphite bearing cataclastic horizon

Leaching processes

According to leaching experiments (see HOMANN & MÜLLER, 1989; KTB-Report 89-2), the reaction of the drilling fluid with sheet silicates (muscovite) in the drilled material leads to an increase of the potassium concentrations. The muscovite content of the drilled biotite gneisses is up to 35 wt.% (quantitative XRD-analyses, see Cap. C.1). The leaching experiments also showed an enrichment in aluminium. The temperature range (25 - 150°C) of the test did not influence the K/Al- ratio (0.3 - 0.4). Of all major mineral compounds of the paragneisses (quartz, plagioclase, biotite, chlorite, muscovite), only muscovite has a similar K/Al-ratio (0.48). No increase of the electrical conductivity of the test fluid could be detected, implying only a small cation exchange between rock flour and drilling fluid. Instead of a cation exchange process, congruent solution of muscovite could be envisaged in the alkaline pH-range (≈ 10) of the drilling fluid.

When drilling fault zones with sulfide impregnation, enrichments both in iron and sulfate (see Figure C.2.5) could be observed, leading to the conclusion that oxidation of pyrite takes place probably caused by atmospheric oxygen introduced with the drilling mud. This oxidation of pyrite can be described by the following reactions:

$$2\ FeS_2 + 7.5\ O_2 + 4\ H_2O = Fe_2O_3 + 4\ SO_4^{2-} + 8\ H^+$$

or in alkaline environment:

$$4\ FeS_2 + 15\ O_2 + 12\ OH^- + 2\ H_2O = 4\ Fe(OH)_3 + 8\ SO_4^{2-} + 4\ H^+$$

The sulfuric acid produced from these reactions leads to a decrease of the pH value of the drilling mud system when drilling shear zones with sulfide mineralization.

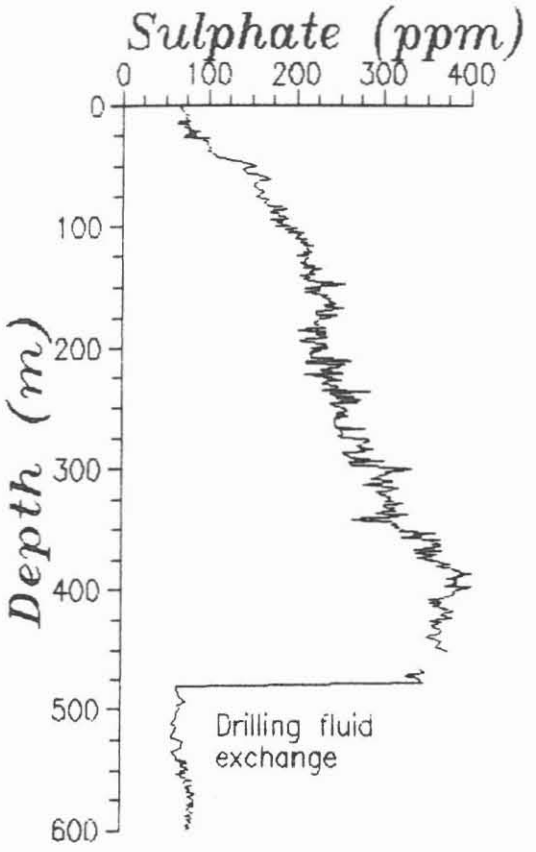

Fig. C.2.5: Sulphate content of the drilling fluid

Artificially produced gases

During drilling the hydrogen content of the liberated gas phase reached values up to 10 vol.% and did not vary systematically with the lithology. However, the occurrence of hydrogen strongly depends on the actual drilling bits, configuration of the drill-string and drilling parameters.

The mining drilling technique (diamond core bits) was used above 1816 m, producing high hydrogen concentrations of up to 10 vol.%. Below a directional drilling with tungsten carbide insert roller cone bits followed, resulting in hydrogen concentrations of less than 0.01 vol.%. During drilling with roller cone bits between 1866 - 1873 m additional stabilizers produced a slight increase in hydrogen contents. Figure C.2.6 shows the measured hydrogen concentrations from 1800 - 1900 m as influenced by the drilling techniques applied.

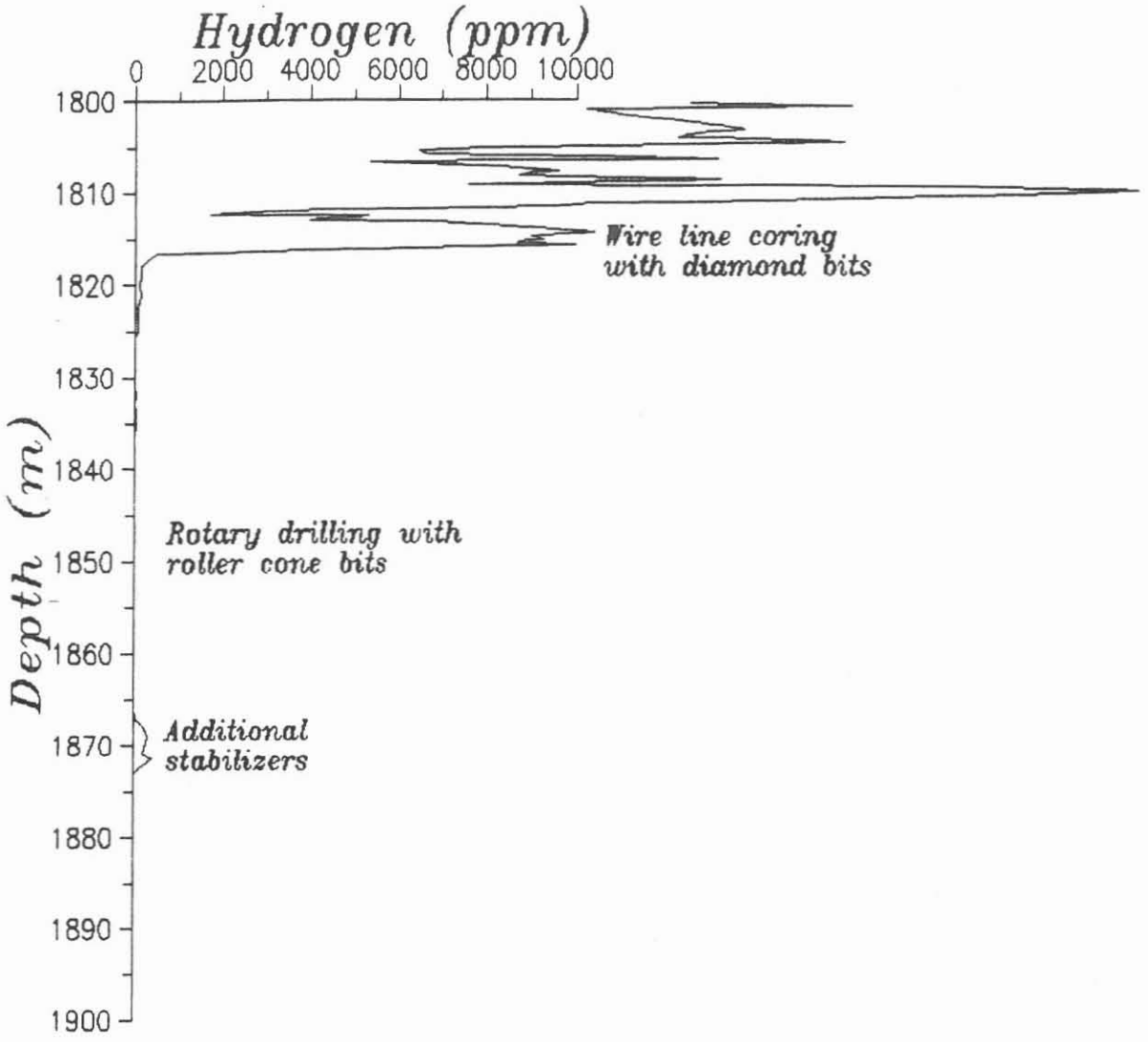

Fig. C.2.6: Variation of measured hydrogen contents between 1800 and 1900 m, as influenced by the drilling technique used

Compared with thermically produced methane, the quantity of artifical methane is small. C-isotope investigations on gas samples showed, that as well as hydrogen a small amount of artifical methane is produced by drilling (WHITICAR & FABER, 1989). The background value of about 100 - 200 ppm methane present during the whole drilling activity could be artifical.

C.2.5 Discussion

As described in Chapter C.2.4 several zones of significantly increased methane and helium concentrations could be identified. A variation plot of methane/helium versus methane allows a significant separation of these "gas rich zones" (Fig. C.2.7).

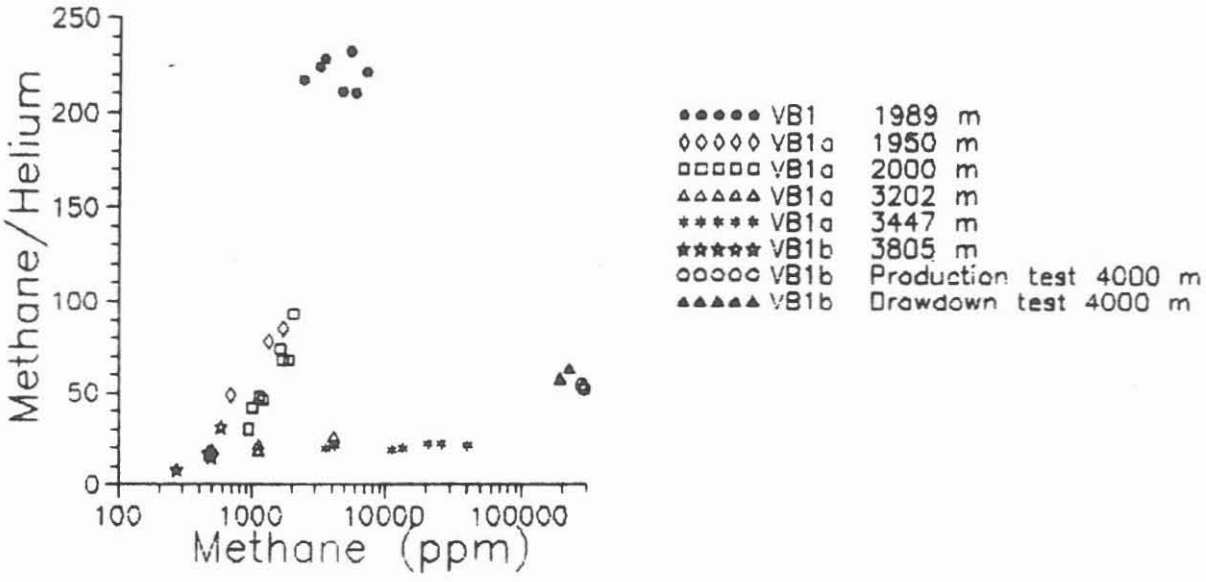

Fig. C.2.7: Characterization of several distinct "gas-bearing" horizons

The helium content of formation water could be partly due to the decay of uranium and thorium (radiogenic helium), which are enriched in the graphite-bearing zones.

Other investigations suggest, that carbon was transported as an CO_2-CH_4-fluid through cataclastic shear zones and precipitated due to an H_2O- and/or temperature- decrease (ZIEGENBEIN et al., 1989).

The chemical composition of the two fluid samples from 3447 m and 4000 m differed significantly, suggesting that these fluids represent separate systems (see Figure C.2.7)

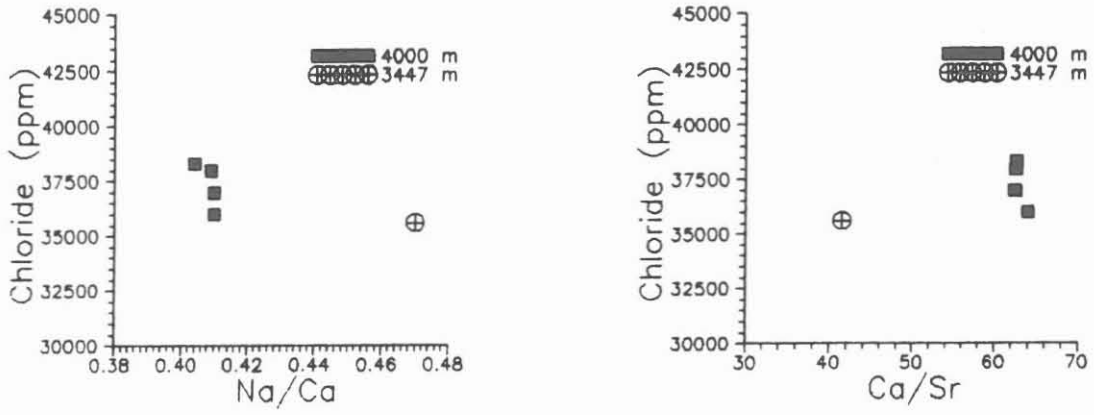

Fig. C.2.8: Characterization of the fluids at 3447 m and 4000 m

Significant inflow of fluids occurred only during drilling standstill. No fractionation of gas and formation water was evident during the circulation out.

At the end of the drilling phase a newly developed bypass-degasser-system was tested for two weeks. The absolute volume of dissolved gases could now be measured for the first time. The amount of the liberated gas (without influx of formation water and gas) was between 2 and 4 l gas/m³ drilling fluid. This corresponds to 0.4 - 0.8 ml CH_4/m³ drilling fluid and 0.02 - 0.04 ml He/m³ drilling fluid.

C.3 References

HACKER,W., KEYSSNER,S., MASSALSKY,T., MÜLLER,H., RÖHR,C., UHLIG,S., GRAUP,G. (1988): Tiefbohrung KTB Oberpfalz VB, Ergebnisse der wissenschaftlichen Bohrungsbearbeitung im KTB Feldlabor Windischeschenbach), Teufenbereich 490-992m, -In: EMMERMANN, R., DIETRICH, H.-G., HEINISCH, M., WÖHRL, T. (Hrsg.): KTB Report 88-2: B1-B37, Hannover.

HEINSCHILD, H.J., HOMANN, K.D., STROH, A.& TAPFER, M, (1988): Tiefbohrung KTB-Oberpfalz VB, Ergebnisse der geowissenschaftlichen Bohrungsbearbeitung im KTB-Feldlabor (Windischeschenbach), Teufenbereich von 0 - 480 m. - In: EMMERMANN, R., DIETRICH, H.-G., HEINISCH, M., WÖHRL, T. (Hrsg.): KTB-Report, 88-1: C1- C73, Hannover.

HEINSCHILD, H.J., HOMANN, K.D., STROH, A.& TAPFER, M. (1988): Tiefbohrung KTB-Oberpfalz VB, Ergebnisse der geowissenschaftlichen Bohrungsbearbeitung im KTB-Feldlabor (Windischeschenbach), Teufenbereich von 480 bis 992 m. - In: EMMERMANN, R., DIETRICH, H.-G., HEINISCH, M., WÖHRL, T. (Hrsg.): KTB-Report,88-2: C1-C107, Hannover.

HEROLD,C.-P., MÜLLER,H., von TAPAVICZA,S. (1987): A New High Temperature Stable Mud Additive for Geological and Deep Drilling Operations. Third International Symposium on Deep Drilling in Crystalline Bedrock. Mora, Sweden 1987.

HOMANN, K.D., HEINSCHILD, H.J., STROH, A.& TAPFER, M. (1988): Tiefbohrung KTB-Oberpfalz VB, Ergebnisse der geowissenschaftlichen Bohrungsbearbeitung im KTB-Feldlabor (Windischeschenbach), Teufenbereich von 1530 bis 1998m. - In: EMMERMANN, R., DIETRICH, H.-G., HEINISCH, M., WÖHRL, T. (Hrsg.): KTB-Report,88-9: C1-C88, Hannover.

HOMANN, K.D. & MÜLLER, H. (1989): Wechselwirkung zwischen Dehydril HT-Bohrspülung und Gesteinsmehl. Tiefbohrung KTB-Oberpfalz VB, Ergebnisse der geowissenschaftlichen Bohrungsbearbeitung im KTB-Feldlabor (Windischeschenbach), Teufenbereich von 1709 bis 2500m. - In: EMMERMANN, R., DIETRICH, H.-G., HEINISCH, M., WÖHRL, T. (Hrsg.): KTB-Report,89-2: F1-F45, Hannover.

RIDLEY, W.I., RHODES, J.M., REID, A.M., JAKES, P.,SHIH, C., BASS, M.N. (1974): Basalts from Leg 6 of the deep sea drilling projekt. J.Petrol., 15, 140-159

SCHÜßLER, U. (1987): Petrographie, Geochemie und Metamorphosealter von Metabasiten im KTB-Zielgebiet Oberpfalz. Verööfftl. Dissertation Würzburg, 1-272

STROH, A. (1988): Quantitative röntgenographische Phasenanalyse von Gesteinen und Mineralgemischen. Unveröff. Dissertation, Gießen 1988

STROH, A., HEINSCHILD, H.J., HOMANN, K.D.& TAPFER, M. (1988): Tiefbohrung KTB-Oberpfalz VB, Ergebnisse der geowissenschaftlichen Bohrungsbearbeitung im KTB-Feldlabor (Windischeschenbach), Teufenbereich von 992 bis 1530m. - In: EMMERMANN, R., DIETRICH, H.-G., HEINISCH, M., WÖHRL, T. (Hrsg.): KTB-Report,88-6: C1-C109, Hannover.

STROH, A., HEINSCHILD, H.J., HOMANN, K.D, TAPFER, M.& ZIMMER, M. (1989): Tiefbohrung KTB-Oberpfalz VB, Ergebnisse der geowissenschaftlichen Bohrungsbearbeitung im KTB-Feldlabor (Windischeschenbach), Teufenbereich von 1709 bis 2500 m. - In: EMMERMANN, R., DIETRICH, H.-G., HEINISCH, M., WÖHRL, T. (Hrsg.): KTB-Report, 89-2: C1-C104, Hannover.

STROH, A. & WÖHRL. T. (1989): Ermittlung der Dispersion von Feststoff im Spülungsstrom. Tiefbohrung KTB-Oberpfalz VB, Ergebnisse der geowissenschaftlichen Bohrungsbearbeitung im KTB-Feldlabor (Windischeschenbach), Teufenbereich von 2500 bis 3009.7m. - In: EMMERMANN, R., DIETRICH, H.-G., HEINISCH, M., WÖHRL, T. (Hrsg.): KTB-Report, 89-4: F1-F9, Hannover.

WALKER, K.R., JOPLIN, G.A., LOVERING, J.F., GREEN, R. (1960): Metamorphic and metasomatic convergence of basic igneous rocks and lime-magnesia sediments of the Precambrian of northwestern Queensland. J. Geol. Soc. Australia, 6, 149-178

WIMMENAUER, W. (1984): Das prävariskische Kristallin im Schwarzwald. Fortschr. Miner., 62, Bh. 2, 69-86

WINCHESTER, J.A. & FLOYD, P.A. (1976): Geochemical magma type discrimination: Application to altered and metamorphosed basic igneous rocks. Earth Planet. Sci. Lett., 28, 459-469

WHITICAR, M.J. & FABER, E. (1989): Hydrocarbon gases in KTB Vorbohrung, 1.Status Report of the ARGE 7 "FLUIDE", Jan. 1989

WOLFF, H. (1987): Cuttings - Korrelations - Untersuchungen. Austragefähigkeit von Cuttings. Unveröfftl. Ergebnisbericht, TU Berlin Institut für Berbauwissenschaften Berlin, Dezember 1987

ZIEGENBEIN, D., SKROTZKI, R., HOEFS, J., MÜLLER, H., REUTEL, C. & EMMERMANN, R. (1989): Fluidtransport und Graphitbildung auf Störungszonen. - In: EMMERMANN, R. und GIESE, P. (Hrsg.): Beiträge zum 2. KTB-Kolloquium Gießen, 15. bis 17.03.1989, KTB-Report 89-3, Hannover

C.4 Acknowledgements

We gratefully acknowledge our technical employees Mrs. A. Heinschild, Miss B. Weber, Mr. H. Kamm, Mr. R. Lippert, Mr. S. Merz and Mr. H.-G. Welker for their support and dedication. We would like to thank Prof. Dr. R. Emmermann, Prof. Dr. H. Wedepohl and Dr. J. Lauterjung for their constructive comments and reviewing of this paper.

C.5 Appendix

C.5.1 Results of XRD/XRF-Analysis

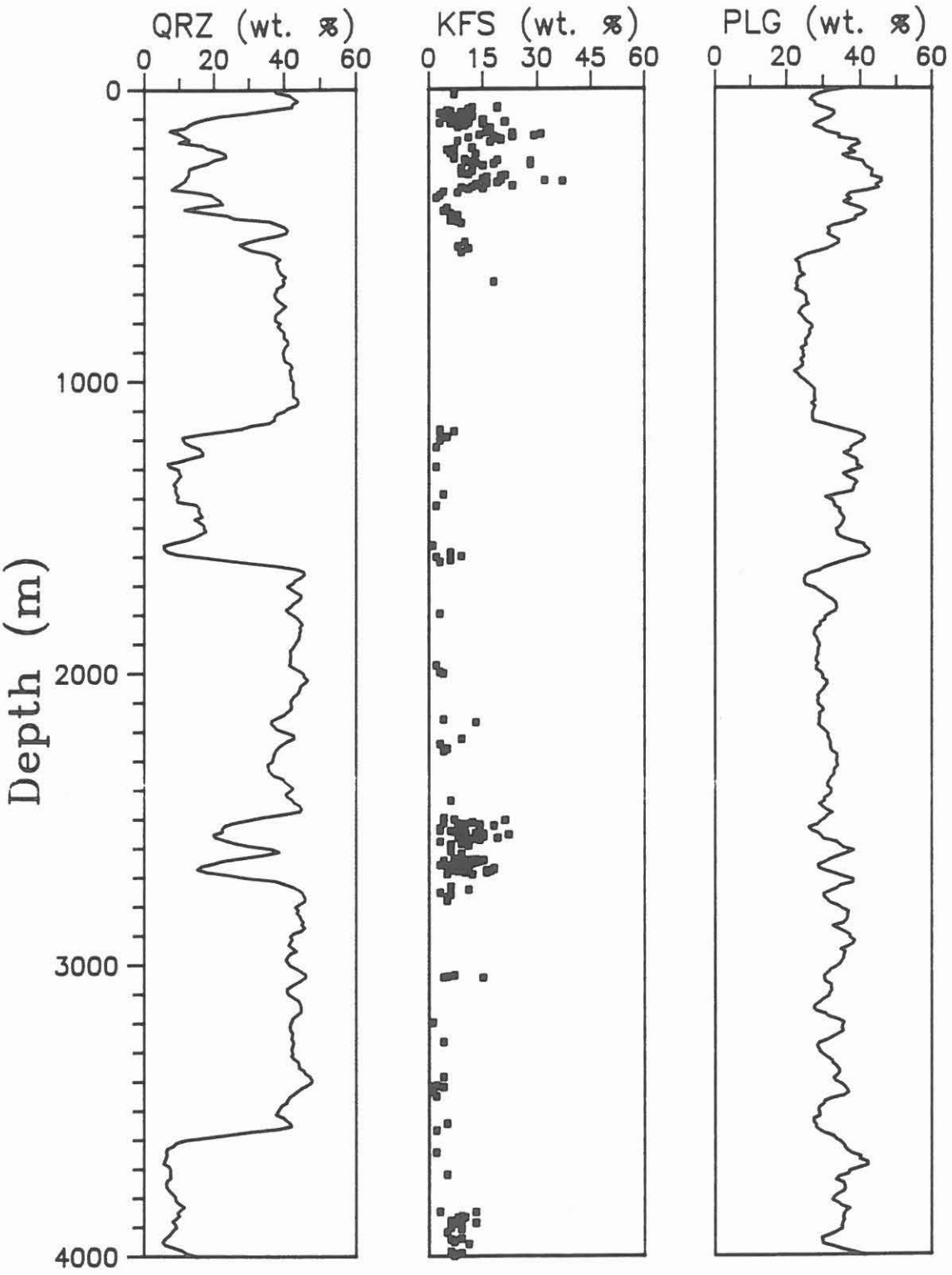

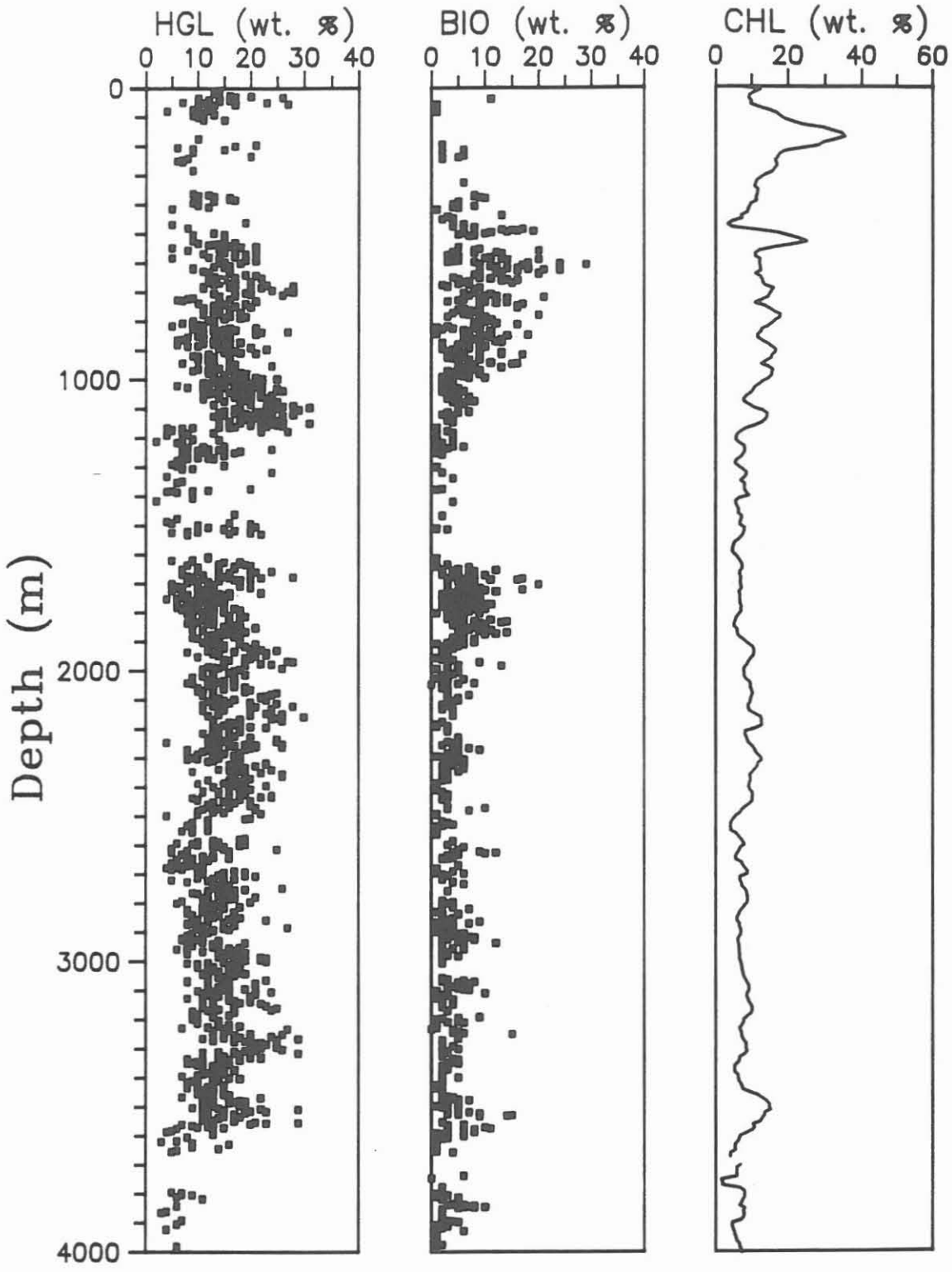
HGL (wt. %)
0 10 20 30 40
BIO (wt. %)
0 10 20 30 40
CHL (wt. %)
0 20 40 60
Depth (m)
0
1000
2000
3000
4000

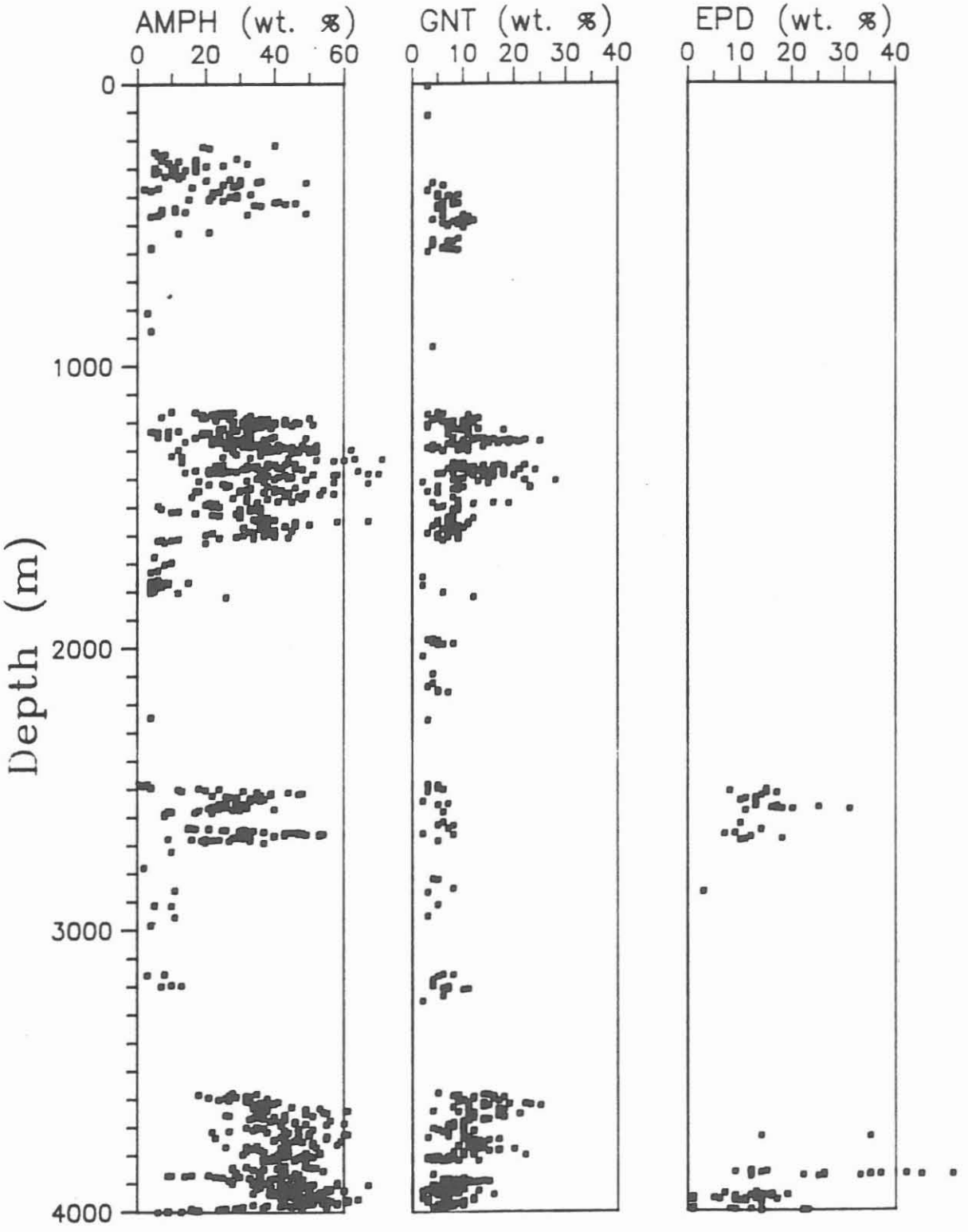
AMPH (wt. %)
0 20 40 60
GNT (wt. %)
0 10 20 30 40
EPD (wt. %)
0 10 20 30 40
Depth (m)
0
1000
2000
3000
4000

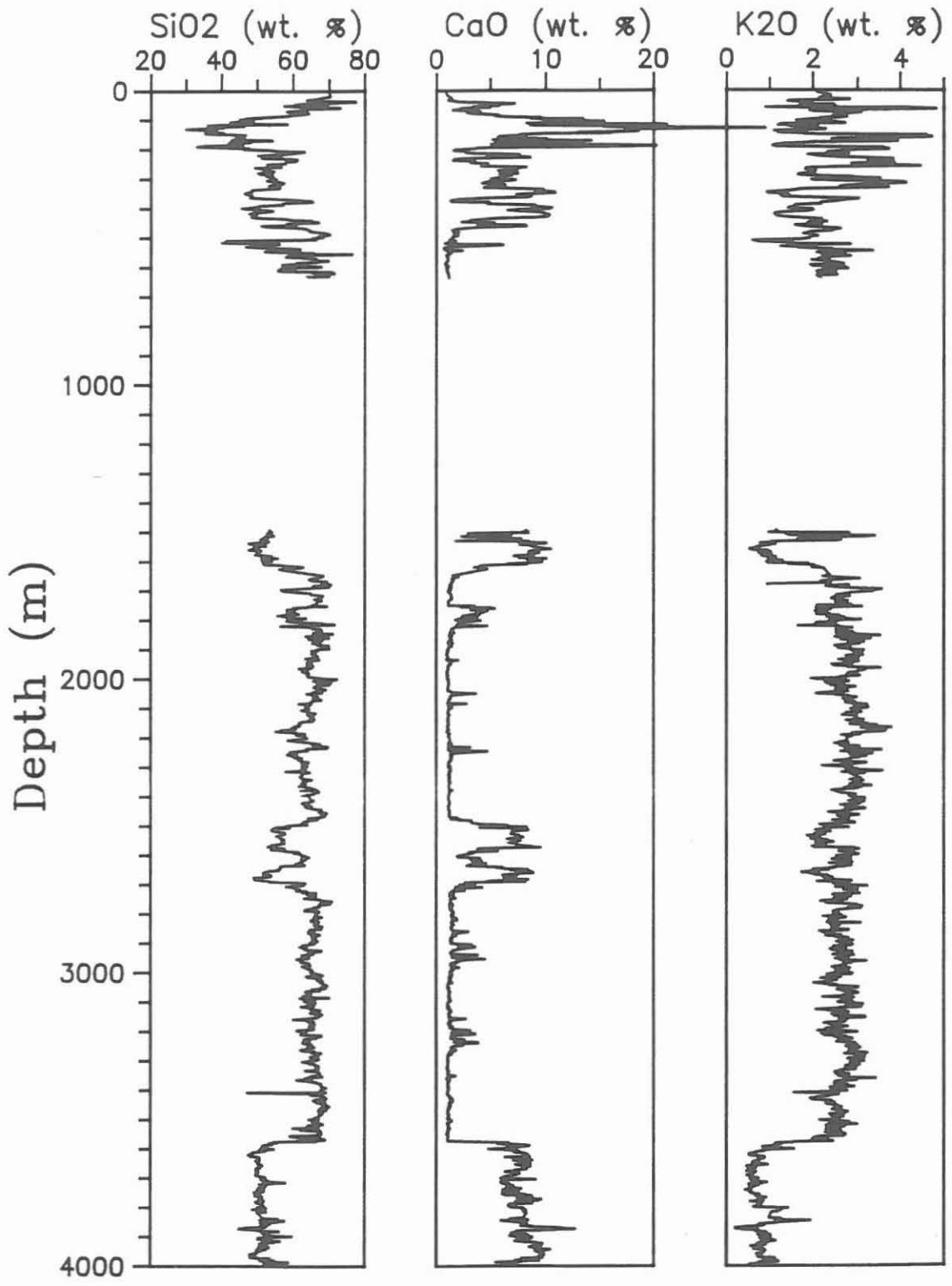
SiO2 (wt. %)
20
40
60
80
CaO (wt. %)
0
10
20
K2O (wt. %)
0
2
4
Depth (m)
0
1000
2000
3000
4000

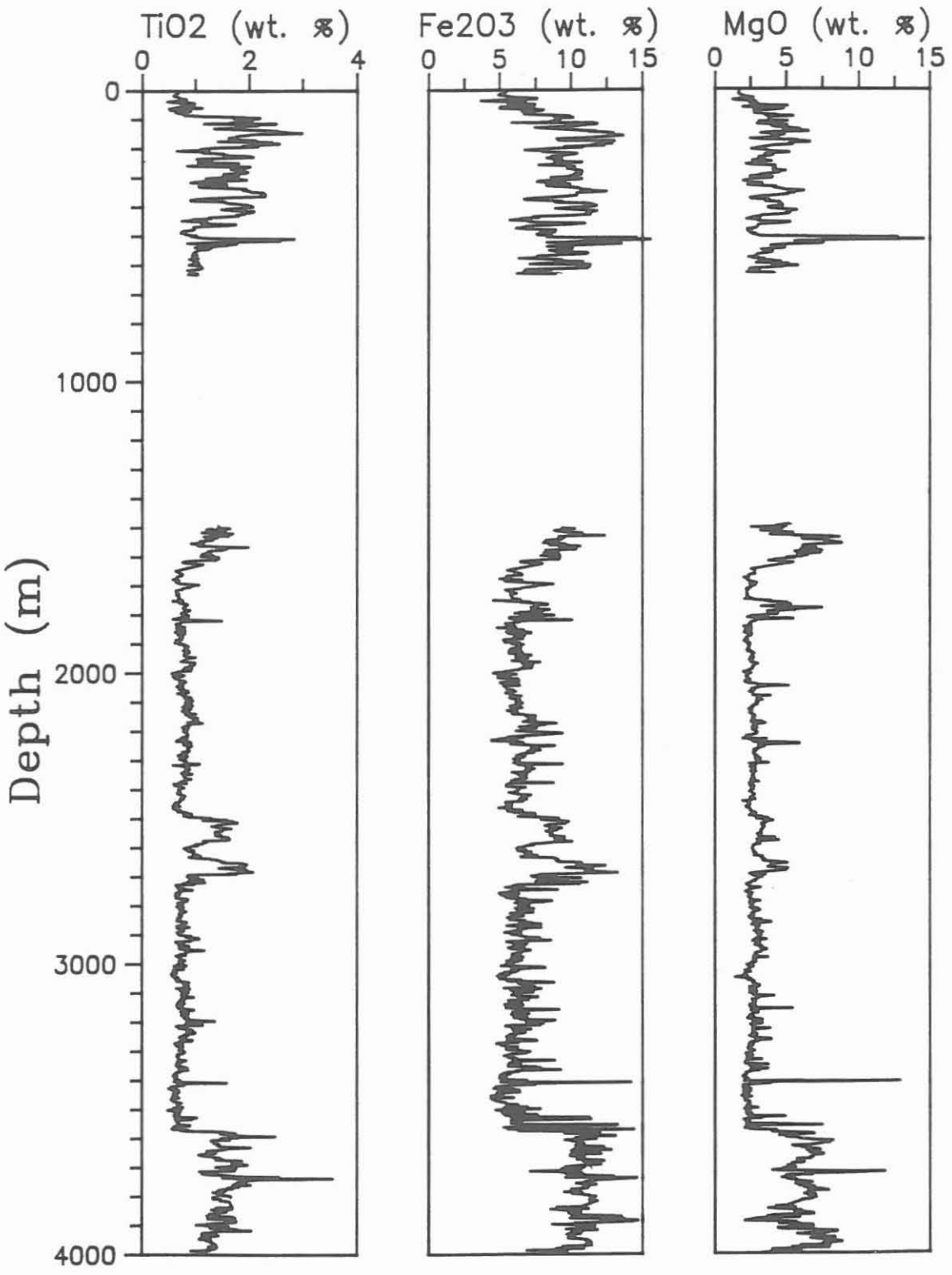
TiO2 (wt. %)
0
2
4
Fe2O3 (wt. %)
0
5
10
15
MgO (wt. %)
0
5
10
15
Depth (m)
0
1000
2000
3000
4000

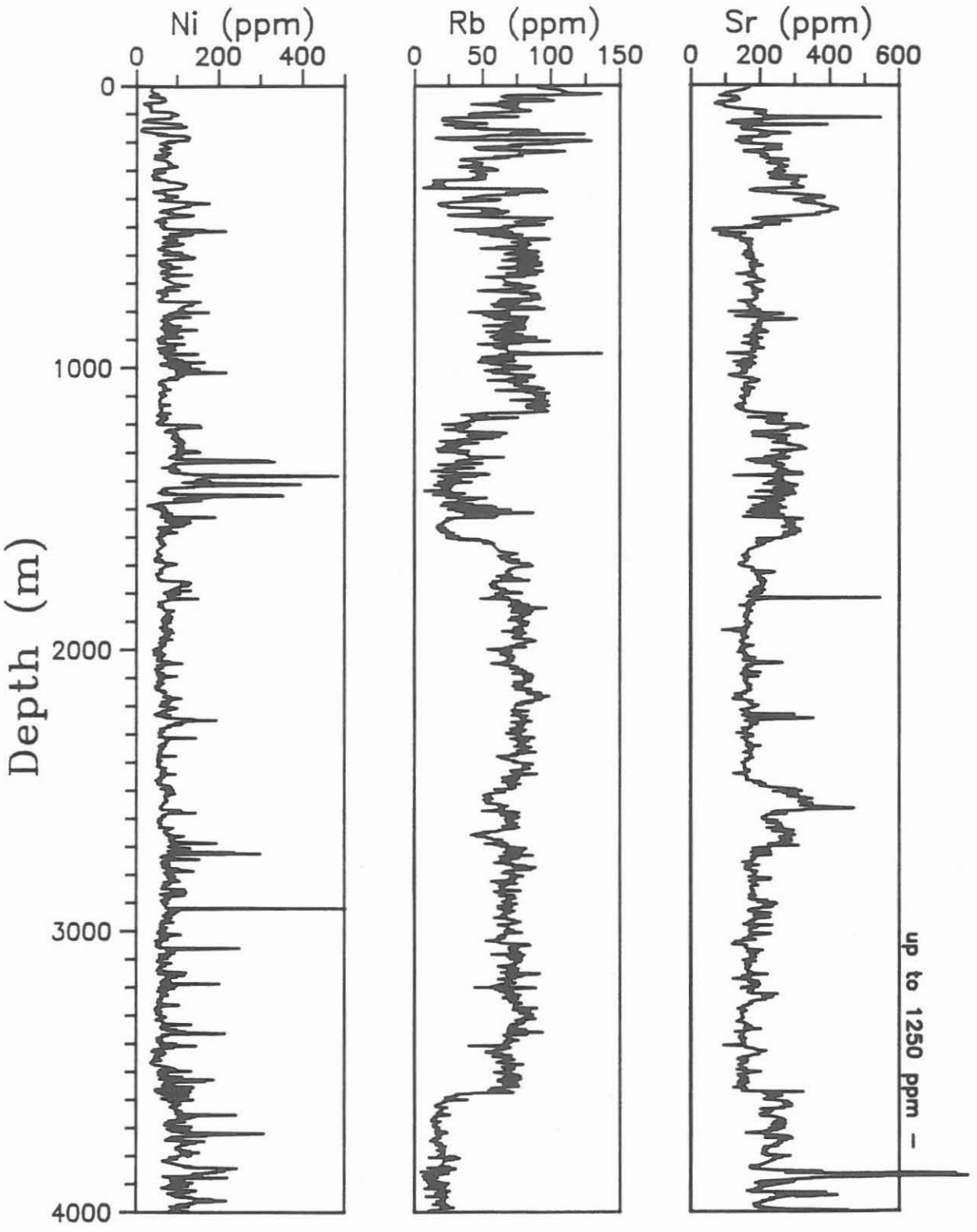
Ni (ppm)
0
200
400
Rb (ppm)
0
50
100
150
Sr (ppm)
0
200
400
600
Depth (m)
0
1000
2000
3000
4000
up to 1250 ppm

C.5.2 Results of cation and anion analyses

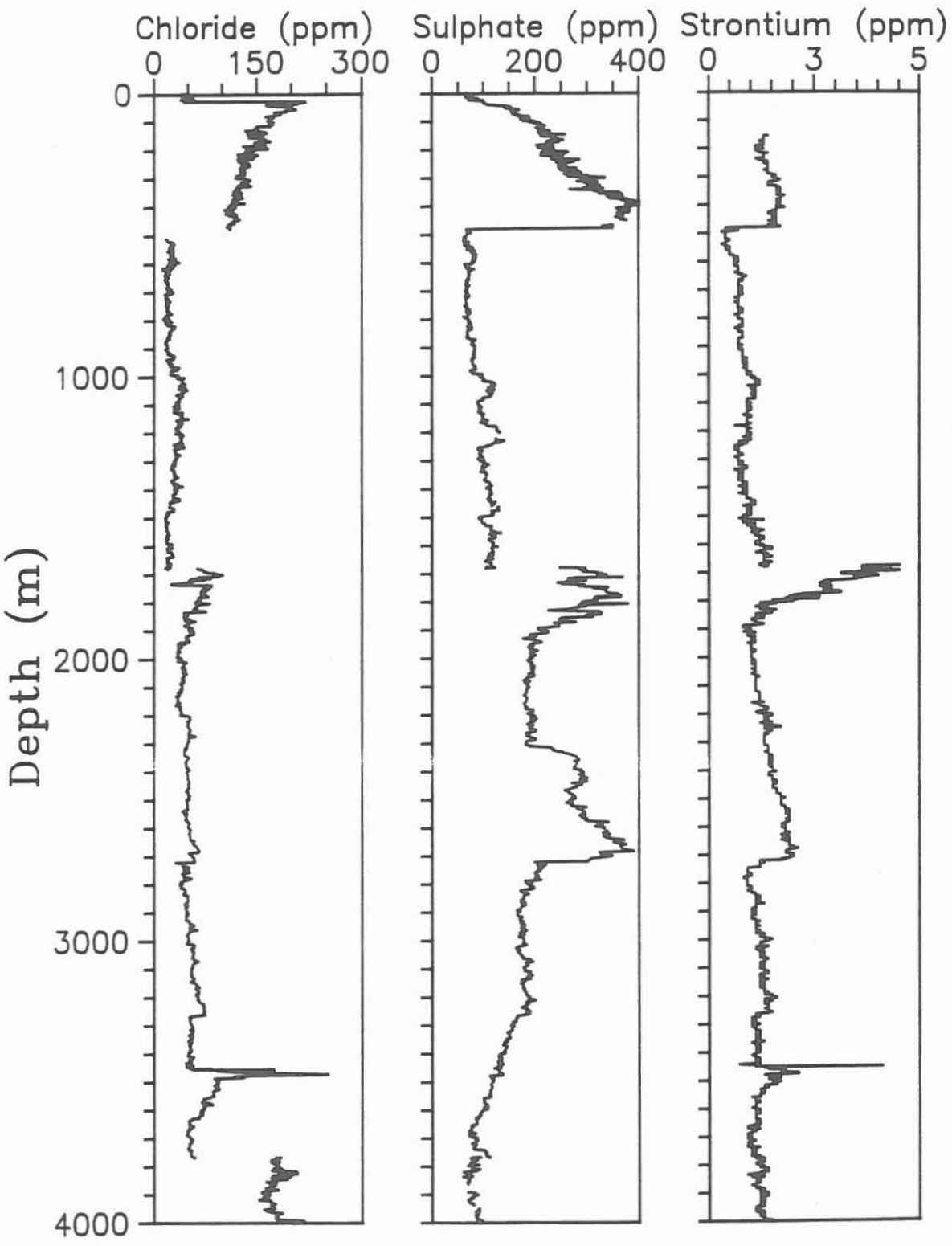

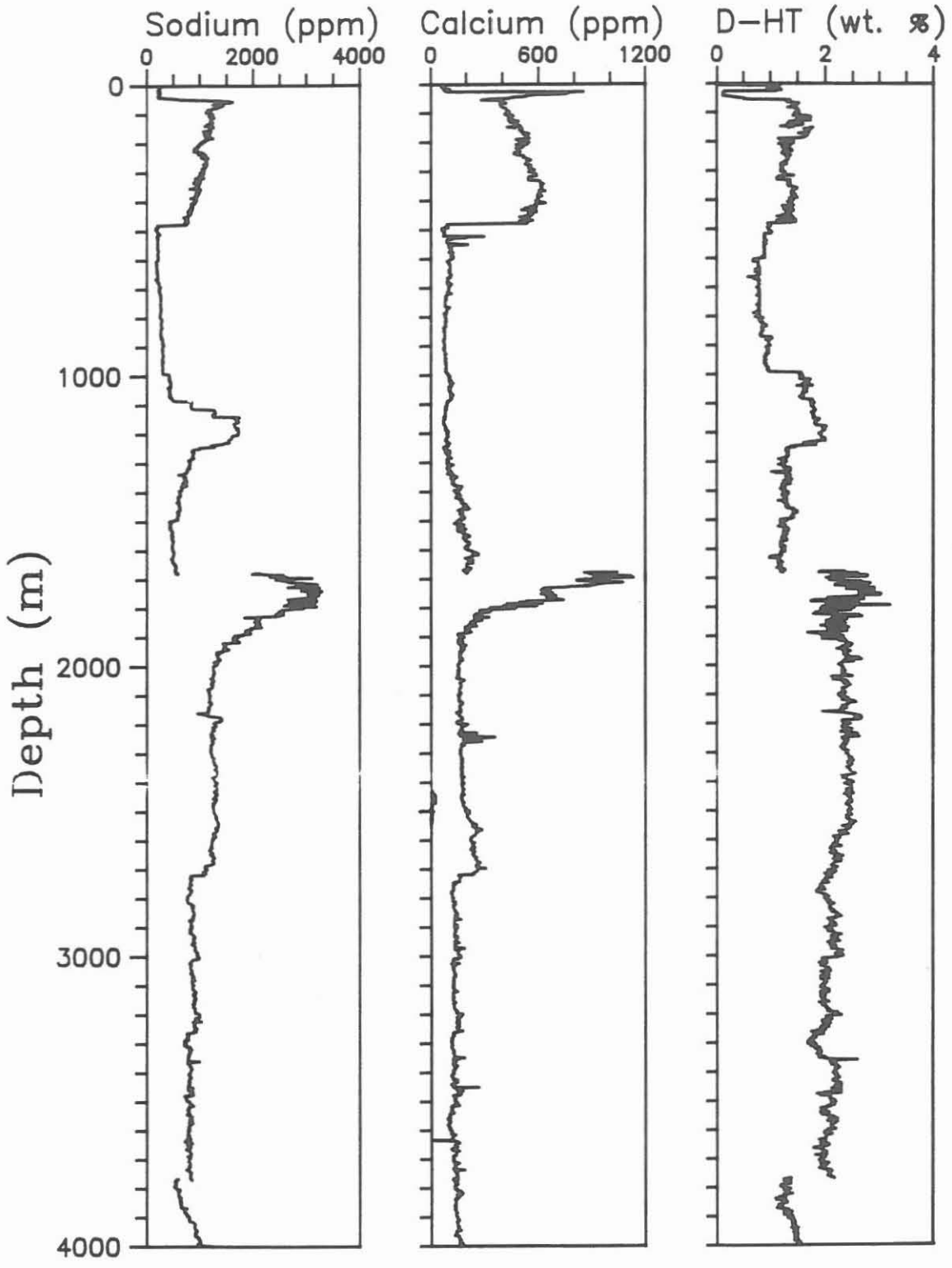
Sodium (ppm)
0
2000
4000
Calcium (ppm)
0
600
1200
D–HT (wt. %)
0
2
4
Depth (m)
0
1000
2000
3000
4000

C.5.3 Results of gas analysis

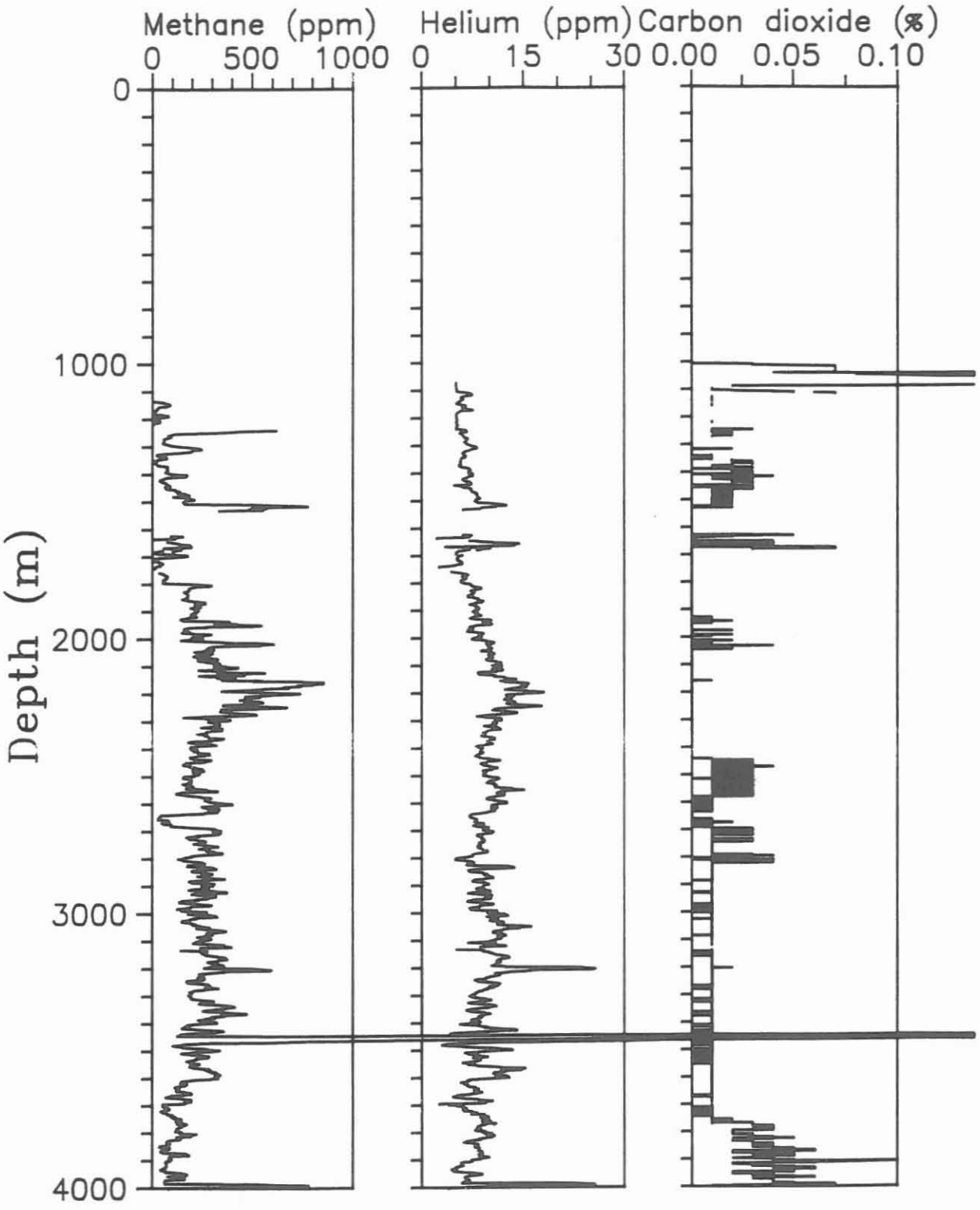

Fig.C.5.3.1: Variations with depth of methane, helium and carbon dioxide contents (average values) of liberated gas phases from KTB pilot well VB 1

KTB-Report	90-8	D1-D29	13 Abb.	Hannover 1990

KTB pilot hole.
Results obtained in the KTB Field-Laboratory.

D. Geophysics

Bücker*, Ch., Huenges*, E., Lippmann*, E., Rauen*, A., Streit*, K.M., Wienand*, J. & Soffel**, H.C.

Contents:

Address of the authors :
* KTB-Feldlabor
D-8486 Windischeschenbach
FRG
** Inst. f. Allgemeine u. Angewandte Geophysik
Theresienstr. 41/IV
D-8000 München 2
FRG

D.0 Summary

The following physical parameters were determined in the KTB field-laboratory: density (2 methods: Archimedian and gamma-ray absorption); sonic longitudinal and shear wave velocity; natural remanent magnetization; magnetic susceptibility; natural gamma-ray activity; electrical conductivity; thermal conductivity; porosity; inner surface; permeability and strain relaxation.

Most experiments and instruments have been specifically developed for the KTB field-laboratory by members from different universities in Germany. By having the laboratory close to the drill hole it is possible to observe irreversible changes in the samples occuring within hours and days after core recovery.

As an overview nearly all results are shown in a composite log in Fig. D.0.1. The results can be summerized as follows:

It has been expected that the lithology is reflected in a simple way by such parameters as density, gamma-ray activity, magnetic properties, thermal conductivity and seismic velocity. Through the measurement of natural remanent magnetization and susceptibility magnetic ore mineralization was detected within gneiss sections. Mean values related to the main lithological units can be found in the text.

The anisotropy of many physical properties of the metamorphic rocks from the KTB pilot hole is remarkable. For the thermal conductivity it is up to 30 % and for the p-wave velocity it is up to 40 %. The high anisotropies are in part due to effects associated with stress release. The in situ anisotropies are believed to be much smaller.

The electrical resistivity correlates with the presence of graphite and of open pores. The intensity of fracturing could be characterized by inner surface data.

Fig. D.0.1: (next page)
Composite log of several physical properties (details see further text).
ϱ = density (2.5 - 3.3 g/cm³), v_p = p-wave velocity (4 - 7 km/s), NRM = natural remanent magnetization (10 - 10^6 mA/m), æ = susceptibility (10^{-4} - 10^{-1} SI), R = electrical resistivity (10 - 10^5 Ωm), ϕ = porosity (0 - 6 %), K = thermal conductivity (2 - 4.5 W/mK).
On the right side: a simplified lithological profile (M = Metabasites, BG = Biotite Gneisses, G = Gneisses).

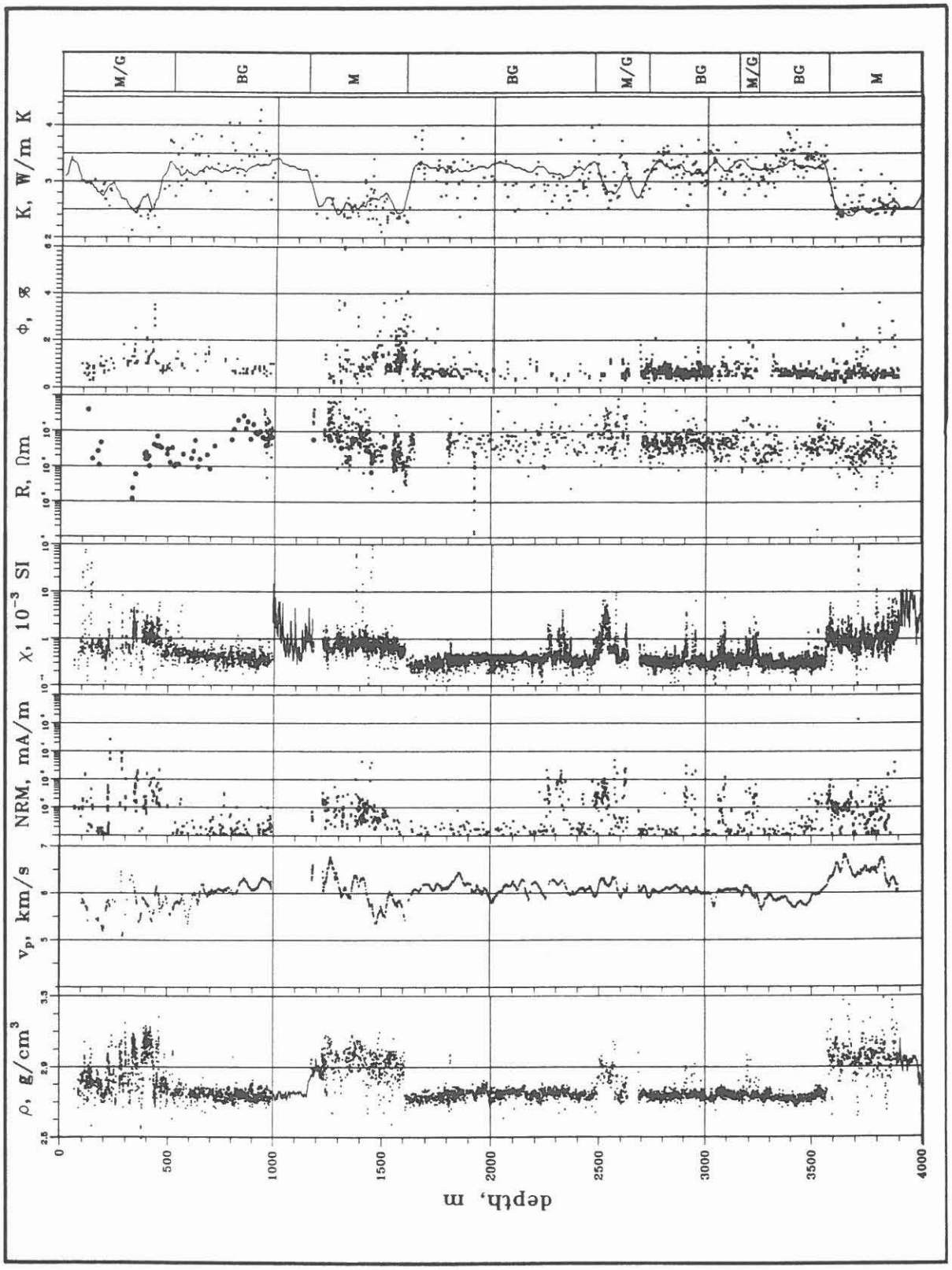
M/G
BG
M
BG
M/G
BG
M/G
BG
M
K, W/m K
Φ, %
R, Ωm
χ, 10⁻³ SI
NRM, mA/m
vp, km/s
ρ, g/cm³
depth, m
0
500
1000
1500
2000
2500
3000
3500
4000

Fig. D.0.1

D.1 Density

D.1.1 Introduction

The knowledge of the density distribution with depth is necessary for example for the interpretation of surface measurements (e.g. gravity). Between 0 and 4000 m the density of 4418 core samples was measured using the "Archimedian method" (BÜCKER et al. 1988). The density of 754 cutting samples was determined with a pycnometer (RAUEN et al. 1988). The cuttings were recovered in sections where a roller cone bit was used. LAUTERJUNG et al. (1990) showed that a model density could also be determined from the mud using the results from the XRD-measurements (see chapter "C" same issue). A comparison of borehole and laboratory density data and methods is shown in GATTO & BÜCKER (1990). The density of cores could also be measured with the gamma-absorption method with a high spatial resolution (BÜCKER et al. 1990).

D.1.2 Results

The complete profile of the density and the lithological units in figure D.1.2 shows that lower values are associated with the gneisses, higher and more scattered data with the metabasites, respectively. The density of gneisses varies from 2.49 g/cm³ to 2.99 g/cm³. The density of the metabasites varies from 2.56 g/cm³ to 3.29 g/cm³. Density data of cuttings and cores are generally in close agreement. Possible differences in special sections are due to a contamination of the cuttings by cavings or abraded particles from the drilling tool. Therefore the data obtained from cuttings are not quite as reliable as those from cores.

A statistical analysis using histograms (figure D.1.1) characterizes the density values. The two maxima can be related to the two principal lithological units. Gneisses show an average density of 2.75 ± 0.04 g/cm³ with a relatively low standard deviation. The average density of the metabasites is 2.93 ± 0.1 g/cm³. The lithological units of the KTB pilot hole can be clearly distinguished by their average densities.

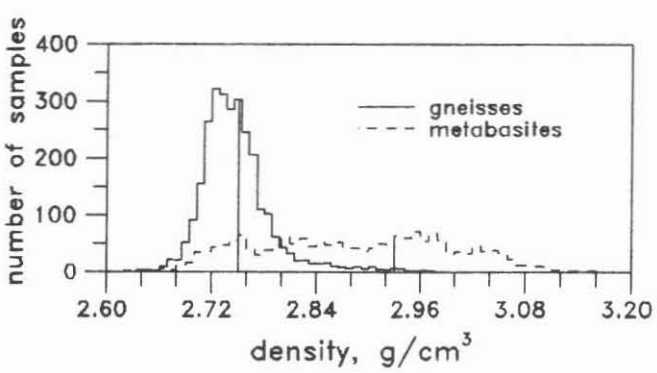

Fig. D.1.1: Frequency distribution of measured densities of cores in the depth range 0 - 3889 m of the KTB pilot drill hole.

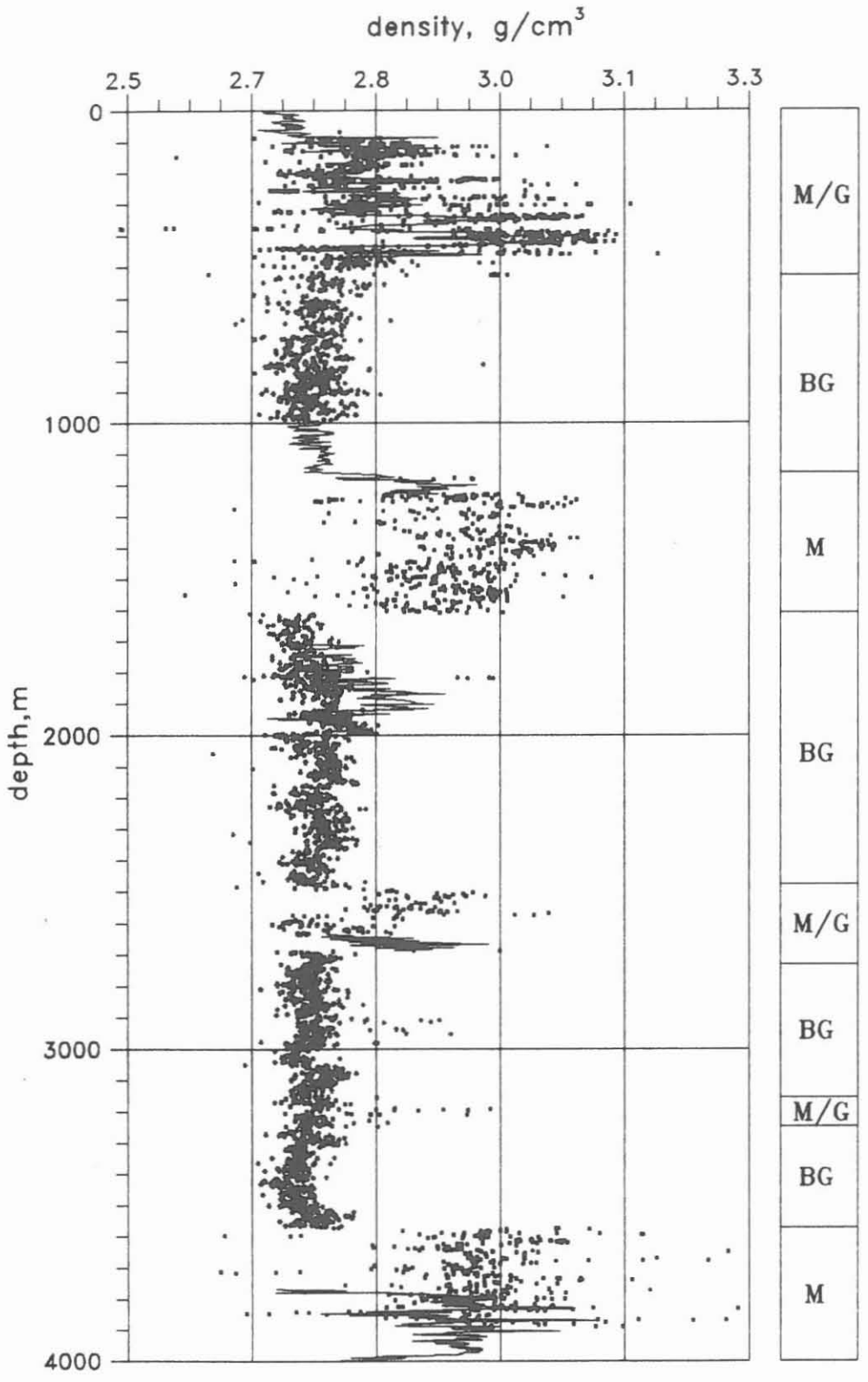

Fig. D.1.2: Density profile of cores (■) and cuttings (-) of the KTB pilot hole measured with the "Archimedian method". On the right side a simplified lithological profile is shown (M=Metabasites, BG=Biotite-Gneisses, G=gneisses).

D.2 Natural Gamma-Ray Activity

D.2.1 Introduction

The analysis of the natural gamma radiation allows to identify various gamma ray emitters.

The quantitative determination of the potassium, uranium and thorium content helps to distinguish between lithological units. Furthermore the heat production rate can be calculated with the formula after RYBACH (1976).

Natural gamma radiation was measured as part of the logging program and in the laboratory on cores, cuttings and mud. This allowed a depth control for logging (BÜCKER & ZIMMERMANN, 1989).

All data reported were measured with NaI crystals. Cuttings were measured in air-tight Marinelli-beakers, and for the measurements of the cores a special equipment with 3 NaI crystals was used. For the quantitative evaluation of the potassium, uranium and thorium content of the samples peaks in the gamma spectra at the energies 1461 keV (K-40), 1764 keV (U-238) and 2614 keV (Th-232) are used and calibrated against measured gamma spectra of standards. A detailed description of the equipment and the data processing is given in HUENGES et al. (1989) and WIENAND et al. (1989), respectively. Some results are also published in RAUEN et al. (1990). As an overview, the results obtained from cuttings are reported.

D.2.2 Results

In the depth ranges 992 - 1240 m, 1900 - 1998 m and 3900 - 4000 m only cuttings were available due to directional drilling phases. The contents of potassium, uranium and thorium in the cuttings are plotted versus depth in figure D.2.1. They characterize in the depth range 1140 - 1200 m the transition from gneisses to metabasites at 1160 m. From 1177 - 1183 m, most cuttings were identified as cavings. The mean contents of K, U and Th are summarized in Table D.2.1 as well as the heat production rate H, which is three times higher for the gneisses than for the metabasites.

A comparison between the laboratory and the logging results of the NGS (Natural Gamma Spectrometer, see DRAXLER & HÄNEL, 1988) shows close agreement for uranium and thorium (see HUENGES et al. 1989). Potassium concentrations, however, differ as much as 0.5% with the higher readings being from the NGS.

In the depth range 1900 - 1998 m a uranium enrichment became apparent (see figure D.2.1). The rocks consists of biotite-

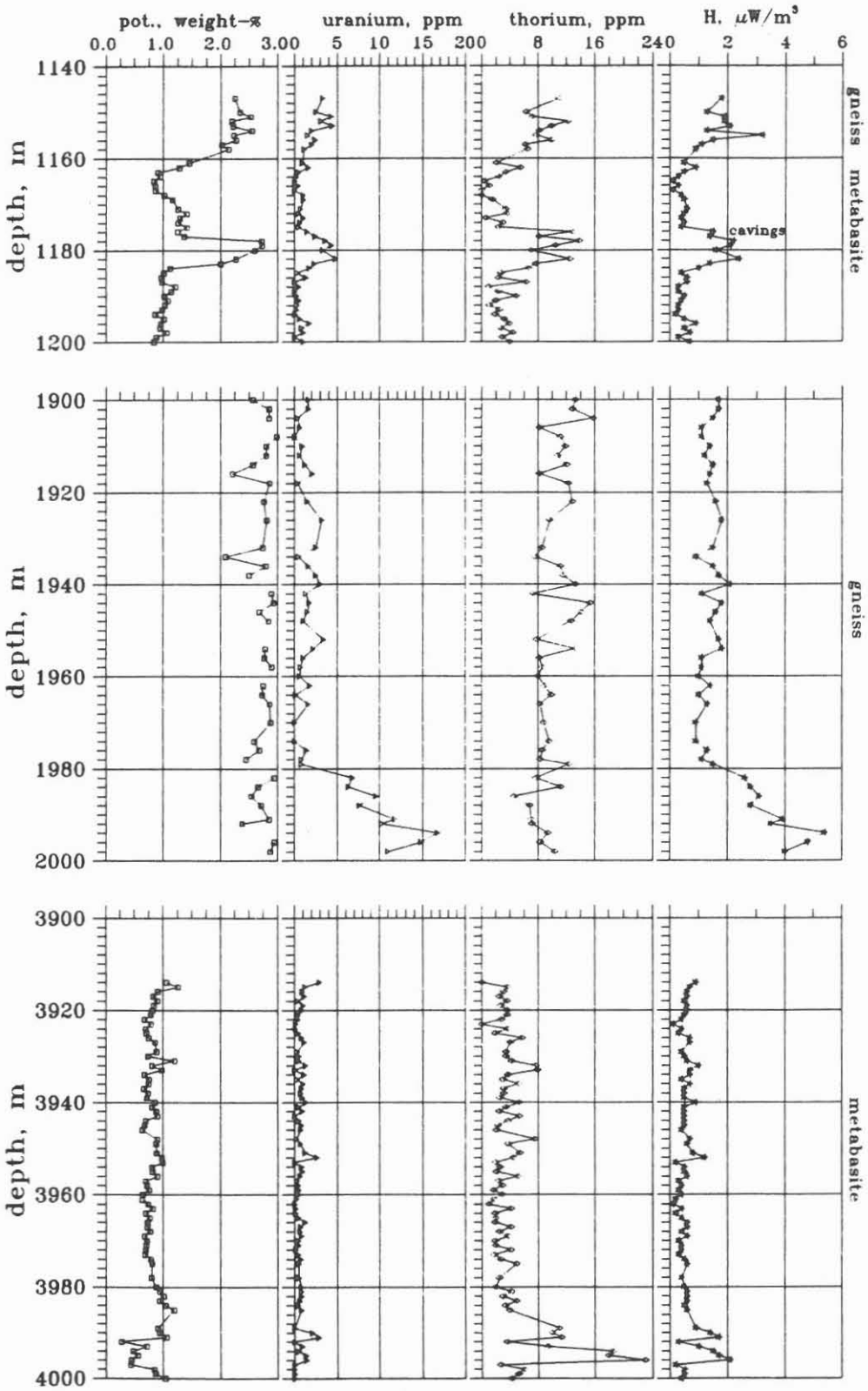

Figure D.2.1: Gamma-ray activity profiles with the potassium, uranium and thorium contents measured on cuttings. The heat production rate H was calculated with the formula after RYBACH (1976).

Table D.2.1: Mean contents of potassium, uranium, thorium and the heat production rate H (± standard deviation) from 1140 to 1210 m.

	K %	U ppm	Th ppm	H µW/m³
gneisses	2.28±0.17	2.6±1.2	8.2±2.0	1.7±0.7
metabasites	1.05±0.16	0.6±0.5	2.5±1.6	0.5±0.2

sillimanite-gneisses. This uranium-enrichment coincides with high graphite- and helium-contents (see MASSALSKY et al. 1988, HOMANN et al. 1988). High helium contents could also be detected below 3985 m, where a thorium-enrichment could be found (see figure D.2.1). Probably the increased helium-content is associated with the α-particles of the uranium and thorium decay sequences.

The histogram of the counting rate obtained from cores (see RAUEN et al. 1990) shows two maxima at 17 c/s and at 77 c/s, separated by a minimum at 40 c/s. These two maxima correlate with the two main lithological units. The higher values occur in gneisses whereas the lower values are associated with the metabasites.

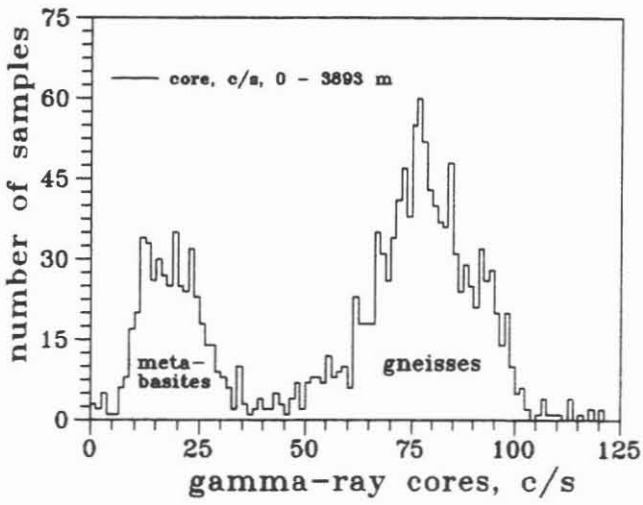

Fig. D.2.2:

Normal frequency distribution of the gamma-ray counting rate of drill cores. All data from 0 - 3900 m are shown. Only a few measurements were above the range of 125 c/s (e.g. for the aplites). The two maxima correspond to the two main lithological units.

D.3 Ultrasonic seismics

D.3.1 Introduction

Ultrasonic velocities are studied in the KTB field laboratory on a routine basis at normal temperature and pressure for several reasons, e.g.
- correlation between seismic velocities and other physical and lithological rock properties,
- improved understanding of seismic velocities and structures derived from seismic field experiments,
- as a basis for a purposeful selection of samples for more detailed laboratory investigations,
- for comparison of rock properties at in-situ and at normal conditions,
- for the investigation of time-dependent petrophysical effects after core recovery.

The last aspect requires measurements as soon as possible after coring and subsequent repetitive measurements.

D.3.2 Methods and Equipment

Ultrasonic wave propagation through core samples is studied in a water tank to insure good signal transmission between transducer, rock specimen and receiver and to avoid time-consuming mechanical preparations.

Down to about 2300 m commercial equipments for ultrasonic testing (USIP11, USL33 and USD10 from KRAUTKRÄMER GmbH) were used and only radial p-wave velocities and their anisotropy (in the plane normal to the core axis) could be measured. Below that depth a specifically designed instrumentation, which was developed at the Institut für Allgemeine und Angewandte Geophysik of the University of Munich was used. In addition to radial v_p-measurements by pulse transmission it allows the determination of axial p- and s-velocities by common mid-point (CMP) refraction experiments, with water as the upper and the core as the lower layer. By rotating the cores, all measurements are performed for variable azimuths. Computer control of all mechanical and electronical operations, digital 10-bit data acquisition, signal stacking and interactive seismogram evaluation are essential features of the system. Seismograms can be stored digitally on magnetic tape for further off-line analysis in the field laboratory or elsewhere.

D.3.2 Results

Fig. D.3.1 shows a synopsis of the results for the pilot hole. It includes from left to right as functions of depth:
- the maximum radial p-wave velocity $v_{p,max}$
- the anisotropy coefficient $(v_{p,max}-v_{p,min})/v_{p,mean}$ of the

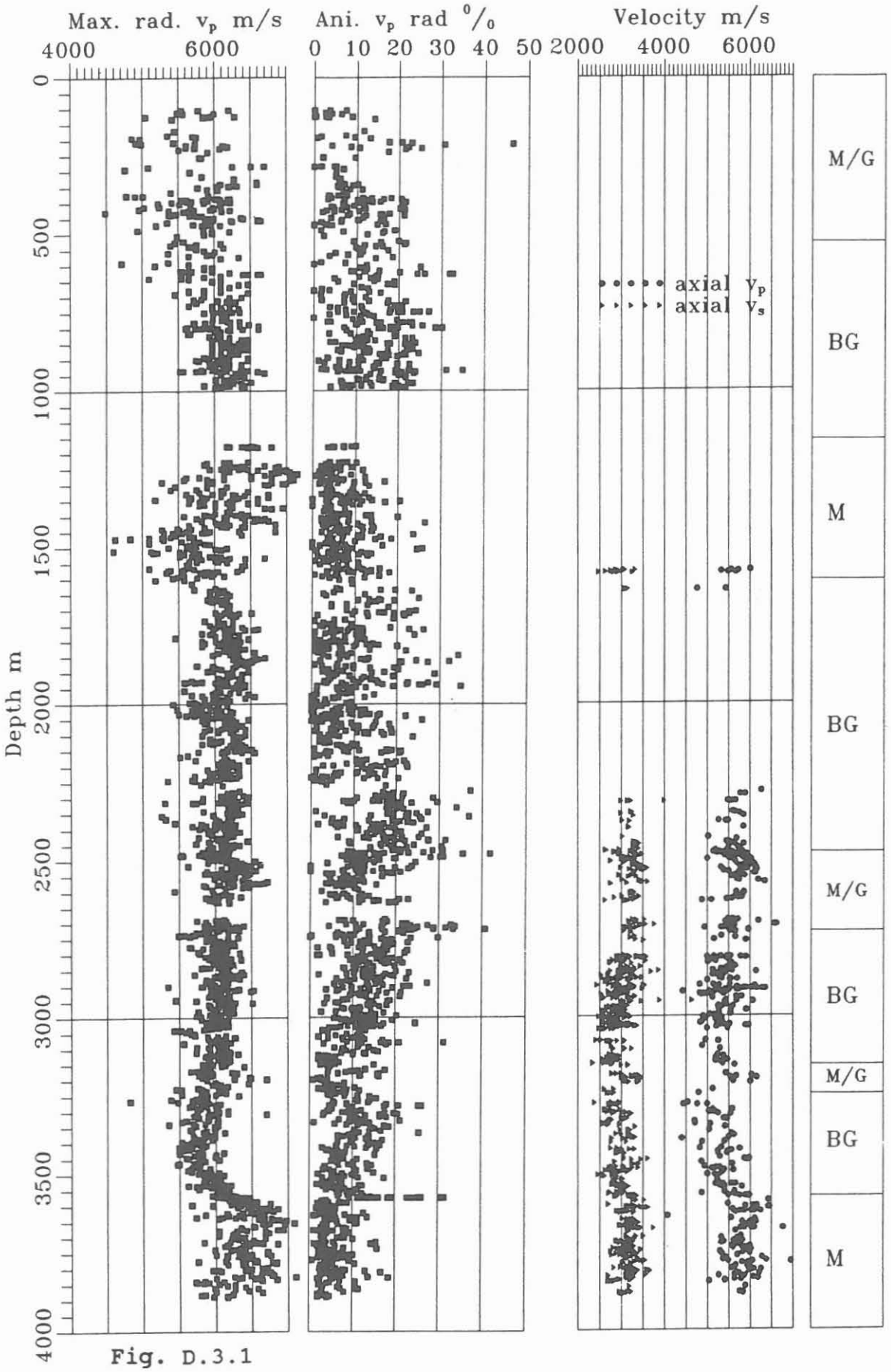
Max. rad. v_p m/s
4000
6000
Ani. v_p rad %
0 10 20 30 40 50
Velocity m/s
2000
4000
6000
axial v_p
axial v_s
Depth m
0
500
1000
1500
2000
2500
3000
3500
4000
M/G
BG
M
BG
M/G
BG
M/G
BG
M

Fig. D.3.1

radial p-wave velocity
- the axial s- and p-wave velocities, and
- a simplified lithology log (G=gneiss,BG=biotite-sillimanite-gneiss, M=metabasite, M/G=metabasite and gneiss intercalations).

In total 1850 core samples have been investigated. The gaps from 1000 to 1230 m and from 2630 to 2680 m are due to directional drilling phases without core recovery.

Ultrasonic velocities measured at normal pressure should be interpreted cautiously in terms of lithology because they may be strongly influenced by pressure relief induced microfracturing and variable water saturation. A time dependent decrease of velocities within hours or days after core recovery is usually observed in the field laboratory (LIPPMANN et al. 1989). The effect is most pronounced for wave propagation normal to foliation, that means in the direction of the smallest velocities. The fastest velocities, which are observed parallel to foliation, seem to be less affected by pressure relief (left column in Fig D.3.1) as indicated by the rather high values of these velocities, exceeding 7.0 km/s for some metabasitic cores, and their weak dependence on water saturation. Nearly all cores exhibit a marked anisotropy of the radial p-velocities. Extremes of more than 40 % have been observed. Multiple values in the anisotropy log at equal depth stem from repetitive measurements; with progressive water saturation the anisotropy decreases. Axial p-wave velocities are usually intermediate between maximum and minimum radial velocities. This can be explained by the mostly steeply dipping foliation.

In spite of the superimposed effects of microfracturing and fabric loosening, velocities and lithology are clearly correlated. Apart from a near surface gradient layer, velocities and their variance are generally larger for metabasites than for gneisses and the opposite correlation holds for the seismic anisotropy.

In cont st to v_p, the axial s-wave velocities show no significant dependence on water saturation. Their variance in Fig. D.3.1 is however clearly influenced by birefringence; s-waves with polarisation parallel to foliation propagate faster than with normal polarization. The average axial v_p/v_s ratio is 1.8 with a weak tendency of increasing v_p/v_s with v_p.

The different anisotropy effects are certainly enhanced at normal conditions, because of prefered orientation of microcracks parallel to foliation. With reduced intensity, however, they are also to be expected under in-situ conditions and should be considered in the evaluation of seismic field experiments.

D.4 Thermal conductivity

D.4.1 Introduction

The knowledge of thermal transport properties of rocks is required for a complete interpretation of the temperature profile of the borehole. In particular the thermal conductivity is used in conjunction with the temperature gradient to calculate the heat flow. A thermal conductivity profile was established from laboratory determinations on cores at intervals of 5 to 10 m, providing a good resolution of the heat flow with depth.

Thermal conductivity measurements were performed on relaxed samples a few months after core recovery using a half space line source. The cut and polished cores were placed in water for more than one hour prior to the measurement under ambient conditions. The heating curve of the source was measured five times at three orthogonal positions on the core and evaluated using a new automatic method giving errors smaller than 5 % (HUENGES et al. 1990).

In general, the thermal conductivity of rocks is anisotropic with the higher value in the plane of foliation and the smaller perpendicular to the foliation. As a consequence of line source measurements the thermal conductivity is determined in the plane approximately perpendicular to the direction of the source. Therefore the data must be transformed to obtain the thermal conductivity in specific directions. HUENGES et al. (1990) described the method to calculate main axis and vertical thermal conductivities of the cores based on a transformation of GRUBBE et al. (1983), using the azimuth of dip and dip angle of foliation.

D.4.2 Results

Figure D.4.1 shows the frequency distributions of the data transformed to the foliation orientation with logs of mean and vertical thermal conductivities. Table D.4.1 lists the thermal conductivities corresponding to the main lithological units.

The mean values are calculated as arithmetic means of the values in the three orthogonal directions. Metabasites are characterized by lower and gneisses by higher mean values, respectively.

The thermal conductivities parallel and perpendicular to the foliation can be summarized as follows: The gneisses from 530 m to 992 m and from 2730 m to 3575 m are strongly anisotropic, whereas the gneisses between 1610 m and 2477 m appear to be less anisotropic. The metabasites between 1160 and 1610 m and below 3575 m are weakly foliated and conse-

quently no significant anisotropy of thermal conductivity was observed.

The anisotropies of the gneisses can be related mainly to the content and distribution of quartz and mica in the rocks (de WALL et al. 1990).

The vertical thermal conductivity is determined by the rock type and by the dip angle. Low to moderate thermal conductivity of 2.9 ± 0.7 W/m K with a high standard deviation characterize the alternating layers of gneisses and metabasites. Moderate to high thermal conductivity of 3.4 ± 0.5 W/m K is measured within the gneiss sections with a high standard deviation due to the local strong variation of the dip angle. Low values of thermal conductivity, with relatively small standard deviation, 2.6 ± 0.3 W/m K characterize the metabasite sections.

Tab. D.4.1: Summary of the transformed mean thermal conductivity results for main lithological units.

depth ranges in m	main lithology	thermal conductivity in W/m K		
		parallel to the foliation	perpendicular to the foliation	parallel to the borehole
530 - 992 1610 - 2477 2730 - 3155 3155 - 3575	gneiss	3.6 ± 0.7	3.0 ± 0.5	3.4 ± 0.5
1160 - 1610 3575 - 3860	metabasite	2.6 ± 0.4	2.5 ± 0.4	2.6 ± 0.3

Although the data are more or less scattering, a comparison of the mean and the vertical thermal conductivities leads interesting observations. As figure D.4.1 shows, the vertical thermal conductivities are higher than the mean values except for the depth range between 2700 and 3400 m. In this section a significant higher difference between both logs with higher mean values is observed. This correlates with a flat dip angle of foliation.

As a conclusion, the variation of the thermal conductivity in the KTB pilot hole is due to the lithology and the layering of the textured rocks.

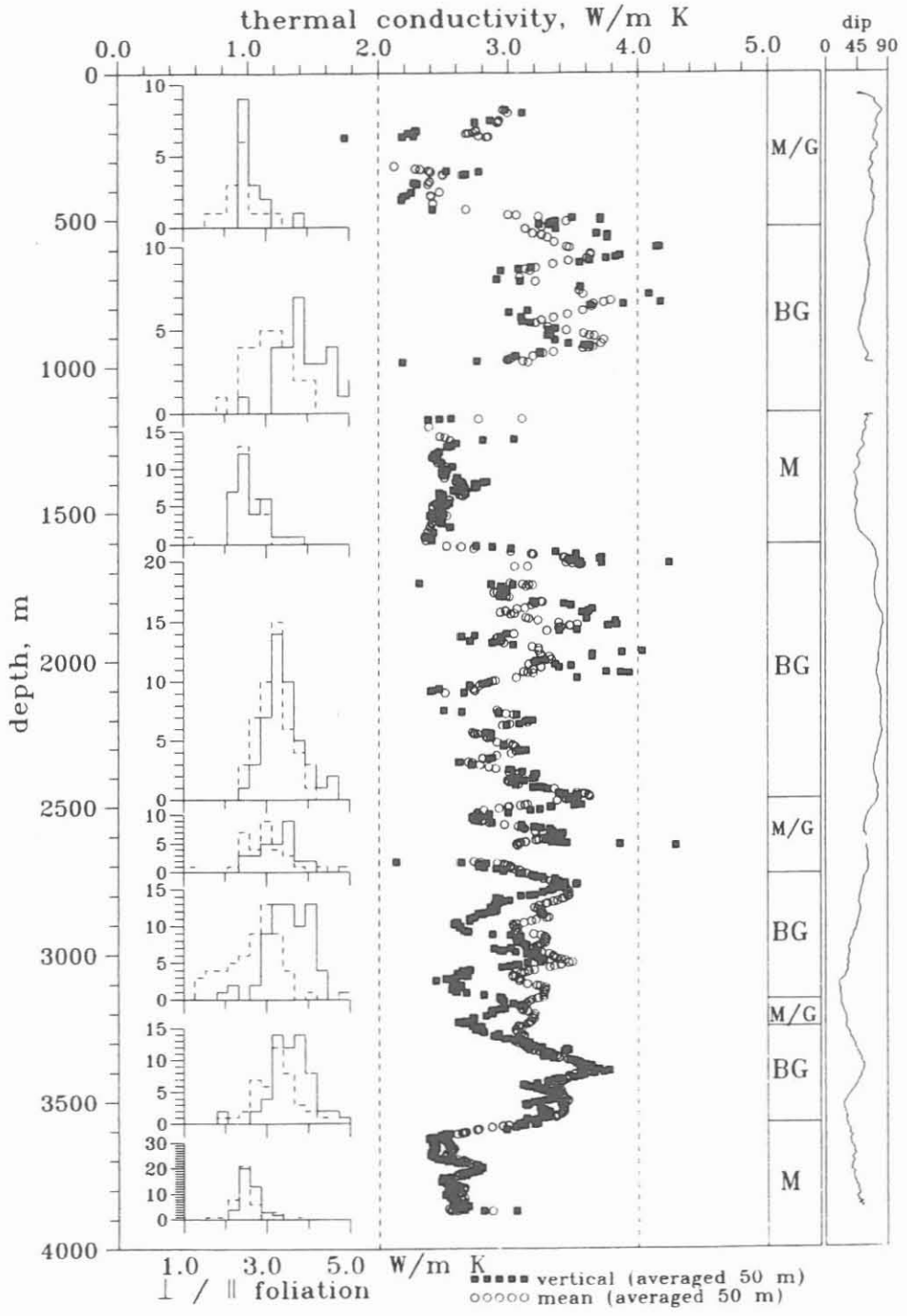

Fig. D.4.1: Mean thermal conductivities of KTB-VB cores (o) and values transformed to the direction parallel to the borehole axis (▪). Within the figure the frequency distributions of thermal conductivities ⊥ foliation (---) and ∥ foliation are shown. The distributions are valid for the depth range given by the length of the frequency axis. On the right side a simplified geological profile (M = Metabasite, BG = Biotite Gneiss, G = Gneiss) and the dip angle are shown.

D.5 Electrical Resistivity

D.5.1 Introduction

From 0 to 3200 m, resistivity was determined on relaxed and below 3200 m on cores short time after drilling. The specimen were placed in a basin of tap-water for approximately 24 hours prior to the measurements, so open and near surface pores could be filled with water. Tap-water was also used to minimize contact resistance between current electrodes and core surface.

In the depth range from 0 to 1530 m a classical 4-electrode technique was applied. An alternating current of 20 Hz was led via plate electrodes into the plane cut ends of the drill core. The voltage was measured between 2 ring-shaped electrodes, which were wrapped parallel around the cylindrical sample (RAUEN et al. 1988).

Below 992 m, current input and measurement of the voltage difference using a lock-in-amplifier at 150 Hz was done with small, nearly point-like electrodes in a WENNER configuration (spacing 2 cm, some mm^2 contact area on the core). Special preparation of the drill core was no longer necessary. Routinely 12 points on the core mantle surface at different azimuths were measured with electrodes parallel to the z-axis . The average resistivity and variation was calculated from these 12 measurements (HUENGES et al. 1989).

D.5.2 Results

The depth log of the resistivities is shown in Fig. D.5.1, covering nearly 6 decades. Measurements on one core sample often scatter in a range of more than 1 decade (e.g. at 2870 m, WOLTER et al. 1989).

The predominant units of lithology (simplified in the middle of fig. D.5.1) cannot be identified from a significant change in resistivity, also the frequency distributions of separated gneiss- and metabasite-data (fig. D.5.2) show a maximum at about 4000 Ωm in both cases (RAUEN et al. 1990). The mean values of porosity show a similar behaviour (see chapter D.8). The logarithms of the resistivity data follow approximately a normal distribution (WIENAND et al. 1989).

Mean values down to 13 Ωm, at single points < 5 Ωm were measured on a graphite bearing gneiss at 1926 m (HUENGES et al. 1989). Low resistivity values are in general associated with graphite indicating electronical conductivity (e.g. 1928 m, HUENGES et al. 1989; 3535 m, RAUEN et al. 1990).

Around 1610 m (change from gneiss to amphibolite) a drop in resistivity is measured due to a shear zone (see chapter "B"

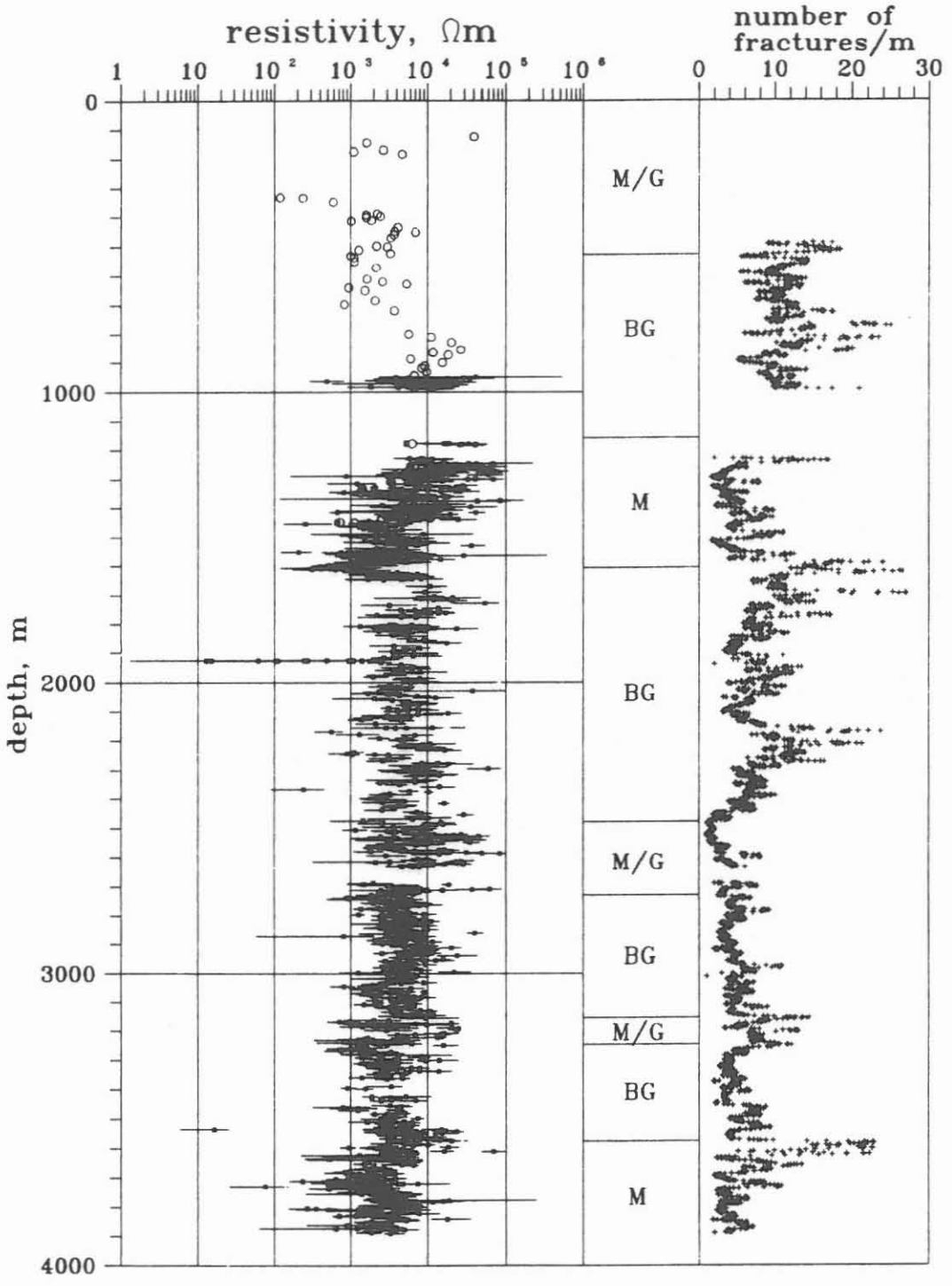

Fig. D.5.1: Resistivities measured on cores from the KTB pilot hole. Open symbols indicate measurements with plate electrodes, closed symbols the mean values gained with the point electrodes in Wenner configuration together with the variation per core. In the middle a simplified lithological profile (M = Metabasite, BG = Biotite-Gneiss, G = Gneiss), on the right side the numbers of fractures per meter, observed on cores are shown (moving average over 10 m).

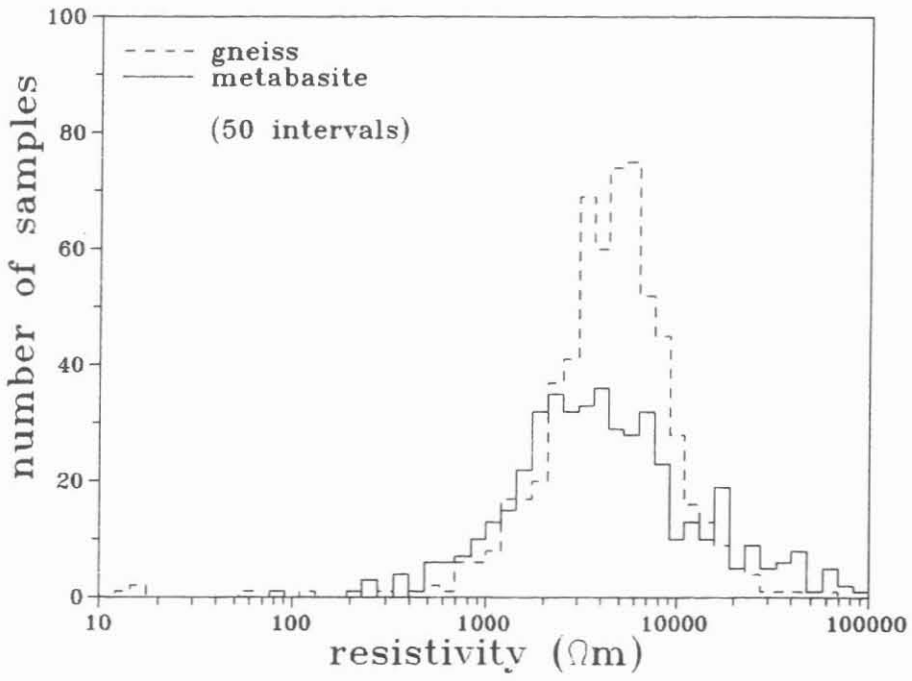

Fig. D.5.2: Log-normal frequency distribution of resistivity data. The data of cores below 1160 m are separated into gneiss- and metabasite-sections (see Fig. D.5.1).

in this issue), with an increasing number of fractures, macroscopically visible on cores (Fig. D.5.1). In these cases the decreased resistivity is due to an increased electrolytical conductivity.

For an analysis of the conductivity processes it is planned to measure the frequency dependence of the complex resistivity.

It can be concluded, that there is no clear correlation between the lithology and the electrical resistivity. The amount of open pores filled with electrolyte and the content of graphite seem to determine the resistivity.

D.6 Natural Remanent Magnetization (NRM)

D.6.1 Introduction

The remanent magnetization between 0 and 3893 m (cored sections) was determined from 1250 core samples with an average sampling interval of 3 m or less where clear anomalies became apparent. The average length of a core fragment was about 30 cm. The magnetic stray field of the core samples was determined with high spatial resolution with 6 flux gate sensors inside a μ-metal tube. Details of the equipment and the precision of the measurements are given by RAUEN et al. (1988). For detailed description of the lithology see chapter B of this report.

D.6.2 Results

The NRM is measured without any AC or thermal demagnetization. The results obtained do not necessarily reflect the in situ properties of the rocks, because of a strong remanence component induced by the drilling process. However, the magnetization is a very sensitive marker for the ferrimagnetic ore minerals. With the help of the NRM and susceptibility, material can be selected for polished section studies of the magnetic ore phases and further rockmagnetic studies.

Table D.6.1: Logarithmic mean values of remanent magnetization of nine depth intervals. In the last two rows the mean values for the strongly and weakly magnetized sections, respectively, are shown.

Interval	Depth, m	Remanence, mA/m	Lithology
A	0 - 480	150	M/G
B	480 - 990	14	G
C	1177 - 1550	71	M
D	1550 - 2220	17	G
E	2220 - 2630	145	G
F	2630 - 2900	16	G
G	2900 - 3250	63	M/G
H	3250 - 3575	28	G
I	3575 - 3893	90	M/G
A,C,E,G,I	Σ = 1961 m	104	M + G
B,D,F,H	Σ = 1775 m	19	G

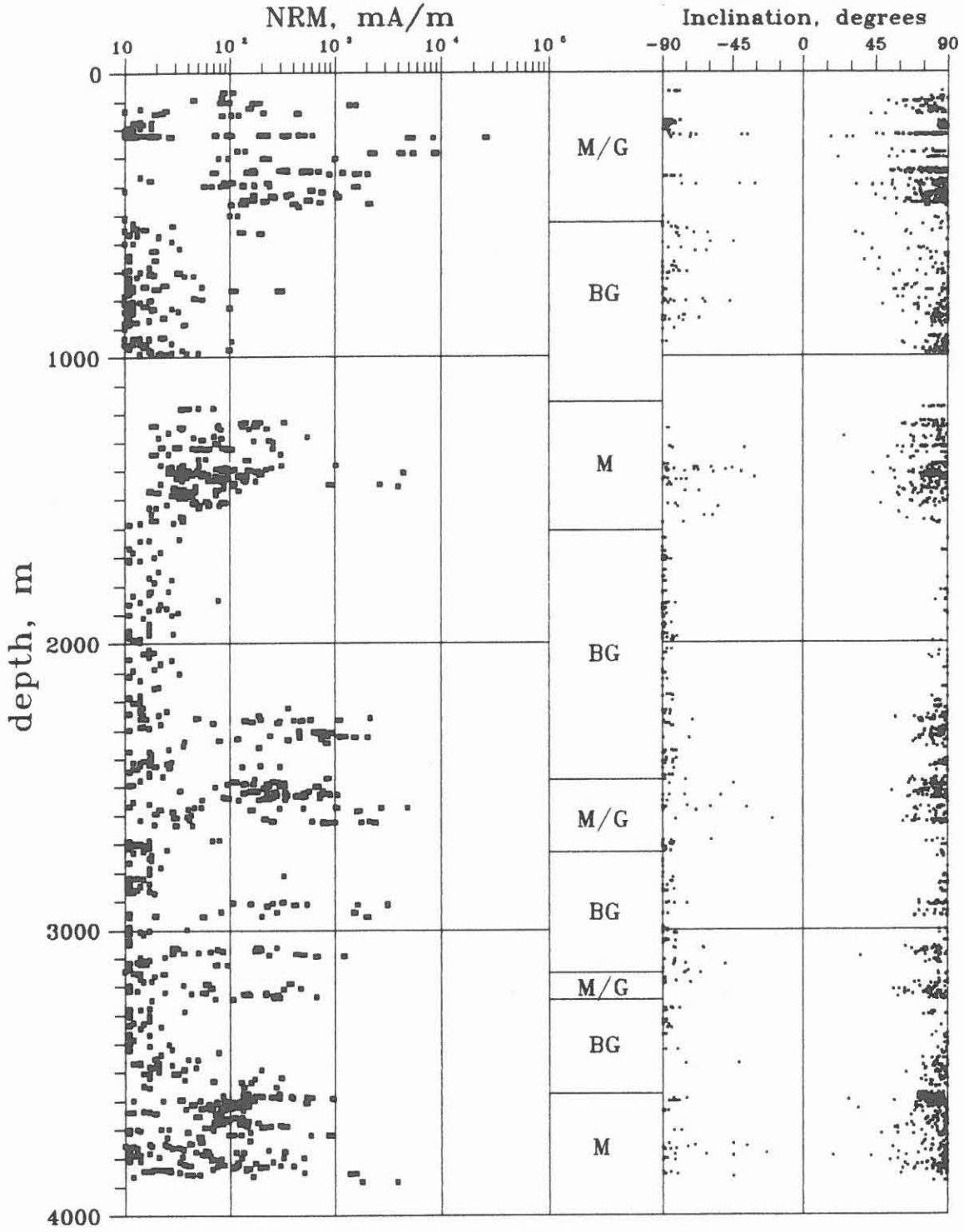

Figure D.6.1: Depth log of natural remanent magnetization (left) and inclination of NRM (right). The main lithologies are shown in the middle: M/G = layering of Metabasites and Gneisses, BG = Biotite-Gneisses.

The depth log of NRM measurements (Fig. D.6.1) allows to discriminate easily between gneisses with low and metabasites with high magnetization. The log can be divided into 9 sections (see Table D.6.1). At depths below 2200 m, however, high magnetizations were detected within gneiss sections, which could otherwise not be distinguished from other gneisses (i.e. by density). Pyrrhotite was found to be the carrier of magnetization in these sections by ore microscopy. Only in the depth ranges near 150 m and 3720 m, magnetite is the dominant carrier of magnetization. Low magnetizations occur only in gneiss sections but not in metabasite sections (see Table D.6.1).

On the right side of Fig. D.6.1 the inclination of NRM is plotted versus depth. Steep negative as well as steep positive inclinations between 60° and 90° are dominant over the whole depth range. It is remarkable, that often the steep negative inclinations were detected in areas with low magnetization. From the DSDP (Deep Sea Drilling Project) and other drilling projects a relation between steep inclinations and soft remanences (weak coercivities) was reported (i.e. ADE-HALL & JOHNSON 1976, BURMESTER 1977, HALL & RYALL 1977, PETERSEN 1978). Probably the drilling process causes the steep inclinations and the measured values are not representative for the in situ properties of the geological units.

The magnetic values determined from the cores of the KTB pilot drill hole are in good agreement with the magnetic models derived from surface measurements (ground magnetics) (see also e.g. BÜCKER 1987, WEBER & VOLLBRECHT 1986).

D.7 Magnetic Susceptibility

D.7.1 Introduction

The magnetic susceptibility was measured on drill cores, side cores (RAUEN et al. 1990) and cuttings by an inductive device (BARTINGTON M.S.2.). Measurements on cores were made every cm by an automatic, computerized equipment. For further graphic display, mean values of 20 cm intervals were calculated (details explained in BÜCKER et al. 1988).

D.7.2 Results

The depth log of susceptibility is shown in Fig. D.7.1, together with a simplified log of the lithology and the occurrence of magnetic ore discovered by ore microscopy on polished sections (see chapter "B" in this volume).

Varying pollution with abraded material of drilling tools caused increased susceptibility values of cuttings, therefore core data and cuttings data of equal depths are slightly different. Due to a different drilling technique in the first 480 m (roller cone bit, producing a large amount of cuttings), data of cuttings and of cores in this depth range are in better agreement (RAUEN et al. 1988).

The highest values of susceptibility up to 0.2 SI occur in metabasite rocks, i.e. in an amphibolite at 120 m and in a section of meta-ultramafitite at 3720 m. Ore microscopy shows, that in both cases magnetite causes the high susceptibility values. In the gneiss sections magnetite occurs less frequent. It is again observed at 2955 m (BÜCKER et al. 1988; RAUEN et al. 1990; WOLTER et al. 1989).

The strongly dominating ferrimagnetic mineral is pyrrhotite, which causes the main susceptibility anomalies in gneiss, e.g. at about 2300 m or around 3000 m (HUENGES et al. 1989; WOLTER et al. 1989 and WIENAND et al. 1989). In gneisses, the susceptibility has values up to $5*10^{-3}$ SI. Pyrrhotite was also detected in metabasitic rocks (e.g. garnet bearing amphibolite at 285 m, RAUEN et al. 1990). (See also the results of investigations of natural remanent magnetization (NRM) in chapter D.6.)

The log shows that metabasite sections are characterized by higher and more scattering values of susceptibilities than gneiss sections (Fig. D.7.1).

The histogram shows two maxima of the total core data separated by a minimum at $0.52*10^{-3}$ SI (fig. D.7.2). The two maxima correspond with the two main lithological units. Higher susceptibility values occur also in gneisses. The metabasites show a broader full width half maximum than the gneisses.

Summarizing the results, one can observe two populations of susceptibility values. Higher susceptibilities occur mainly in metabasites and also in some paragneiss sections.

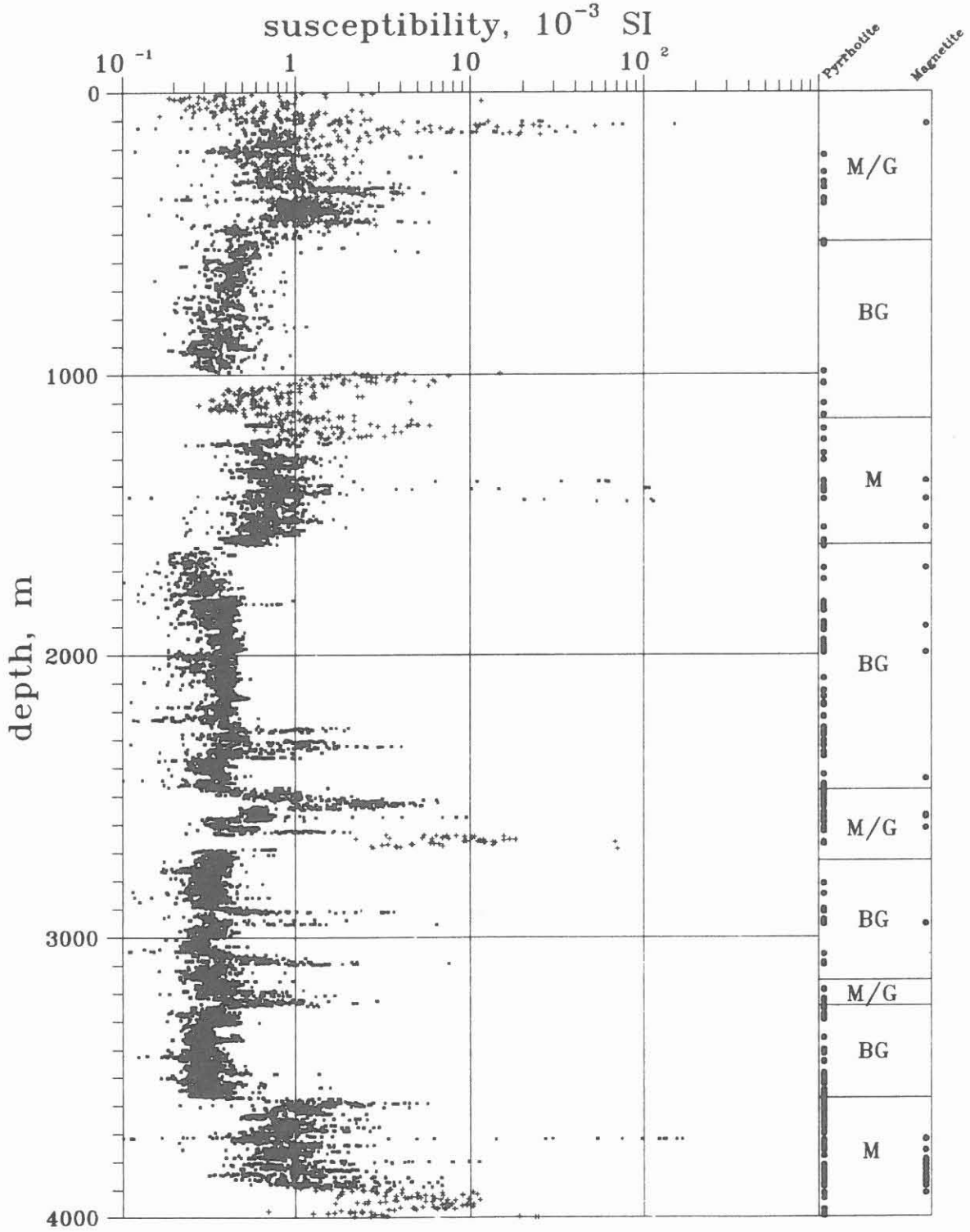

Fig. D.7.1: Depth log of magnetic susceptibility, measured on cores (points) and on cuttings (crosses). At the right side a simplified lithological profile and the occurrence of magnetite and pyrrhotite detected by ore microscopy, is shown (BG=Biotite-Gneisses, M=Metabasites, G=Gneisses).

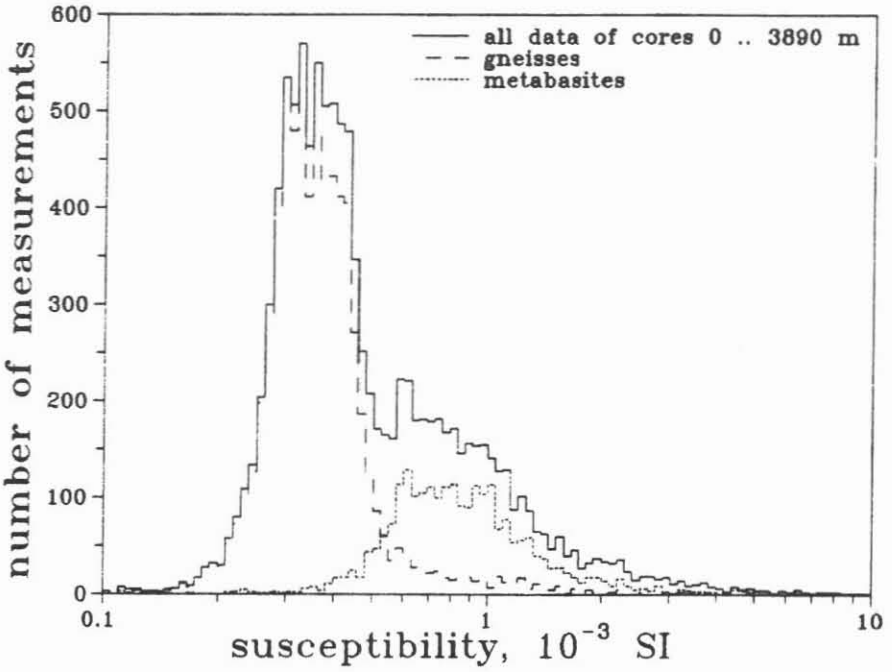

Fig. D.7.2: Log-normal frequency distribution of magnetic susceptibility of drill cores. Total data and data separated into the two main rock types (metabasites and gneisses) are shown. The susceptibilities range between 10^{-4} SI and 10^{-2} SI.

D.8 Porosity and inner surface

D.8.1 Introduction

Porosity and pore geometry are main parameters to understand the electrical and elastic properties of rocks. The porosity and inner surface were measured quasi-continuously a few months after core recovery. Therefore the pore space due to deformation and microcracks caused by drilling and decreasing temperature and pressure contributes to the measured porosity. The porosity is determined from 1316 plugs (diameter = 15 mm, length ≈ 30 mm) using the "Archimedian method" with distilled water (HUENGES et al. 1989). The inner surface was measured with the monomolecular nitrogen adsorption method on 204 plugs (WOLTER et al. 1989).

D.8.2 Results

Figure D.8.1 shows the porosity, the observed macroscopic fractures per meter, the inner surface and a simplified lithological profile as a function of depth. The average

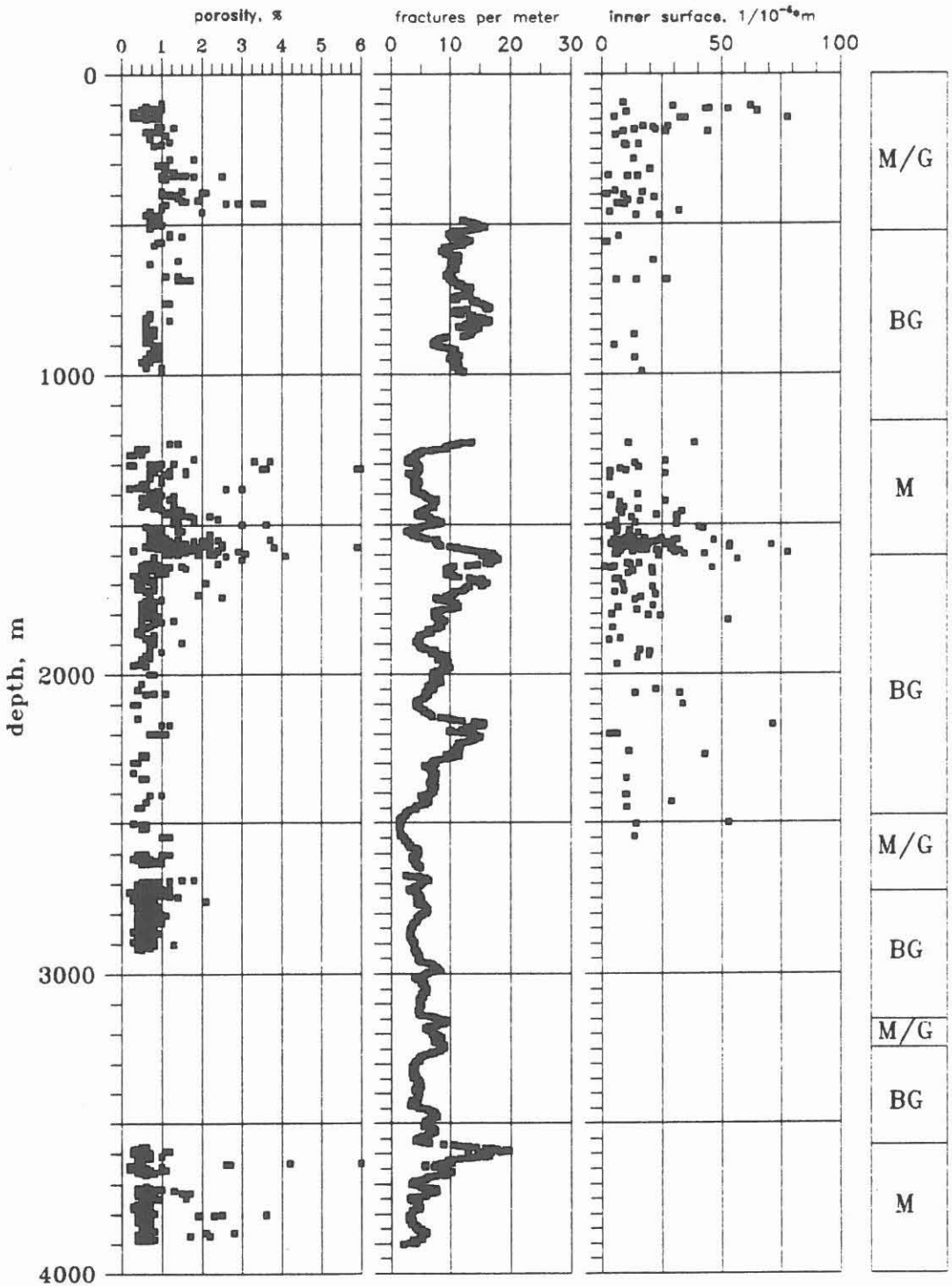

Fig. D.8.1: Porosities measured on plugs (diameter = 15 mm, length ≈ 30 mm) with the "Archimedian method", fractures per meter and inner surface measured on the same plugs with the monomolecular nitrogen adsorption method. On the right side a simplified lithological profile is shown (M=Metabasites, BG=Biotite-Gneisses, G=Gneisses).

porosity of gneisses is 0.7 ± 0.3 % with 3.0% the highest and 0.2% the lowest value. Metabasites have porosities of 1.1 ± 0.9 % with a maximum of 6.0 % and a minimum of 0.2 %. It should be outlined, that low porosities characterize the gneisses and also low but more scattering values the metabasites. Taking into account that core-disking only occurs in metabasites, this different scatter can be explained by different elastic properties (see chapter "H" of this issue). Possible leaching or hydratazation processes may effect porosity too.

The inner surface of KTB cores spreads from 2 to 78 μm^{-1}. A dependence on lithology can not be observed. Figure D.8.1 shows that in a first approximation the inner surface correlates with the fractures per meter. See for example the shear zone at about 1600 m which is characterized by an increase of inner surface and an increase of fractures per meter. Higher inner surface indicates intensive fracturing on a microscopic scale.

D.9 Acknowledgements

The measurements were mainly performed by our technicians Robert Fürnrohr, Michaela Jäger, Adelheidi Kick and Hubert Köstler. We thank them very much.

The authors are grateful to all colleagues of the geophysical institutes of the universities of Berlin and München, not mentioned here, for their support and cooperation. Special thanks are due to the members of the mechanical workshop in München: O. Bühler, H. Reichel, M. Thuringer and H. Khek.

We would also like to thank Prof. R. Emmermann, Prof. Dr. H.C. Soffel, Dr. J. Lauterjung, Dr. H.-G. Dietrich, Dr. M. Heinisch, Th. Wöhrl and Dr. H. Müller for their excellent suggestions.

The authors wish to thank the Deutsche Forschungsgemeinschaft (DFG) and especially the DFG Priority Program of the Continental Deep Drilling Project and the Niedersächsisches Landesamt für Bodenforschung for financial support of our investigations.

D.10 References

ADE-HALL, J.M. & H.P. JOHNSON (1976): Palaeomagnetism of basalts.- Leg 34, Init. Rep. Deep Sea Drill. Proj., 34: 513-532.

BÜCKER, Ch. (1987): Die Anomalien der Schwere im Bereich der Kontinentalen Tiefbohrlokation (KTB) Oberpfalz und ihre Interpretation.- Diss., Ludwig-Maximilians-Universität, München.

BÜCKER, Ch., EIGNER, K.-H., RAUCH, E., RAUEN, A., WIENAND, J. & K.E. WOLTER (1988): Tiefbohrung KTB Oberpfalz VB, Ergebnisse der geowissenschaftlichen Bohrungsbearbeitung im KTB-Feldlabor, Teufenbereich 0-480 m.- D. Geophysik. In: Emmermann, Dietrich, Heinisch, Wöhrl (Hrsg.), KTB-Report 88-1: D1-D42, Hannover.

BÜCKER, Ch. & G. ZIMMERMANN (1989): Vergleichende Untersuchungen der Gamma-Ray-Messungen (GR) im Bohrloch und an Bohrkernen im Teufenbereich 3000-3500 m.- In: Emmermann, Dietrich, Heinisch, Wöhrl (Hrsg.), KTB-Report 89-5, E1-E9, Hannover.

BÜCKER, Ch., LÖFFEL, R. & A. SCHULT (1990): Hochauflösende Dichtemessungen an Bohrkernen mittels Absorption von Gammastrahlung.- In: Emmermann & Giese (Hrsg.), Beiträge zum 3. KTB-Kolloquium, KTB-Report 90-4, (im Druck).

BURMESTER, R.F. (1977): Origin and stability of drilling induced remanence.- Geophys. J.R. astr. Soc., 48: 1-14.

DRAXLER, J.K. & R. HÄNEL (1988b): Grundlagenforschung und Bohrlochgeophysik, Bohrlochmessungen in der KTB-Oberpfalz VB, Intervall 1529.4-3009.7 m. - KTB-Report 88-7, Hannover.

GATTO, H. & C. BÜCKER (1990): Vergleich der Gesteinsdichte mittels Messungen von Schlumberger (litho-density log) und an Kernen durch das Feldlabor.- In: Draxler (Hrsg.), KTB-Report 90-1, Hannover.

GRUBBE, K., HÄNEL, R. & ZOTH, G. (1983): Determination of the vertical component of thermal conductivity by line source methods.- Zbl. Geol. Paläont. Teil I; H.1/2, 49-56.

HALL, J.M. & P.J.C. RYALL (1977): Paleomagnetism of basements rocks, Leg 37. In Aumento, F., Melson, W.G. et al., Initial Reports of the Deep Sea Drilling Project, v. 37: p. 423-424, Washington (U.S. Government Printing Office).

HOMANN, K.D., HEINSCHILD, H.-J., STROH, A. & M. TAPFER (1988): Tiefbohrung KTB Oberpfalz VB, Ergebnisse der geowissenschaftlichen Bohrungsbearbeitung im KTB-Feldlabor, Teufenbereich 1530-1998 m: C. Geochemie.- KTB-Report 88-9: C1-C88, Hannover.

HUENGES, E., BÜCKER, Ch., WOLTER, K.E., WIENAND, J., RAUEN, A. & E. LIPPMANN (1989): Deep Drilling KTB-Oberpfalz VB, Results of the Geoscientific Proceedings in the KTB-Laboratory; Depth Interval:

1709 - 2500 m.- D. Geophysik.- In: Emmermann, Dietrich, Heinisch, Wöhrl (Hrsg.), KTB-Report 89-2, D1-D83, Hannover.

HUENGES, E., BURKHARDT, H. & ERBAS, K. (1990): Thermal Conductivity Profile of the KTB Pilot Corehole.- Sci. Dri., in preparation.

LAUTERJUNG, J., HUENGES, E., STROH, A., REIBELT, M. & Ch. BÜCKER (1990): Abschätzung physikalischer Parameter aus dem quantitativen Mineralbestand.- In: Emmermann & Giese (Hrsg.), Beiträge zum 3. KTB-Kolloquium, KTB-Report 90-4, (im Druck).

LIPPMANN, E., C. BÜCKER, E. HUENGES, A. RAUEN, J. WIENAND, K. WOLTER and H.C. SOFFEL (1989): Rock physical properties: first results of the KTB-field-laboratory.- Scientific Drilling 1, 143-149.

MASSALSKY, T., H. MÜLLER, C. RÖHR, G. GRAUP, W. HACKER, S. KEYSSNER & J. KOHL (1988): Tiefbohrung KTB Oberpfalz VB, Ergebnisse der geowissenschaftlichen Bohrungsbearbeitung im KTB-Feldlabor (Windischeschenbach), Teufenbereich von 1530 bis 1998 m: B. Geologie.- KTB-Report 88-9: B1 - B66, Hannover.

PETERSEN, N. (1978): Glomar Challenger Drillings: The Magnetic Field Produced By The Drill And Drill String.- Initial Reports of the Deep Sea Drilling Project, Volume XLVI, Washington (US Government Printing Office).

RAUEN, A., LIPPMANN, E., HUENGES, E., BÜCKER, Ch., WIENAND, J. & K.E. WOLTER (1988): Tiefbohrung KTB Oberpfalz VB, Ergebnisse der geowissenschaftlichen Bohrungsbearbeitung im KTB-Feldlabor (Windischeschenbach), Teufenbereich von 992 bis 1530 m: D. Geophysik.- In: Emmermann, Dietrich, Heinisch, Wöhrl (Hrsg.), KTB-Report 88-6: D1-D60, Hannover.

RAUEN, A., BÜCKER, Ch., HUENGES, E., LIPPMANN, E.,WIENAND, J. und K.E. WOLTER (1989): Natürliche remanente Magnetisierung und Suszeptibilität.- In: R.Emmermann & Giese (Hrsg.): Beiträge zum 2. KTB-Kolloquium, KTB-Report 89-3, Hannover.

RAUEN, A., LIPPMANN, E., HUENGES, E., BÜCKER, Ch., WIENAND, J., K.E. WOLTER & Streit, K.M. (1990): Tiefbohrung KTB Oberpfalz VB, Ergebnisse der geowissenschaftlichen Bohrungsbearbeitung im KTB-Feldlabor (Windischeschenbach), Teufenbereich von 3509 bis 4000 m: D. Geophysik.- In: Emmermann, Dietrich, Heinisch, Wöhrl (Hrsg.), KTB-Report 90-2: D1-D60, Hannover (in press).

RAUEN, A., LIPPMANN, E., HUENGES, E. & SOFFEL, H.C. (1990): Elektrische Widerstandsmessngen an Bohrkernen - Vergleich mit Bohrlochmessungen.- In: Emmermann & Giese (Hrsg.), Beiträge zum 3. KTB-Kolloquium, KTB-Report 90-4, (in press).

RYBACH, L. (1976): Radioactive heat production, a physical property determined by the chemistry of rocks. In: R.G.J. Strens (ed.):"The Physics and Chemistry of Minerals and Rocks", Wiley & Sons, London.

WALL de, H., HUENGES, E., JUCKENACK, C. & K. WEBER (1990): Beziehungen

zwischen Gefügeanisotropie und der Richtungsabhängigkeit gesteinsphysikalischer Eigenschaften - Untersuchungen an Paragneisen der KTB-Vorbohrung.- In: Emmermann & Giese (Hrsg.), Beiträge zum 3. KTB-Kolloquium, KTB-Report 90-4, (im Druck).

WEBER, K. & A. VOLLBRECHT (eds.) (1986): Kontinentales Tiefbohrprogramm der Bundesrepublik Deutschland, Ergebnisse der Vorerkundungsarbeiten Lokation Oberpfalz.- 2. KTB-Kolloquium Seeheim/Odenwald, 19.9.-21.9.86.

WIENAND, J., RAUEN, A., HUENGES, E., BÜCKER, Ch. & K.E. WOLTER (1989): Tiefbohrung KTB-Oberpfalz VB, Ergebnisse der geowissenschaftlichen Bohrungsbearbeitung im KTB-Feldlabor (Windischeschenbach), Teufenbereich 3000 - 3500 m: D. Geophysik.- In: Emmermann, Dietrich, Heinisch, Wöhrl (Hrsg.), KTB-Report 89-5, D1-D50, Hannover.

WOLTER, K.E., WIENAND, J., RAUEN, A., LIPPMANN, E., HUENGES, E. & BÜCKER, CH. (1989): Tiefbohrung KTB Oberpfalz VB, Ergebnisse der geowissenschaftlichen Bohrungsbearbeitung im KTB-Feldlabor (Windischeschenbach), Teufenbebereich von 2500 bis 3009 m: D. Geophysik.- In: Emmermann, Dietrich, Heinisch, Wöhrl (Hrsg.), KTB-Report 89-4, D1-D39, Hannover.

KTB-Report	90-8	E1- E18	4 Fig.	Hannover 1990

KTBase (KTB database) - THE CORE OF A SCIENTIFIC/TECHNICAL INFORMATION SYSTEM

J. Wächter

Contents

Address of the author:

KTB-Feldlabor, Postfach 67, D-8486 Windischeschenbach

E.1. Introduction

The KTB is an interdisciplinary geoscientific research project. The conversion of the geoscientifical objectives form an interdisciplinary methodological diverse, extensive data gain. A continuous investigation of core material, rock flour, drilling fluid, and formation waters is carried out using a wide variety of methods in the field laboratory within the framework of the working groups: Geology/Tectonics, Petrology/Petrography, Geochemistry and Geophysics. The parameters of the fluid circulation are continuously measured through the mud-logging unit. An extensive geophysical borehole measurement program (wireline logging, experiments within the borehole) forms an important part of the underground data recovery. Scientific investigations in the surrounding areas provide data for a spatial or regional interpretation of the above mentioned information. The results of present and further research projects lead to a continuous expanding of the database.

A central computer system has been set up in the field laboratory for the management, documentation and use of this extensive, dynamically growing database. Based on presently modern hardware equipment a central database system is being implemented. The KTBase (KTB database) forms the core of a scientific/technical information system, which will guarantee the integrated interactive use of all data.

In this report we would like to present the actual status of the development. Chapter E.2 introduces the hardware components of the KTB computer centre and gives an overview of the computer network within the KTB field laboratory.

Chapter E.3 is devoted to the KTB database KTBase. Based on the standard architecture of database systems the complete definition of the KTBase contains the conceptual, the internal, and the external scheme. The conceptual scheme defines the data structures of the analysed miniworld, in this case the KTB project. Both the data structures and the data flow within the miniworld are integrated to generic information structures, which support the functions of the KTB Information System.

Chapter E.4 explains the functions of the KTBase within the framework of the information system. The internal structure of the information system is composed of the KTBase and the application layer embedding the KTBase. The efficient implementation of the information system within the KTB computer network requires a decomposition of this complex database application into client and server components.

E.2. The computer network in the KTB field laboratory

The targets of the KTB data processing include the effective administration and the interdisciplinary evaluation of the project data. This high level concept can only be established by a translation into a basic concept i.e. computer hard- and software. Effective archiving means a centralized data management on central storage units under a single security domain. An interdisciplinary evaluation of data requires access to the centrally stored data, sufficient computing power for numeric calculations and devices for high resolution graphic output. This basic concept, the hardware configuration and the software components of the KTB data processing centre, will be introduced in this chapter.

The local computing environment within the KTB field laboratory is a special type of computer network called **L**ocal **A**rea **VAX** **C**luster (LAVC). The hardware is composed of computers produced by the DIGITAL EQUIPMENT CORPORATION (DEC). The operating system is VAX/VMS 5.3. A cluster is a highly integrated organisation of computer systems, which share processing and storage resources as well as devices, for example, printers, plotters or tape units. All systems within the cluster have direct access to all cluster resources.

A typical cluster configuration contains a boot server, which should be the most powerful machine, and satellite nodes. All satellites boot from the same boot server's system disk, which contains only a single copy of the operating system. In th actual configuration the KTB-VAXCluster contains a VAX 6210, which is the boot server, a MikroVAX II and serveral workstations (one VAXstation 3200, nine VAXstation 2000). All computer systems joined in the cluster communicate over ETHERNET (fig. 1).

In order to use the computing power of the cluster efficiently, the workload caused by power consuming applications is distributed among the cluster nodes:
- Because of its considerable computing power, the **VAX 6210** is selected to serve the database to the cluster and to perform special numerical calculations.
- The office information system ALLIN1 including text processing facilities is available on the **MikroVAX** II which also connects the cluster to the telecommunication services of the public networks.
- The **workstations** provide an efficient window environment for the development of applications as well as the statistical evaluation and the graphical presentation of data.

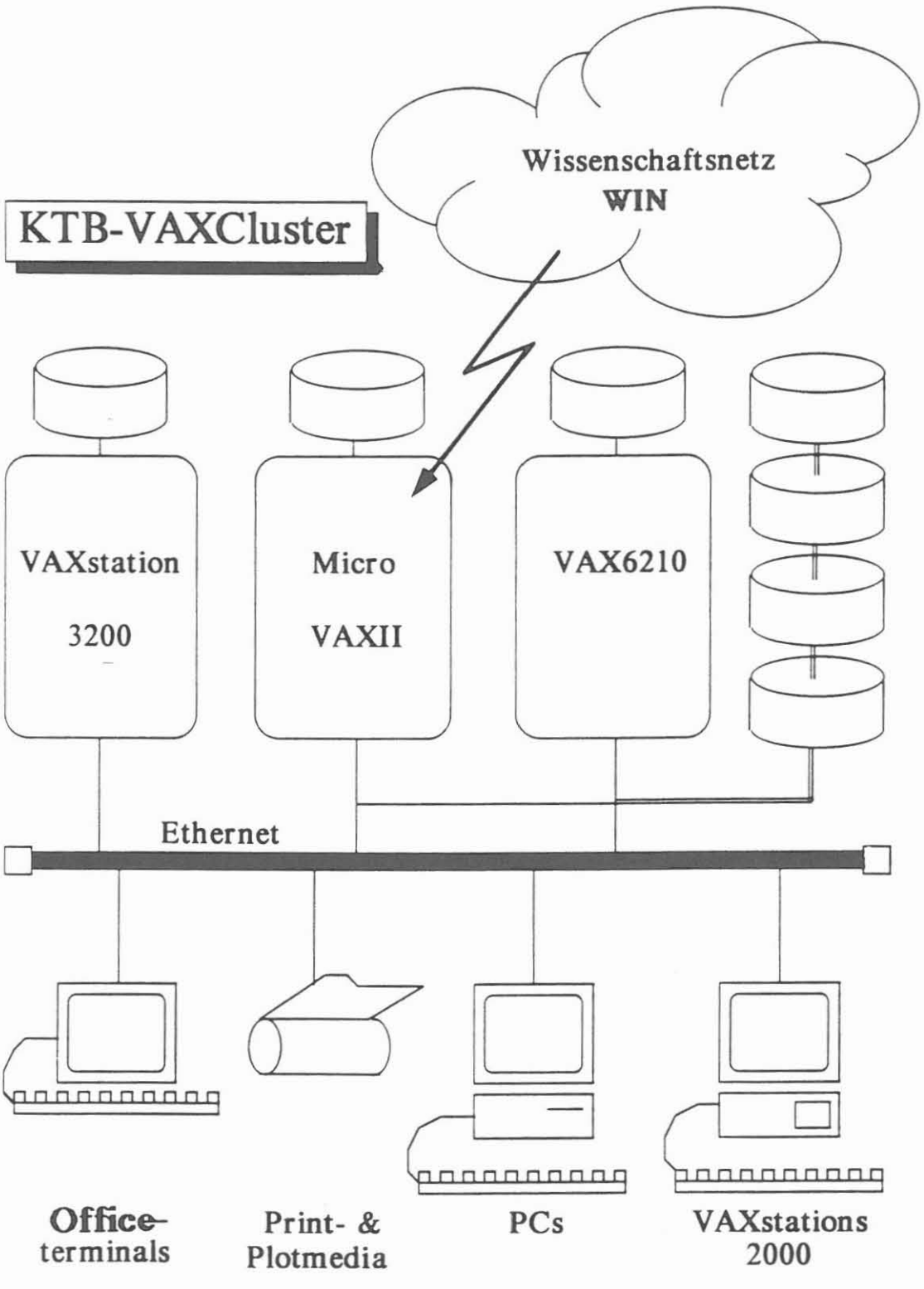

Fig. 1: Configuration of the KTB-VAXCluster.

The resources of the KTB-VAXCluster can be summarized as follows:

- The total disk storage capacity amounts to 5.8 GByte.

- Among the peripheral devices are tape drive stations, a high capacity streamer, matrix and laser printers, pen plotters and a special color plotter.

- The main standard software products offered to the user are an office information system (Allin1 - DEC), Spreadsheet software (Teamdata - DEC), a database management system (Rdb/VMS - DEC), database manipulation languages (SQL,RDO - DEC), statistical analysis software (SAS - SAS Institute), 4GL-development tools (UNIFACE - GEI) and compilers (FORTRAN, Pascal, C -DEC).

Besides the configuration of the KTB-VAXCluster, the integration of personal computers is another important characteristic of the computer network in the field laboratory. By an interface personal computers (IBM AT, IBM XT and compatible PCs) are interconnected to the local area network (ETHERNET). The PCSA software (DEC) establishes a close connection between the PCs and the cluster allowing the PCs to store data on cluster disks and to use peripheral devices of the KTB-VAXCluster (printer, plotter). Another advantage of the PC integration is data security. By storing scientific data on cluster disks, the data are automatically be saved by the daily backup operations.

The KTB-VAXCluster is a member of the scientific network WIN (Wissenschaftsnetz) supported by the DFN (Deutsches Forschungsnetz).

E.3 Development and structure of the KTBase

The KTBase is a database system containing the data of all KTB project, administrated by a database management system. This software product provides functions for the data definition, data manipulation and definition storage parameters. Additional functions define the parameters of the file where database is stored and the way data is accessed. The most important capabilities of database management systems (DBMS) are explained in chapter E.3.1. The implementation and administration of the KTBase by using a DBMS in this case Rdb/VMS make these performance capabilities available as functions of the database system (ch. E.3.1).

A further characteristic of present day database systems is the three level architecture. The structure of the database is defined by three independent schemes. The conceptual scheme contains the data definition and relations between the data structures. This scheme provides the basis to define the internal and external schemes. The database design, containing

the complete definition of the database, is therefore developed in three steps, which are outlined in chapter E.3.2.

The database design is based on an information analysis, which documents the data structures and data definitions. The other aim of the information analysis is the description of the future usage of the database system as basic functions. Both data structures and basic functions are integrated into the conceptual scheme. The most important results of the information analysis within the KTB field laboratory are presented in the chapters E.3.3 and E.3.4.

E.3.1 Functions of a database system

With the constantly increasing performance potential of computer systems, the usage has shifted from numerical calculation methods to management of information. Database systems are important tools for computer supported management of large data accumulations. Database systems are composed of two parts, (1) the database, in which related information of a miniworld are stored, and (2) the database management systems (DBMS), which assist in the management and updating of data as well as support of application programs in order to access data in a suitable form. An important advantage of a database system is its independence from both the physical presentation and the external views. This allows the flexible adaptability of the database system, for example

- new database applications should not necessitate a change of the current application programs, data structures and data storage,

- changes in the information structure should have no effect on current database applications,

- changes in the storage system of the database, to increase performance, should not have reverse effects on the database concept or application programs.

The ANSI/SPARC architecture has been proposed to accomplish data independence for concrete database systems. The complete definition of a database system can be divided into three levels each having its own scheme:

- Conceptual scheme: this scheme contains the complete list of global definitions describing the miniworld in question, whose relevant information is stored in the database. The information structures are expressed by a data model. The conceptual scheme forms the basis for the definition of the external and the internal scheme.

- External scheme: this scheme involves the determination of the individual views of the database. User and application programs have access only to selected areas of the conceptual scheme. The user gets the impression that the database contains only information, which is relevant to him.

- Internal scheme: the scheme defines the physical structure of the database and determines how and where the data will be stored. This includes the set up and control of system parameters (for example buffer size) and data access.

A central administration of the complete data of a miniworld by a DBMS and a 3-level-architecture of the database ha essential advantages in comparison with the decentral storage and management of data:

- By a global conceptual scheme of the database, redundant information can easily be detected and removed. During the development of the conceptual scheme possible negative effects on the consistence of the database, for example, caused by update operations like deletion, insertion and data correction can be discovered.

- Access to data is controlled by the DBMS. Due to this inconsistencies, which can be caused by uncontrolled updates, are avoided. The central control function guarantees an effective multiuser operation of the database and the implementation of integrated backup and security concepts.

- For individual users of the database the logical view of the data can be freely formulated within the external scheme. Therefore the database system can provide data in a suitable form for the user or application program.

In addition to the above mentioned advantages a furthe important characteristic of a database system should be pointed out: Recovery of the original conditions in the case of a system breakdown or a hardware failure. During operation, changes in the database are recorded by the DBMS. Using this redundantly stored information, the DBMS can reconstruct the database as it existed before the breakdown (detailed discussion: Date 1986, Vossen 1987, Lockemann and Schmidt 1987).

E.3.2 Steps in the development of the KTBase

The KTBase is responsible for both effective archiving of the KTB data and flexible information retrieval. With respect to a continuously enlarged database, these aims can only be achieved by a detailed documented, clear database structure, which allows for a flexible addition of further data structures and data.

As pointed out in chapter E.3.1 the definition of a database is subdivided into three levels, the internal, external and

conceptual scheme. The conceptual scheme contains the entire information structures of the miniworld. The external an internal schemes are deduced from the conceptual scheme.

The first and most important step of the database design is the development of the conceptual scheme. The data structures and data relations within the KTB project are quite complex. Due to data reflux from external research projects new data definitions are being continuously added to the conceptual scheme. Therefore description of information structures is conducted by means of a semantic data model, in this case the entity relationship model.

Semantic data modelling provides the basis for a distinc graphical presentation of data structures both at the level of the working group data and global generic scheme of the database. A further advantage of this kind of presentation is the independence of the database scheme from the data definition language of the specific database management system used to implement the database. This means the portability of the database to other operating systems or database management systems is achieved.

The basis for the development of the conceptual scheme is a information analysis, which establishes the relevant information of the examined miniworld. An integrated, interdisciplinary use requires a clear definition of both data structures and applied methods of investigation. Another important point of information analysis is the description of the future usage of the database i.e. the data flow. The results are formulated as abstract basic functions. Both data structures and basic functions are fundamental for the design of the general, integrating information structures of the database.

During implementation the semantic conceptual scheme is translated into the data model of the DBMS used for the construction of the real database on a concrete computer system. In the KTB field laboratory the DBMS Rdb/VMS (DEC) is used for this purpose. It is based on the relational data model. Data structures are internally represented in form of flat tables, consisting of rows and columns.

The next step is the design of the internal scheme which defines the physical storage of the database. Rdb/VMS allows for the distribution of the database into several files (multifile database), definition of indices and modification of buffer sizes. A proper designing of the internal scheme results in a short response time during updating or query operations.

Defining of the external scheme is not of actual importance for setting up the KTBase and will be done during development of the application programs.

E.3.3 Basic functions of the KTBase

The conceptual scheme of a database contains the global data definitions of the miniworld and describes the information structures (entities) as well as the relations between them (entity relations). Therefore the scheme describes the data structures as well as the flow of information within the miniworld and its information requirements.

Future tasks of the database system have been defined in the form of basic functions, which are useful for the definition of the key concept and generic, integrating information structures of the conceptual scheme. They are required to describe the information flow and information demands of the database users.

The basic function of the KTBase can be derived from the aims of the KTB data processing. They include the archiving an documentation of data and samples as well as the utilization of the documentation, data and samples for scientific purposes. The selection and distribution of samples an d data for external projects has also to be supported as well as control of the sample and data reflux. The data reflux not only includes data in the form of flat ASCII tables but also publications and reports i.e. text documents.

The following basic functions describe the main responsbilities of the database system:

1. **storage** of

a) documentation of:

- probe types, sampling methods and storing of samples,
- finalized and current investigations,
- data structures and definitions.

b) data:

- internal data (working groups of the field laboratory)
- external data (reflux from universities or other research institutes),
- time series data.

c) **documentation of depth corrections**

2. retrieval of

a) **information about samples and data:**

- storing of samples,
- geological context,
- finalized and current investigations,
- structure of data,
- joining of data,
- depth corrections.

b) **data:**

- internal and external data,
- time series data.

3. **definition of reference systems** for

- retrieval of data and samples,
- presentation of results,
- interpretation of results.

E.3.4 Conceptual scheme of the KTBase

The conceptual scheme of the KTBase contains five generic information structures (fig. 2) whose complex internal structure will not be outlined in detail. The information structures and their functions are explained below:

Central Archives

Information with special importance for the KTB is stored at this most central place of the database. The Central Archives contain documentation of samples, documentation of geophysical borehole measurements and online data, which document the course of drilling and mudlogging. Further important data structures contain depth corrections for drilling cores and for drilling fluid samples.

The Central Archives support the following functions of the information system:

- supervision of data integrity,
- joining of information,
- access to depth corrections for samples,
- access to the reference system.

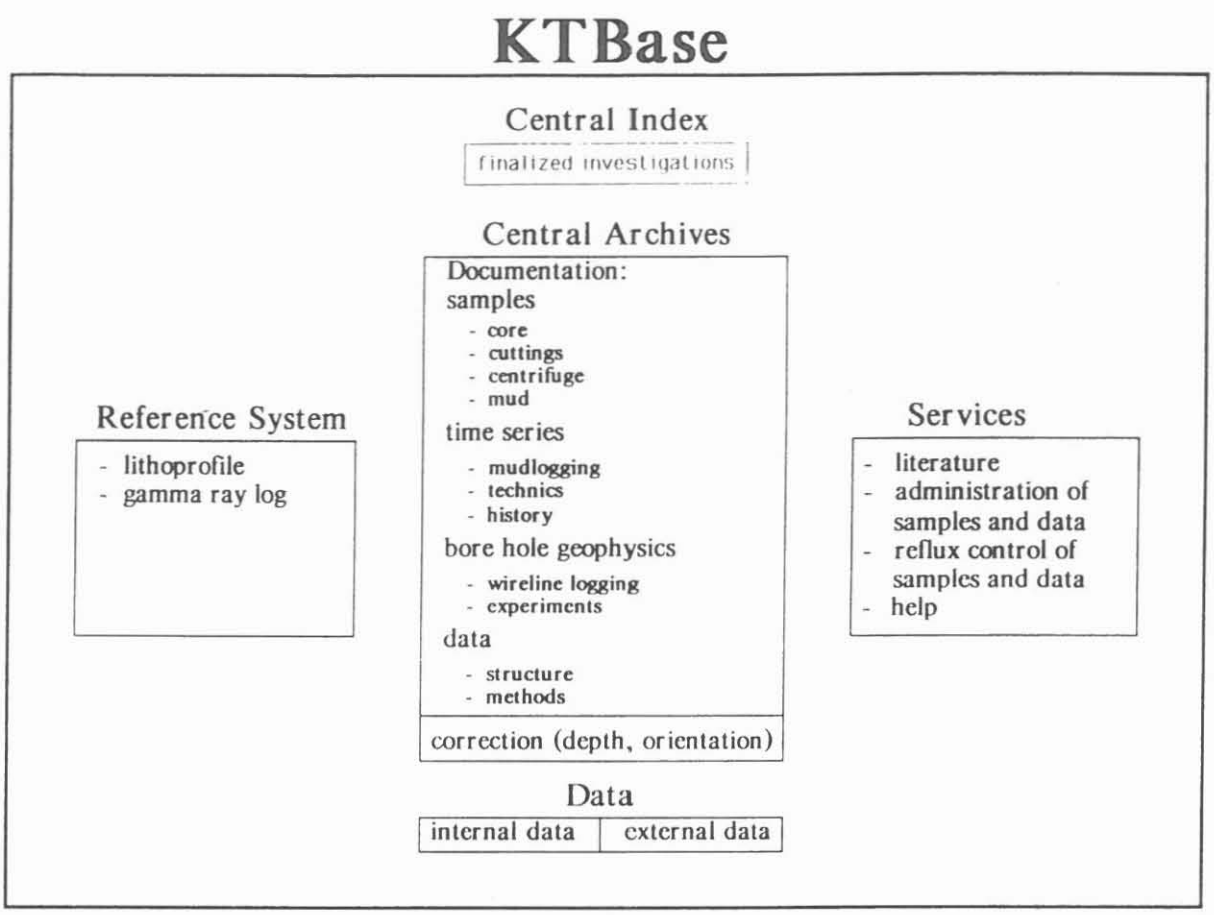

Fig. 2: The conceptual scheme of the KTBase

Data

This area of the database contains the data structures for research groups working in the KTB field laboratory (internal data) and for the numerous research projects being conducted at universities and other research institutions.

Central Index

The Central Index provides information of the type of investigations conducted on samples. The information system uses the Central Index to join information from the Central Archives with the Data structures.

Reference System

The Reference System contains logs being used by the database application programs to support

- interpretation of data,
- graphical presentation of data,
- selection of samples,
- presentation of technical drilling parameters and mudlogging data, and
- geotectonical interpretation of data.

Service

The service data structures support the following functions of the information system:

a) The literature processing supports the administration of abstract internal and external data i.e. text documents and graphics.

b) Sample and data administration. The data structures support distribution of samples and data.

c) Data reflux control. The data structures are an interface between the external data producers and the database.

d) Help. The Help function includes various information on data definition, the methods used for sample investigation and also allows the combination of different information sources. This function supports the scientific usage of the database.

E.4 The KTB Information System

The target of the KTB data processing can be divided into two major functions: (1) documentation, storing and security of the project data, and (2) support of an interdisciplinary interpretation of data. This will be realized by the development of the KTB scientific/technical Information System.

Within commercial database applications for most users only selected parts of the database are accessible. In contrast to this the authorized user of a scientific/technical information system has access to the whole database. In addition a scientific information system has to support the researcher to use the entire existing information for his creative scientific work.

In chapter E.3.1 the general features of database systems have been explained. By using retrieval languages such as SQL and RDO the user has many possibilities to select and join information. In respect to the demands of scientific research these functions are not sufficient. The retrieval of geological or geophysical data produces a listing of alphanumeric or numeric values. It is obvious that the interpretation of data cannot be achieved in this way.

Preparing data for interpretation processes is rather the task of a software shell, which is in the perspective of the information flow, a layer between the database and the user. The information requested by users are extracted from the database and committed to the database shell by an interface. The database shell converts the data for example into a chart, which is presented to the user as the result of his information demands.

The main tasks of the KTB data processing are realized by two different components in the scientific/technical information system:

- documentation, storing and security of data is the main task of the KTBase, which administrates the database as the core of the information system.

- the preparation and presentation of the data for scientific interpretations. This is realized by the database shell consisting of serveral applications with a homogeneous user interface.

In the following the structure of the application layer and its future implementation on the KTB computer network is outlined in detail.

E.4.1 The application layer

For communication with the database the core of the KTB Information System is surrounded by a layer of application programs. The application layer consists of the mask, the graphic and the evaluation interface (fig. 3).

The functions of the mask interface are input and output of data, sample and literature administration as well as administration of data documentation and generation of reports. The user communicates with the database by means of a scheme displayed at the terminal screen. Input and output consists of alphanumeric values.

The graphic interface with read-only access to the database enables a flexible graphical display of data in relation to reference systems like the litholog and/or the gamma ray log. The main tasks are graphic display of actual drilling parameters, support of data interpretation, and selection of interesting samples and data for special research studies. Standard charts displaying the course of drilling will be stored as bitmaps in picture files. The output can be directed to a screen, a plotter or a printer device.

The evaluation interface has read-only access to the database. The purpose of this interface is to support the user in sta-

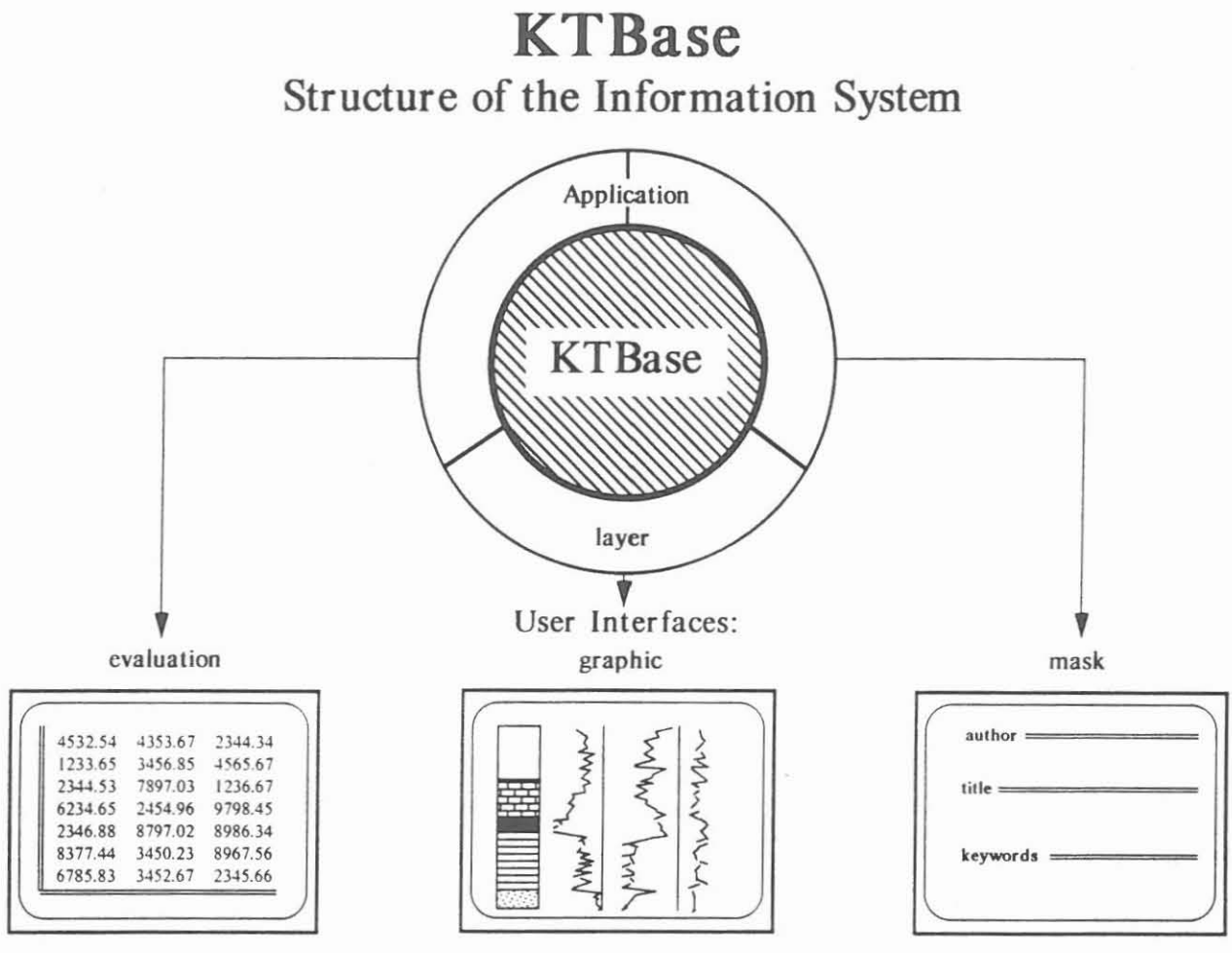

Fig. 3: Structure of the KTB Information System.

tistical and graphical evaluation of data as well as data manipulation. Within the KTB Information System the statistic software package SAS is introduced to the user at this place. The software offers both an interface to the database and fully developed graphic features.

E.4.2 Client-server architecture

The structure of the information system was explained above in its conceptual structure. Considering the computer hardware available in the field laboratory, it is obvious that the total amount of computing power is not concentrated on one mainframe but distributed among several computing systems. The effective usage of the processing power in this environment requires the decomposition of the application architecture into several application components by using a client-server model. This model has become very popular for implementing distributed applications. Applying this model to the design of the KTB Information System, it has to be decomposed into a server com-

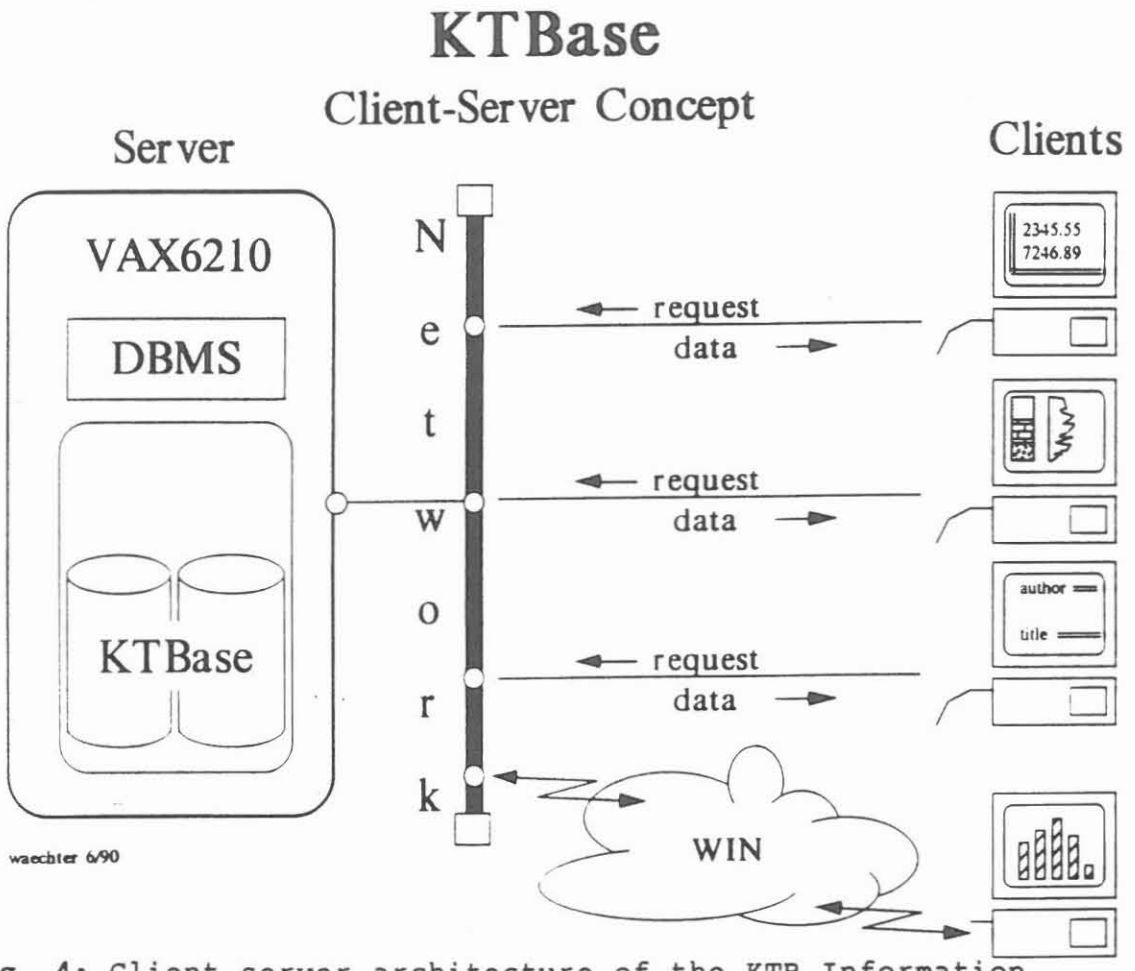

Fig. 4: Client-server architecture of the KTB Information System.

ponent managing the database access, and a client component providing the services of the application layer (fig. 4). Although client and server components are distinct, physically separated entities, they cooperate to implement the information system as a whole.

The VAX 6210, the most powerful computer of the KTB-VAXCluster, has the function of the server and performs exclusively database management requests, for example updating and retrieval of data, thus the duration of transactions with the database is minimized resulting in short response times for database queries, even with a significant number of simultaneous users.

The programs implementing the application layer of the information system reside as client processes on workstations of the KTB-VAXCluster. Therefore the local computing power of workstations is used for controlling of the display unit and communication with the user. Whenever a user requests data, the client initiates a network connection to the server by sending a message containing the data request. The server processes the database lookup request and sends a message to the

client containing the requested data. The subsequent processing of data takes place at the workstation, the client resides on.

The client-server architecture of the information system provides a full utilization of the cluster processing power. The performance of the information system will be sufficient, even there is a significant number of users.

E.5 Concluding remarks

The actual status of the KTB data processing can be summarized as follows:

- The setting up of the KTB-VAXCluster is finalized. This includes the installation of software and the integration of the PCs used by the working groups of the field laboratory. The VAXcluster supports a broad variety of software products and provides an effective storage management of data as well as data and system security.

- The development of the KTBase, which is the core of the future scientific/technical information system, has reached its final stage. Because the data administration has been a task of the working groups up to the present, the data has to be loaded into the central database. For this special purpose upload programs have been developed, transforming the data into the data structures defined in the conceptual scheme of the database. Besides the upload programs examine the integrity of the data.

- The implementation of the mask interface (input and retrieval of data, reports) will begin in August 1990 by using a 4GL application development tool (UNIFACE - GEI). Besides UNIFACE provides the network communication services to set up a client -server architecture, which supports access to one or more (distributed) databases.

The development and opening of the KTBase is an important step in establishment of the KTB data processing concept. The target of future efforts will be the development of an efficient application layer.

The KTB project is a teamwork of geoscientific and technical disciplines with an extensive data gain. The administration and the scientific/technical utilization can only be achieved by effective data processing. The future information system has to deal with different data objects as common data in the form of flat ASCII tables and complex data, which contains text documents and graphics. Under a homogeneous user interface the information system will offer input and retrieval functions, spreadsheet applications as well as evaluation and graphic software. A help function providing information about the

structure of the database, data and method description will support the scientific user to understand and evaluate the data.

The KTB project is a demanding task for an integrated information processing. The KTB Information System will become an encouraging example for the successful integration of information systems into geoscientific research.

E.6 References

Date, C.J. (1986): An Introduction to Database Systems, Vol 1. - Addison Wesley Publ. Co., Reading, MA.

Vossen, G. (1987): Datenmodelle, Datenbanksprachen und Datenbank-Management-Systeme. - Addison Wesley Verlag, Bonn.

Lockemann, P.C. and J.W. Schmidt (1987) [eds.]: Datenbankhandbuch. - Springer Verlag, Berlin, Heidelberg.

KTB-Report	90-8	F1-F21	12 Fig.	Hannover 1990

INFERRING THE IN-SITU STATE OF STRESS FROM STRESS RELIEF MICROCRACKING IN DRILL CORES

A. Zang and H. Berckhemer
Institut für Meteorologie & Geophysik, Feldbergstr. 47,
6000 Frankfurt (F.R.G.)

K. E. Wolter
KTB-Feldlabor, Postfach 67,
8486 Windischeschenbach (F.R.G.)

Directory:

Abstract

In this paper the state of stress in the KTB pilot hole is inferred from anelastic strain recovery (**ASR**) and ultrasonic wave velocity analysis (**WVA**) on oriented crystalline core samples. The calculation of in-situ stress magnitudes from **ASR**-results was carried out only in case of structurally isotropic material (i.e., lamprophyre core samples), whereas the **WVA**-method leads to a more or less continuous stress profile. Investigating 41 core samples in the depth range from 130 to 3900 m by this new **WVA**-method, the KTB pilot hole may be divided into three major stress regimes: above 500 m both the minimum and maximum horizontal stress are greater than the overburden pressure, from 500 to 3000 m the vertical stress is intermediate and below 3000 m horizontal stress magnitudes are smaller than the vertical stress. The orientation of maximum horizontal stress determined from the **ASR**-data on five core samples fulfilling structural isotropy criteria is N168°E ± 25° in the depth range from 2000 to 3600 m. In contrast, the direction of maximum horizontal stress derived from minimum wave velocity of **WVA** on the same core samples has a mean value of N5°E ± 20°. Taking into account all 17 spatially oriented core samples irrespective of their structure, a rotation of minimum velocity azimuth from North at 1000 m to NE at 3000 m is found.

Keywords: acoustic emission, crack closing pressure, drill core, in-situ stress, strain recovery, velocity anisotropy, stress relief microcracking.

F.1 Introduction

Determining in-situ stresses at mid-crustal depth is one of the motivating aspects for deep drilling programs. The overall scientific objective of the Stress Measurement Group in the Continental Deep Drilling Program (KTB) of the Federal Republic of Germany is to establish a "continuous" profile of the orientation as well as the magnitude of the in-situ stress with depth. Techniques applicable for estimating the in-situ state of stress in a wellbore may be divided into:

(1) in-situ methods such as hydraulic fracturing (e.g., Rummel 1989) and borehole wall condition logs (Televiewer, Caliper and Formation MicroScanner) to examine borehole breakouts (e.g., Zoback et al. 1986) and

(2) drill core analyses such as anelastic strain recovery (**ASR**, Teufel 1983), differential strain curve analysis (**DSCA**, e.g., Ren & Roegiers 1983, Dey & Brown 1986), differential wave velocity analysis (**DWVA**, Ren & Hudson 1985) and core disking phenomena (e.g., Maury et al., Dyke 1989, Perreau et al 1989, Wolter et al. 1990).

In this paper we restrict ourselves presenting data from two methods applied to oriented core samples from the KTB pilot hole, which was finished in April 1989 at a final depth of 4000 m. The results of strain recovery measurements

and ultrasonic wave velocity analysis on crystalline core samples from depths between 130 m and 3900 m of the KTB pilot hole are summarized and their significance with respect to in-situ stress estimates is discussed.

The primary physical mechanism generated by stress relief upon removal of the core sample from depth is the formation of microcracks (Teufel 1983, Carlson & Wang 1986, Teufel 1989, Wolter & Berckhemer 1989a, Zang & Berckhemer 1989). The crack opening process is studied as well as quantified on 32 freshly recovered water saturated drill cores by means of **ASR**-method and simultaneous acoustic signal detection (Wolter et al. 1988). On the other hand the crack closing mechanism is monitored by the determination of P-wave velocity on 43 dry core samples during a gradually increase of hydrostatic confining pressure. A combination of both methods is carried out on 24 core specimen. By inferring that drill cores will create microcracks in proportion to the pre-existing effective state of stress (Charlez et al. 1986), one can in case of micromorphically isotropic material obtain an estimate of the orientation, as well as the magnitudes of in-situ principal stresses.

F.2 Time-dependent strain analysis

After extraction the drill core adapts to its new stress free surface condition. This process is accomplished by an instantaneous release of elastic strain as well as time dependent strain recovery (Teufel 1982). Due to the redistribution of internal stresses in polycrystalline materials acoustic emissions occur by formation of micro-cracks. The time dependent strain recovery and the occurrence of acoustic emissions of oriented drill cores of different lithologies are investigated.

F.2.1 Principle of strain recovery measurements

The **ASR**-method is used measuring the retarded strains of a freshly recovered drill core (Teufel 1982, El Rabaa 1989, Warpinski & Teufel 1989, Wolter & Berckhemer 1989a). For this purpose a cylindrical core sample with 94 mm in diameter and 100 mm in length hermetically sealed by a wax coating is mounted in a multi-component dilatometer (Fig. F.1). This device has been built in the Frankfurt Institute by E. Aulbach. The retarded strains are measured by means of inductive displacement-transducers in the core axis and in three different radial directions at constant temperature and moisture content (Wolter et al. 1988, Wolter & Berckhemer 1989a). The principal horizontal strains (maximum: e_1 and minimum: e_2) can be calculated, using the strain values measured in three different radial directions. It is assumed that the vertical strain e_v is a principal strain, too. For measuring the emission of acoustic signals a piezoelectrical sensor is attached to the surface of the

core sample. The events are counted and summed up by an ultraacoustic emission monitoring system. In addition

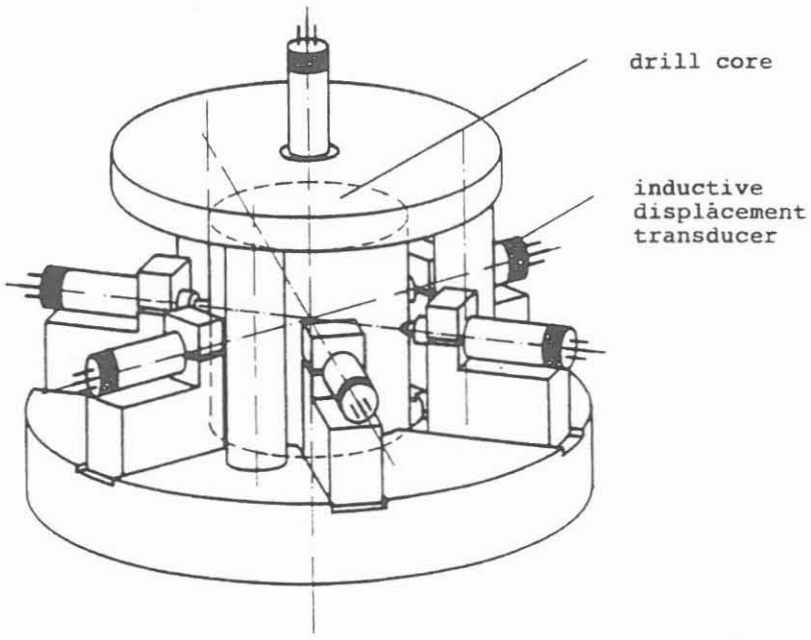

Fig. F.1: Measuring device for strain recovery experiment on drill cores (diameter 94 mm) from KTB pilot hole.

recording of the time function of selected acoustic events is possible.

F.2.2 Strain magnitudes and acoustic emissions

The time dependent strain recovery and the emission of acoustic signals is demonstrated in Fig. F.2 for a gneiss-sample from the depth of 3237 m. In Fig. F.2a the retarded strains (e_1, e_2, e_v) and in Fig. F.2b the

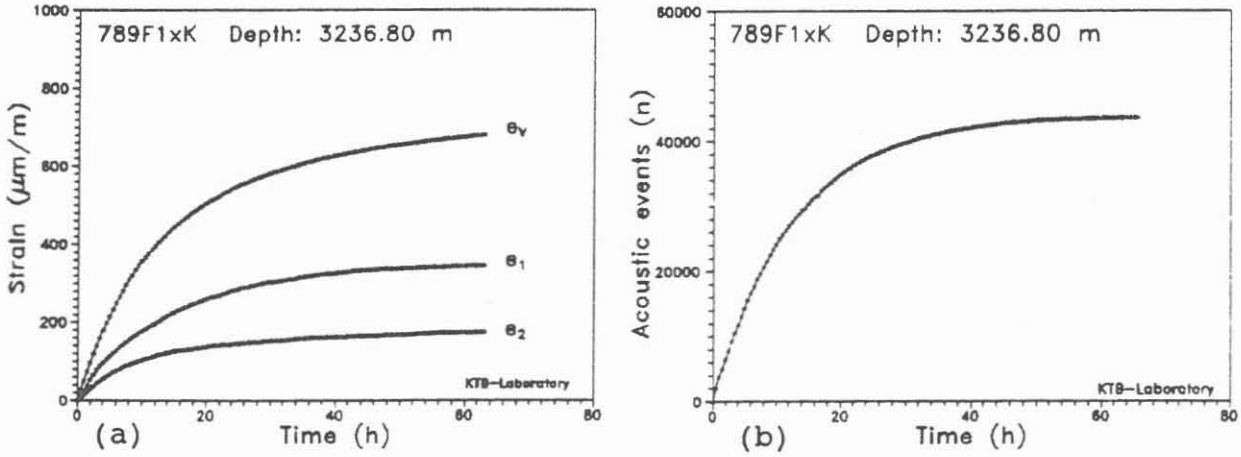

Fig. F.2: Principal strains (a) and cumulative number (b) of acoustic emissions versus time for a paragneiss sample from a depth of 3237 m.

cumulative number of acoustic events is plotted versus time.

The zero point of time scale for all relaxation measurements is about 5 hours after the sample was overcored in-situ. The final value of recording time (here: 66 hours) varies for different core samples from 40 to 300 hours depending on the decrease of retardation process (i.e., until the asymptotic value of strain or acoustic emission was reached approximately). The strain retardation process as well as the occurrence of acoustic emissions show an exponential behaviour.

In this way 32 core samples from depth between 1400 and 3800 m were investigated. There is no significant dependence of the final magnitude of retarded strain with depth (see Fig. F.3). This can be explained by the variety of material

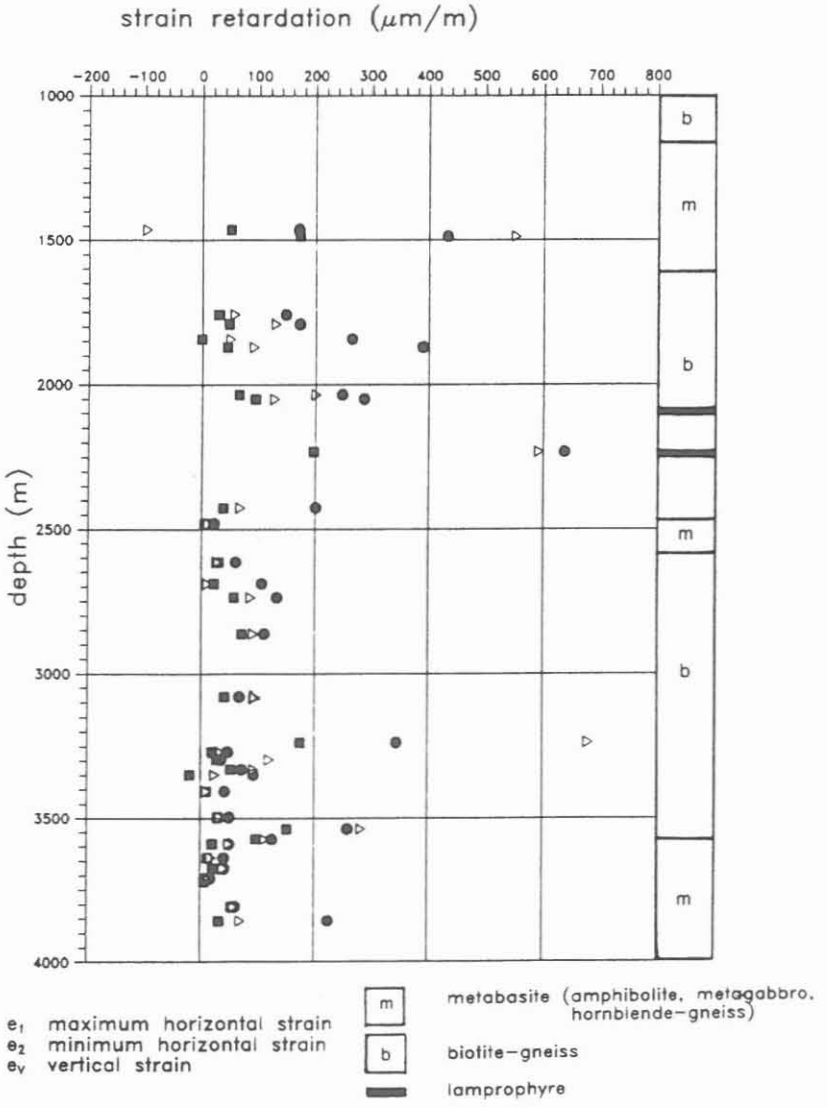

Fig. F.3: Final amplitude of principal retarded strains as a function of depth.

properties (e.g., composition, texture, structure, elastic moduli and strength). For strongly foliated paragneisses the orientation of maximum horizontal strain (e_1) in drill cores

tends to be perpendicular to the strike of foliation. The orientation of maximum horizontal strain with respect to geographic North is compared to the strike of the foliation for different core samples in Fig. F.4.

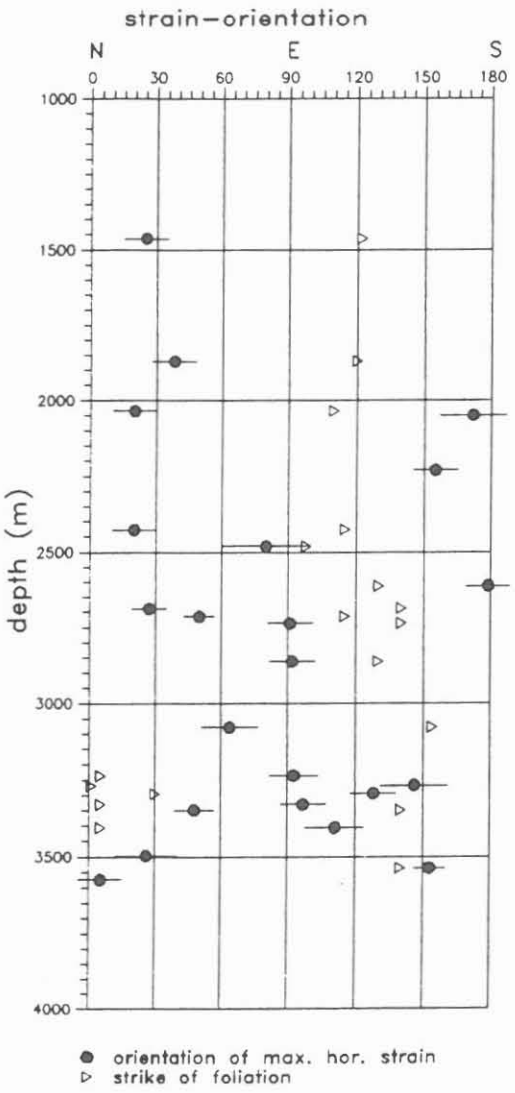

Fig. F.4: Orientation of horizontal principal strains and foliation with respect to geographic North versus depth.

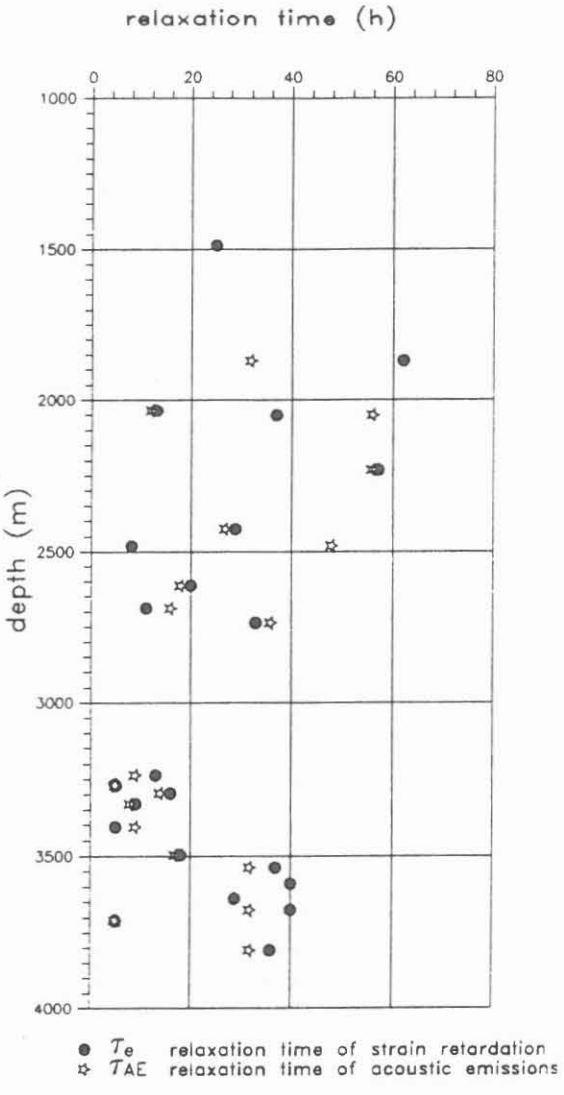

Fig. F.5: Time constants for strain retardation process and acoustic emissions versus depth.

The frequency content of the acoustic signals ranges from 100 to 500 kHz for all rock samples investigated. The characteristic features of the acoustic emissions (e.g., the number of events, frequency of occurence, and magnitude) depend on the rock properties and the process of microcrack formation. Preliminary results of the magnitude-frequency distribution of acoustic emissions show a preference of signals of characteristic magnitude with increasing time (Wolter & Berckhemer 1989b).

F.2.3 Relaxation times of recovery process

The relaxation time (τ) is the time elapsed until 1-1/e ≅ 63% of the final strain is reached (Wolter & Berckhemer 1989a). It is possible to determine relaxation times for strain retardation (τ_e) as well as for the cumulative number of acoustic emissions (τ_{AE}). These time constants are given

sample #	lithology	depth [m]	τ_e [h]	τ_{AE} [h]
526G2u	lamprophyre	2231	57	56
588E5ac	paragneiss	2426	29	27
789F1xK	paragneiss	3237	13	9
928E1pK	amphibolite	3808	36	32

Table F.1: Relaxation times for different core samples

in Table F.1 for some core samples. The similarity of the respective time constants demonstrates the intimate relationship between strain recovery and emission of acoustic signals caused by the formation of microcracks. The relaxation times for both strain retardation and the acoustic emissions of all core samples investigated are shown in Fig. F.5. There is no trend which indicates a depth dependence of the relaxation times.

F.3 Ultrasonic wave velocity analysis

After briefly reviewing the ultrasonic core analysis method, in this chapter the velocity data of the core samples during repressurisation are presented. The pressure dependent velocity anisotropy is used to separate crack-caused from textural anisotropy. Eliminating textural influence the remaining crack-caused part of velocity anisotropy is interpreted with respect to in-situ stress magnitudes as described in the following chapter.

F.3.1 Ultrasonic method

Crack distribution, as well as fabric elements in cases of preferred orientation, cause a considerable velocity anisotropy. This anisotropy is determined by means of P-wave travel time measurements of an ultrasonic pulse through a dry core sample. The rock cylinders with 30 mm in length and diameter used for this experiment are cut from the original drill core (diameter 94 mm) with axis parallel to wellbore axis (z-direction) and oriented with respect to the (arbitrary) KTB reference line (x-direction) in the horizontal xy-plane. All data below are referred to these sample fixed

xyz-axes. The specimen is dried and sealed with epoxy resin against hydraulic pressure fluid. The sample is rotated in 10° increments about the z-axis and the travel times are measured for three different wave paths (horizontal, conical and vertical, see Fig. F.6) in the pressure vessel. After

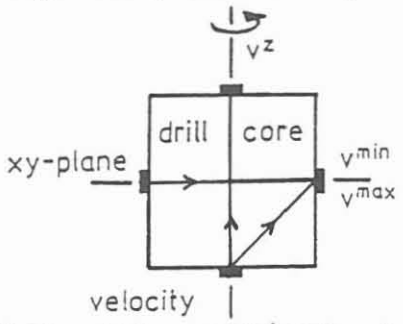

Fig. F.6: Horizontal (→), conical (↗) and vertical (↑) transmission of cylindrical core sample, which is rotated in 10 degree increments about core axis.

collecting the travel time data for a complete 2π-rotation, the hydrostatic confining pressure is increased stepwise up to a final value of 350 MPa. From these travel time data we are able to calculate a velocity distribution assuming one dominating set of parallel, dry and penny-shaped cracks within the core sample (Zang et al. 1989). The crack fit of velocity data has to be done after eliminating the textural influence on velocity (reduction of texture, see below). One final result of such an ultrasonic wave velocity analysis is shown in Fig. F.7 for a gneiss sample from 3406 m depth. The lower hemisphere plot of velocity data is characterized by

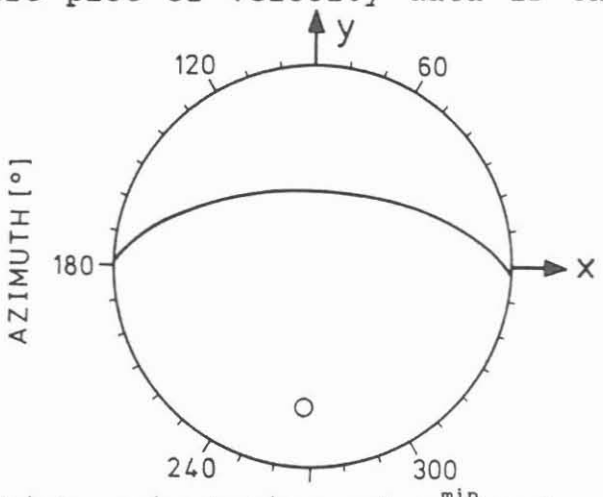

Fig. F.7: Spatial orientation of v^{min}-pole in a gneissic core sample from 3406 m depth.

the plane of maximum velocity (v^{max}-plane or crack plane) and, perpendicular to it, by the pole of minimum velocity (v^{min}-pole or crack normal). The azimuth of the v^{min}-pole is 268° and its dip 59° referred to the sample-fixed xyz co-ordinates. The position of v^{min}-pole does not change with increasing confining pressure, whereas the velocities increase from v^{min} = 1.72 km/s and v^{max} = 5.15 km/s at 1 MPa to v^{min} = 5.66 km/s and v^{max} = 6.37 km/s at 350 MPa.

F.3.2 Cracks and texture

The velocity anisotropy of the gneiss sample from 3406 m decreases from 67% at 1 MPa to 11% at 350 MPa. Assuming crack closure to be responsible for the decrease of velocity anisotropy with increasing confining pressure the remaining anisotropy of 11% at maximum pressure may be interpreted as the contribution of rocks texture to the velocity anisotropy. Therefore 56% of the total velocity anisotropy at 1 MPa may be caused by freshly opened microcracks during unloading of core sample. This separation into crack and textural anisotropy of P-waves has been performed for 42 drill cores from the KTB pilot hole and is shown in Fig. F.8. The P-wave velocity anisotropy inferred from the lower

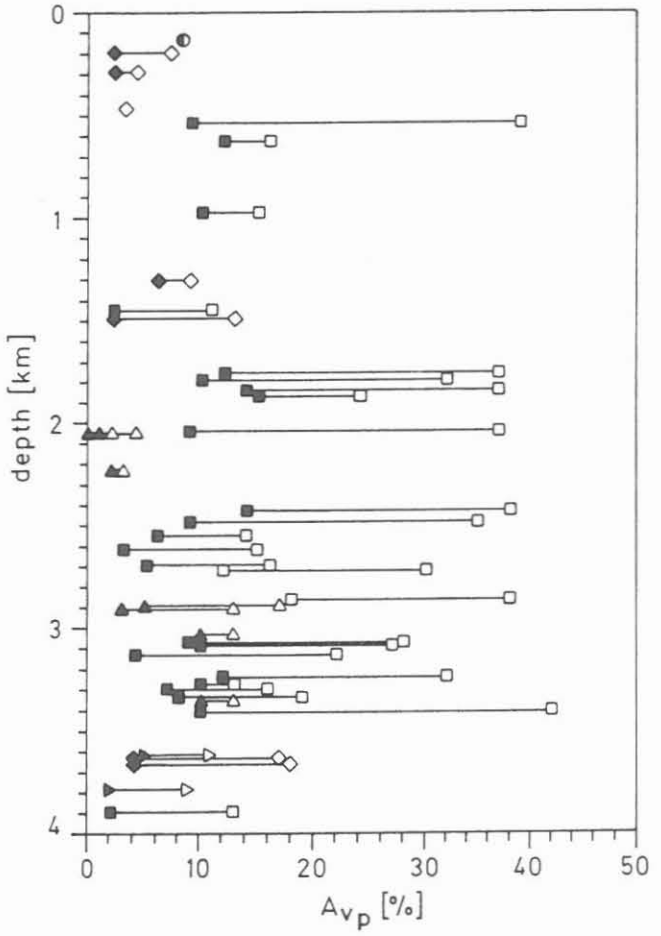

Fig. F.8: P-wave velocity anisotropy at 10 MPa (open symbols) and 350 MPa confining pressure (solid symbols) versus depth for different rock types (◆ = amphibolite, ▲ = lamprophyre, ▶ = metagabbro, ■ = gneiss and ● = marble).

hemisphere projections is plotted versus depth firstly for a reference pressure level of 10 MPa (open symbols) and secondly for 350 MPa confining pressure (solid symbols). The horizontal line for each depth level in Fig. F.8 represents the crack caused part of velocity anisotropy.

F.3.3 Textural reduction

After the separation into crack and textural velocity anisotropy in this section we address the question how to eliminate numerically the influence of preferred fabric elements on P-wave velocity from the measured ultrasonic data set. This operation - the so-called textural reduction - is shown in Fig. F.9 for the horizontal transmission (see Fig. F.6) of a paragneiss core sample from 2036 m depth. In

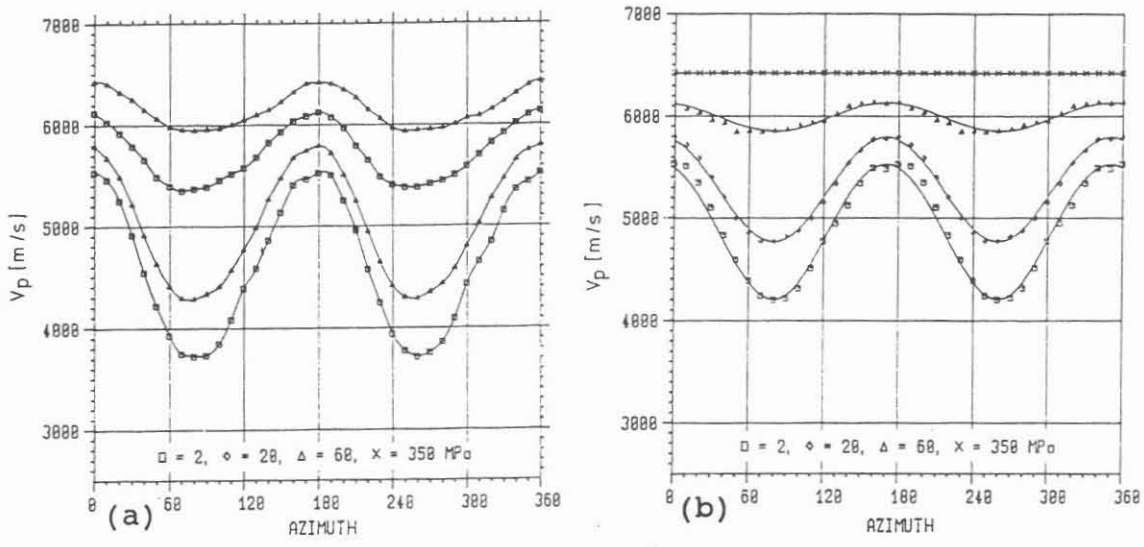

Fig. F.9: Textural reduction in case of horizontal transmission for a paragneiss sample from a depth of 2036 m.

Fig. F.9a the P-wave velocity is plotted versus azimuth for four selected pressure levels. Here the velocity anisotropy consists of one part due to microcracks and a second part caused by the rocks texture. The remaining velocity anisotropy at 350 MPa (assumed to be a purely textural one), is now subtracted from all velocity anisotropy curves at lower pressure levels. The result of this procedure is seen in Fig. F.9b. Now all curves at lower pressure levels consist of a pure crack-caused velocity anisotropy, which will be interpreted with respect to in-situ stresses in the following section.

F.4. In-situ stress estimates

In this chapter the maximum (S_H) and minimum (S_h) horizontal stresses are calculated from the values of anelastic strain recovery. A second independent estimate of in-situ stress magnitudes results from pressure differences determined from the crack-caused velocity anisotropy of drill cores. In case of structurally isotropic material the direction of maximum strain recovery and minimum wave velocity should coincide with the orientation of the maximum in-situ stress.

F.4.1 Stress magnitudes

Under the assumption of linear viscoelasticity it is possible to calculate the relative magnitudes of princial horizontal stresses directly from the values of recovery strains of the core samples (Blanton 1983). Absolute values are obtained by normalisation with S_v assumed to be the weight of the overburden. Estimating the principal stress magnitudes in this way for two lamprophyric core samples of the KTB pilot hole (Zang et al. 1989, Wolter & Berckhemer 1989a) one obtains the data in Table F.2.

sample #	depth [m]	S_H [MPa]	S_h [MPa]	S_V [MPa]
468G1r	2051	73	52	57
526G2u	2232	63	47	61

Table F.2: Stress magnitudes inferred from ASR-results of two lamprophyric core samples.

The basic concept for estimating in-situ stress magnitudes from ultasonic velocity data is presented in Fig. F.10. After the elimination of the textural influence (see Fig. F.9b) the P-wave velocity is plotted versus confining pressure for three different directions of wave paths (v^{min}, v^{max}, v^z see Fig. F.6) in Fig. F.10. Because of the correction for textural anisotropy the set of pressure dependent velocity curves has a common velocity value at the maximum pressure of 350 MPa. In Fig. F.10 three different cases for velocity relationships are distinguished, depending whether the vertical value of P-wave velocity lies in between (case 1), below (case 2) or above (case 3) the two horizontal ones. For estimating stress magnitudes the first step is to determine a horizontal (Δp_h) and a vertical (Δp_v) pressure difference (see Fig. F.10). These difference pressures are necessary to remove the crack-caused velocity anisotropy of drill cores. In a second step from these pressure differences the in-situ stress magnitudes are calculated according to the scheme on the right hand side of Fig. F.10. The idea behind this stress estimate is, that ultrasonic wave velocity is influenced by a distribution of stress relief microcracks. Closing these cracks by applying the pressure differences $\Delta p_{h,v}$ one obtains the values of in-situ stress differences. Therefore the relationship $S_H > S_v > S_h$ may be deduced from the velocity relationship $v^{min} < v^z < v^{max}$ keeping stress relief microcracking as connecting link in mind.

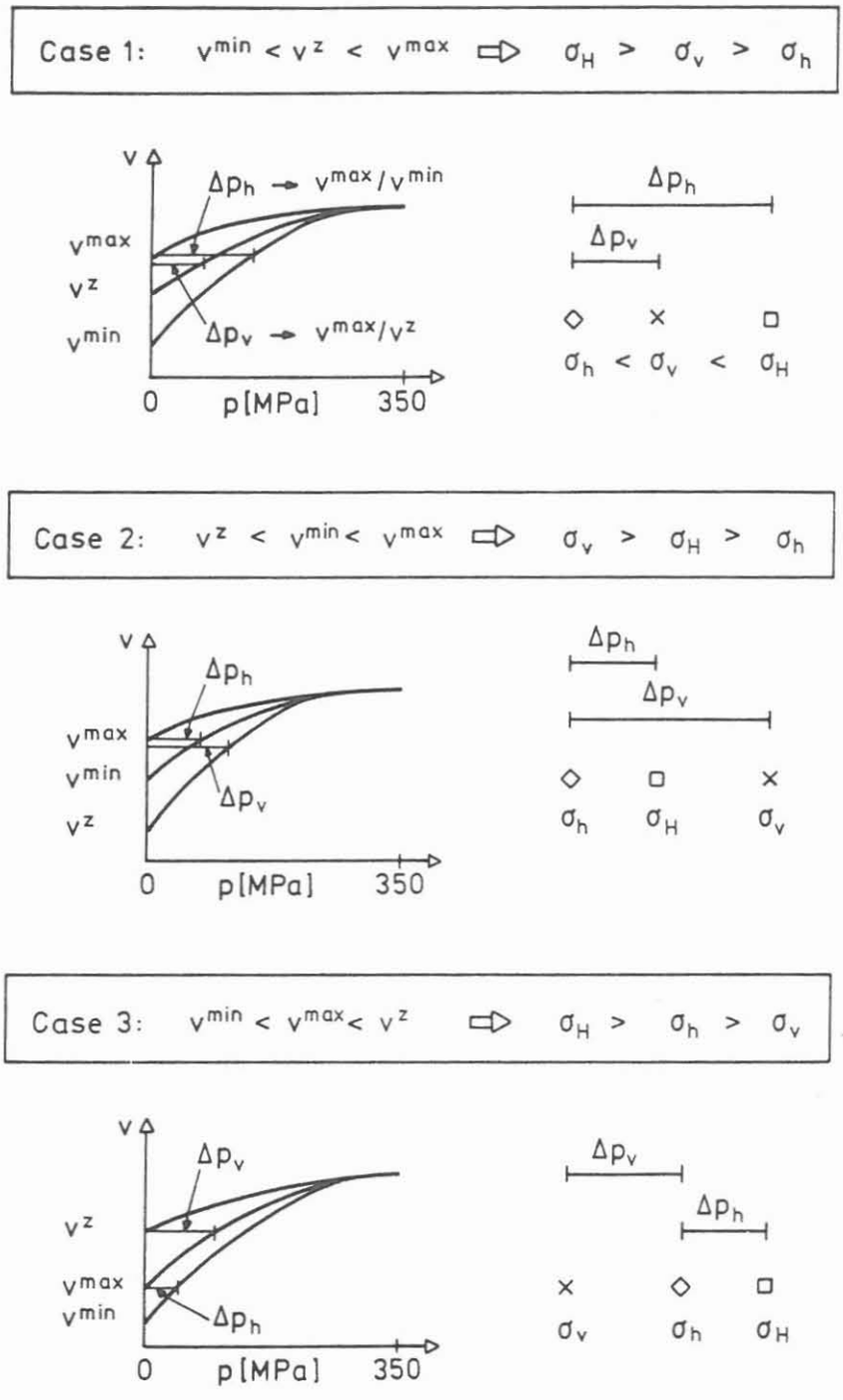

Fig. F.10: Scheme for stress estimates by WVA-method based on pressure dependent ultrasonic velocity measurements on drill cores.

This method for in-situ stress estimates from ultrasonic velocity data was applied to 41 KTB-drill cores. Absolute pressure values are obtained by normalisation of the vertical stress in Fig. F.10 to the lithostatic overburden pressure calculated from a mean rock density of 2750 kg/m^3. The stress magnitudes S_h , S_H and S_v resulting from this

procedure are plotted versus depth on Fig. 11. At the right margin the pilot hole is divided into several stress regimes based on the velocity classification introduced in Fig. F.10. From Fig. F.11 it is evident, that near surface stresses ($z \leq 500$ m) are characterised by case 3, that means the horizontal principal stresses both are greater than the vertical stress ($S_H > S_h > S_v$). A reasonable explanation for

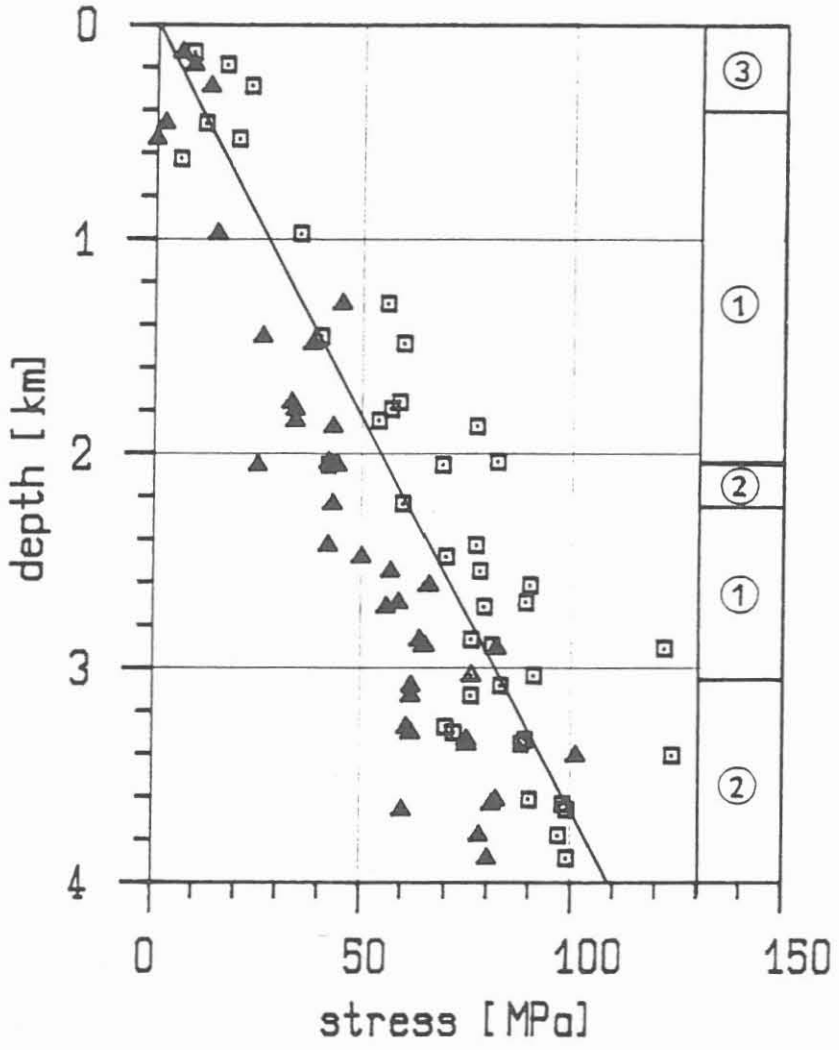

Fig. F.11: Stress magnitudes necessary to remove crack-caused velocity anisotropy of KTB drill cores (⊡ = S_H, ▲ = S_h, —— = S_v).

this stress regime is the presence of high horizontal tectonic stresses exceeding the low overburden pressure at shallow depth. Below a depth of 500 m the state of stress in the pilot hole is dominated by case 1, i.e. the vertical stress is intermediate ($S_H > S_v > S_h$). This stress relation covers the depth range from 500 to about 3000 m and is interrupted only at 2050 m to 2250 m depth by stress regime 2, which was confirmed by analysing three lamprophyric core samples. Below 3000 m the state of stress is characterized by case 2 where horizontal stress magnitudes are smaller than the vertical stress ($S_v \geq S_H > S_h$).

Linear regression of 41 data points allows to estimate a continuous stress profile for the horizontal stresses: S_h = 21z (correlation 0.866), and S_H = 23z + 15 (correlation 0.843) based on a vertical overburden pressure of S_v = 27z with stresses S in MPa and depth z in km. For example at 4 km depth one obtains the stress magnitudes S_h = 85 MPa, S_H = 107 MPa and S_v = 108 MPa.

F.4.2 Stress field orientation

The direction of the maximum horizontal compressional stress S_H should be parallel to the orientation of maximum recovery strain and minimum wave velocity in case of structurally isotropic material.

Teufel (1982) found a good agreement between directions of principal horizontal stresses and principal horizontal strains in vulcanic tuff, determined from both elastic and anelastic strain recovery. The orientation of maximum horizontal in situ-stress deduced from the direction of maximum retarded strain is given in Table F.3 for five selected KTB core samples.

sample #	lithology	depth [m]	S_H [N°E]
468G1r	lamprophyre	2051	172 ± 15
526G2u	lamprophyre	2232	155 ± 10
632G2r	metabasite	2614	179 ± 9
865E2zK	gneiss	3537	153 ± 7
874G1vK	metabasite	3573	185 ± 10

Table : F.3: S_H-orientation deduced from strain retardation measurements.

The samples 468G1r and 526G2u are fine-grained, non-foliated, quasi-isotropic lamprophyres. It can be presumed that the orientation of maximum horizontal retarded strain of those samples does coincide with the orientation of maximum compressional horizontal in situ-stress. This means that the orientation of S_H at the KTB-lokation deduced from strain retardations of two lamprophyre core samples leads to NNW - SSE (mean value: N163°E ± 21) in the depth range from 2000 to 2250 m. If we take into consideration three additional core retardation measurements (see Table F.3) than the mean value of S_H-orientation is N168°E ± 25 in

the depth range from 2000 to 3600 m. Two of three additional core samples are weakly foliated metabasites (high Young's modulus and high uniaxial compressive strength) and one is a garnet-mica-gneiss with a modest dip angle of foliation.

The ultrasonic data set leads to a different estimate of S_H-orientation (mean value of minimum velocity azimuth is about N30°E, see Fig. F.12), but one has to take into account the influence of rocks texture on stress relief microcracking when discussing the v^{min}-orientation with respect to stress direction. From Fig F.9b it is evident that v^{min}-orientation does not change with increasing confining pressure for gneissic core samples. Therefore the preferred orientation of cracks and fabric elements (here: foliation) is likely to be the same. The foliation of gneisses is responsible for the preferred orientation of stress relief microcracks, and therefore the v^{min}-direction does not necessarily correspond to the orientation of S_H. Loosing the stress direction by rocks texture, the crack closing pressure derived from ultrasonic measurements still may be a reasonable approach for in-situ stress magnitudes.

In spite of foliation influence on the S_H-orientation, in Fig. F.12 the azimuth of v^{min}-direction after textural reduction is plotted versus depth for 17 oriented core samples. It is worth mentioning that the azimuth of

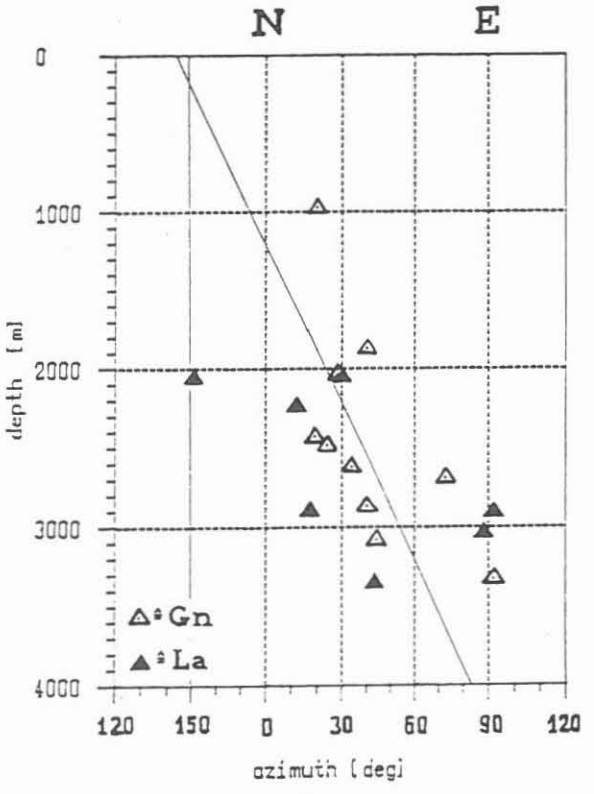

Fig. F.12: Orientation of v^{min}-azimuth with respect to geographic North versus depth for foliated gneisses (open triangles) and structurally isotropic lamprophyres (solid triangles).

v^{min}-pole for gneiss samples (open triangles) and lamprophyres (solid triangles) shows a rotation in Eastward direction with increasing depth. One has to test if this clockwise rotation of the v^{min}-azimuth from NNE near surface to about EW at 4 km depth is a realistic indicator for a change in stress field orientation with depth.

F.5 Discussion and conclusions

The two different methods applied to estimate the state of stress in the KTB pilot hole using oriented drill core samples are: the anelastic strain recovery method (**ASR**) and the ultrasonic wave velocity analysis (**WVA**). Both methods make use of stress relief by tension crack opening upon removal of the core from its environment. The measurement- and analysis techniques have been developed to a quite advanced stage within the KTB-project.

A first and most important result of the **ASR** method was the proof that the so-called "viscoelastic" relaxation of the core which follows a simple exponential law is at least in part the effect of retarded dilatancy by microcrack generation. In principle it is possible to derive relative components of the in-situ stress field from strain retardation measurements if the rock behaves as an isotropic viscoelastic body (Blanton 1983). Unfortunately the crystalline rock in the KTB pilote hole consists in large parts of steeply inclined foliated gneisses. It was to be expected that anisotropy in tensile strength (which is measured by the Brazilian test but not described here) will lead to a microcrack pattern which is strongly influenced by the rock texture as seen in Fig. F.4.

The same microcrack pattern is also the cause of elastic anisotropy in the **WVA** ultrasonic experiments at low confining pressure after the effect of intrinsic textural anisotropy has been eliminated as described in Chapter F.3.3. Although it is of considerable interest to have a convenient tool to study by an integrating physical method open microcrack populations in rocks it is, for the reasons mentioned above, problematic to derive information on the in-situ stress field from strongly texturised rocks. The large variety in strain retardation amplitude (Fig. F.3), maximum strain direction (Fig. F.4), relaxation times (Fig. F.5) and direction of minimum velocity (Fig. F.12) reflects the complex petrographic setting in the borehole.

At present, the only way to obtain significant data on the stress field by core analysis is a careful selection of those specimens which are from their macroscopic structural appearance nearly isotropic. Foliated rocks, too, might be useful to derive the direction of S_H if the foliation is subhorizontal and free of linear flow structures.

Among the 32 specimens analysed by ASR five samples from a depth range 2000 to 3500 m seemed to fulfil the above requirements. They are listed in Table F.3. These are mainly lamprophyres but also a gneiss with slight and flat foliation. A mean value for the S_H-direction of N163°E ± 21° is obtained from the direction of the maximum horizontal strain. This is in good agreement with the mean value of N149°E ± 15° for S_H from hydrofrac tests (Baumgärtner et al. 1990). In the present paper stress magnitude components derived from strain retardation are exemplified for two samples in Chapter F.4.1.

The orientation of the elastic anisotropy obtained by the ultrasonic method seems to be quite sensitive to the orientation in particular to phylosilicates. If one uses the same samples as listed in Table F.3 one obtains an S_H-direction of N5°E ± 20°. Taking, however all spatially oriented samples irrespective of their structure, a rotation of v^{min}-azimuth from North at 1000 m to NE at 3000 m is found in Fig. F.12. One has to be very careful in correlating this result with stress directions, although a similar clockwise rotation of S_H-orientation with depth can also be seen from the breakout analysis in the borehole (Fuchs et al. 1990, unpublished). It also agrees to some extent with the strike of the saddle of core disking faces (Wolter et al. 1990).

Rather independent on structural anisotropy and therefore more reliable seems to be the stress values obtained from **WVA** as described in Chapter F.4.1 and shown in Fig. F.11. It is one of the interesting results from this study to see how the stress regime changes with depth. This result agrees in general trend with the hydrofrac data (Baumgärtner et al. 1990), and may be classified in terms of thrust faulting regime for depth below about 500 m, strike slip regime in the depth range from 500 to 3000 m and normal faulting regime below 3000 m. More detailed structural analysis of samples, more reliable core orientation, and future developments in interpretation theory may improve the significance and quality of our results.

F.6 Acknowledgements

The authors thank Dipl. Ing. E. Aulbach for designing and building the measuring devices used in this study. Dipl. Ing. E. Aulbach and Dipl. Phys. M. Lienert although carried out parts of the measurements, from which data were used for further investigation. This work was supported by the "Deutsche Forschungsgemeinschaft (DFG)" and the "Niedersächsisches Landesamt für Bodenforschung (NLfB)".

F.7 References

Baumgärtner, J., Rummel, F. & Zoback, M. D. (1990): Hydraulic fracturing in situ stress measurements to 3 km depth in the KTB Pilot Hole VB1. KTB-Report (in press).

Blanton, T. L. (1983): The relation between recovery deformation and in situ stress magnitudes. Symp. SPE/DOE 11624, Denver (CO), 213-218.

Carlson, S. R. & Wang, H. F. (1986): Microcrack porosity and in situ stress in Illinois borehole UPH 3, J. geophys. Res. 91, 10421-10428.

Charlez,P., Hamamdijan, C. & Despax, D. (1986): Is the microcracking of rock a memory of its initial state of stress? Proc. Int. Symp. on Rock Stress and Rock Stress Measurements, Stockholm, 341-350.

Dey, T. & Brown, D. (1986): Stress measurements in deep granitic rock mass using hydraulic fracturing and differential strain curve analysis. Int. Sym. on Rock Stress and Rock Stress Measurements, Stockholm, 351-357.

Dyke, C. G. (1989): Core discing: Its potential as indicator of principal in-situ stress directions.- In: Rock at Great Depth, Balkema, Rotterdam, 1057-1064.

El Rabaa, A. (1989): Determination of the stress field and fracture direction in the Danian chalk. In: Maury & Fourmaintraux, Rock at Great Depth, Balkema, Rotterdam, 1017-1024.

Fuchs, K., Wilhelm, H., Mastin, L. & Krammer, A. (1990): Untersuchung des Spannungsfeldes in der KTB-Tiefbohrung mit kombinierten Methoden. Endbericht zum Forschungsvorhaben Fu 55/31, 21 p.

Maury, V., Santardelli, F. & Henry, J. P. (1988): Core Discing: a review.- Proc. 1st African Conf. on Rock Mech., Swaziland, 1057-1064.

Perreau, P., Heugas, O. & Santarelli, F. (1989): In-situ stresses evaluated from measurements on core samples. European Geothermal Update, Proc. of the 4th Int. Seminar on the Results of EC Geothermal Energy Research and Demonstration, Florence, 27-30 Apr., 253-270.

Ren, N. K. & Roegiers, J. C. (1983): Differential strain curve analysis - a new method for determinig the pre-existing in situ stress state from rock core measurements. Proc. 5th Int. Congr. Rock Mech. 5, F117-F127.

Ren, N. K. & Hudson, P. J. (1985): Predicting the in-situ state of stress using differential wave velocity analysis. Proc. 26th U.S. Symposium on Rock Mech., E. Ashworth (ed.), Rapid City, SD, 1235-1244.

Rummel, F. (1989): Hydraulic fracturing stress measurements theory and practice. European Geothermal Update, Proc. of the 4th Int. Seminar on the Results of EC Geothermal Energy Research and Demonstration, Florence, 27-30 Apr., 335-344.

Teufel, L. W. (1983): Determination of in-situ stress from anelastic strain recovery measurements of oriented core. Symp. on Low Permeability Gas Reservoirs SPE/DOE 11649, Denver (CO), 421-430.

Teufel, L. W. (1989): A mechanism for anelastic strain recovery of cores from deep boreholes: time-dependent microcracking. EOS 70, #15, 476.

Warpinski, N. R. & Teufel L. W. (1989): In-situ stresses in low- permeability, nonmarine rocks. J. Petr. Techn., 405-414.

Wolter, K., Aulbach, E. & Berckhemer, H. (1988): Spannungsnachwirkungsuntersuchungen: - Messung der Retardation und der akustischen Emission. In: Emmermann, Dietrich, Heinisch & Wöhrl (eds.), KTB-Report 88-6, NLfB, Hannover D47-D60.

Wolter, K. & Berckhemer, H. (1989a): Time dependent strain recovery of cores from KTB-Deep drill hole. Rock Mech. & Rock Engineering 22, 273-287.

Wolter, K. & Berckhemer, H. (1989b): Retardierte Entspannungsdeformation an KTB-Bohrkernen. In: R. Emmermann & P. Giese (eds.), KTB-Report 89-3, NLfB, Hannover, 245-249.

Wolter, K. E., Röckel, Th., Bücker, Ch., Dietrich, H.-G. & Berckhemer, H. (1990): Core disking in KTB Drill Cores and the Determination of the in-situ stress orientation. This volume.

Zang, A. & Berckhemer, H. (1989): Residual stress features in drill cores. Geophys. J. Int. 99, 621-626.

Zang, A., Wolter, K. & Berckhemer, H. (1989): Strain recovery, microcracks and elastic anisotropy of drill cores from KTB deep well. Scientific Drilling 1, 115-126.

Zoback, M., Mastin, L. & Barton, C. (1986): In-situ measurements in deep boreholes using hydraulic fracturing, wellbore breakouts, and stonely wave polarization. Int. Sym. on Rock Stress and Rock Stress Measurements, Stockholm, 289-299.

KTB-Report	90-8	G1-G13	8 Fig.	Hannover 1990

Core Disking in KTB Drill Cores and the Determination of the in situ Stress Orientation

[1] WOLTER, K.E., [1] RÖCKEL, Th., [1] BÜCKER, Ch., [1] DIETRICH, H.G. & [2] H. Berckhemer

Contents:

Authors adresses:

[1])KTB-Feldlabor, P.O.-Box 67, D-8486 Windischeschenbach
[2])Inst. f. Geophysik u. Meterologie, Feldbergstr. 47
D-6000 Frandfurt am Main

Abstract

Core disking is frequently found in cores (ø=94 mm) of the KTB pilot well below 3574 m depth. There the lithology changes from strongly foliated paragneisses to weakly textured metabasites. The core disks have a saddle-shaped morphology which is closely related to the in situ stress orientation. The stress orientation determined by the analysis of the saddle-shaped morphology is in accordance with the results of different stress measurement methods. The core disking morphology is a good indicator for the orientation of the maximum horizontal in situ stress (S_H). The S_H-orientation at the KTB drill site derived from the saddle-shaped disks is NNW-SSE (N163°E ± 22, depth range: 1200-3600 m).

G.1 Introduction

The occurrence of the core disking phenomenon of drill cores is characterized by disks with thicknesses of 1-10 cm. Disking fractures are perpendicular to the borehole axis and the morphology of the disks is often buckled and saddle-shaped (Fig. G.1). Disking takes place during coring. Different zones of stress concentrations at the bottom of the hole lead to failure on the drill core. The disking fractures do not correspond with paleotectonical textures. OBERT & STEPHANSON (1965) and PANET (1969) propose relations between core disking, in situ stress and rockmechanical properties of the drilled rocks. First investigations of core disking in drill cores from the crystalline basement of southern Germany indicate a relation of failure orientation of disks and the in situ stress field (SCHÄDEL & DIETRICH 1982). The failure is primarily caused by tensional stress concentrations (SUGAWARA et al. 1978, STACEY 1982, BORM et al. 1989, DYKE 1989). After PERREAU et al. (1989) there are also zones of high level compressive stresses which can lead to shear failure. Secondarily, the failure is influenced by mechanical disturbances during the drilling process as well as by tensional stresses induced by thermal contraction of the drill cores (BORM et al. 1989). In a review about core disking presented by MAURY et al. (1988), it is outlined that the occurrence of core disking and the shape of a disk is a good indicator of the in situ stress direction.

Core disking may lead to drilling difficulties and cause problems to petrophysical research on the samples. MAURY et al. (1988) point out that a better understanding of the conditions which lead to core disking would be extremely profitable, either to prevent disking, or to control the occurrence of disking. A controlled occurrence of disking gives good informations of the state of stress.

G.2 Core Disking in the KTB Pilot Hole

An extensive occurrence of core disking was found below 3574 m. This coincides with the lithological change of foliated paragneisses to weakly textured metabasites. The first occurrence of a disk in drill cores of the KTB pilot well in a foliated biotite-gneiss was detected at 2904 m depth. The core disking fracture plane is not controlled by the foliation. Almost all disks show a saddle-shaped morphology. The first saddle-shaped cracks occur already at 1180 m depth (metabasite), but no dissection into disks could be found. A depth dependence of the thickness of the disks is not recognizable. The disks of KTB drill cores often have a thickness of 2-4 cm (depth range: 3574-3893m).

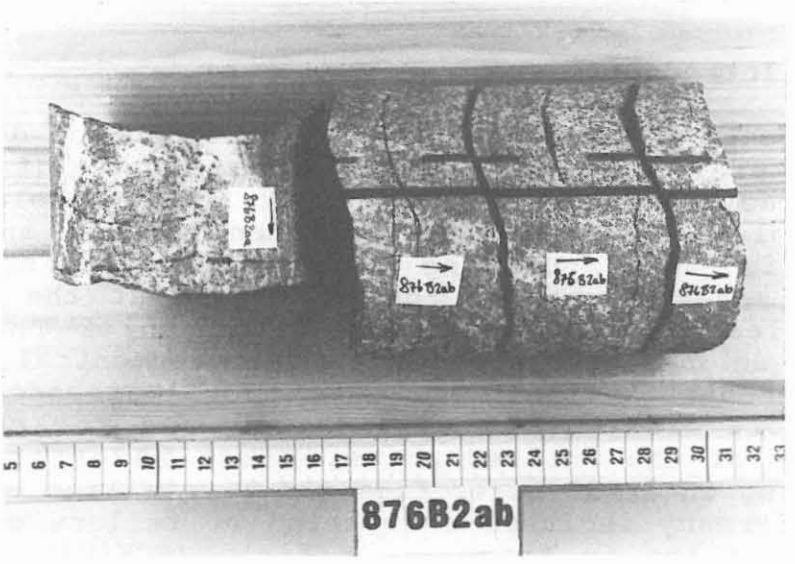

Fig. G.1: Saddle-shaped disks in metabasite (depth: 3581 m)

Core disking in KTB drill cores predominantly occurs in brittle rocks (metabasites). In strongly foliated biotite gneisses a strain relief microcracking along the foliation planes (WOLTER & BERCKHEMER 1989) prevents the expected disking across the foliation planes.

G.2.1 Disk Shape and Stress Direction

The latest publications on core disking furnish evidence for a close relationship between in situ stress distribution and the morphology of the disks. Disk shapes ("high"- and "low"-points, Fig.G.2) can be used as an indication of the in situ stress orientation (MAURY et al. 1988, DYKE 1989, PERREAU et al. 1989, WOLTER et al. 1990). Fig. G.2 shows a sketch of the saddle-shaped disk. The axis of the "low"-points indicates the direction of maximum horizontal in situ stress S_H.

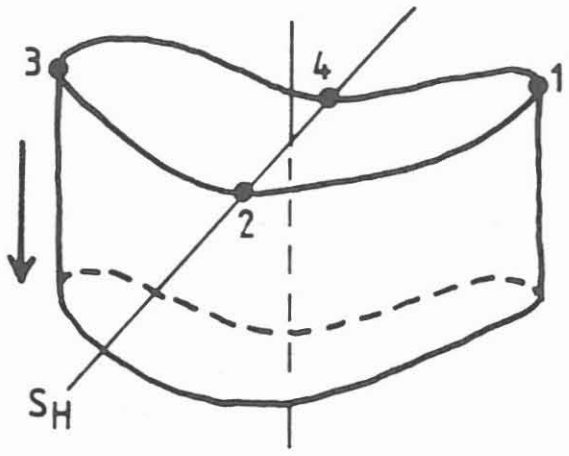

Fig. G.2: Shape of disk. Definition of "high"-points (1,3) and "low"-points (2,4)

DYKE (1989) investigated the initiation of disking and the formation of disk shapes. He used a 3-D elastic boundary element analysis to calculate the stress and extension strains within a core during unloading. Results of this calculations are shown in Fig. G.3. It displays the location of failure initiation for a vertical borehole subjected to unequal horizontal stresses. The plot shows the extensional strain paths in two different vertical planes perpendicular to each other.

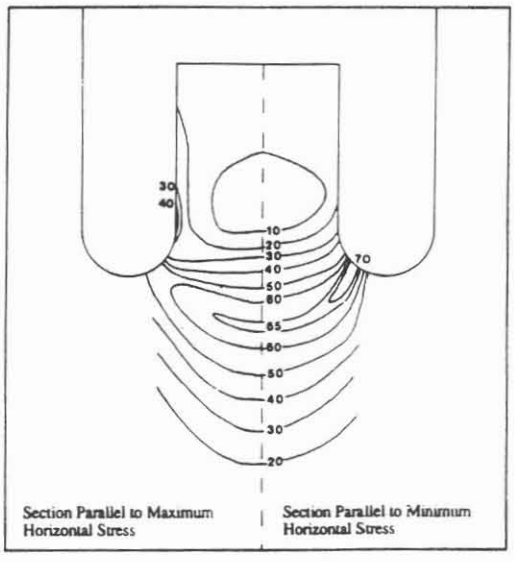

Fig. G.3: Vertical extension strains for a vertical borehole subjected to the stresses σ_H=2MPa, σ_h=1MPa, σ_v= 1MPa, E=17GPa, ν=0.25 (DYKE 1989).

The most important results of the calculations are:

I. In the direction of maximum horizontal stress (S_H) failure initiation takes place in the center of the core and develops outward at a shallow angle.

II. In the direction parallel to the minimum horizontal stress (S_h) failure would initiate at the surface of the core and propagate inwards and steeply downwards to the center.

This results explain the formation of a saddle-shaped disks and confirm that the axis of "low"-points (2-4, Fig. 4) does coincide with the orientation of maximum horizontal in situ stress (S_H).

Fig. G.4 shows the pattern of cracks within a core sample (amphibolite, depth: 3837 m) on two vertical planes perpendicular to each other. The two planes are parallel to the direction of S_H (axis of "low"-points) and parallel to S_h (axis of "high"-points). It can be seen that the cracks are wider in the interior than at the surface of the core. The fact that the failures do not penetrate each other suggest that failure initiation starts from different zones in the core. This is in good agreement with the results of DYKE's calculations.

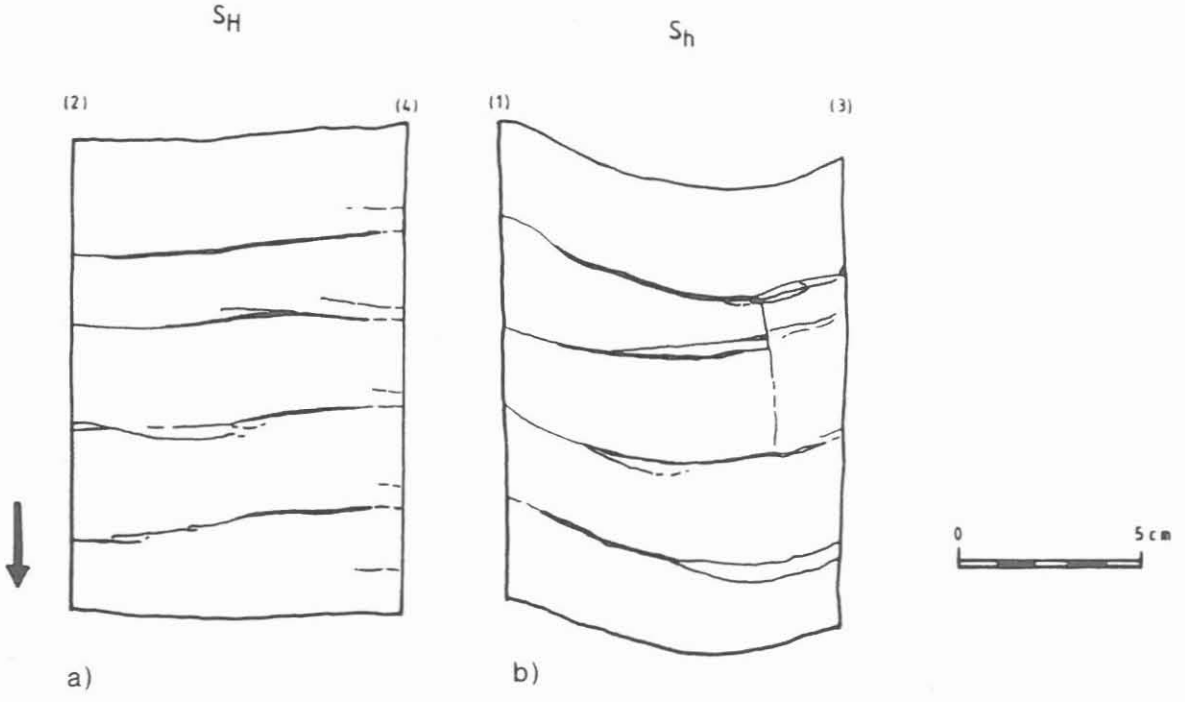

Fig. G.4: Crack pattern inside of a drill core (amphibolite, depth: 3837m).
a) parallel to S_H (axis of "low"-points; 2-4)
b) parallel to S_h (axis of "high"-points; 1-3)

G.2.2 Subaxial Fractures

Another fracture phenomenon in KTB drill cores is the appearance of subaxial fractures (BORM et al. 1989). The subaxial fractures predominantly appear below 3574 m depth within series of metabasites. Subaxial fracturing and core disking may occur together (Fig. G.5). The subaxial fractures are mainly subparallel to the axis of "low"-points or parallel to the maximum horizontal in situ stress (S_H). When subaxial fracturing and core disking exist in the drill core together, in most cases the failure of disk is displaced by the subaxial fracture (Fig. G.5). This shows, that subaxial fracturing is generated before core disking occurs. We propose, that subaxial fractures below the bottom of the hole are induced by the drilling process. After BORM et al.(1989) it is very likely that the subaxial fractures are technically induced hydraulic fractures at the very bottom of the hole. Theoretically, the vertical hydraulic fractures are parallel to the direction of maximum horizontal in situ stress (e.g. RUMMEL 1988). Then, during drilling of the core, core disking takes place in the drill core which is already subaxial fractured.

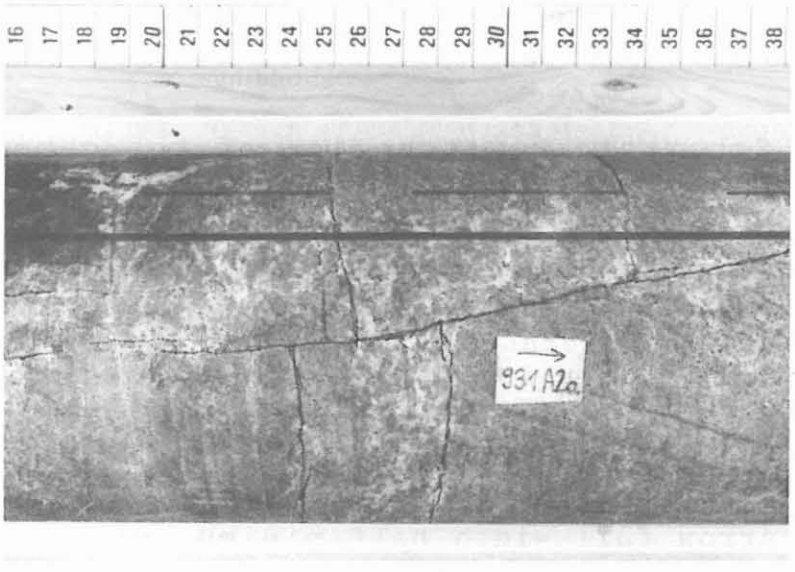

Fig. G.5: Subaxial fracturing and core disking in drill core (metabasite, depth: 3720 m)

G.3 Gamma-Ray Absorption; A Method to Detect Internal Cracks

Several cores do not show any visible failures of the core surface that indicate core disking. High resolution density measurements with the gamma-ray absorption method, however suggest that there are open cracks inside of the core.

These measurements can be performed with a high spatial resolution. Differences in density lower than 0.005 gcm^{-3} can be resoluted. The radiation source is a commercially available gamma source (Cs-137) having a photon energy of 662 keV and an activity of 26 GBq. The principal design of the measurement equipment is sketched in Fig. G.6. The scintillation detector is a very fast polyvinyltoluol plastic scintillator. A detailed description of the equipment is given by BÜCKER et al. (1990).

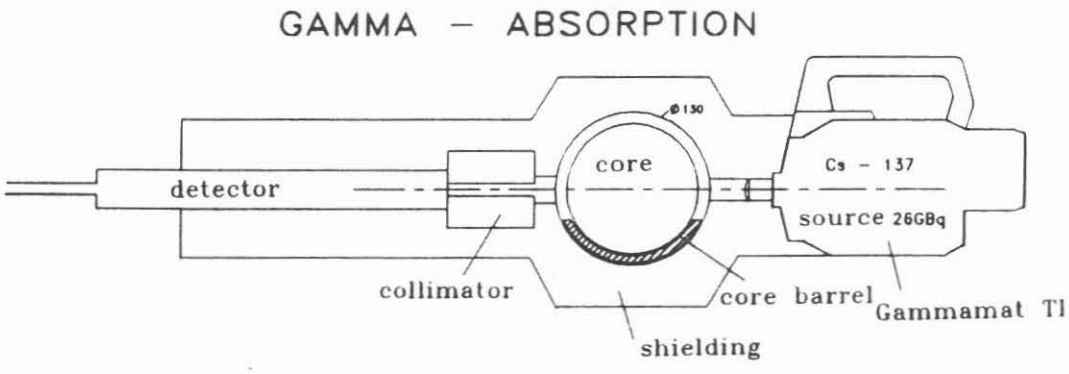

Fig. G.6: Schematic construction of the gamma-density measurement equipment used for the determination of invisible open cracks in cores.

Results of these density determinations on one core sample (metagabbro, depth: 1262 m) are shown in Fig. G.7. This core already shows saddle-shaped cracks on the surface of the core. The core with a length of 15 cm was measured in axial steps of 1 mm under different azimuths (0°, 90°, related to the field laboratory reference line). The decrease in density at 50 mm and at 130 mm can be explained by visible cracks. This does not apply to the minimum in density at 25 mm. The narrow full width half minimum of this decrease (Fig. G.7) could be explained by an open crack inside of the core. This interpretation confirms the results of the investigations of DYKE (1989), who showed an initiation of disking failure in the center of the core parallel to the s_H-direction.

By means of the gamma-ray absorption method it is possible to detect open fractures within the core, which are not visible at the core surface. Furthermore, a spatial determination of failure propagation inside the core sample might be used as an indication of stress orientation.

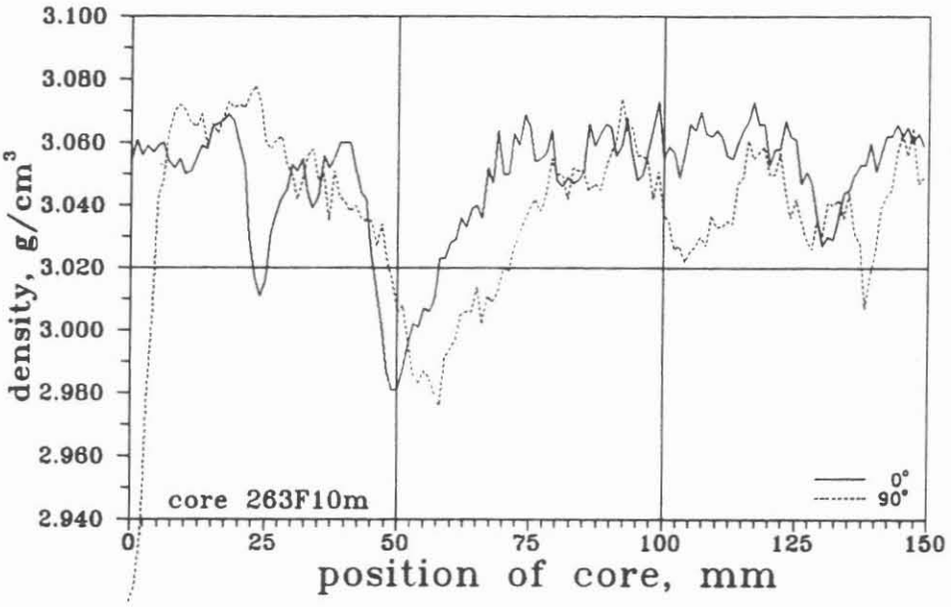

Fig.G.7: Density profiles in two azimuth-positions of a metagabbro core from 1262 m depth (core 263F10m). The minima in density are related to core-disking failures. The minimum in density at 25 mm can not be explained by a visible crack at the core surface.

G.4 Results of the Observations with Respect to the in situ Stress Orientation

The axis of "low"-points of a saddle-shaped disk coincides with the orientation of the horizontal maximum in situ stress. So, the in situ stress orientation is determinable if the core samples are oriented. In the following we compare the orientation of core disking shapes with the results of the analysis of the Anelastic Strain Retardation (ASR-method) on drill cores (TEUFEL 1983, WOLTER et al. 1988, WOLTER & BERCKHEMER 1989). Fig. G.8 shows the orientation of "low"-points of saddle-shaped disks and the orientation of maximum horizontal strain retardation (e_1). The e_1-orientation of isotropic and linear viscoelastic core samples coincides with the orientation of S_H. The e_1-data (Fig. G.8) are obtained from quasi-isotropic core samples (lamprophyres, metabasites).

The orientation of maximum horizontal stress (S_H) estimated by evaluation of anelastic strain retardation is N168°E ± 21 in the mean. This S_H-direction coincides with the mean value of the axis-orientation of "low"-points of core disks (N163°E ± 22). In general, the orientation of the maximum horizontal in situ stress (S_H) is NNW-SSE. The data from the depth range of 3200-3500 m (Fig. G.8) suggest a change in the stress orientation from NNW-SSE to N-S. Until now it is not possible to determine stress magnitudes inferred from saddle-shaped disks.

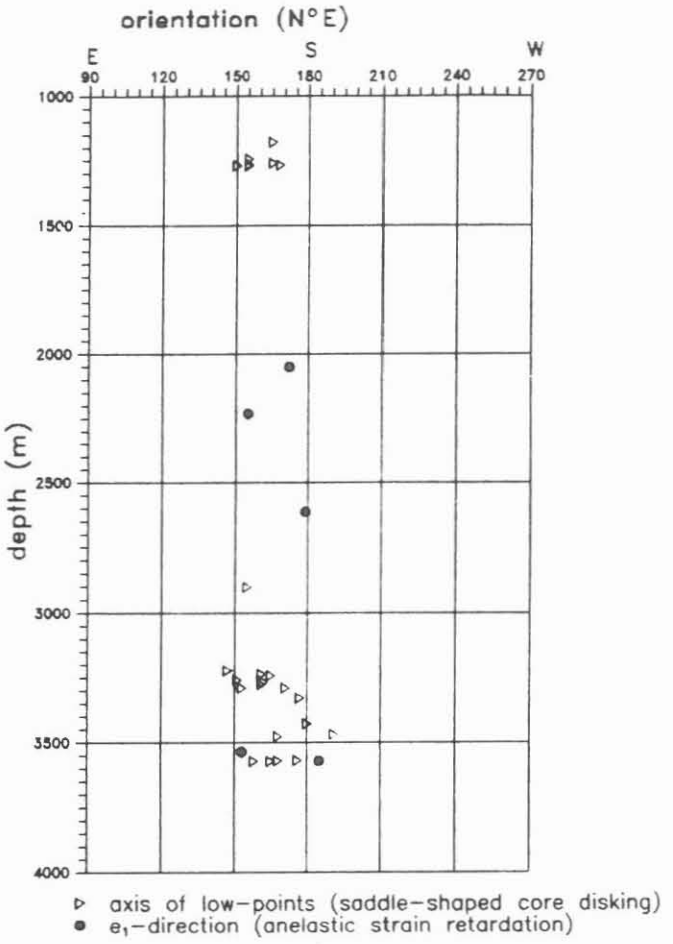

Fig. G.8: Data of orientation of saddle-shaped disks and anelastic strain retardation

G.5 Conclusions

Core disking in the KTB pilot hole predominantly occurs below 3574 m depth within a series of weakly textured metabasites. The formation of core disking within strongly foliated paragneisses is prevented by strain relief microcracking along the foliation planes. The orientation of maximum horizontal in situ stress derived by strain retardation measurements on KTB drill cores (ZANG et al. 1989, WOLTER & BERCKHEMER 1990) correlates well with the axis of "low"-points of saddle-shaped disks. MAURY et al. (1988), DYKE (1989) and PERREAU et al. (1989) already proposed a close relation between the morphology of a saddle-shaped disk and the orientation of the maximum horizontal in situ stress (S_H) by field observations and theoretical modelling. If core disking occurs in the form of saddle-shaped disks we are able to determine the in situ stress direction, provided that the cores are oriented. Analyses of KTB borehole breakouts (MASTIN et al. 1990) below 3000 m confirm the S_H-direction estimated by analyses of saddle-shaped disks of KTB drill cores.

G.6 Acknowledgements:

The authors are grateful to G. Borm, R. Löffel, and H.C. Soffel for helpfull discussions. This work was funded by the Deutsche Forschungsgemeinschaft (DFG) and the Niedersächsisches Landesamt für Bodenforschung (NLfB).

G.7 References

BORM, G., LEMPP, Ch., NATAU, O. & RÖCKEL, Th. (1989): Instabilities of borehole and drillcores in crystalline rocks, with examples from the KTB pilot hole.- Scientific Drilling, 1, 105-114, Springer.

BÜCKER, Ch., LÖFFEL, R. & A. SCHULT (1990): Hochauflösende Dichtemessung an Bohrkernen mittels Absorbtion von Gammastrahlung. - In: Beiträge zum 3. KTB-Kolloquium, Emmermann & Giese (eds.), KTB-Report 90-4, NLfB, Hannover (in press).

DYKE, C.G. (1989): Core discing: Its potential as an indicator of principal in situ stress directions. - In: Rock at Great Depth, Maury & Fourmaintraux (eds.), 2, 1057-1064, Balkema, Rotterdam.

MASTIN, L., HEINEMANN, B., KRAMMER, A., FUCHS, K. & ZOBACK, M.D. (1990): Stress orientation in the KTB pilot hole determined from stress-induced wellbore breakouts.- In: Beiträge zum 3. KTB-Kolloquium, Emmermann & Giese (eds.), KTB-Report 90-4, NLfB, Hannover.

MAURY, V., SANTARELLI, F. & HENRY, J.P. (1988): Core Discing: a review. - Proc. 1st African Conf. on Rock Mech., 1057-1064, Swaziland.

OBERT, L. & STEPHANSON, D.E. (1965): Stress conditions under which core discing occurs. - Soc. Min. Engrs. Trans., Vol.232, 227-234.

PANET, M (1969): Quelques problèmes de mécanique des roches posés par le tunnel du Mont-Blanc. - Annales de l'Institut Technique du bâtiment et des travaux publics, No.264, 1968-1979.

PERREAU, P.J., HEUGAS, O. & SANTARELLI, F.J. (1989): In situ stresses evaluated from measurements on core samples. - In: European Geothermal Update. Louwrier, Staroste, Garnish & Karkoulias (eds.), 253-270, Kluwer Academic Pub.

RUMMEL, F. (1988): Hydraulic fracturing stress measurements - theory and practice. - In: Spannungsmessungen und Bohrlochstabilität. Borm (ed.), KTB-Report 88-8, 53-65, NLfB, Hannover.

SCHÄDEL, K. & DIETRICH H.G. (1982): Results of the fracture experiments at the geothermal research borehole Urach-3. - In: The Urach Geothermal Project. Haenel (ed.). 323-343, Schweizerbart, Stuttgart.

STACEY, T.R. (1982): Contribution to the mechanism of core discing. - J. South Afr. Inst. Min. Metall., Vol. 83, 269-274.

SUGAWARA, K., KAMEOKA, Y., OKA, Y. & HIRAMATSU, Y. (1978): A study of core discing of rock. - J. Min. Inst. Japan, Vol. 94, 797-803 (in japanese).

TEUFEL, L.W. (1983): Determination of in situ stress from anelastic strain recovery of oriented core.- Symp. on low permeability gas reservoirs, SPE/DOE 11649, 421-430, Denver (CO).

WOLTER, K.E., AULBACH, E. & H. BERCKHEMER (1988): Spannungsnachwirkungsuntersuchungen: Messung der Retardation und der akustischen Emission: D. Geophysik.- In: Ergebnisse der geowissenschaftlichen Bohrungsbearbeitung im KTB-Feldlabor. Emmermann, Dietrich, Heinisch & Wöhrl (eds.), KTB-Report 88-6: D47-D60, Hannover.

WOLTER, K.E. & H. BERCKHEMER (1989): Time Dependent Strain Recovery of Cores from the KTB-Deep Drill Hole. - Rock Mech. and Rock Eng., Vol.22, 273-287, Springer.

WOLTER, K.E. & BERCKHEMER, H. (1990): Estimation of in situ stresses by evaluation of time-dependent strain recovery of KTB drill cores. Extended Abstract - Tectonophysics, Vol.178, Elsevier (in press).

WOLTER, K.E., BERCKHEMER, H., BÜCKER, CH., DIETRICH, H.G. & RÖCKEL, TH. (1990): Korrelation von Core Disking-Strukturen mit den Ergebnissen der Entspannungsdeformation an KTB-Bohrkernen.- In: Beiträge zum 3. KTB-Kolloquium. Emmermann & Giese (eds.), KTB-Report 90-4, NLfB, Hannover.

ZANG, A., WOLTER, K.E. & BERCKHEMER, H. (1989): Strain recovery, microcracks and elastic anisotropy of drill cores from KTB deep well. - Scientific Drilling, 1, 115-126, Springer.

KTB-Report	90-8	H1-H13	8 Fig.	Hannover 1990

German Continental Deep Drilling Programm (KTB) - Results from Rock Mechanical Index Tests of the Pilot Hole "KTB Oberpfalz VB"

Th. Röckel* & O. Natau**

Contents

*KTB Field Laboratory
D-8486 Windischeschenbach
Federal Republic of Germany

**Head of the Department of Rock Mechanics
University of Karlsruhe
D-7500 Karlsruhe 1
Federal Republic of Germany

H. 1 Introduction

Rock mechanical parameters are of great scientific as well as technical importance for deep drilling projects. They are an integral part for the determination of the state of stress in the earth's crust and are of direct interest to the borehole stability.

Since the fall of 1988 we have performed laboratory tests on rock samples of the KTB pilot hole to determine uniaxial compressive strength (Fig. H.1) and indirect tensile strength. The tests were carried out at the Institute for Rock Mechanics, University of Karlsruhe and the KTB Field Laboratory.

The selection of samples, the sample geometry, test equipment, methods and results have been described by RÖCKEL & NATAU (1989).

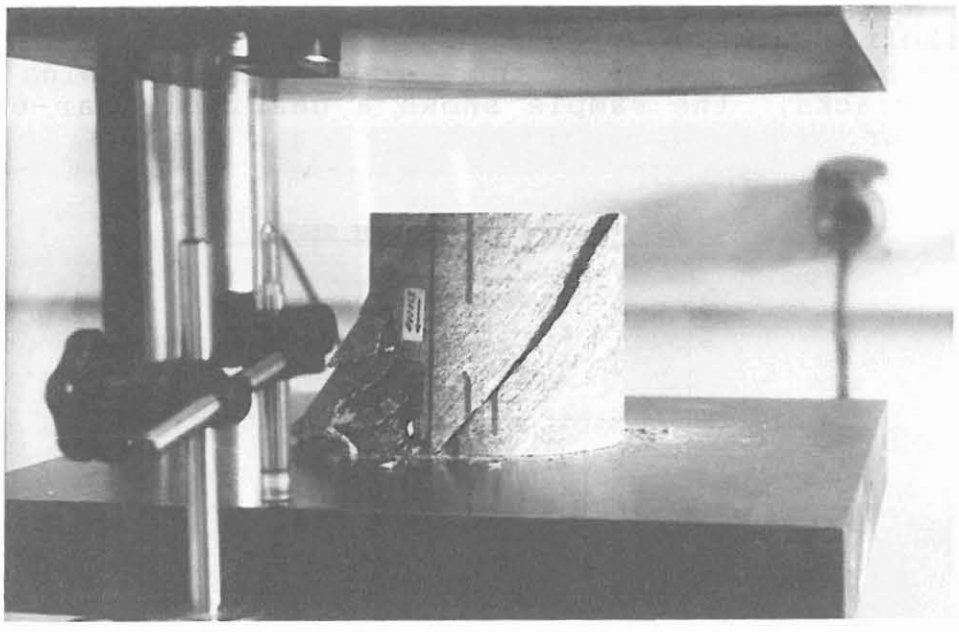

Fig. H.1: Uniaxial compression test with shear failure along the foliation in a biotite-gneiss sample from 3402 m. The dip angle of the foliation is about 50°. The uniaxial comressive strength is 31.0 MPa and the Young's modulus is 28.6 GPa.

H. 2 Test Results

The main lithological components of the rocks of the KTB pilot hole are massive, non-textured metabasites and foliated biotite-gneisses. In general, samples of the biotite-gneisses show a strongly anisotropic behaviour compared to the metabasites with a more isotropic rock-strength behaviour.

H. 2.1 Uniaxial Compression Tests

The uniaxial compressive strengths and the Young's moduli measured on cores from the pilot hole vary over a wide range. The massive metabasites show high mean values of the uniaxial compressive strength (140.5 MPa) and the Young's modulus (53.8 GPa). The minimum and maximum uniaxial compressive strengths in the metabasites are 36.5 MPa at 189 m depth and 265.4 MPa at 3816 m. The Young's moduli vary from 31.2 GPa to 90.0 GPa. The metabasites show a tendency to have higher uniaxial compressive strengths with increasing depth. The metabasites between 189 m and 452 m have a mean value of 71.2 MPa. The samples between 1178 m and 1558 m depth have a mean value of 128.7 MPa. The metabasites below 3575 m, with a mean value of 217.2 MPa, show very high uniaxial compressive strengths (Tab H.1). In this depth range, the cataclastic deformation is of lower degree.

Fig. H.2 shows a stress-strain diagram of a garnet-amphibolite from about 1434 m. Typical for the metabasites is the high elasticity of these rocks. After closing of the micro-cracks, the sample shows a nearly linear-elastic behaviour.

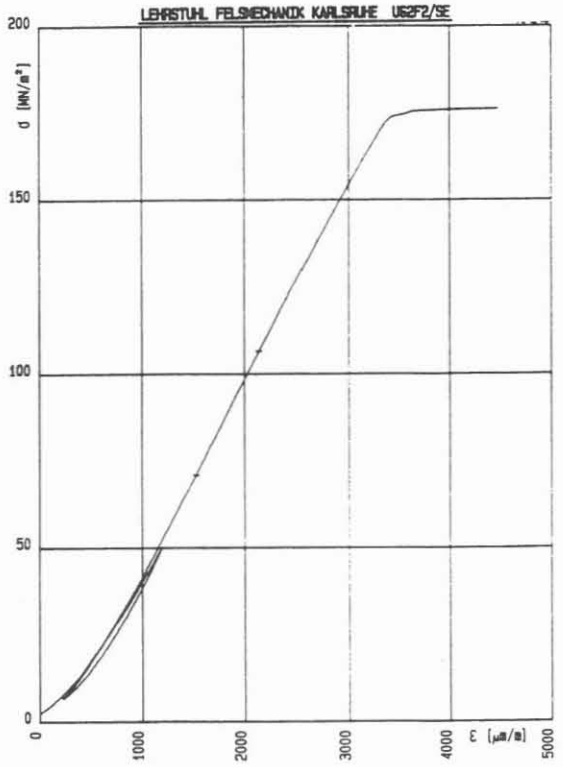

Fig. H.2: Stress-strain diagram of a massive metabasite sample (garnet-amphibolite) from 1434 m. The uniaxial compressive strength is 176.2 MPa and the Young's modulus is 58.0 GPa.

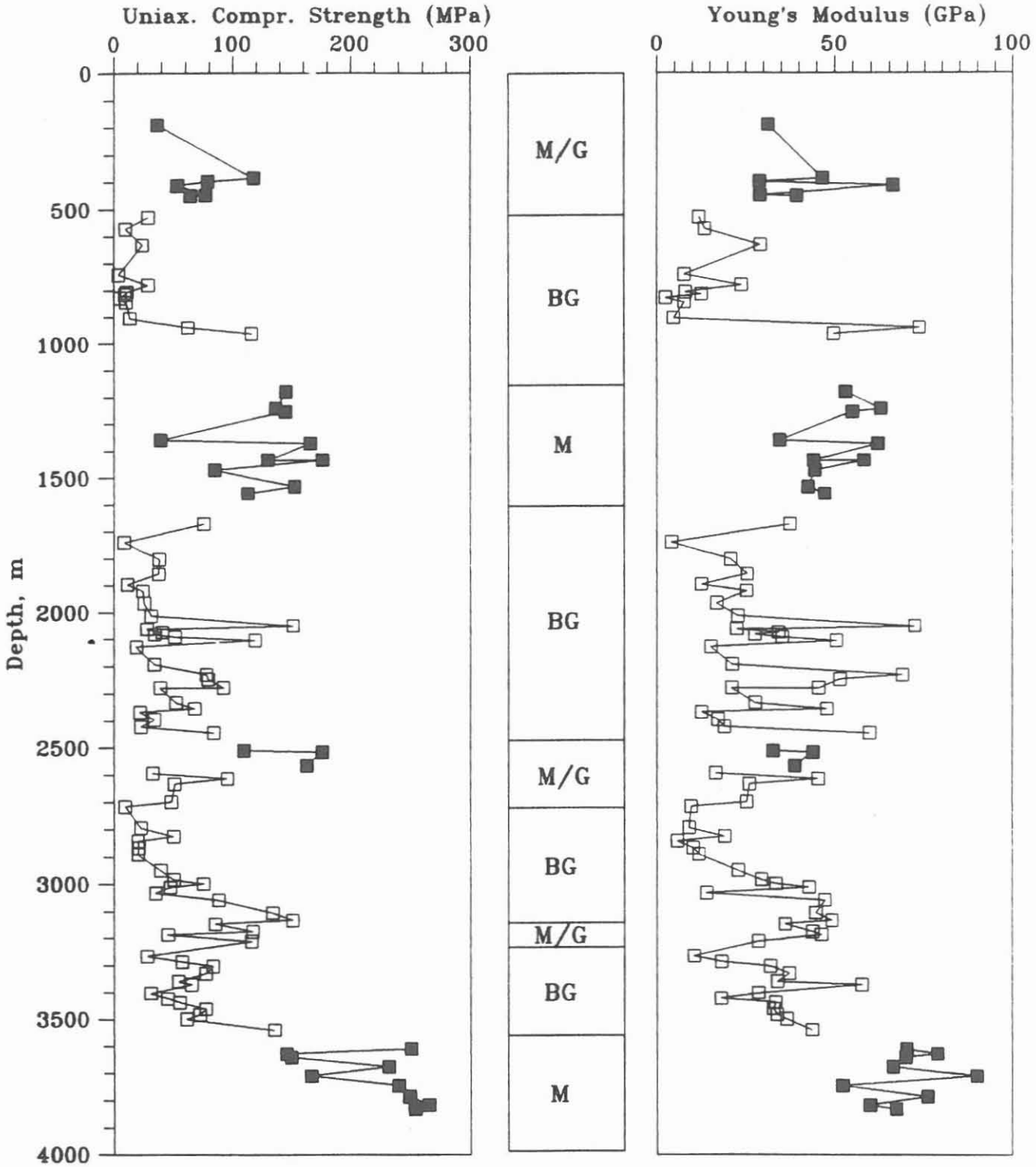

Fig. H.3a: Dependence of uniaxial compressive strength on depth.

Fig. H.3b: Dependence of the Youngs's modulus on depth.

(open squares: biotite-gneisses (BG), black squares: metabasites and hornblende-gneisses(M)).

In contrast to the massive metabasites, the foliated biotite-gneisses show lower mean values for the uniaxial compressive strength (50.5 MPa) and the Young's moduli (27.3 GPa). Fig. H.3a and H.3b show the uniaxial compressive strengths and the Young's moduli with relation to the depth. The measured uniaxial compressive strength of the biotite-gneisses varies over a wide range. For uniaxial compressive strength in foliated rocks, the dip angle of the foliation is the most important factor. The highest value measured (151.1 MPa) is found in a sample from about 3133 m where, the foliation is horizontal. The Young's modulus (49.2 MPa) of this sample is one of the highest in biotite-gneisses. Fig. H.4a shows the stress-strain diagram of this sample with a linear elastic behaviour over a wide range. Only at loads lower than 50 MPa, the material is not linear-elastic due to closing of micro-cracks and deformation of mica.

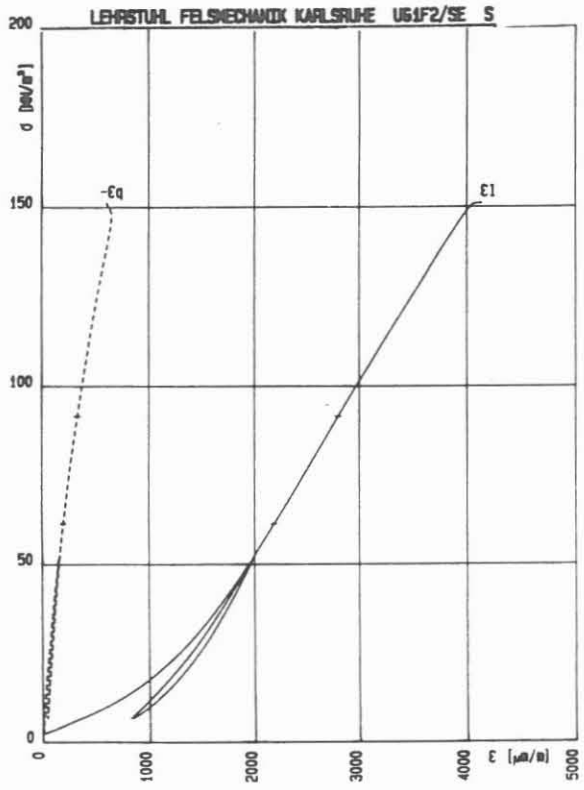

Fig. H.4a: Stress-strain diagram of a biotite-gneiss sample with horizontal foliation from about 3133 m.

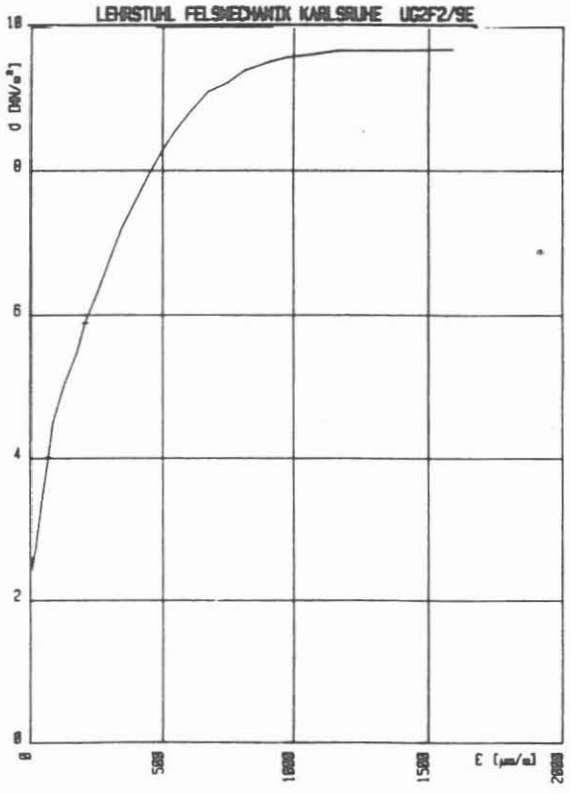

Fig. H.4b: Stress-strain diagram of biotite-gneiss sample from about 573 m (Dip angle 60°-70°).

A biotite-gneiss sample from about 573 m depth with 60° - 70° dipping foliation shows a completely different stress-strain behaviour (Fig. H.4b). With increasing load, the micro-cracks begin to open immediately and shear failure occurs at an uniaxial compressive strength of only 9.7 MPa.

The dependence of uniaxial compressive strength of biotite-gneisses on the dip angle of the foliation in the depth interval from 2000 to 3500 m is shown in Fig H.5. The samples with low dip angles of foliation have the highest strength. At dip angles of about 60°, the uniaxial compressive strength reaches a minimum, and at steeper dipping, the uniaxial compressive strength increases again.

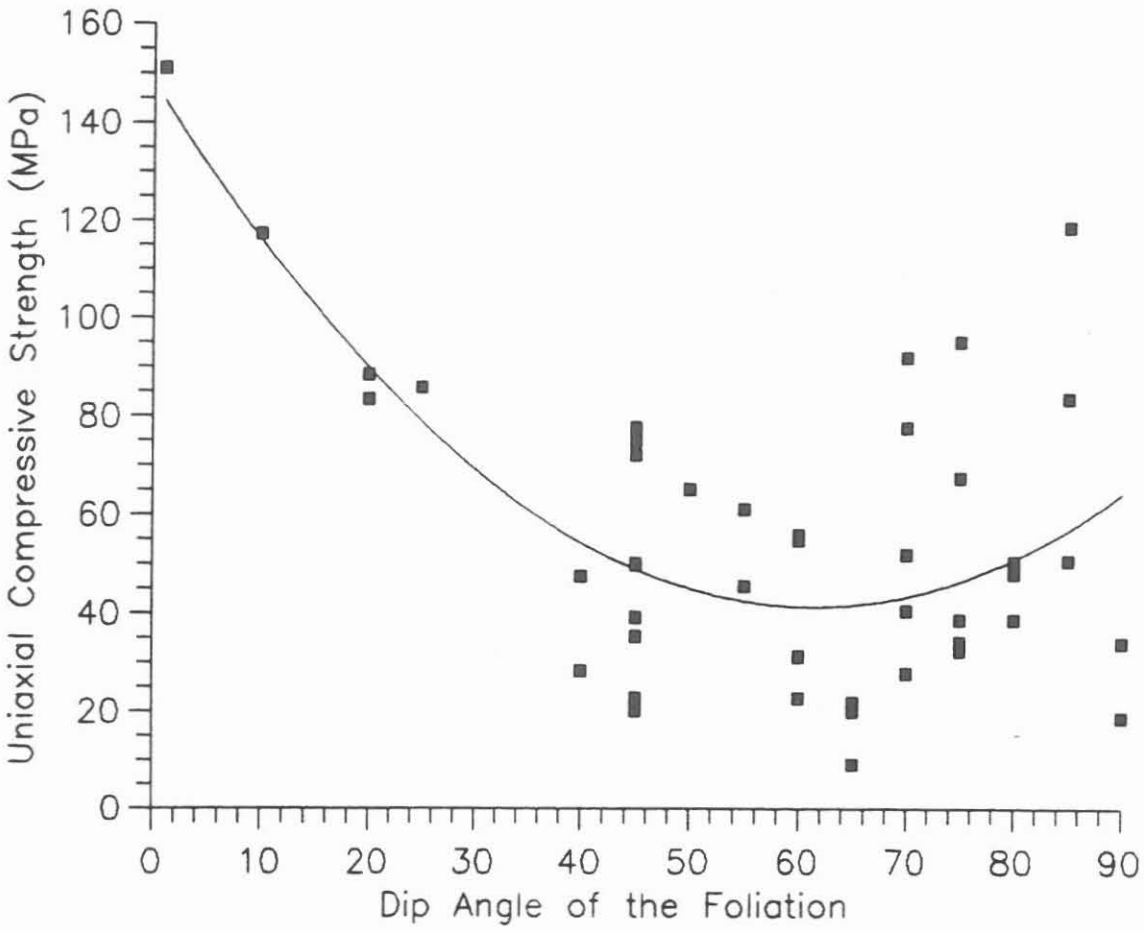

Fig. H. 5: Dependence of the uniaxial compressive strength of the biotite-gneisses on the dip angle of the foliation (depth between 2000 m and 3500 m).

For the uniaxial compression tests, rock samples without macroscopically visible cracks were used. In cataclastic shear zones - especially with graphite joints - no samples without macroscopically visible cracks could be prepared. Therefore, no uniaxial compressive strength data from these zones are available.

In the depth range between 2156 m to 2187 m, for example, the strong cataclastic deformation leads to significant borehole breakouts (RÖHR et al. 1989). The rock strength in these zones is lower than the smallest value measured in the biotite-gneisses.

H. 2.2 Indirect Tensile Tests (Brazilian Tests)

The tensile strength was measured using the Brazilian-test on 94 mm diameter cores (Fig. H.6). The results of the indirect tensile tests clearly show the contrast in the mechanical behaviour of the foliated biotite-gneisses and the massive, non-textured metabasites. The metabasites have relatively high tensile strength, and the anisotropy is low. The tensile strength of the biotite-gneisses is of stronger anisotopic character due to the foliation.

In the biotite-gneisses the indirect tensile strength was measured parallel and perpendicular to the strike of the foliation. In the massive metabasites, the indirect tensile strength was measured in two directions perpendicular to each other. The mean values for the biotite-gneisses parallel and perpendicular to the strike of the foliation for the different lithological sections are shown in table H.1. as well as the minimum and maximum mean values of the massive metabasites.

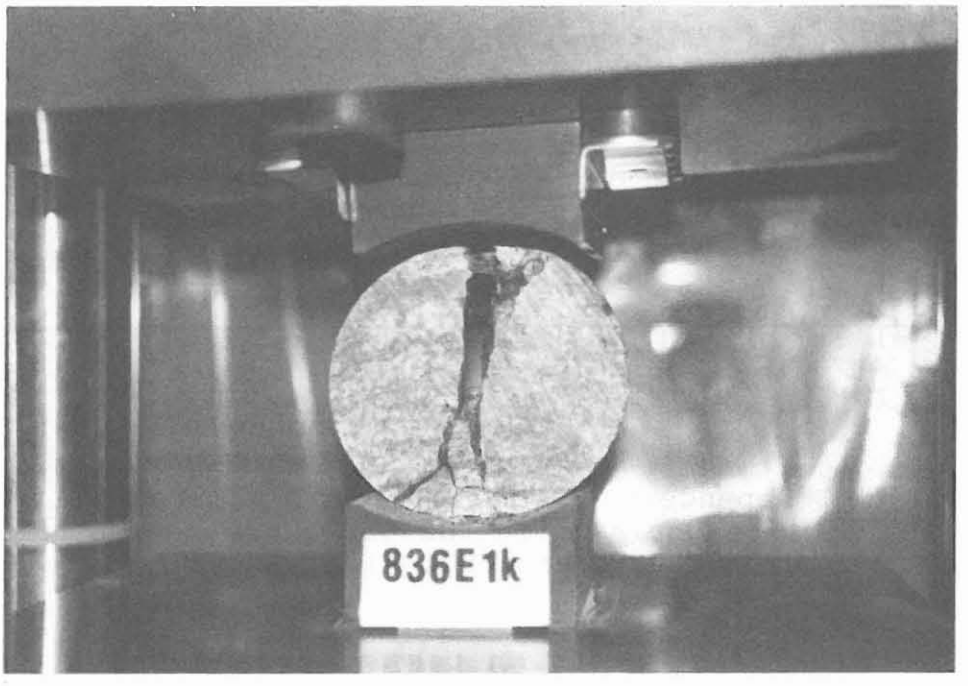

Fig. H.6: Brazilian-test to determine the tensile strength parallel to the strike of the foliation in a biotite-gneiss sample from 3421 m.

The minimum and the maximum tensile strengths in the metabasites are 3.9 MPa and 15.3 MPa, respectively. The mean tensile strength from all metabasites is 10.0 MPa.

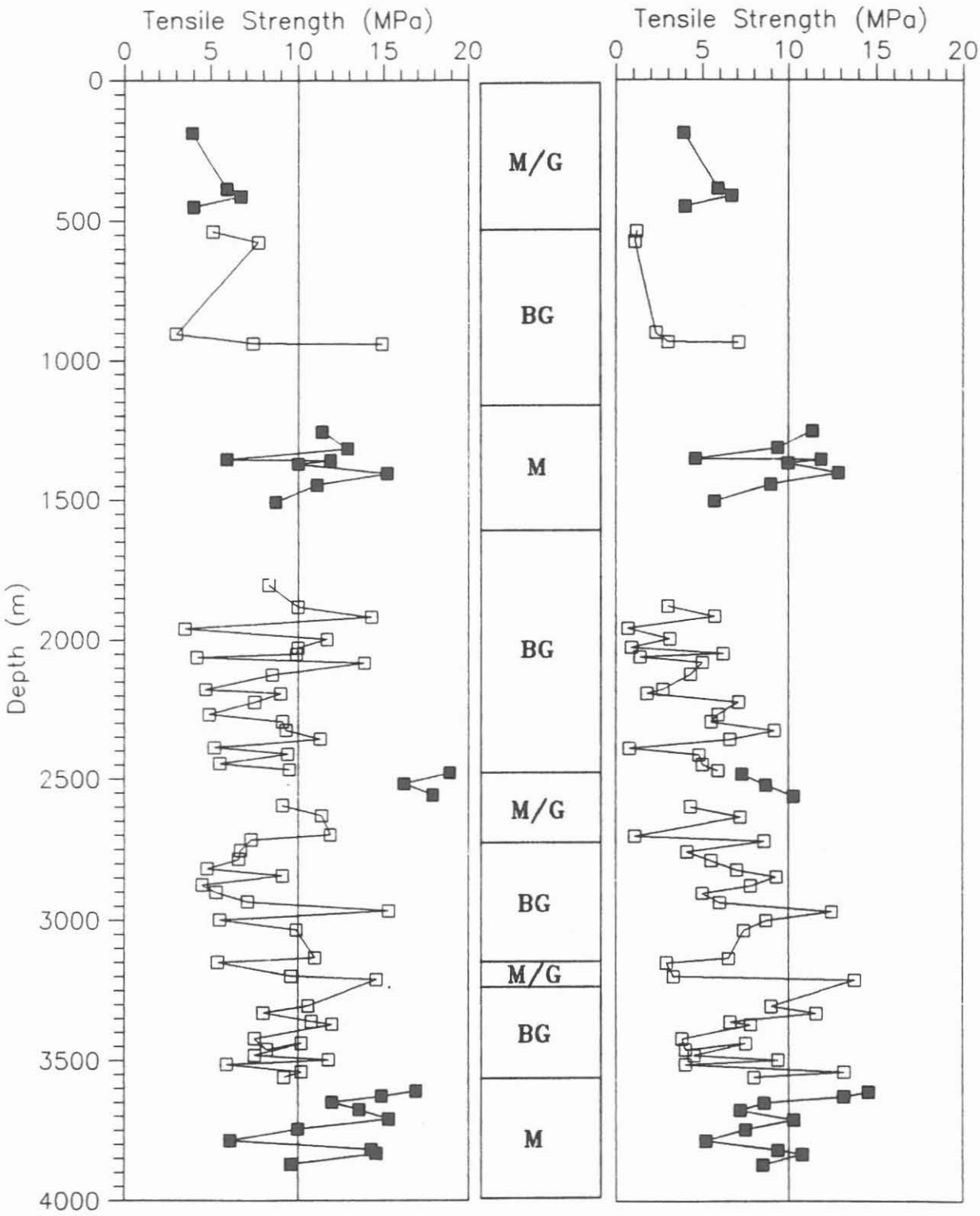

Fig. H.7a: Tensile strength of the biotite-gneisses parallel to the foliation (open squares, BG) and the maximum values of the metabasites (black squares, M).

Fig. H.7b: Tensile strength of the biotite-gneisses perpendicular to the strike of the foliation and minimum values of the metabasites

In the depth range between 188 m and 452 m, the metabasites have a mean tensile strength of 6.8 MPa, and the ratio between mean maximum value (7.3 MPa) and mean minimum value (6.3 MPa) is 1.2. In the depth range from 1256 m to 1508 m, the metabasites have a mean tensile strength of 10.2 MPa, and the ratio between mean maximum value (10.9 MPa) and mean minimum value (9.4 MPa) is also 1.2. The deepest metabasite-series below 3.575 m show the highest mean tensile strength with an average of 11.2 MPa. The ratio between mean maximum values (12.9 MPa) and mean minimum values (9.5 MPa) is 1.4 (Tab. H.1). The stronger variation of the mean values below 3575 m may be caused by a preferential orientation of micro-cracks. Fig. H.7a and H.7b show the dependence of the tensile strength of the biotite-gneisses and metabasites on depth.

The weakly foliated hornblende-gneisses between 2478 m and 2556 m show the highest mean values (17.7 MPa) parallel to the strike of the foliation. Perpendicular to the foliation, the mean value is still high (8.8 MPa).

Table H.1: Mean values of the rock mechanical index-parameters.

Lithology	Depth Range	UCS	E	gn-par & max. $\sigma_{(t)}$	gn-per & min. $\sigma_{(t)}$
metabasites	189 - 452	71.2	40.4	7.3	6.3
metabasites	1178 - 1558	128.7	50.3	10.9	9.4
metabasites	3575 - 3832	217.2	70.0	12.9	9.5
metabasites	189 - 3832	140.5	53.8	11.1	8.9
hbl.-gneisses	2478 - 2613	121.2	40.4	17.7	8.8
biot.-gneisses	530 - 963	26.9	20.4	7.6	2.9
biot.-gneisses	1671 - 2467	42.8	27.1	8.5	4.2
biot.-gneisses	2632 - 3559	63.8	29.8	8.9	6.8
biot.-gneisses	530 - 3559	50.5	27.3	8.7	5.6

Legend:
UCS = uniaxial compressive strength (MPa), E = Young's modulus (GPa), gn-par = gneisses parallel to the strike of foliation, gn-per = gneisses perpendicular to the strike of foliation, max. = maximum mean values of the metabasites, min. = minimum mean values of the metabasites, $\sigma_{(t)}$ = tensile strength (MPa).

In contrast to the metabasites, the biotite-gneisses show a stronger anisotropic behaviour of the tensile strength. Parallel to the strike of the foliation, the biotite-gneisses show high average tensile strength (8.7 MPa), whereas perpendicular to the strike of the foliation they show lower average tensile strengths (5.6 MPa). The ratio of the indirect tensile strengths parallel and perpendicular to the strike of the foliation is 1.6.

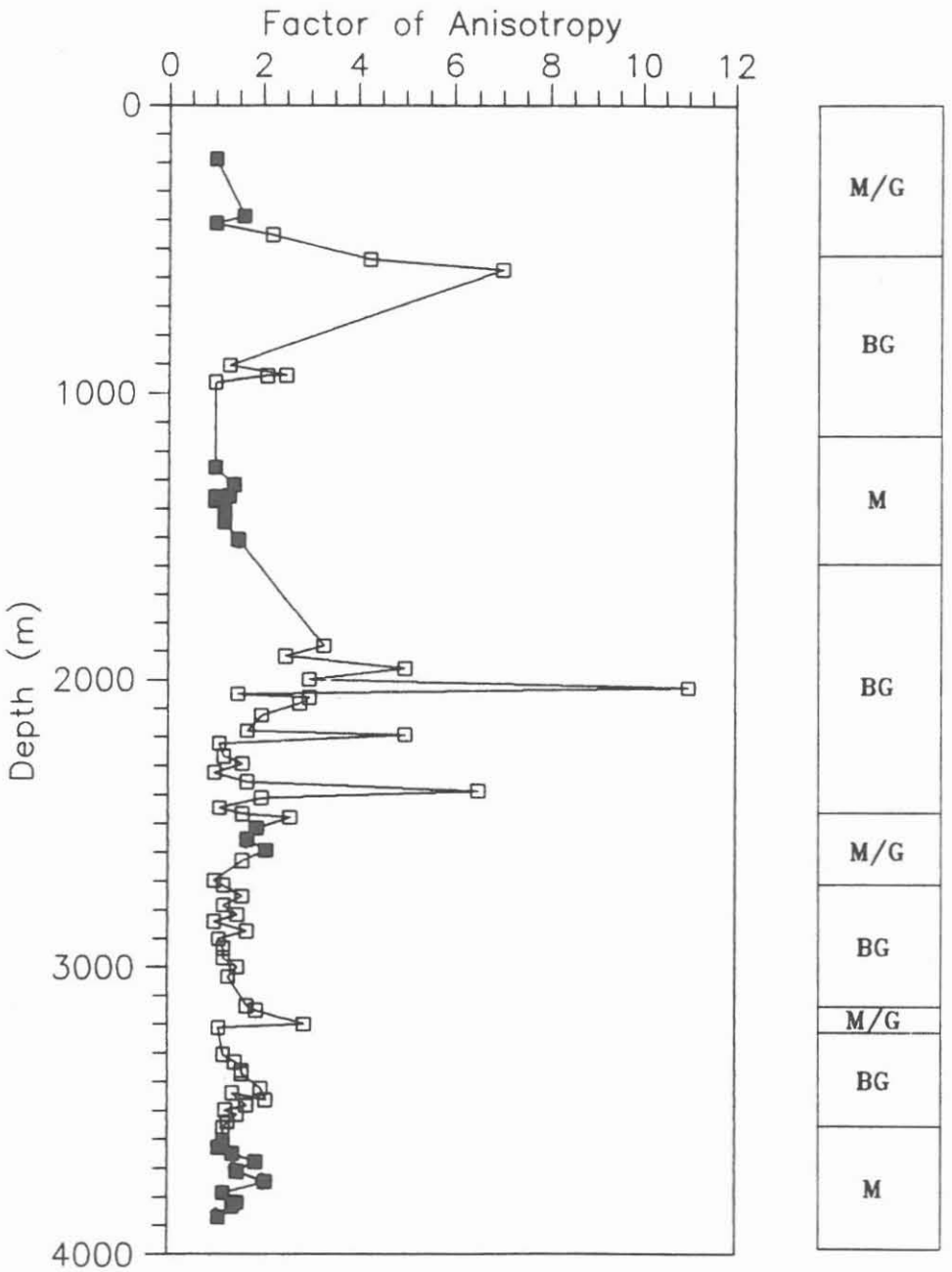

Fig. H.8: Dependence of tensile strength anisotropy ratio on depth. (open squares = biotite-gneisses, black squares = metabasites and hornblende-gneisses).

The biotite-gneiss samples from between 1671 m and 2467 m depth show a strong anisotropic behaviour (Fig H.8). In this depth range, the foliation dips very steeply. The mean value of the tensile strength of the biotite-gneisses parallel to the strike of the foliation is 8.5 MPa, whereas perpendicular to the strike of the foliation it is only 4.2 MPa. The anisotropy ratio is 2.0. The tensile strength anisotropy in some samples, especially at very steeply dipping foliation, is still much higher. A biotite-gneiss sample from 2028 m, for example, has a tensile strength of 10.0 MPa parallel to the strike of the foliation and only 0.9 MPa perpendicular to it. The anisotropy ratio is very high (11.1). Between 1671 m and 2467 m depth the mean tensile strength parallel to the foliation (8.5 MPa) is similar to that of the biotite-gneisses from between 2593 m und 3558 m (8.9 MPa). Only the biotite-gneisses from between 537 m und 940 m show lower tensile strength values (7.6 MPa) parallel to the strike of the foliation.

The tensile strength of the biotite-gneisses perpendicular to the strike of foliation varies over a wide range and is strongly dependent on the dip angle of the foliation. Between 1671 m and 2467 m, where the gneisses dip very steeply, the mean tensile strength is only 4.2 MPa.

Some samples show tensile strengths below 1.0 MPa. The values vary from 0.7 MPa at 1960 m to 9.2 MPa at 2324 m. In the depth range from 2593 m to 3558 m, where the biotite-gneisses have lower dip angles, the mean tensile strength value is 6.7 MPa. The lowest average tensile strength value (2.9 MPa) is observed in the biotite-gneisses perpendicular to the strike of the foliation at the depth range between 537 m and 940 m. The lower tensile strength in this depth range may be caused by a stronger cataclastic deformation and a higher degree of alteration.

H. 3.0 Conclusions

The measured uniaxial compressive strengths and tensile strengths show variations over a wide range. In general, the massive metabasites have higher uniaxial compressive strengths and tensile strengths. The biotite-gneiss samples with dip angles of about 60° show low uniaxial compressive strength whereas at steeper dip angles and especially at low dip angles the uniaxial compressive strength increases. The compressive strength in cataclastic shear zones, e. g. between 2156 m and 2187 m, is lower than the lowest value measured in biotite-gneisses. The tensile strength of biotite-gneisses parallel to the strike of the foliation is significantly higher than the tensile strength perpendicular to the foliation.

H. 4.0 References

RÖCKEL, Th., und O. NATAU., (1989): Tiefbohrung KTB Oberpfalz VB-Erste Ergebnisse felsmechanischer Indexversuche bis 1998 m. In: EMMERMANN R. & GIESE P. (Hrsg.), KTB-Report 89-2, H1-H22, Hannover.

RÖCKEL, Th., und O. NATAU., (1989): Tiefbohrung KTB Oberpfalz VB-Erste Ergebnisse der felsmechanischen Indexversuche im Teufenbereich von 2000 m - 3000 m. In: EMMERMANN, DIETRICH, HEINISCH und WÖHRL (Hrsg.), KTB-Report 89-5, H1-H13, Hannover.

RÖHR, C., HACKER, W., KEYSSNER, S., KOHL, J. & MÜLLER, H. (1989): Tiefbohrung KTB-Oberpfalz VB, Ergebnisse der geowissenschaftlichen Bohrungsbearbeitung im KTB-Feldlabor, Teufenbereich von 1709 bis 2500 m: Geologie; In: EMMERMANN R. & Giese P. (Hrsg.), KTB Report 89-2, B1-B114.

KTB-Report	90-8	I1-I6	1 Abb.	Hannover 1990

KTB Pilot Hole: Permeability Profile

HUENGES[1], E., J. WIENAND[1] & G. NOVER[2]

Content:

Adresses of the authors:

[1]KTB-Feldlabor, Postfach 67, 8486 Windischeschenbach
[2]Mineralogisches Institut, Poppelsdorfer Schloß, 53 Bonn

I.1 Introduction

In order to understand fluid movements in crystalline rocks it is essential to quantify the geometry of the fluid pathways. As a rough estimation one can distinguish between the microscopic and macroscopic permeability. The microscopic permeability is associated with microcracks and grain boundary permeability in the scale of a few millimeter or less and the macroscopic permeability is due to larger cracks. Because of experimental limitations of laboratory measurements on cores in the scale of a few centimeters, only microscopic permeability could be determined in laboratory.

I.2 Methods

The permeability of 50 cores (30 mm in diameter, 15 mm height) was measured as a function of a quasi hydrostatic pressure up to 80 MPa, using a gas pressure transient method. During the measurements the pore pressure was increased up to a maximum value of 5 MPa. For further details see HUENGES (1987). The transient curves were evaluated using a formula of ZOBACK & BYERLEE (1975).

In addition to these instationary measurements, 30 further experiments were performed on core samples (30 mm in diameter, 50 mm height) using the stationary d'Arcy method. These measurements were made at a constant confining pressure of 5 MPa. Because of the low pore pressure during the measurements the data had to be corrected for the effect of gas slipping along the matrix wall, the so called Klinkenberg effect. Further details regarding equipment and evaluation are given by PUSCH et al. (1986) .

I.3 Results

The results were published by WOLTER et al. (1989), WIENAND et al. (1989), and RAUEN et al. (1990). A significant dependence of permeability on pressure and on the direction of the flow in the foliated rocks could be observed. Thus it was possible to establish the factor of anisotropy ranging from 1 to 500 for permeability parallel and perpendicular to the foliation. Due to the fact that most of the measurements were performed in different orientations to the foliation and at various pressures an additional processing was necessary. So it can be established a common basis, the quasi in situ permeability, using all informations on pressure and orientation dependence of the permeability.

I.4. Quasi-in-situ permeability with respect to directions

Equation (1) describes the transformation of the permeability k_α to main axis permeabilities assuming a rotation

ellipsoid. The direction is given by the angle α to the rotation axis with permeabilities k_p parallel and k_s perpendicular to the foliation plane. In a first step the data measured at the pressure closest to the in situ pressure were transformed to permeabilities k_p und k_s using equation (1) with minimum and maximum values due to the scatter of anisotropy factor from 1 and 500.

$$k_\alpha^2 = k_p^2 * \sin^2(\alpha) + k_s^2 * \cos^2(\alpha) \qquad (1)$$

The pressure correction is based on the empirical equation (2) (DEBSCHÜTZ et al. 1989), which describes the exponential decrease of the permeability $k(p_1)$ to $k(p_2)$ caused by the pressure increase from p_1 to p_2.

$$k(p_2) = k(p_1) * \exp(-(p_2 - p_1) / p_c) \qquad (2)$$

The parameter p_c was taken from the fit of equation (2) to about 50 pressure dependent data sets. P_c scatters from 10 to 35 MPa and is in a first approximation independent on lithology and direction of flow. Therefore this scatter was used for the maximal estimation of the permeability ellipsoid. Increased pore pressure was not taken into consideration.

The calculated quasi in situ main axis permeability is plotted in Fig. I.1. Some data have a small scatter because of isotropic core material, e.g. a lamprophyre in 2050 m, or because of complete measurements in two orientations to the foliation, e.g. a biotite gneiss of 3535 m. Most data have large error bars due to a lack of detailed information about the anisotropy and the pressure dependence of the permeability.

Because of the steep dip of foliation there is a higher permeability vertical than the mean value horizontal. This was shown by the transformation of the data to borehole coordinates using equation (1) and the dip angle of foliation.

In order to quantify additional "Klinkenberg-" and porosity-corrections for the instationary measurements, which were performed at about 3 MPa pore pressure, must be done. This leads to a decrease of the permeabilities within one half order of magnitude (SIEBERT & PUSCH pers. communications). Moreover the permeability of a (not gas) fluid is lower than the gas permeability (SCHOPPER pers. communication). The work on all these corrections is in progress. Therefore the upper limitation of permeability is used for first considerations.

The maximum estimation allows to conclude that the measured permeability in all directions is most lower than 1 µd. Assuming a reasonable pressure gradient for the environmental conditions one can expect that fluid movement on the scale of micro permeability is neglectible.

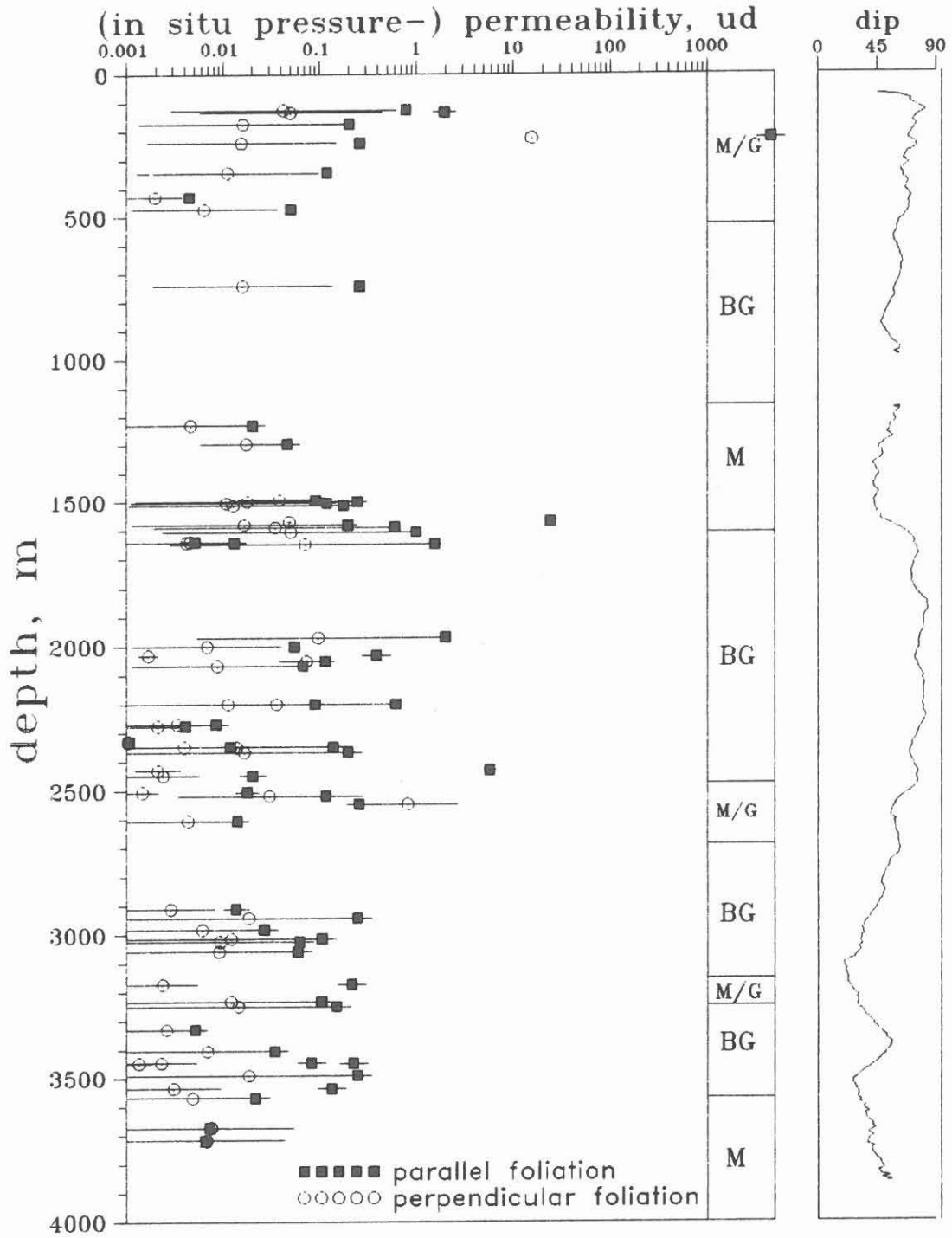

Fig. I.1 (Main axis-) Permeability of KTB core samples determined with the pressure transient method (core diameter ⌀ = 30 mm, height h = 15 mm; all data above 2800 m) and the d'Arcy method (⌀ = 30 mm, h = 50 mm below 2800 m). The scatter is calculated from a maximum estimation including all available pressure and orientation dependent measurements on KTB core samples. The values are corrected to in situ pressure and valid for gases. Simplified lithological profile (M = Metabasite, BG Biotite Gneiss) and dip angle of foliation in degrees.

I.4. References

DEBSCHÜTZ, W. U. KRÜCKEL & J.R. SCHOPPER (1989): Der Einfluß des Überlagerungs- und Porendrucks auf die Permeabilität, den Klingenbergfaktor und andere Strömungsparameter.- Rock at Great Depth, Maury & Fourmaintraux (eds.), 179-185, Balkema Rotterdam.

HUENGES, E. (1987): Messung der Permeabilität von niedrigpermeablen Gesteinsproben unter Drücken bis 4 kbar und ihre Beziehung zu Kompressibilität, Porosität und komplexem elektrischen Widerstand.- PhD thesis University Bonn (West Germany).

PUSCH, G., P. Schweizer & O. Gaminger (1986): Stationäre und instationäre Gaspermeabilitätsmessung an niedrigpermeablen Gesteinen. Erdöl Ergas Kohle, **102.** Jahrgang, Heft 5, 235-239.

RAUEN, A., E. HUENGES, Ch. BÜCKER, M. STREIT, K.E. WOLTER & J. WIENAND (1990): Tiefbohrung KTB-Oberpfalz VB, Ergebnisse der geowissenschaftlichen Bohrungsbearbeitung im KTB-Feldlabor (Windischeschenbach), Teufenbereich 3500 - 4000 m: D. Geophysik.- In: Emmermann, Dietrich, & Wöhrl (Hrsg.), KTB-Report 90-2, D1-D50, Hannover.

WIENAND, J., A. RAUEN, E. HUENGES, Ch. BÜCKER & K.E. WOLTER (1989): Tiefbohrung KTB-Oberpfalz VB, Ergebnisse der geowissenschaftlichen Bohrungsbearbeitung im KTB-Feldlabor (Windischeschenbach), Teufenbereich 3000 - 3500 m: D. Geophysik.- In: Emmermann, Dietrich, Heinisch & Wöhrl (Hrsg.), KTB-Report 89-5, D1-D50, Hannover.

WOLTER, K.E., J. WIENAND, A. RAUEN, E. LIPPMANN, E. HUENGES & Ch. BÜCKER (1989): Tiefbohrung KTB-Oberpfalz VB, Ergebnisse der geowissenschaftlichen Bohrungsbearbeitung im KTB-Feldlabor (Windischeschenbach), Teufenbereich 2500 - 3009 m: D. Geophysik.- In: Emmermann, Dietrich, Heinisch & Wöhrl (Hrsg.), KTB-Report 89-4, D1-D39, Hannover.

ZOBACK, M.D. & J.D. BYERLEE (1975): The Effect of Microcrack Dilatancy on the Permeability of Westerly Granite.- J. Geophys. Res., 80 (5), 752-755.

KTB-Report	90-8	J1 - J19	17 Fig.	Hannover 1990

OBSERVATIONS ON THE DUCTILE DEFORMATION PATH OF THE PARAGNEISSES OF THE KTB PILOT HOLE

Weber, K. *)

Contents:

* Institut für Geologie und Dynamik der Lithosphäre (IGDL)
Universität Göttingen
Goldschmidtstr. 3
3400 Göttingen
Federal Republic of Germany

OBSERVATIONS ON THE DUCTILE DEFORMATION PATH OF THE PARAGNEISSES OF THE KTB PILOT HOLE

K. Weber (Göttingen)

Zusammenfassung: Korn- und Reaktionsgefüge der Paragneise der KTB-Vorbohrung lassen auf einen retrograden Deformationspfad im Deckenkomplex der Zone von Erbendorf-Vohenstrauß (ZEV) schließen, der sich in 3 ductile Deformationsstadien gliedern läßt. Die ältesten Gefüge (Stage 1) sind HT-Mylonite, die durch sekundäre Quarzrekristallisation und feinkörnige (primäre) Feldspatrekristallisation unter trockenen, amphibolitfaziellen Metamorphosebedingungen entstanden. Es folgt ein metablastisches Deformationsstadium (Stage 2), das durch Kornvergröberung im Quarz-Feldspatgefüge und durch syntektonische Neubildung von Muscovit I und Biotit II sowie lokale Migmatisierung gekennzeichnet ist. Im anschließenden diaphthoritischen Stadium (Stage 3) zeigt Quarz primäre Rekristallisation, während Feldspat kataklastische verformt wird. Diaphthoritische Mineralneubildungen sind Muscovit II, der schwach bis ungeregelt ist und häufig Fibrolith einschließt, sowie Serizit, Chlorit, Ilmenit und Quarz.
Die Interpretation dieses Pfades erfolgt auf der Basis eines Deckenkonzepts. Danach können die Edukte der Paragneise als unterdevonische Flyschsedimente einem variszischen aktiven Kontinentalrand des Bohemikums zugeordnet werden. Im Verlauf der Subduktion und der mit ihr verbundenen druckbetonten Metamorphose wurden sie mit mafischen Gesteinen verschuppt. Als intrakrustaler Deckenkomplex wurde dieser Gesteinsverband weitgehend isothermal unter HT-mylonitischer Verformung in höhere Krustenstockwerke transportiert. Zunehmende Infiltration wässeriger Fluide führte zu metablastischer bis migmatischer Überprägung. Die Inkorperation und Obduktion von Inselbogengesteinen (Erbendorfer Grünschiefer) und von Sedimenten eines passiven Kontinentalrandes (Wetzldorf-Folge) führte im Verlaufe des Kollisionstadiums und des suprakrustalen Deckentransportes zur Infiltration großer Mengen hoch gespannter Fliude und zu kräftiger Diaphthorese, verbunden mit hydraulischer Bruchbildung. Alle duktilen Gefüge entstanden vor und während dieses SW-polaren Deckentransportes.

Abstract: Grain and reaction fabrics in the paragneisses of the nappe complex of the Zone of Erbendorf-Vohenstrauß (ZEV), exposed in the KTB pilot hole, document a ductile, retrograde metamorphic deformation path, which can be subdivided into three stages. Fabrics representing the early stage are HT-mylonitic (stage 1), and are characterized by primary recrystallization of feldspar and secondary recrystallization of quartz. The fabrics formed in dry amphibolite facies metamorphic conditions. Stage 1 is followed by the metablastic deformation stage (stage 2) which is characterized by grain growth of quartz and feldspar and the syntectonic formation of muscovite I und biotite II. During the diaphthoritic stage (stage 3) quartz shows primary recrystallization whereas feldspar is cataclastically deformed. Common diaphthoritic minerals are muscovite II, sericite, chlorite, ilmenite and quartz. Muscovite II has a weak preferred or random orientation and frequently contains inclusions of fibrolite.
These deformation stages are interpreted on the basis of the nappe concept of the ZEV. The protoliths of the paragneisses can be interpreted as Lower Devonian flysch sediments, deposited at an early Variscan active continental margin of the Bohemian terrane. In the course of subduction and HP-metamorphism they were tectonically intercalated with mafic rocks. Subsequently, they were displaced more or less isothermally as an intracrustal nappe complex into higher crustal levels. In the course of this deformation HT-mylonitization took place under dry amphibolite facies conditions, followed by metablastic grain growth and local migmatization due to infiltration of hydrous fluids. The incorporation and obduction of island arc rocks (Erbendorf greenschists) and sediments of a passive continental margin (Wetzldorf Formation) indicate the collisional stage and supracrustal nappe displacement. The emplacement of the crystalline rocks onto oceanic sediments abounding in water led to immigration of large amounts of overpressured hydrous fluids and to strong diaphthoritic mineral reactions, accompanied by hydraulic fracturing. All ductile fabrics were formed before and during the SW-directed nappe transport.

1. Introduction

The Variscan basement around the Continental Deep Drilling Site (KTB) Oberpfalz on the western margin of the Bohemian Massif is composed of three polyphasely deformed tectonometamorphic units (Fig. 17): the Saxothuringian, the Moldanubian and the Bohemian unit. The Saxothuringian of the Fichtelgebirge represents a former passive continental margin. The boundary of the Saxothuringian and Moldanubian is interpreted as a cryptic suture and is represented by the northwestern rim of the HT-mylonitic belt of the Zone of Tirschenreuth-Mähring (ZTM). This zone forms part of a formerly active continental margin. Dextral shearing played an important role in the ZTM during the advanced stage of collision, i.e. during the indentation stage (Weber & Vollbrecht, 1989). The klippen of the ZEV and the Münchberg Massif (MM) form part of a previously coherent nappe complex which was connected with the Zone of Tepla-Taus (ZTT) at the western margin of the Bohemian terrane.
The following investigations of rocks from the KTB pilot hole aims at a preliminarycharacterization of the microscopic deformation and reaction fabric of the paragneisses of the ZEV. The investigations deal with rocks from as deep as 4000 m. The data are interpreted on the basis of the nappe concept, developed for the Zone of Erbendorf-Vohenstrauß (ZEV) in the course of the presite studies (KTB, 1986) and succeeding investigations (Weber and Vollbrecht, 1989). Several stages of the deformation path can be distinguished in the paragneisses. The younger stages, which represent retrograde metamorphic stages of the strain path, are much better preserved than older prograde metamorphic stages. Their reconstruction will be subjected to further investigation, particularly of mafic rock, where the early stages in the deformation path seem to be better preserved.

2. Stages of the deformation path

2.1 Stage 0: Prograde metamorphic deformation

This stage refers to all possible earlier deformation stages which preceded the HT-mylonitic stage and which possibly form part of the prograde metamorphic deformation path.

2.2 Stage 1: HT-mylonitic deformation

The HT-mylonitization stage is characterized by dynamic primary recrystallization of Fsp. The minimum temperature of Fsp recrystallization is 500°C (White, 1978; Voll, 1980). The acid Plg of the paragneisses form a fine-grained, equigranular fabric with well equilibrated grain boundaries (Fig.1). Partly recrystallized Plg-clasts can be preserved (Fig.2). Together with coarsely grained ribbon quartz (see below) they evidence a coarsely grained metamorphic protolith of the HT-mylonites. No Kfsp-clasts have been observed. Plg-Qz symplectites (myrmekite) are found around clasts of chessboard albite that could have developed from Kfsp.

Bio I is fine-grained, homogeneous in grain size, and shows a strong preferred orientation which tends to be oblique to the metamorphic foliation or compositional layering, as observed in sections parallel to the mineral lineation. Bio I has grown syntectonically only outside Qz grains and recrystallized Fsp grains, preferably in stretching shadows (Fig.3). The sense of shear derived from this oblique orientation fabric is identical with that of delta- and sigma-clasts. The syncrystalline strain seems to be high, but cannot be determined quantitatively. However, pervasive microboudinage in the recrystallized Fsp-Bio I matrix indicates high strain in sections parallel to the mineral lineation (Fig.4). Indications of high strain are also given by strongly stretched corona structures of Ga+Qz surrounding Hbl-Qz symplectites after Cpx in a completely recrystallized anorthositic gneiss. The corona structures reveal a pronounced prolate strain with X:Y:Z approx. 50:3:1.
Qz grains are mostly larger than Fsp. Unlike Fsp, Qz shows highly unequilibrated grain boundaries and no primary recrystallization (Fig.5). The coarse grain size and the highly lobate grain boundaries of Qz can be interpreted as resulting from secondary dynamic recrystallization. Due to high dislocation mobility at temperatures above 500°C (the minimum temperature of Fsp recrystalliza-

tion), migration recrystallization dominates recrystallization by subgrain rotation. Mortar textures due to primary recrystallization develop at lower temperatures in the course of the diaphthoritic strain path (see below).

The HT-mylonitic part of the deformation path is characterized by the formation of ribbon quartz (Fig.6). These document high strain and show the abovementioned characteristics of secondary dynamic recrystallization and indications of low viscosity, enabling them to protrude (intrusion in the solid state) along grain boundaries of the recrystallized Fsp fabric (Fig.2 and 7). In several cases single quartz grains may coalesce into larger grains of ribbon quartz in the course of the strain-induced protrusion process.

During the HT-mylonitic stage small-scale internal folds developed contemporaneously with the s_1-foliation. These F_1-folds can occur as sheath folds (Weber, 1988). Their pronounced asymmetry refers to a SW-directed sense of shear in accordance with the abovementioned rotational and oblique orientation fabrics. In sections perpendicular to the stretching lineation rotational fabrics have formed with changing vorticity around the stretching lineation.

HT-mylonitic fabrics of the paragneisses are preserved predominantly in those high-grade gneisses that were primarily free of Ksp. Gneisses bearing Ksp possibly were transformed into Ms bearing gneisses and micaschists during the metablastic deformation stage.

2.3 Stage 2: Metablastic deformation

Metablastic grain coarsening, particularly in the Fsp fabric (Fig.8), took place with the occurrence of Ms I and Bio II under amphibolite facies metamorphic conditions (675°±50°C, 7±1 kbar, Reinhardt and Kleemann, 1989). Locally, concordant and discordant migmatic mobilisates are present. Ms I has grown syntectonically parallel to the s_1-foliation (Fig.9). It is (unlike Ms II) free of Sil (Fibrolite)-inclusions. The amount of Ms I varies. Bio II is intergrown with Sill (Fibrolite). It formed during the metablastic deformation stage from:

$$\text{Ga} + \text{Kfsp (or } K^+\text{-bearing hydrous fluids)} \dashrightarrow \text{Bio II} + \text{Sill} + \text{Qz}$$

In contrast to Bio I, the Bio II-fibrolite-aggregates are more coarsely grained (Fig. 10) and do not occur in pressure shadows around recrystallized Fsp grains. In addition, fibrolith has been formed from prismatic Sil.

Metablastic Plg (Oligoclase) does not show recrystallization. Quartz and ribbon quartz have instable (lobate) grain and phase boundaries and show, like the entire Qz-Fsp fabric, increasing grain size. Inside larger Qz grains there is an internal development of lobate grain boundaries and lobate to plane subgrain boundaries (Fig.8) There is still no primary recrystallization. The degree of oblique preferred orientation of Bio I decreases with increasing metablastic grain growth. At the same time metamorphic differentiation continues, in the course of which the s_1-foliation is intensified by enrichment of Ms I and Bio II.

During the metablastic deformation stage no new penetrative foliation developed in those F_2-folds that refold the metablastic and migmatic fabrics. Together with the lack of Fsp-recrystallization, this can be regarded as an indication of low effective stress due to high P_{H2O} during F_2-folding (see chapter "Interpretation"). In the observed cases the F_2-fold axes are parallel to the F_1-axes, evidencing largely homoaxial folding. Surface exposures in the ZEV support this assumption.

2.4 Stage 3: Diaphthoritic deformation

With decreasing temperature more and more mineral phases sink below their metamorphic conditions of stability. Retrograde retrograd metamorphic mineral reactions therefore becoming increasingly dominant and affecting the rock fabric.

In the Qz-Fsp fabric the beginning of stage 3 is indicated by primary recrystallization of Qz (Fig. 11 and 12) and cataclastic deformation of Fsp (Fig.13). The recrystallized Qz grains are undulous (Fig.12) and there are all transitions to subgrain fabrics and continuous undulosity, particularly inside larger Qz grains. Strongly strained layers of diaphthoritic gneisses show some characteristics of LT-mylonites.

During stage 3 a new Qz generation appears, represented by millimeter to centimeter thick veins parallel to the s_1-foliation (Fig.14) that are polyphasely mineralized. Individual Qz-mineralizations within a vein are separated by thin, more or less continuous films of wall-rock minerals, which indicates incremental dilation and mineralization ("crack-seal"). These crack-seal veins are formed by syntectonic hydraulic fracturing and indicate an abnormally high fluid pressure during this diaphthoritic deformation stage. The volume of crack-seal quartz reaches 30% of the total rock volume in the 300 m deep borehole "Püllersreuth" (Heidelbach 1989) approx. 2 km SW of the KTB pilot hole. The source of these large volumes of hydrous fluids for solution and precipitation of Qz is unknown (see "Interpretation"). The Sr-isotopes of the Quartz veins, however, are significantly different from those in the country rocks (Albat et al.1989, Grauert, pers. comm.).

The crack-seal veins predate the cataclastic deformation. The intensity of ductile strain varies in different veins and is generally much higher in the KTB pilot hole than in the Püllersreuth drillhole, where most veins are weakly deformed (Fig.15). In such veins the Qz-crystals are oriented with their rhombohedral planes preferably parallel to the vein boundary (Heidelbach et al 1988). These growth fabrics are transformed by ductile deformation and recrystallization into cross-girdle and oblique-girdle fabrics (Heidelbach et al. 1988, Heidelbach, 1989).

Ms II occurs in different form during stage 3. It shows all transitions between a preferred orientation parallel to s_1 and a random orientation. The varyring degrees of preferred orientation of Ms II presumably do not reflect an age sequence, but represent a spatially and temporarily inhomogeneous strain.

Ms II frequently has inclusions of fibrolite and sometimes of prismatic Sil. Very often Ms II adopts the fibrous and curly texture of fibrolithic Sil and forms aggregates of flaky to fibrous sericite. Sericite is also formed in ductile shear zones by dynamic recrystallization of Ms I and Ms II. Coarsely grained random Ms II is locally developed as poikiloblasts, or as symplectites by intergrowth with Qz. It cannot be proven with certainty whether Ksp was involved in the formation of Ms II. Usually the following reaction is observed (Fig. 16):

$$\text{Bio} + \text{Sil} \dashrightarrow \text{Ms II} + \text{Ilmenite} + \text{Qz}$$

Chloritization of Bio takes place contemporaneously with the formation of Ms II, but it continues into the cataclastic stage. At the end of stage 3 the ductile deformation path terminates and stage 4, the cataclastic deformation begins, which will not be described here.

Also in the course of stage 3 the s_1-foliation remains active and represents the dominant penetrative foliation. Extensional cleavage, SC-fabrics (Fig. 16) and delta- or sigma-clasts can occur between s_1- foliation planes, particularly during the diaphthoritic deformation stages. Some F_2-folds show a very weakly developed intersection cleavage.

3. Interpretation

The Ga, Ky-Sil, Bio paragneisses, interpreted as high-temperature mylonites, are characterized by ribbon quartz and Plg-recrystallization. Rare Plg-clasts show core and mantle structures and indicate a coarsely grained precursor. These rocks, free of Ms at the end of the prograde metamorphic strain path, developed their HT-mylonitic fabric at high deviatoric stress and low water activity, i. e. under dry amphibolite facies conditions. Therefore, almost no Ms has been formed during amphibolite facies HT-mylonitization.

Supply of hydrous fluids under amphibolite facies conditions induced metablastic processes and locally partial melting. Ms I appeared as a new mineral phase. HT-mylonites are relics in metablastic gneisses.

During the diaphthoritic stage substantial amounts of overpressured hydrous fluids invaded the rocks contemporaneously with uplift, cooling and reduction of effective stress. Strain, accordingly, became increasingly inhomogeneous.

The source of the fluids is not known. Since the crack-seal Qz-veins are isotopically different from their host rocks, the source of the fluids was possibly outside the gneisses of the ZEV nappe complex. The post-tectonic granites cannot be regarded as their source because the crack-seal veins of the pilot hole are strongly strained and therefore older than the granites. Nonmetamorphic or very low-grade metamorphic rocks are a possible source, provided they were tectonically drained under the load of the crystalline nappes, and have released water from prograde metamorphic mineral reactions. In fact, the Erbendorf greenschists and their associated greenschist-facies phyllonitic to quartz-phyllonitic Wetzldorf sequence constitute the basal units of the ZEV-nappe complex at the present outcrop level. They represent a possible source of fluids in the course of the nappe transport. Younger fluids entered the rocks after the emplacement of the nappe complex in the course of late diaphthoresis and brittle faulting. Outside the cataclastic faults proper the formation of retrograde metamorphic minerals (e.g. Biotite --> Chlorite) took place under static conditions in all three types of paragneisses described.

The maintenance of unstable grain boundaries and subgrain boundaries in Qz from HT-mylonitic, metablastic and diaphthoritic gneisses shows that no post-tectonic annealing took place. In this respect the Qz-grain and Qz-subgrain boundaries of the ZEV differ from those of the LP-HT metamorphic Moldanubian and Saxothuringian.

The post-tectonic granites did not influence the rock fabric of the drilling site. In spite of the short distance to the post-tectonic Falkenberg granite the KTB pilot hole is situated outside its thermal contact area. However, the ZEV at the Waldnaab fault zone has been downthrown about 3000 m (Stettner, pers. comm.), so at the time of granite intrusion the rocks of the drilling site could have been at another position relative to the granite body than they are now.

There are continuous transitions between the different deformation stages described. The older fabrics are relics inside rocks overprinted during younger deformation stages of variable intensity. HT-mylonites e.g., can be strongly overprinted diaphthoritically without substantial metablastic grain growth or can be altered during the brittle deformation stage.

The following tectonic interpretation can be derived from the described ductile deformation path: According to the character of metamorphism, the MP- to HP- metamorphism must be related to the subduction stage, whereas the LP-metamorphism took place in the course of the complex collision of the Bohemian, Moldanubian and Saxothuringian terranes (Weber & Vollbrecht, 1987). The nappe complexes of Münchberg and the ZEV escaped the younger LP-metamorphism by obduction and supracrustal displacement.

The chemical composition of the described paragneisses corresponds to greywackes, clayey greywackes and shales (Röhr et al., this vol.). Findings of acritarchs point to a Lower Devonian age of these sediments (Pflug & Prössl, 1989). Therefore, they can be interpreted as flysch deposits at a Hercynian active continental margin of the Bohemian terrane. During subduction they underwent progressive metamorphism at about 390 Ma. In the course of the HT-mylonitic part of the deformation path, the presumably MP-granulite facies rocks were transported together with slices of mafic and ultramafic HP-metamorphic rocks as an intracrustal nappe from deep into higher crustal levels. During the early stage of this transport the effective stress was high due to low water activity. In the course of advancing intracrustal transport, i.e. during the metablastic stage, a gradually inreasing infiltration of hydrous fluids took place possibly from underlying subducting and prograde metamorphosed rocks.

During the diaphthoritic stage the crystalline nappe has been emplaced as a supracrustal nappe onto oceanic sediments abounding in water. The island arc affinity of the Erbendorf greenschists

(Schüssler et al, 1989) as basal parts of the ZEV nappe complex indicates collision with a presumably late Proterozoic island arc. Silurian metacherts (Reitz et al. 1988, Pflug and Reitz 1987), associated with the Wetzldorf Formation along the eastern rim of the ZEV may idicate the incorporation of oceanic sediments in the nappe complex. The highly mature phyllitic-quartzitic sediments of the Wetzldorf Formation must have been deposited on a passive continental margin. They were incorporated into the nappe pile during the early collision stage. Equivalents of the Wetzldorf Formation are presumably preserved along the nordwestern margin of the Zone of Tepla-Taus (Stettner, pers. comm.) and in the Silurian rocks (Reitz & Pflug 1987) of the Kühnesche Gebirge.

Under the load of the crystalline rocks high pore fluid pressures were generated inside the basal nappe units abounding in water (Erbendorf greenschists and Wetzldorf beds), thus reducing effective stress and internal friction. The overpressured sediments acted as glide horizon during the diaphthoritic stage of nappe transport. Correspondingly, the deformation concentrated inside the basal nappe unit producing their mylonitic to phyllonitic fabric. Overpressured fluids migrated into the overlying crystalline rocks leading to diaphthoritic mineral reactions and producing hydraulic fractures and corresponding crack-seal Qz mineralizations, preferably along the foliation as planes of lower cohesion.

The temporal and spatial relationship between the Moldanubian LP-metamorphism at about 320 Ma (Teufel, 1987) and the obduction of the ZEV nappe, which were subjected to prograde metamorphism during Devonian subduction prior to 380 Ma, is still open to question. If the crack-seal Qz-veins were formed at about 360 Ma (Albat et al.,1989), the diaphthoritic stage of the nappe transport and the incorporation of the basal nappe unit must have taken place prior to the 320 Ma old LP-metamorphism of the Moldanubian. The Rb/Sr-mineral ages of 365 to 370 Ma of Bio and Ms from gneisses of the ZEV (Teufel, 1987) support this assumption. A correlation of the ZEV with the Münchberg nappe complex, the basal unit of which contains Lower Carboniferous wildflysch (Franke, 1984), shows that the nappe transport continued into late to post-Lower Carboniferous time. Overthrusting of the ZEV over the Moldanubian could then have taken place during the time of its LP-metamorphism as a supracrustal nappe, i.e. in a high structural level outside the area of the Moldanubian metamorphism, similarly to the Münchberg nappe complex. Stretching lineations and associated shear sence indicators evidence, that the polarity of the tectonic transport was in SW direction through all stages of the ductile deformation path.

LP-metamorphic overprint increases from the NW to the SE. There is no LP-metamorphic overprint in the MM and it has not yet been proven in the northern ZEV. It seems, that the Wetzldorf Formation suffered lower grade metamorphism in the NW than in the SE. Further to the SE, the LP-metamorphic overprinted eclogites of Winklarn (Blümel, 1986; O'Brien, 1989) could be interpreted as basal relics of the ZEV nappe complex on top of the Moldanubian, affected by the Moldanubian metamorphism (Fig. 17). The western rim of the ZTT has been overprinted by the Moldanubian metamorphism. Still open to question are the younger Hbl cooling ages east of, and in the roof of, the post-tectonic granites forming the eastern rim of the ZEV (Kreuzer at al.,1989). It can be assumed that these granites reset the Hbl cooling ages of the ZEV.

References

ALBAT,F., GRAUERT, B. & HANSEN, B. (1989): Sr-Isotopenverteilung in einem Kleinbereichsprofil durch Gneise der Bohrung Püllersreuth (ZEV).-KTB Report 89-3: 442.

BLÜMEL, P. (1986): Metamorphic processes in the Variscan crust of the Central Segment.-Third EGT Workshop: The Central Segment, Bad Honnef, 14.-16.4.1986: 149-155.

FRANKE, W. (1984): Variszischer Deckenbau im Raume der Münchberger Gneismasse, abgeleitet aus der Fazies, Deformation und Metamorphose im umgegbenden Paläozoikum.- Geotekt. Fosch. 68: 253 pp.

HEIDELBACH, F. (1989): Gefügekundliche Untersuchungen an mylonitischen Gneisen der Bohrung Püllersreuth (ZEV).- Diplomarbeit Univ. Göttingen: 68 pp.

HEIDELBACH, F., VOLLBRECHT, A., de Wall, H. & WEBER, K. (1988): Lagenparallele Quarzmineralisationen in Gneisen der Bohrung Püllersreuth. Kontinentales Tiefbohrprogramm der

Bundesrepublik Deutschland, 1. KTB Schwerpunkt-Kolloquium, Giessen 28.-29. 1. 1989: p. 56.

KOSSMAT, F. (1927): Gliederung des varistischen Gebirgsbaues.-Abh. Sächs. Geol. L. A., 1: 39 p.

KTB (1986): Ergebnisse der Vorerkundungsarbeiten Lokation Oberpfalz. 2. KTB-Kolloquium, Seeheim/Odenwald, 19.-21.9.1986: 186 pp.

KREUZER, H., SEIDEL, E., SCHÜSSLER, U., OKRUSCH, M., LENZ, K.-L., RASCHKA, H. (1989): K-Ar geochronology of different tectonic units at the northwestern margin of the Bohemian Massif.- Tectonoph.,157: 149-178.

O'BRIEN, P.J. (1989): The petrology of retrograded eclogites of the Oberpfalz Forest, northeastern Bavaria, West Germany. Tectonoph., 157: 195-212.-

PFLUG,H.D. & REITZ, E. (1987): Palynology in metamorphic rocks: Indication of early land-plants: Naturwissenschaften, 74, p. 386-387.

PFLUG, H.-D. & PRÖSL, K.F. (1989): Palynology in gneiss. Results from the Kontinental Deep Drilling Program. Naturwissenschaften 76: 565-567.

REINHARDT, J. & KLEEMANN, U. (1989): Phasenpetrologische Analyse und Geothermobarometrie der Metapelite in der Zone von Erbendorf-Vohenstrauß (ZEV), Oberpfalz.- Europ. J. Mineralogy, Vol. 1, Beih., p. 152.

REITZ, E., PFLUG, H.-D. & FRANKE, W. (1988): Biostratigraphie im Kristallin. 1. KTB-Schwerpunkt-Kolloquium Giessen 1988, Zusammenfassung der Beiträge, p. 32.

SCHÜßLER et al. (1989): Metabasites from the KTB Oberpfalz target area, Bavaria - geochemical characteristics and examples of mobile behaviour of "immobile" elements.- Tectonoph.,157: 135-148.-

TEUFEL, S. (1987): Vergleichende U-Pb und Rb-Sr Altersbestimmungen an Gesteinen des Übergangsbereiches Saxothuringikum/Moldanubikum, NE-Bayern.- Diss. Univ. Göttingen: 110 pp.

VOLLBRECHT, A., WEBER, K. & SCMMOLL, J. (1989): Structural model for the Saxothuringian-Moldanubian suture in the Variscan basement of the Oberpfalz (Northeastern Bavaria, F.R.G.) interpreted from geophyscal data.- Tectonoph., 157: 123-133.

VOLL, G. (1980): Deformation, Crystallization and Recrystallization.-Intern. Conf. on "The effect of deformation on rocks", Göttingen 9.-12.4.1980, Abst. Appendix:1-9.

WEBER, K. & VOLLBRECHT, A. (1989): The Crustal Structure at the Continental Deep Drilling Site, Oberpfalz. In: Emmermann and Wohlenberg (Eds.): The German Continental Deep Drilling Program (KTB), Site-selection Studies in the Oberpfalz and Schwarzwald: p.5-36, Spinger-Verlag

WHITE, S. (1975): Tectonic deformation and recrystallization of oligoclase.-Contrib. Mineral. Petrol., 50: 287-304.-

Fig. 1: Quartz (Q) grain surrounded by recrystallized plagioclas. Most of the Plg grains are untwinned. The Qz grain shows no primary recrystallization. Its acute offshoots are interpreted as resulting from ductile protrusion along grain boundaries of the recrystallized feldspar fabric. HT-mylonitic deformation stage. Sample VB 447 C2h, 1977,69 m, x pol., short picture length: 0,45 mm.

Fig. 2: Coarsely grained plagioclas relic showing subgrains and recrystallized grains along its rim. HT-mylonitic deformation stage. Sample VB 447 C2h, 1977,69 m, x pol., short picture length: 3,4 mm

Fig. 3: Biotite-rich HT-mylonite showing untwinned recrystallized Plg. Bio is oriented parallel to the finite stretching direction. Sample VB 449 B2e, 1983,39 m, oblique pol., short picture length: 1,2 mm.

Fig. 4: Microboudinage fabric inside a Bio-rich HT-mylonite. The orientation of Bio indicates the direction of finite elongation. Sample VB1a 500 B2h, 2170,81 m, one pol., short picture length 1,5 mm.

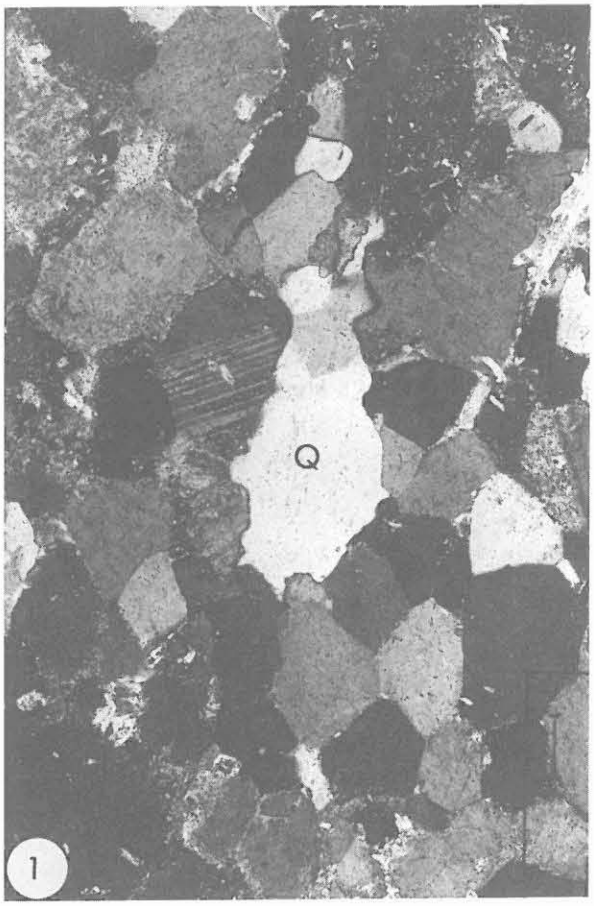
Q
1

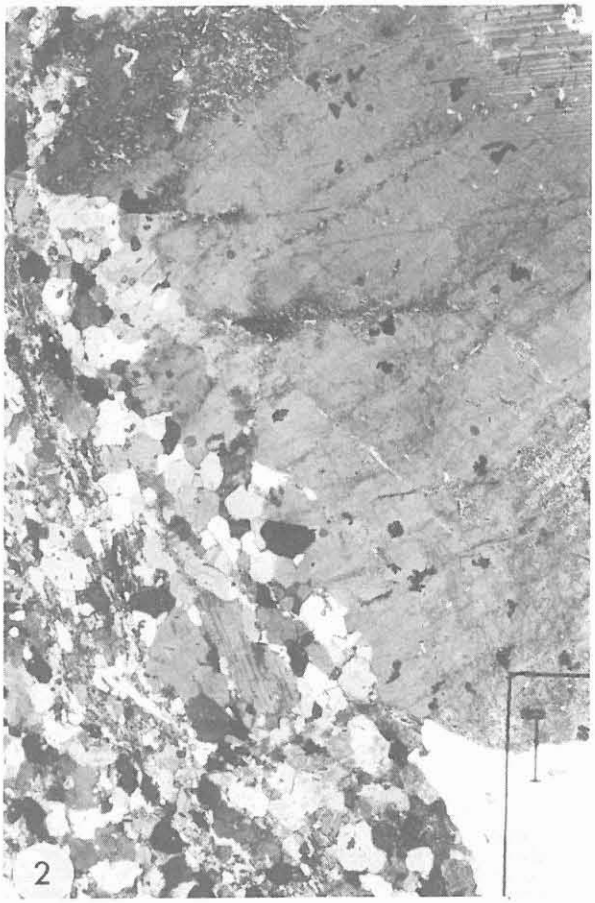
2

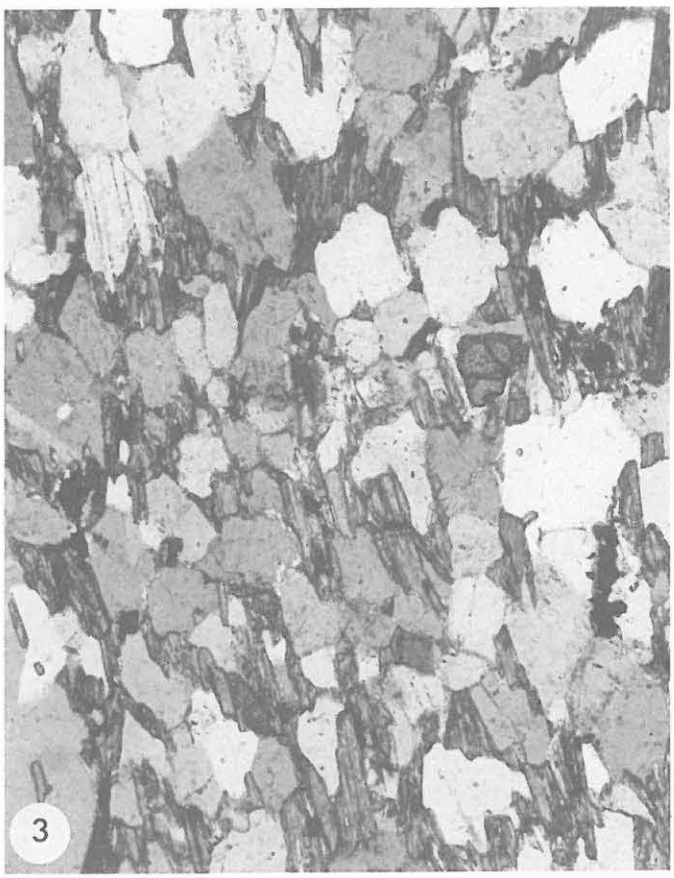
3


4

Fig. 5: Quartz grain (Q) showing strongly unequilibrated internal grain boundaries resulting from secondary recrystallization. Sample VB 1a 480 E1o, 2099,52 m, x pol., short picture length: 1,8 mm.

Fig. 6: Ribbon quartz inside a matrix of recrystallized plagioclase. The quartz grain shows no primary recrystallization, but small acute offshoots along grain boundaries of the recrystallized plagioclase, interpreted as in Fig. 1. HT-mylonitic deformation stage. Sample VB 447 C2h, 1977,69 m, x pol., short picture length: 1,8 mm.

Fig. 7: Detail from Fig. 6, short picture length: 0,45 mm

Fig. 8: Metablastic grain coarsening of the quartz (Q) - plagioclase (P) fabric together with newly formed muscovite I (MI) and biotite II (BII). biotite II is intergrown with fibrolite. Metablastic deformation stage. Sample VB 401, x pol., short picture length: 4,5 mm.

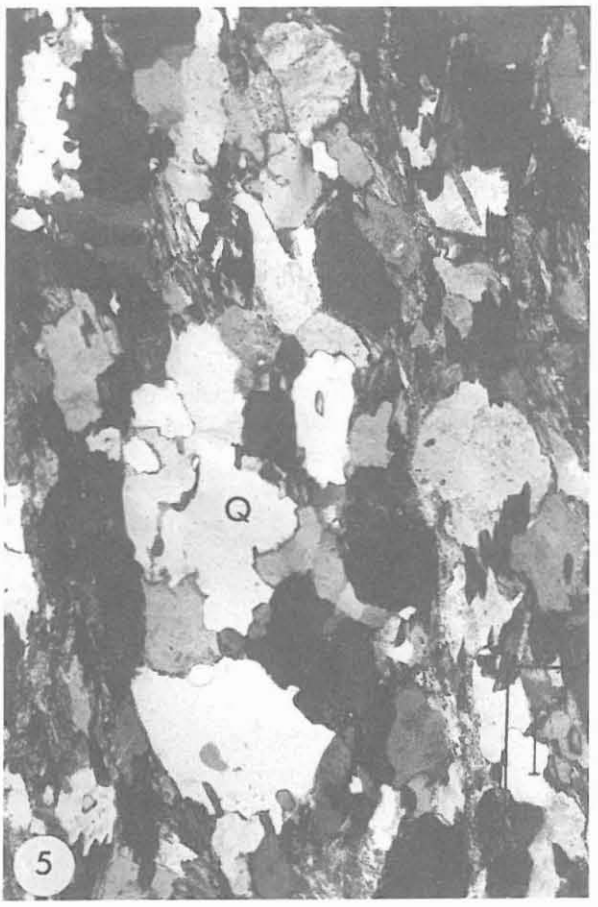
Q
5


6


7

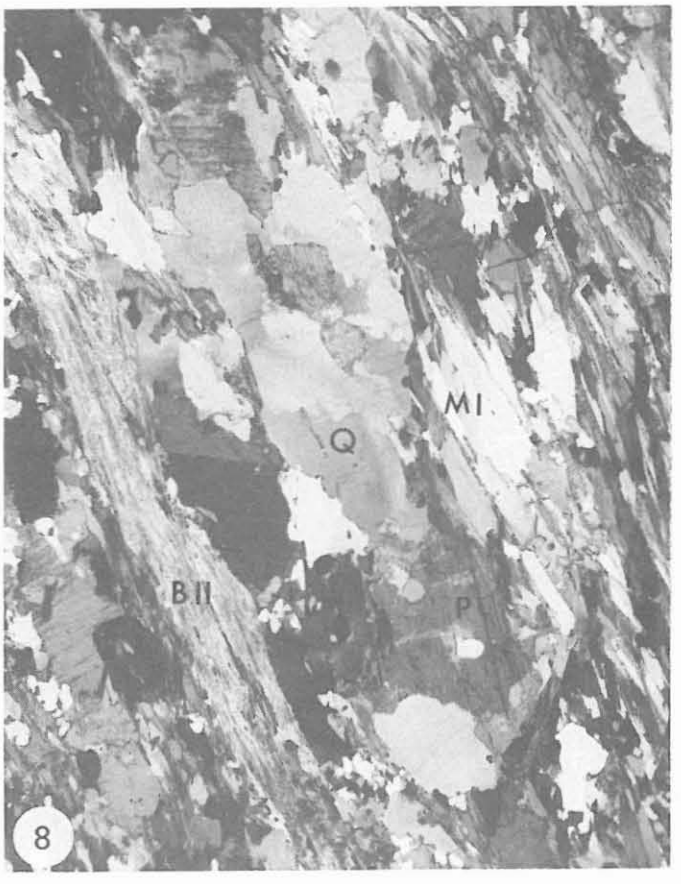
MI
Q
BII
P
8

Fig. 9: Muscovite I (MI), syntectonically grown parallel to the s1-foliation. Biotite I (BI) forms a relic of the HT-mylonitic defornmation stage and is, in contrast to the younger Ms I, located dominantly in pressure shadows of feldspar grains. Sample VB 465 E4b, 2040,32m, oblique pol., short picture length: 1,7 mm.

Fig. 10: Biotite II - fibrolite aggregates. They formed during the metablastic deformation stage. In contrast to biotite I, biotite II has not grown in pressure shadows, but only on the s1 foliation planes. Sample VB 422 D11, 1869,60 m, one pol., short picture length: 1,7 mm.

Fig. 11: Incipient primary recrystallization of quartz, overprinting the metablastic fabric; beginning of the diaphthoritic deformation stage. Micas are biotite I and muscovite I. Sample VB 426 A1ekI, 1889,78 m, x pol., short picture length 4,5 mm.

Fig. 12: Primary recrystallized ribbon quartz, surrounded by a diaphthoritic host rocks. Oblique orientation of elongated recrystallized grains indicate sinistral sense of shear. Sample 206 B1B, layer A, x pol., short picture length: 3,2 mm.

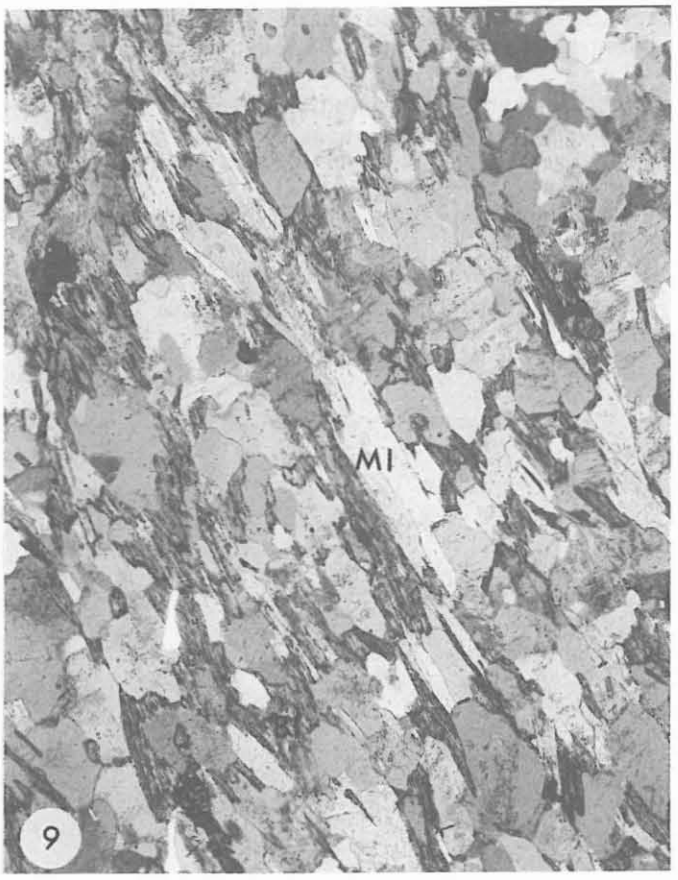
MI
9


10

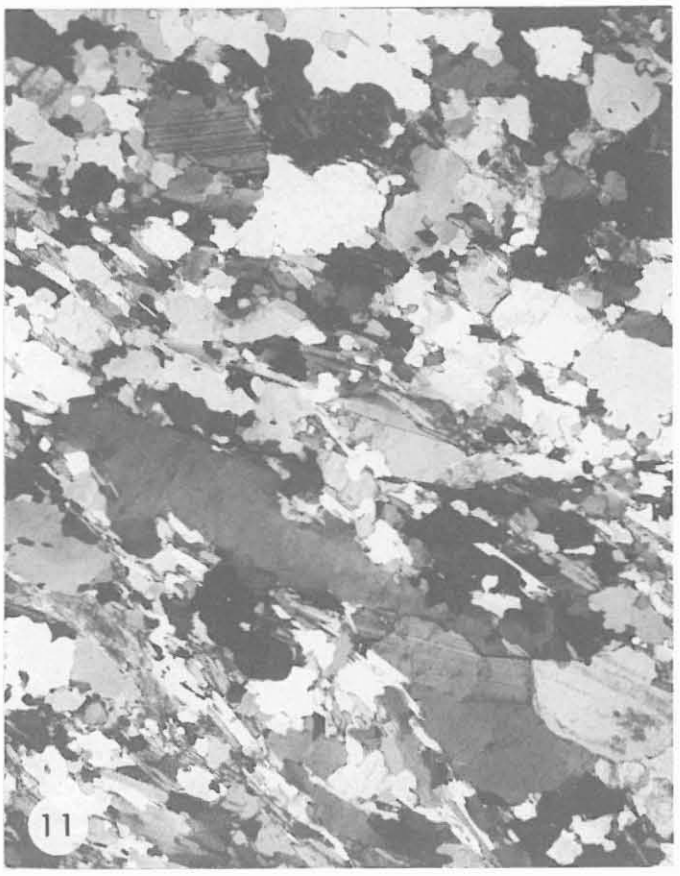
11

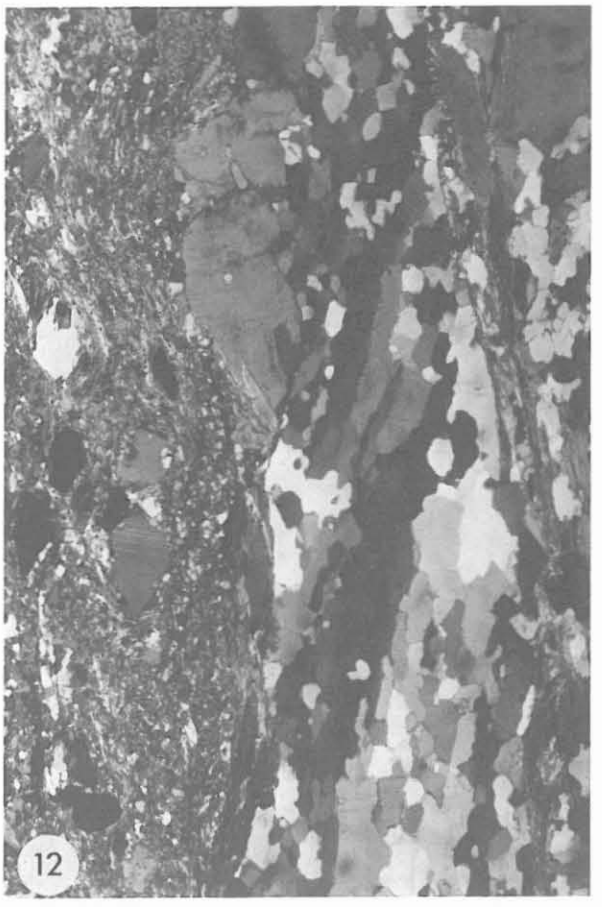
12

Fig. 13: Cataclastically deformed plagioclase, surrounded by recrystallized quartz. Diaphthoritic deformation stage. Sample 206 B1B, layer A, x pol., short picture length: 3,6 mm.

Fig. 14: Crack-seal quartz vein surrounded by diaphthoritic country rocks. Individual quartz mineralizations within the vein are separated by thin, more or less continuous films and lenses of wall-rock minerals. Sample VB 447 C2h, 1977,69 m, x pol., short picture length: 3,2 mm.

Fig. 15: Weakly deformed crack-seal quartz veins from the bore hole "Püllersreuth". Sample 193,1 m, x pol. short picture length: 24 mm.

Fig. 16: Diaphthoritic mica schist with SC-fabric indicating sinistral sense of shear. Sample 206 B1B, layer A, one pol., short picture length: 1,2 mm.


13

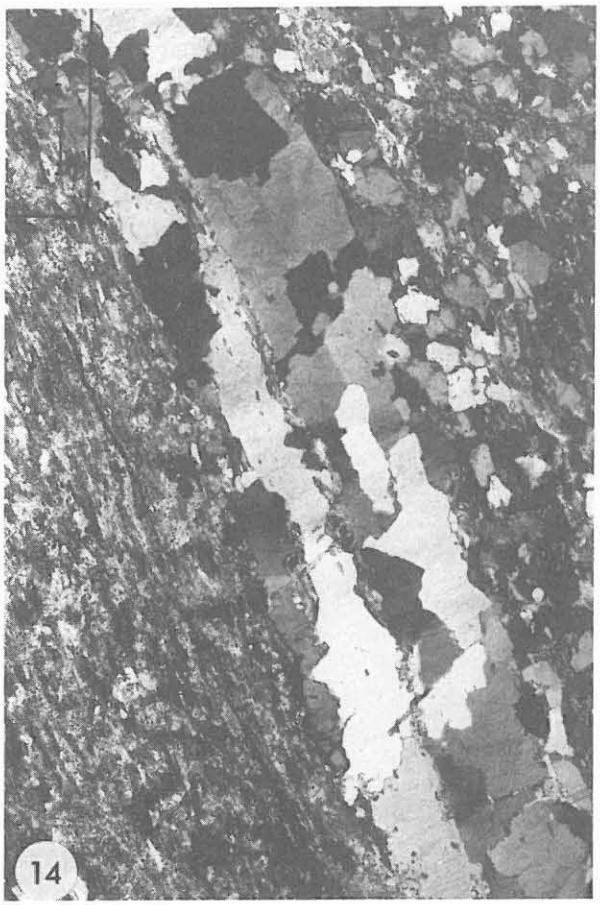
14

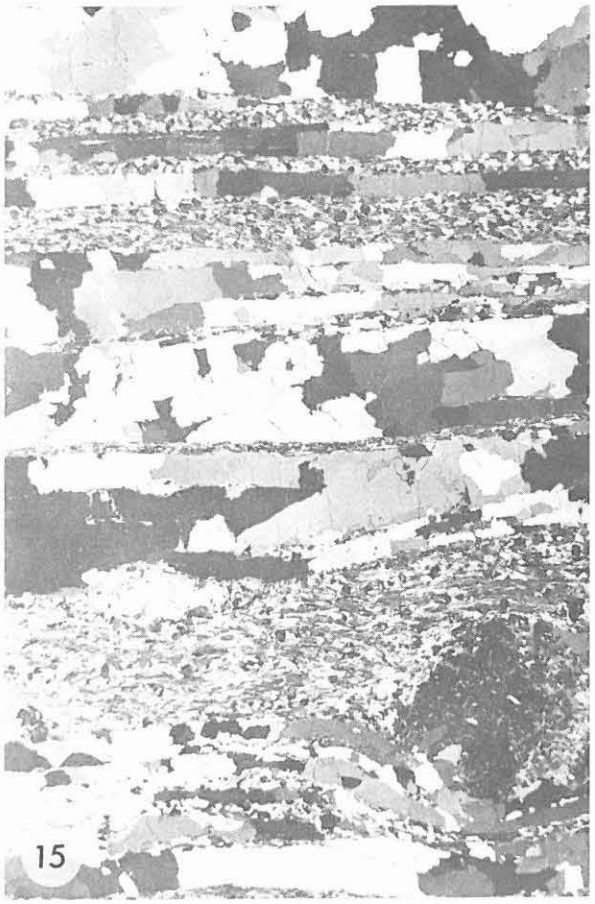
15


16

Fig. 17: Geological sketch map of the western rim of the Bohemian Massif in NE Bavaria. A: Variscan basement outcrops in Middle Europe with zones according to Kossmat (1927). RH: Rhenoherzynian Zone; ST: Saxothuringian Zone; MN: Moldanubian Region. B: Geological map with the tectonometamorphic units. 1: crystalline nappe complexes; 2: basal units of the nappe complexes; MM: Münchberg nappe complex; ZEV: nappe complex of the Zone of Erbendorf-Vohenstrauß; ZTT: Zone of Tepla-Taus, forming the western part of the Bohemian terrane (Bohemicum); 3: Saxothuringian; 4: Moldanubian of the Oberpfälzer Wald; 5: late- to post-tectonic granites; 6: KTB drilling site. 7: overthrust; ZTM: Zone of Tirschenreuth-Mähring; W: Winklarn.

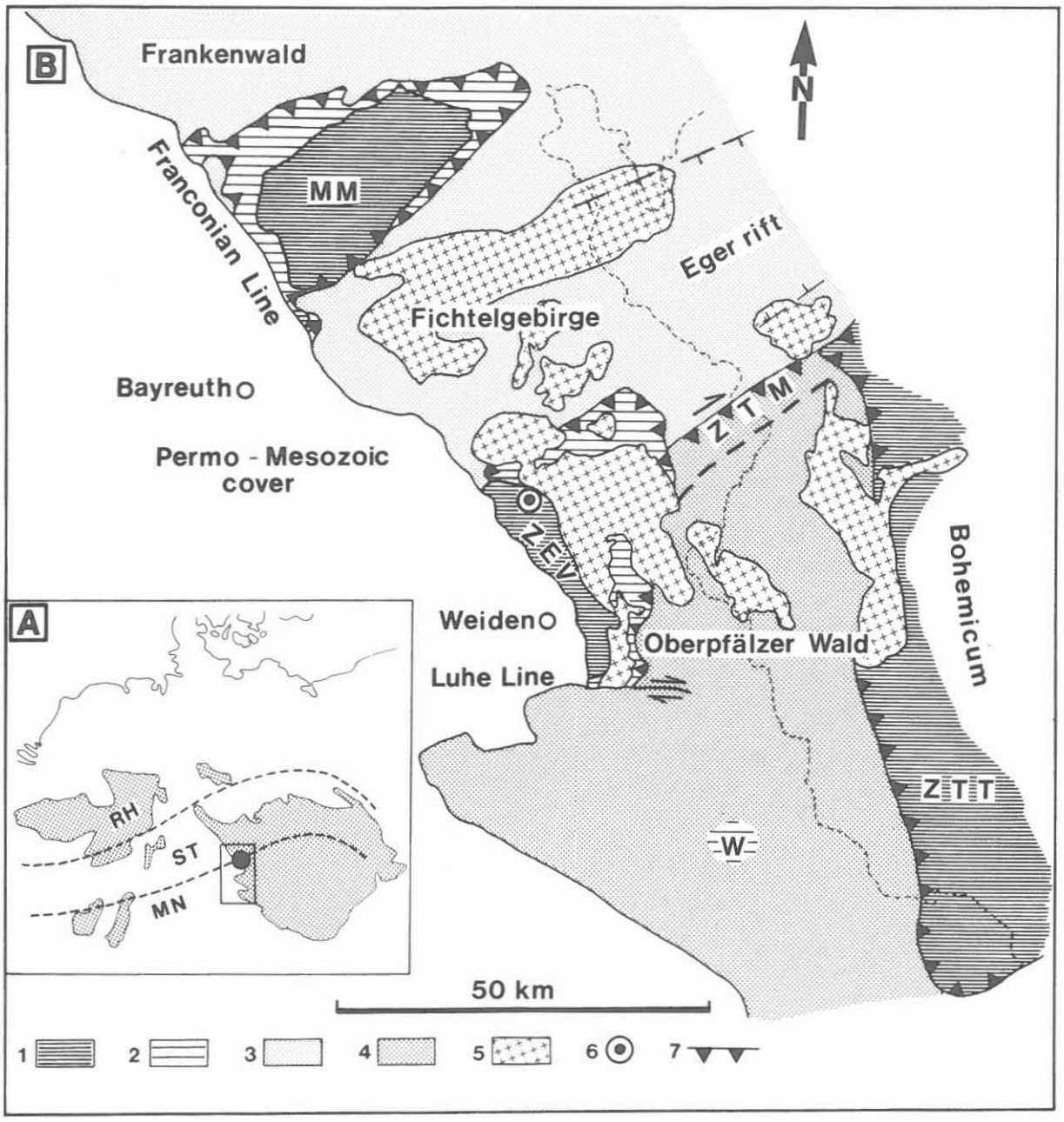
B
Frankenwald
N
MM
Franconian Line
Eger rift
Fichtelgebirge
Bayreuth
Permo - Mesozoic cover
ZTM
ZEV
Bohemicum
A
Weiden
Oberpfälzer Wald
Luhe Line
RH
ST
MN
ZTT
W
50 km
1
2
3
4
5
6
7